SE818-18

REPORT NO. F694

PART B4 ALTERNATIVES, ANALYSES, SELECTION

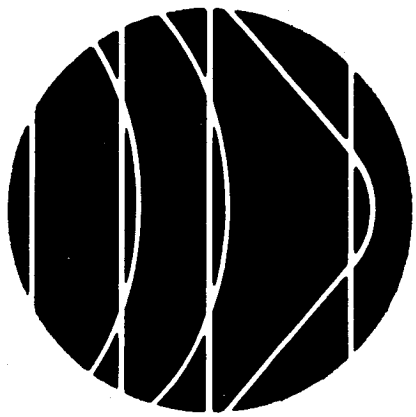

VOLUME II CAPSULE BUS SYSTEM

MCDONNELL ASTRONAUTICS

REPORT NO. F694
31 AUGUST 1967

PART B4 ALTERNATIVES, ANALYSES, SELECTION

VOYAGER CAPSULE PHASE B FINAL REPORT

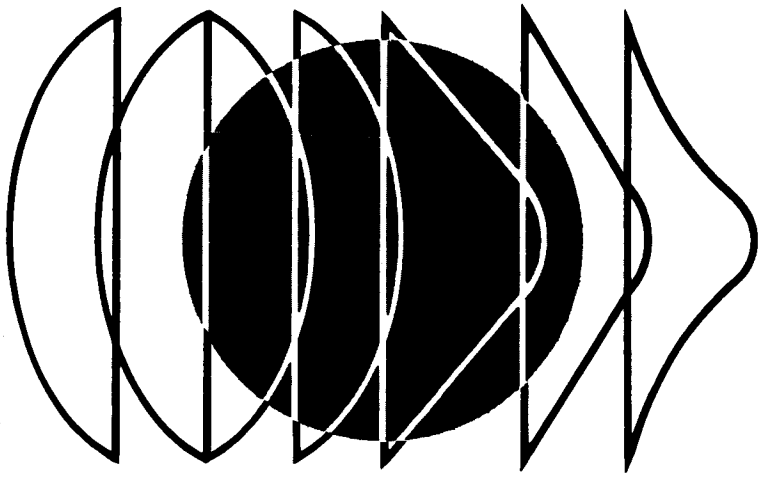

VOLUME II CAPSULE BUS SYSTEM

PREPARED FOR:
CALIFORNIA INSTITUTE OF TECHNOLOGY
JET PROPULSION LABORATORY
PASADENA, CALIFORNIA
CONTRACT NUMBER 952000

COPY NO. 15

MCDONNELL ASTRONAUTICS

REPORT ORGANIZATION

VOYAGER PHASE B FINAL REPORT

The results of the Phase B Voyager Flight Capsule study are organized into several volumes. These are:

Volume I	Summary
Volume II	Capsule Bus System
Volume III	Surface Laboratory System
Volume IV	Entry Science Package
Volume V	System Interfaces
Volume VI	Implementation

This volume, Volume II, describes the McDonnell Douglas preferred design for the Capsule Bus System. It is arranged in 5 parts, A through E, and bound in 11 separate documents, as noted below.

Part A	Preferred Design Concept	2 documents, Parts A_1 and A_2
Part B	Alternatives, Analyses, Selection	5 documents, Parts B_1, B_2, B_3, B_4 and B_5
Part C	Subsystem Functional Descriptions	2 documents, Parts C_1 and C_2
Part D	Operational Support Equipment	1 document
Part E	Reliability	1 document

In order to assist the reader in finding specific material relating to the Capsule Bus System, Figure 1 cross indexes broadly selected subject matter, at the system and subsystem level, through all volumes.

SYSTEM/SUBSYSTEM \ VOLUME II PARTS		PART A DESCRIPTION OF PREFERRED SYSTEM OBJECTIVES, MISSION, DESIGN, SUBSYSTEMS, OPERATIONS, SUPPORTING FUNCTIONS	PART B ALTERNATIVES, ANALYSIS AND SELECTION – METHODS TRADE STUDIES, OPTIMIZATION STUDIES RESULTS	PART C DETAILED DESCRIPTION OF SUBSYSTEM FUNCTIONS	PART D OPERATIONAL SUPPORT EQUIPMENT – SYSTEM, SUBSYSTEM, LAUNCH COMPLEX, MISSION, HANDLING, SOFTWARE	PART E RELIABILITY CONSTRAINTS, ANALYSIS, RESULTS, PROGRAM TESTING, CONTROL
CAPSULE BUS SYSTEM						
Mission	Objectives	1.1–Summary	2–Analysis	N/A	1–General	1–Constraints
	Profile	1.2–Summary	2–Analysis 2.4–Selection	N/A	N/A	3.1.1–Analysis
	Operations	4–Description by Phase	2.3–Analysis 2.3.7–Landing Site Select	N/A	4.4–LCE Description 4.5–MDE Description	3–Estimates
Design	General	2–Criteria Summary 3.1–Configuration	1–Study Approach 3–Functional Requirements	N/A	3.2–Concept 3.3–Summary 6.1–AHSE	4–Program Requirements 5–Component Reliability
	Standardization/Growth	2.5–Summary 11–Future	(See Specific Subsystem Below)	N/A	4.3.8-STC 4.4.8-LCE 4.5.8-MDE } Growth	N/A
	Weight	3.1.2.4–Summary 5–Breakdown	(See Specific Subsystem Below)	N/A	N/A	2.3.2–Reliability vs Weight
Interfaces (See Also Vol. V)		3.1–Summary 9.0–Operational	(See Volume V)	N/A	4.2.1,4.3.5,4.4.5, 4.5.5	N/A
Implementation (See Also Vol. VI)		10–Schedule 8.11–OSE	(See Volume VI)	N/A	(See Specific Subsystem Below)	N/A
Planetary Quarantine		7–General	(See Volume VI, C,7 Sterilization Plan)	N/A	None Required	N/A
O.S.E. (See Also Part D)		8–General (See Also–D1,D2, D3,D4)	(See D2.5-Selection Criteria, D9-Analysis, D10 - Alternatives)	(See D5-Subsystem Level Test Equipment, See Also D4, D6, D7)	Complete OSE Description	(See D4.3.6–STC D4.4.6–LCE D4.5.6–MDE)
SUBSYSTEMS						
Sterilization Canister		3.2.1.1–Description 3.1.2–Summary	5.1–Analysis	1.1	6.1.5.2,6.1.5.3, 6.1.5.6 6.1.5.8–AHSE 6.2.15–Servicing	(See Part C Sections 1.1.1.7 1.1.2.7 1.1.3.7)
Adapter		3.2.1.2–Description 3.1.2–Summary	5.2–Analysis	1.2	None Required	(See Part C, 1.2.7)
Aeroshell		3.2.1.3–Description	4.1–Configuration	1.3	None Required	(See Part C, 1.3.7)

Figure 1

Aerosheil	3.1.2–Summary	Selection 4.6–Separation 5.3.1–Structure 5.3.2–Heat Shield			
Lander	3.2.1.4–Description 3.1.2–Summary	4.2–Configuration Selection 5.4–Analysis	1.4	6.1.5.9–Fixture	(See Part C, 1.4.7)
Telecommunications	3.2.2.1–Description	4.9–In-Flight Monitoring 5.5–Analysis	2–Telemetry 3–Radio 4–Antenna 5–Data Storage 6–Command	4.3.9.1–STC Console 5.7–Test Set	(See Part C, Sections 2.1.7, 2.2.7, 2.3.7, 3.1.7, 3.2.7, 4.5, 5.1.7, 5.2.7, 6.1.7, 6.2.7)
Power	3.2.2.2–Description	5.6–Analysis	7	4.3.9.1–STC Console 5.3–Test Set	(See Part C, Sect. 7.7)
Sequencing and Timing	3.2.2.3–Description	5.7–Analysis	8	4.3.9.1–STC Console 5.4–Test Set	(See Part C Sections 8.1.7, 8.2.7)
Guidance and Control	3.2.2.4–Description	4.7–De-orbit Attitube Reqm't. 5.8–Analysis	9	4.3.9.1–STC Console 5.5–Test Set	(See Part C, 9.7)
Radar	3.2.2.5–Description	5.9–Analysis	10	4.3.9.1–STC Console 5.6–Test Set	(See Part C, Sections 10.1.7, 10.2.7)
Aerodynamic Decelerator	3.2.3–Description	4.4–Selection 5.10–Analysis	11	None Required	(See Part C, 11.7)
Pyrotechnics	3.2.4–Description	5.11–Analysis	12	4.3.9.1–STC Console 5.9–Test Set	(See Part C, 12.7.1)
Thermal Control	3.2.5–Description	5.12–Analysis	13	4.3.9.1–STC Console 5.8–Test Set	(See Part C, 13.6)
De-orbit Propulsion	3.2.6.1–Description	5.13.1–Analysis	14	5.10–Test Set 6.1.5.10–AHSE	(See Part B, 5.13.4.5) (See Part C, 14.7)
Reaction Control	3.2.6.2–Description	5.13.2–Analysis	15	5.10–Test Set 6.2–Servicing	(See Part B, 5.13.4.5) (See Part C, 15.7)
Terminal Propulsion	3.2.6.3–Description	4.3–Configuration Selection 4.5–Terminal Deceleration 5.13.3–Analysis	16	4.3.9.1–STC Console 5.10–Test Set 6.2–Servicing	(See Part B, 5.13.4.5) (See Part C, 16.7)
Packaging and Cabling	3.2.7–Description	5.14–Analysis	17	4.3.9.8–Special Purpose Complex Equipment	Not Required

Note: Parentheses Refer Reader to Volumes/Parts Outside of the Respective Notation

TABLE OF CONTENTS

This document consists
of the following pages:

Title Page
i through iv
5.5-1 through 5.5-88
5.6-1 through 5.6-17
5.7-1 through 5.7-17
5.8-1 through 5.8-22
5.9-1 through 5.9-95

5.5 TELECOMMUNICATIONS - The Capsule Bus telecommunications design was severely influenced by the large uncertainties in the Martian environment and the wide range of orbits and entry trajectories which must be accommodated. Maintaining the link between the CB and Spacecraft necessitated examining such problems as multipath interference and entry ionization as well as geometrical considerations, Spacecraft to CB line of sight and CB orientation.

To resolve these questions, we examined the entire spectrum of orbits/entry trajectories/atmospheres, candidate modulations, antenna patterns, data storage-retransmission techniques, ablator effects upon the wake ionization and diversity transmission approaches. Figure 5.5-1 is a summary of the computer programs, tests and simulations which were employed to solve the Martian entry telecommunications questions. Our design provides a maximum return of entry data within the design requirements and constraints.

The solutions derived to the multipath and entry ionization questions indicated that a significant increase in low frequency science data retrieval probabilities could be achieved by interleaving the CB and ESP packages prior to transmission. This interleaving is achieved with minimum interference to the CB.

PROPAGATION COMPUTER PROGRAMS AND SIMULATIONS

REFERENCE PARAGRAPH	COMPUTER PROGRAM	TEST/SIMULATION	DESCRIPTION
5.5.1.1	Echo		Computation of all of the geometric parameters required for the multipath problem
5.5.1.1	LS2 to LS8		Solutions to the complex statistical functions necessary to evaluate FSK in a multipath environment
5.5.1.1		Bit sync simulation	Simulation of the multipath environmental effects upon candidate bit synchronizer designs
5.5.1.2	KA1F		Chemical equilibrium program for hot gas mixtures*
5.5.1.2	–		Mixing and diffusion program for any gases*
5.5.1.2	–		Ray trace program – electromagnetic profile*
5.5.1.2		Test	Seeding tests with an RF plasma generator
5.5.1.2	T–684		Pointed cone – aerodynamics
5.5.1.2	T–785		Shear layer – aerodynamics
5.5.1.2	T–299		Method of characteristics – aerodynamics
5.5.1.2	T–805		Entropy layer patch – aerodynamics
5.5.1.2	T–687		Charring ablation program – thermodynamics
	T–689		Laminar boundary layer with mass addition – thermodynamics
	T–666		Chemical equilibrium composition of gas – thermodynamics
5.5.4		Test	Antenna pattern-Pattern Development Tests

*Plasma Programs

Figure 5.5–1

5.5.1 Propagation Analysis - The capsule link propagation analysis is based upon a 340-400 MHz relay link to the spacecraft.

The frequency range from 150 to 500 MHz was investigated in detail. Frequencies below 150 MHz were excluded because of galactic noise and antenna size limitations. Frequencies above 500 MHz were excluded because of the higher space loss incurred when the antenna beamwidths must be held constant. The results of the study indicated that the total vehicle weight was minimized at a 350 MHz transmission frequency. The two specific frequencies for the preferred design are required to be 60 MHz apart in order to minimize the equipment complexity in the spacecraft (see Section 5.5.3). 400 MHz was chosen to be compatible with the space research and telemetry bands, and 60 MHz below it, 340 MHz.

A relay, rather than a direct-to-earth, link was chosen primarily because the necessary high gain steerable antenna for a direct link is not compatible with the entry geometry.

The heart of the propagation analysis is the design control table (Figure 5.5-2). The transmitter power, five watts, is a design parameter which must be adjusted to provide an adequate signal margin under the most severe propagation conditions. The transmitting circuit losses are an engineering estimate based upon the cable routing within the vehicle configuration. The transmitting antenna gain and design space loss are predicated upon the allowable envelope of spacecraft-capsule positions at the time of entry. The derivation of this envelope is given in the first part of the multipath analysis (Section 5.5.1.1). The transmitting antenna gain figure includes the efficiency of the candidate antenna (see Section 5.5.4). Polarization loss in the right hand circularly polarized antenna subsystem is principally due to the "loss" of circularity off axis. The degree of off-axis look angles required is given in the first part of the multipath analysis, while the antenna ellipticity is discussed in the antenna analysis section.

The receiving antenna design gain is based upon the allowable envelope of spacecraft-capsule look angle variations, discussed in the multipath section, together with the envelope of orbit orientations with respect to the Sun and Canopus, discussed in Paragraph 5.5.4. The gain includes the receiving antenna efficiency. The receiving circuit loss, as was the transmitting circuit loss, is estimated based upon the vehicle configuration. The noise temperature analysis is given in Section 5.5.3.

The capsule bit rate of 2730 bps is derived from formatting the capsule instrumentation requirements given in Figure 5.5-3. The formatting techniques and trades

TELECOMMUNICATION DESIGN CONTROL TABLE

ITEM NUMBER	PARAMETER	VALUE	TOLERANCE (dB)		SOURCE
1	Transmitter Power (5W)	37.0 dBm	+0.5	−0.5	Design variable
2	Transmitting Circuit Loss	−0.5 dB	+0.2	−0.3	Engineering judgement
3	Transmitting Antenna Gain	5.1 dB	+0.5	−0.5	5.5.1.1 and 5.5.4
4	Transmitting Antenna Pointing Loss	Included in Line 5	–		–
5	Space Loss (f = 400 MHz, R = 10,000 Km)	−164.5 dB	–		5.5.1.1
6	Polarization Loss	0.0 dB	+0.0	−0.5	5.5.4
7	Receiving Antenna Gain	5.5 dB	+0.0	−3.0	5.5.1.1 and 5.5.4
8	Receiving Antenna Pointing Loss	Included in Line 7	–		–
9	Receiving Circuit Loss	−1.0 dB	+0.2	−0.2	Engineering judgement
10	Net Circuit Loss	−155.4 dB	+0.9	−4.5	Sum Lines 2 through 9
11	Total Received Power	−118.4 dBm	+1.4	−5.0	Sum Lines 1 and 10
12	No ($T_s = 555\ ^{+25}_{-80}\ ^{\circ}K$)	−171.2 dBm/Hz	+.3	−.8	5.5.3
13	Bit Rate (2730 bps)	34.4 dB-bps	–		5.5
14	Required E/N_o	13.1 dB	–		5.5.1.1
15	Threshold Power	−123.7 dBm	+.3	−.8	Sum Lines 12 through 14
16	Margin	5.3 dB	+2.2	−5.3	Line 11 minus Line 15

Figure 5.5–2

CAPSULE BUS INSTRUMENTATION LIST

PARAMETER NUMBER	PARAMETERS	RANGE	TYPE	ACCURACY	SAMPLES/SECOND				
					LAUNCH & CRUISE	PRESEPARATION CHECKOUT	DE-ORBIT	ENTRY	TERMINAL DESCENT
	Guidance & Control								
GC1–6	System Temperatures (6)	± 10°	LL	3%	.05	.05	.05	.05	.05
GC7–9	Gyro Temperatures (3)	175° ± 5°F	LL	3%		0.1	0.1	0.1	0.1
GC10–12	Accelerometer Temperatures (3)	175° ± 5°F	LL	3%		0.1	0.1	0.1	0.1
GC13–15	Gyro Speed (3)		BL			0.1	0.1	0.1	0.1
GC16	AC Power Supply Input Voltage		HL	10%		0.1	0.1	0.1	0.1
GC17	DC Power Supply Input Voltage		HL	10%		0.1	0.1	0.1	0.1
GC18	G&C Battery Voltage		HL	10%		0.1	0.1	0.1	0.1
GC19–26	Power Supply Voltages (8)		HL	10%		0.1	0.1	0.1	0.1
GC27	Computer Data (Includes Self Tests, Guidance Parameters, Status Parameters)		D	20 bits		6.0	6.0	6.0	6.0
	Sequencer & Timer								
SQ1	S&T Master Oscillator Temperature	50°–100°F	LL	3%	.001	.05	.01	0.1	.01
SQ2	Frequency Monitor Reference		BL				.01	0.01	.01
SQ3	Command Receipt Parity Check		BL			(1)			
SQ4	Address Decoder Entry	128 cmd	D	7 bits		(1)			
SQ5	Driver Output Counter	80	D	7 bits		.01	.01	.01	.01
SQ6–8	Power Supply Voltage (3)	0–20 Vdc	HL	2%		.05	.01	.01	.01
SQ9	S&T Memory Readout – 128 24 Bit Words (8)		D						
	Radar Altimeter								
RA1	Power Input		BL			.05		0.1	0.1
RA2	Regulator	28 ± 5Vdc	HL	2%		.05		0.1	0.1
RA3–9	Power Supplies (6.3, –7.3, 12, –12, 15, 450, 1 kv) (7)		HL	2%		.05		0.1	0.1
RA10	Temperatures	–200°–300°F	LL	3%	.001	.05	.01	0.1	0.1
RA11–12	AFC (2)	±2.5 Hz	HL	3%		.05		0.1	0.1
RA13–14	AGC (2)	70 Db	HL	2%		.05		0.1	0.1
RA15	Transmitter Incident Volts		HL	2%		.05		0.1	0.1
RA16	Transmitter Reflected Volts		HL	2%		.05		0.1	0.1
RA17	Transmitter Pulse Width	0–10 μs	HL	2%		.05		0.1	0.1
RA18–19	Tracker Lock-on (2)		BL			.05		0.1	0.1
RA20–21	Transmitter Current (2)	0–1 amp	LL	2%		.05		0.1	0.1
RA22	Modulator Hold-off		BL			.05		0.1	0.1
	Mode Switch		BL			.05		0.1	0.1

Figure 5.5–3

RA23	Mode Switch								
RA24–26	Discrete Altitude Marks (3)		BL			.05		0.1	0.1
RA27–28	Mixer (2)	0–20 mV	D	7 bits		.05		0.1	0.1
RA29	False Alarm Count	0–16 FA	D	4 bits		.05		0.1	0.1
RA30	Altitude	50–300 kft	D	14 bits		1.0		1.0	1.0
RA31–32	Range Accumulator (2)		BL			0.1		0.1	0.1
RA33	Temperature	−50°–250°F	LL	3%	.001	.05	.01	0.1	0.1
RA34–35	Reliable Operation (2)		BL			.05		0.1	0.1
	Landing Radar								
LR1–2	Transmitter Power (2)	0–200 mw	HL	3%		0.1		0.1	0.1
LR3	Modulator Sweep Amplifier	8 & 40 Hz	HL	2%		1.0		0.1	1.0
LR4	Modulator Sweep Frequency	130 cps	HL	2%		1.0		0.1	1.0
LR5–9	Tracker Lock-on (5)		BL			(2)			(2)
LR10	Range	f = 150 Hz	HL			1.0			1.0
LR11–14	Velocity (4)	f = 150 Hz	HL			1.0			1.0
LR15	150 kHz Pulse Train	f = 150 Hz				1.0			1.0
LR16–18	Velocity Output (V_x, V_y, V_z) (3)	0–500 fps	D	15 bits		1.0			1.0
LR19	Range Output	10–15 kft	D	15 bits		1.0			1.0
LR20–29	Preamp Outputs (10)		LL	3%		1.0			1.0
LR30–34	Preamp AGC Gain States (5)		BL			(2)		0.1	(2)
LR35–38	Doppler & Range Simulator Signals (4)		LL	2%		1.0			
LR39–42	Power Supply Voltages (4)	±30, −4, 6	HL	2%		0.1		0.1	0.1
LR43–44	Temperatures (2)	−60°–185°F	LL	5%	.001	0.1	.01	0.1	0.1
LR45	Range Low Scale Factor		BL			1.0			1.0
LR46–50	Received Beam Signal Strength (5)		HL			1.0			1.0
	Terminal Propulsion								
LC1	Source Pressure	0–4500 psia	HL	3%	.001		.01	.05	1.0
LC1–5	Regulator Pressure (4)	0–1500 psia	HL	3%	.001		.01	.05	1.0
LC6–14	Temperatures (9)	−50°–300°F	LL	3%	.001		.01	.05	1.0
LC15–17	Cartridge Valve Actuations (3) (3)		BL					(4)	(4)
LC18	.05g Relay (Subsystem Activation Sensor)		BL					.1	
LC19	Engine Start Valve		BL			1.0			(5)
LC20–23	Throttle Position Transducers (4)	0–5 in.	HL	3%		1.0			1.0
LC24–27	Engine Chamber Pressure (4)	0–500 psia	HL	3%					1.0
LC28–39	Propellant Level Sensors (12) (9)		BL			0.1			
	Reaction Control System								
RJ1	Source Pressure	0–4500 psia	HL	3%	.001	0.1	.01	1.0	
RJ2	Regulator Pressure	0–500 psia	HL	3%	.001	0.1	.01	1.0	
RJ3–6	Temperatures (4)	−50°–300°F	LL	3%	.001	0.1	.01	1.0	
RJ7–9	Cartridge Valve Actuations (3) (3)		BL			(4)		(4)	
RJ10–25	Thrust Chamber Valve Opening (16)		D	4 bits		(6)	(6)	(6)	
	De-orbit Propulsion (7)								
DP1	Case Temperature	−50°–300°F	LL	3%	.001	.01	1.0		
DP2	Motor Ignition		BL				(5)		
DP3	Nozzle Release		BL				(5)		
DP4	Ignitor Arm Verification		BL						

2-5-5.5

CAPSULE BUS INSTRUMENTATION LIST (Continued)

PARAMETER NUMBER	PARAMETERS	RANGE	TYPE	ACCURACY	SAMPLES/SECOND				
					LAUNCH & CRUISE	PRESEPARATION CHECKOUT	DE-ORBIT	ENTRY	TERMINAL DESCENT
	Electrical Power								
EC1	Battery Voltage	15–35 Vdc	HL	1%	.001	.01	.01	.01	.01
EC2–5	Battery Temperature (4)	0–120°F	LL	3%	.001	.01	.01	.01	.01
EC6	Battery Charge Current	0–2 amp	LL	1%	.001				
EC7–8	DC-to-DC Converter Output Voltage (2)	25–30 Vdc	HL	1%	.001	.01			
EC9	Battery Current	0–25 amp	LL	1%	.001	.01	.01	.01	.01
EC10–11	DC-to-DC Converter Output Current (2)	0–8 amp	LL	3%	.001	.01			
EC12–13	DC-to-DC Converter Temperature (2)	0–120°F	LL	3%	.001	.01			
EC14	DC-to-DC Converter Operation		BL		.001	.01			
EC15–17	Squib Battery Voltage (3)	20–35 Vdc	HL	1%		.01	.01	.01	.01
EC18	Power Transfer Switch Operation		BL		.001	.01			
EC19	Redundant Battery Switch Operation		BL				.01	.01	.01
	Thermal Control								
TC1–10	Insulation Blanket Temperatures (10)	−350° to 200°F	LL	3%	.001	.01	.01	.01	.01
TC11–20	Aeroshell Bond Line Temperatures (10)	−200° to 1000°F	LL	2%	.001	.01	.01	.01	
TC21–30	Capsule Bus Equipment Temperature (10)	−200° to 200°F	LL	3%	.001	.01	.01	.01	
TC31–40	Aeroshell Heater Current (10)	0–2 amp	LL	3%	.001	.01	.01	.01	
TC41–46	Aeroshell Surface Temperature (6)	−200°–3000°F	LL	3%	.001	.01	.01	.5	
	Radio Subsystem								
RC1–2	UHF Transmitter Power (2)	25°–150°F	HL	3%		.05	.01	.01	.01
RC3–4	UHF Crystal Temperature (2)		LL	3%		.05	.01	.01	.01
RC5–6	UHF Oscillator Drive (2)		HL	3%		.05	.01	.01	.01
RC7	UHF Antenna Reverse Power		HL	3%		.05			
RC8–9	UHF Transmitter Frequency (2)		HL	3%		.05			
RC10–11	Modulator Verification (2)		HL	3%		.05			
	Aerodynamics								
AR1	Accelerometer – No. 1 Axial	± 5g	HL	.5%				.5	.2
AR2	Accelerometer – No. 2 Axial	0–70g	HL	1%					
AR3	Axial Accelerometer Range		BL						
AR4	Accelerometer – Lateral	± 5g	HL	.5%				.5	.2
AR5	Accelerometer – Vertical	± 5g	HL	.5%				.5	.2
AR6	Lateral Accelerometer Range		BL					.5	.2
AR7	Vertical Accelerometer Range		BL					.5	.2
			HL					.25	.25

Figure 5.5–3 (Continued)

AR25	Pitot Pressures of Lander		HL						.5
	Telemetry Subsystem								
DC1	Oscillator Temperature	25°–150°F	LL	3%		.01	.01	.01	.01
DC2	Telemetry Mode		D	4 bits		.01	.01	.01	.01
DC3	Vehicle Time		D	10 bits		.01	.01	.01	.01
DC4	DC Power	15–35 Vdc	HL	3%		.01	.01	.01	.01
DC5	Slaved to Reference Frequency		BL			.01	.01	.01	.01
DC6–8	ADC Linearity Voltages (3)	0–5 V	HL	3%		.01	.01	.01	.01
DC9–11	Low Level Amplifier Linearity Voltages (3)	0–40 mV	LL	3%		.01	.01	.01	.01
DC12	Transducer Voltage Source	0–40 mV	LL	3%		.01	.01	.01	.01
DC13	Cruise Commutator DC Power	15–35 Vdc	HL	3%	.001	.01	.01	.01	.01
DC14–16	Cruise Commutator ADC Linearity Voltages (3)	0–5 V	HL	3%	.001	.01	.01	.01	.01
DC17–19	Cruise Commutator Low Level Amplifier Linearity Voltages (3)	0–40 mV	LL	3%	.001	.01	.01	.01	.01
DC20	Cruise Commutator Mode		D	4 bits	.001	.01	.01	.01	.01
DC21–23	ADC Linearity Voltages (3)	0–5 V	HL	3%		.01			
DC24–26	Low Level Amplifier Linearity Voltages (3)	0–40 mV	LL	3%		.01			
DC27	Telemetry Memory Readout (8)								
	Pyrotechnics								
PY1	Battery Activation Squib Bus		BL			.05			
PY2	Redundant Battery Activation Squib Bus		BL			.05			
PY3	Battery Activation Arm & Fire Relays		BL			.05			
PY4	Redundant Battery Activation Arm & Fire Relays		BL			.05			
PY5–7	Battery Activation Initiator (3)		BL			.05			
PY8–10	Redundant Battery Activation Initiator (3)		BL			.05			
PY11	CBS Auto Activated Squib Bus		BL			.05			
PY12	RCS Pressurant Activation Arm & Fire Relays		BL			.05			
PY13	Redundant RCS Pressurant Activation Arm & Fire Relays		BL			.05			
PY14	RCS Propellant Activation Arm & Fire Relays		BL			.05			
PY15	Redundant RCS Propellant Activation Arm & Fire Relays		BL			.05			
PY16–17	RCS Pressurant Activation Initiator (2)		BL			.05			
PY18–19	Redundant RCS Pressurant Activation Initiator (2)		BL			.05			
PY20	RCS Propellant Activation Initiator		BL			.05			
PY21	Redundant RCS Propellant Activation Initiator		BL			.05			
PY22	De-orbit Motor Arm & Fire Relay		BL				0.1		
PY23	Redundant De-orbit Motor Arm & Fire Relay		BL				0.1		
PY24	De-orbit Motor Initiator		BL				0.1		
PY25	Redundant De-orbit Motor Initiator		BL				0.1		
PY26	De-orbit Motor Thrust Termination Arm & Fire Relay		BL				0.1		
PY27	Redundant De-orbit Motor Thrust Termination Arm & Fire Relay		BL				0.1		

2-9-5'5

CAPSULE BUS INSTRUMENTATION LIST (Continued)

PARAMETER NUMBER	PARAMETERS	RANGE	TYPE	ACCURACY	SAMPLES/SECOND				
					LAUNCH & CRUISE	PRESEPARATION CHECKOUT	DE-ORBIT	ENTRY	TERMINAL DESCENT
PY28	De-orbit Motor Thrust Termination Initiator		BL				0.1		
PY29	Redundant De-orbit Motor Thrust Termination Initiator		BL				0.1		
PY30	De-orbit Motor Separation Arm & Fire Relays		BL				0.1		
PY31	Redundant De-orbit Motor Separation Arm & Fire Relays		BL				0.1		
PY32	De-orbit Motor Separation Initiator		BL				0.1		
PY33	Redundant De-orbit Motor Separation Initiator		BL				0.1		
PY34	De-orbit Motor Electrical Interface Separation Initiator		BL				0.1		
PY35	Redundant De-orbit Motor Electrical Interface Separation Initiator		BL				0.1		
PY36	RCS Deactivate Arm & Fire Relay		BL					.1	
PY37	Redundant RCS Deactivate Arm & Fire Relay		BL					.1	
PY38	RCS Deactivate Initiator		BL					.1	
PY39	Redundant RCS Deactivate Initiator		BL					.1	
PY40	Aerodynamic Decellerator Deploy Initiator		BL					.1	
PY41	Redundant Aerodynamic Decelerator Deploy Initiator		BL					.1	
PY42	TPS Pressurant Activation Arm & Fire Relay		BL					.1	
PY42	Redundant TPS Pressurant Activation Arm & Fire Relay		BL					.1	
PY43–45	TPS Pressurant Activation Initiator (3)		BL					.1	
PY46–48	Redundant TPS Pressurant Activation Initiator (3)		BL					.1	
PY49	TPS Propellant Activation Arm & Fire Relay		BL					.1	
PY50	Redundant TPS Propellant Activation Arm & Fire Relay		BL					.1	
PY51–53	TPS Propellant Activation Initiator (3)		BL					.1	
PY54–56	Redundant TPS Propellant Activation Initiator (3)		BL					.1	
PY57	Aeroshell Electrical & Mechanical Separation Arm & Fire Relay		BL					.1	
PY58	Redundant Aeroshell Electrical & Mechanical Separation Arm & Fire Relay		BL					.1	
PY59	Aeroshell Electrical Separation Initiator		BL					.1	
			BL					.1	

Figure 5.5–3 (Continued)

PY60	Redundant Aeroshell Electrical Separation Initiator		BL						
PY61–62	Aeroshell Mechanical Separation Initiator (2)		BL					.1	
PY63–64	Redundant Aeroshell Mechanical Separation Initiator (2)		BL					.1	
PY65	Aerodynamic Decelerator Separation Arm & Firing Relay		BL						.1
PY66	Redundant Aerodynamic Decelerator Separation Arm & Firing Relay		BL						.1
PY67–68	Aerodynamic Decelerator Separation Initiator (2)		BL						.1
PY69–70	Redundant Aerodynamic Decelerator Separation Initiator (2)		BL						.1
PY71	TPS Motor Termination Arm & Firing Relay		BL						.1
PY72	Redundant TPS Motor Termination Arm & Firing Relay		BL						.1
PY73–74	TPS Motor Termination Initiator (2)		BL						.1
PY75–76	Redundant TPS Motor Termination Initiator (2)		BL						.1
PY77	Stab Legs Release Arm & Firing Relay		BL						.1
PY78	Redundant Stab Legs Release Arm & Firing Relay		BL						.1
PY79–81	Stab Legs Release Initiators (3)		BL						.1
PY82–85	Redundant Stab Legs Release Initiator (3)		BL						.1
	Test Programmer								
TP1			BL			.05			
TP2			D	6 bits		.05			
TP3			HL	3%		1			
TP4–7			HL	3%		.01			

2-7-5.5

(1) Event Parameter – Time of event must be known within 10 sec. Event occurs only at capsule up-date

(2) Event Parameter – Time of event must be known within 1 sec

(3) Three signals only; two at system arming, the third at system deactivation

(4) Event Parameter – Time of event must be known to within 10 sec. Event occurs one time only

(5) Event Parameter – Time of event must be known to within 0.1 sec. Event occurs one time only

(6) Count valve openings each sec and telemeter the result once per sec

(7) De-orbit Propulsion System operating time is between 35 and 115 sec

(8) Memory content verification. Readout entire memory on command.

(9) Checkout must be performed under induced "g" environment.

Definitions:
HL – Single endedhigh level – 0 to 5 volts
LL – Double ended low level – 0 to 40 millivolts
D – Digital
BL – Bilevel event

are presented in Section 5.5.2., while the actual formats are given in the Flight Capsule Telemetry Subsystem functional description Section C2.

The sum of the adverse tolerances is -5.2 dB, thus with a power margin to just overcome the adverse tolerances, a "threshold" signal energy to noise density ratio of 13 decibels is established. From the bit error histories illustrated in Section 5.5.1.1, this signal level would result in an average probability of bit error of 1.8×10^{-3} for the preferred design in the worst case atmosphere-trajectory.

5.5.1.1 Multipath Analysis - The capsule-to-spacecraft communications link will be corrupted by an indirect transmission path reflected off the surface of the planet. This analysis is concerned with identifying the degree of this interference. The problem is divided into three parts: geometry, modulation, and effects. The geometric consideration identifies those parameters concerned with the direct and indirect path lengths, antenna look angles, entry trajectories, and reflectivity models. The modulation consideration identifies the gross effects of multipath upon various modulation schemes, i.e., coherent vs noncoherent, wideband vs narrowband, and diversity. The final part of the analysis combines the previous sections to provide bit error histories during entry.

The results of this analysis indicate (1) that multipath is more severe in the period near the end of plasma blackout and (2) that a noncoherent wideband 2FSK frequency diversity system will provide the best performance on the Martian multipath entry environment.

- Geometric Considerations - The entry geometry problem appears at first to be multidimensional and unbounded. The major trajectory parameters are orbit size, de-orbit anomaly, de-orbit velocity, de-orbit deflection angle, atmosphere, entry angle and attitude. In order to bound the problem, thirty-four trajectory cases have been examined for the period from de-orbit thrust to 100 kilofeet altitude. These cases range over de-orbit deflection angles from -10 to 120 degrees, entry angles of -20 and -14 degrees, and both large (4,400 x 23,400 km) orbits. De-orbit anomalies from 190° to 270° were considered. The envelope of these cases is given in Figure 5.5-4. A ten degree angle uncertainty is added to give the required antenna pattern. Assuming a gaussian shaped pattern, the optimal pattern would be squinted 25° off the roll axis. However, a steady roll at a rate of 3-4 revolutions/hour occur down to entry; thus, the pattern must be symmetrical about the roll axis. In order to provide an adequately effective radiated power

DESCENT TRAJECTORY GEOMETRY – EFFECTS ON CB ANTENNA PATTERN SHAPE

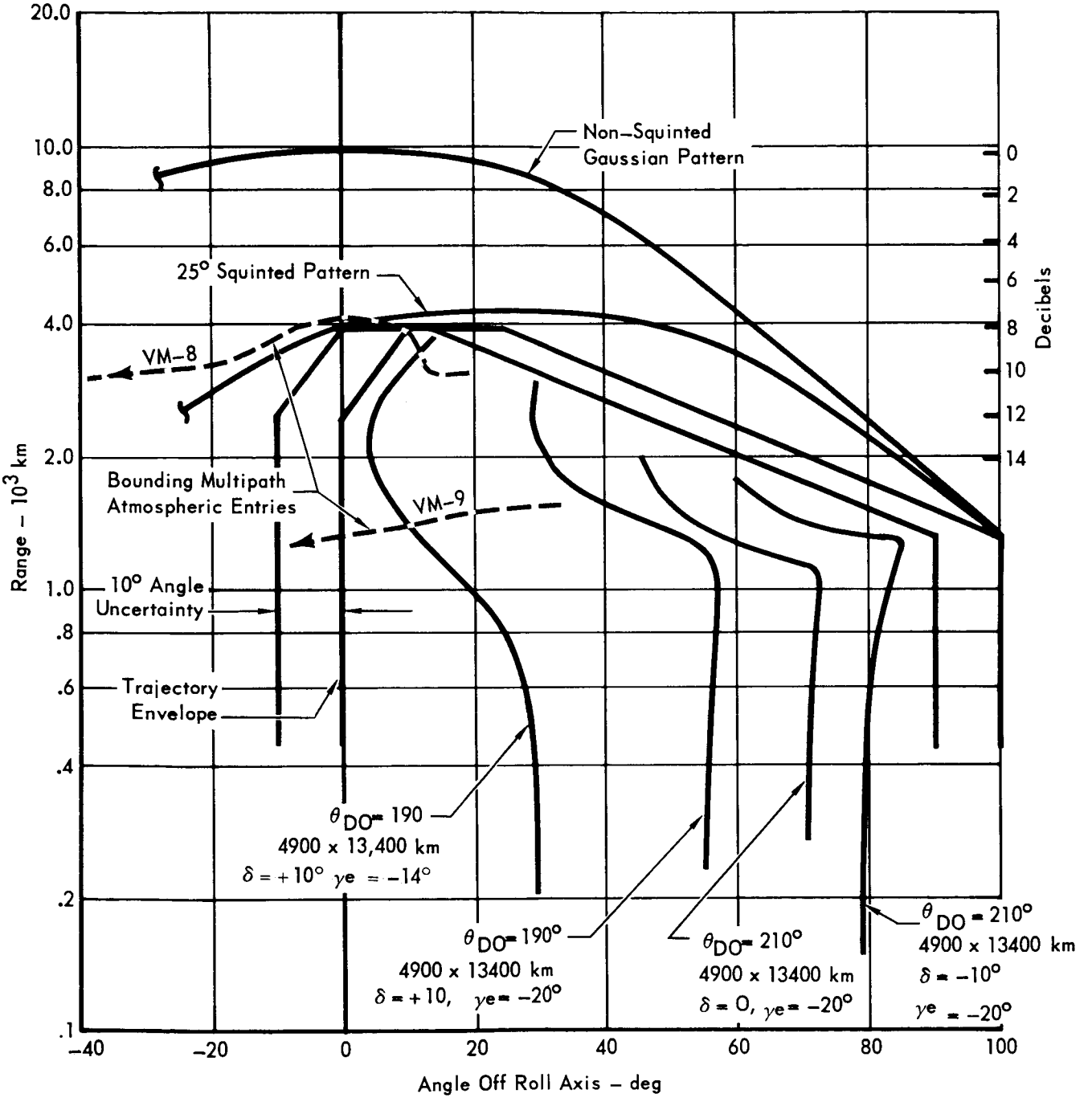

Figure 5.5–4

(gain x transmitter power) at the extreme view angles where the gaussian antenna pattern gain is low, the "on-axis" gain provides a range capability greater than the experienced on any trajectory. This is designated the design range and is 10^4 km for a symmetrical pattern about the roll axis.

The relative spacecraft position at the time of capsule entry as seen from the capsule is shown in Figure 5.5-5a. Superimposing the pattern requirement from Figure 5.5-4 and allowing both a $\pm 20°$ entry attitude tolerance (initial angle of attack) and a 3 decibel entry range tolerance, an envelope of allowable spacecraft positions may be computed. This is given in Figure 5.5-5b. A second boundary is the trailing horizon visibility limit. This is computed by assuming that the relative spacecraft/capsule lead angle is constant during entry, and assures that the spacecraft will not fall below 34° on the trailing horizon.

From the envelope of allowable spacecraft-capsule positions (and the entry trajectory constraints discussed in Section 2.3), two bounding cases are chosen; the first at 313° FSC anomaly, 9° CB lead for VM-9, and the second at 300° FSC anomaly, 27° CB lead for VM-8.

Observations of Mars (References 5.5-3 and 4) have indicated that the average power reflectivity is 3 to 10% (ρ = .17 to .32) at 10 to 20° latitude. However, one measurement produced a reflectivity of 13% (ρ = .36) and greater values would certainly have been measured if greater resolution were available. In these measurements, a pure sine wave was transmitted at S-band, but because of rotational doppler the echo spanned a frequency of 7.6 kHz. Most of the reflected power was contained in a band of only 450 Hz, corresponding to reflections from a disk about 250 miles wide. The Arecibo measurements (Reference 5.5-4) noted that there is a tendency for high values of radar reflectivity to be associated with the dark region on Mars.

The measurements substantiate a reflectivity assumption of $\rho \sim 0.3$ at normal incidence, i.e., poor ground. From the Arecibo measurements, it is evident that there is a probability of about 0.05 of experiencing a mean reflectivity of approximately 0.4 over an extended area (greater than 250 miles wide). Assuming that this reflectivity is equally probable at any latitude, there is a significant probability (~ 0.05) that the capsule relay will operate over this area for essentially its entire descent.

ANTENNA PATTERN LIMITS

- 3dB Range Margin
- ± 20° Attitude Margin
- Situation at Entry

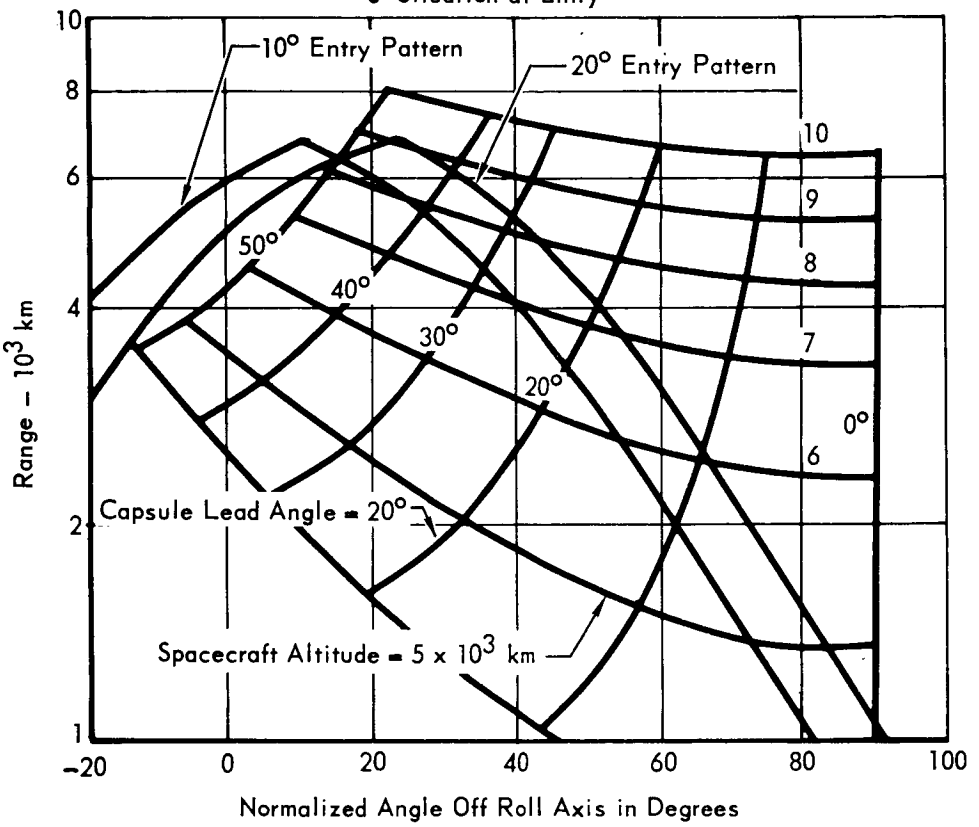

Figure 5.5–5a

b) TELECOMMUNICATIONS MULTIPATH/VIEW BOUNDARY FOR THE –20° ENTRIES.

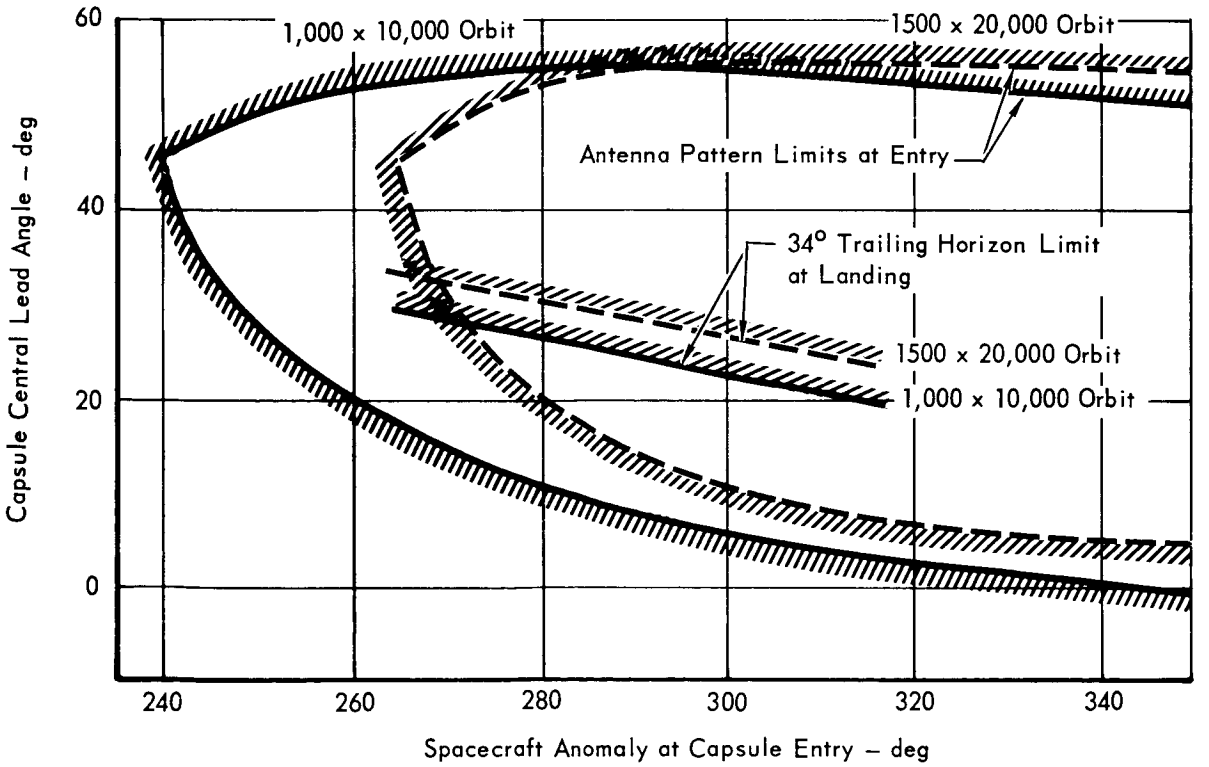

Figure 5.5–5b

The Arecibo measurements give a mean square reflectivity of $\rho^2 = 0.06$ with a variance of about 0.03, assuming a normal distribution of reflectivity. If the same ratio of variance to mean square applies to the higher mean square of $\rho^2 = 0.13$, then the variance would be 0.06. This would yield the following probabilities of experiencing a given reflecitivity in the "worst-case" reflectivity zones.

ρ^2	ρ	$P(\rho)$
.13	.36	.5
.19	.44	.2

The fact that most power was reflected in a band of 450 Hz implies that a reflection with a specular component can be expected. As pointed out by Dyce (Reference 5.5-4), surface roughness cannot be ignored and results in a Rayleigh-distributed scatter reflection component. Hence, the reflection can, in general, be expected to consist of a specular plus scatter component.

Given the bounding orbits, the antenna characteristics, and the surface reflection coefficients, the direct (D) to indirect (J) path geometry ratios may be defined. The D/J ratio is the summation of the delta free space loss (Δ FS), the delta antenna gains (Δ AG) and the surface reflectivity (Δ RC). Figure 5.5-6 gives the bounding D/J histories. Note that the most severe multipath (lowest D/J) occurs immediately after plasma blackout! This is the period when the most significant entry package data is acquired, and where the spacecraft-borne bit synchronizer must reacquire synchronization. This is also the time during which the blacked out, delayed storage bits are transmitted.

- o Modulation Selection - Several modulation techniques were considered for use on the Capsule Bus relay link. Noncoherent FSK operating with a wideband nontracking receiver was selected because of its simplicity and predictable performence in a multipath environment.

Five basic judgments were made in the selection of a modulation technique for the Capsule Bus link.

a. Coherent or noncoherent modulation
b. Wideband or narrow-band tracking receiver
c. Choice of specific modulation technique
d. Bit synchronization techniques
e. Use of diversity

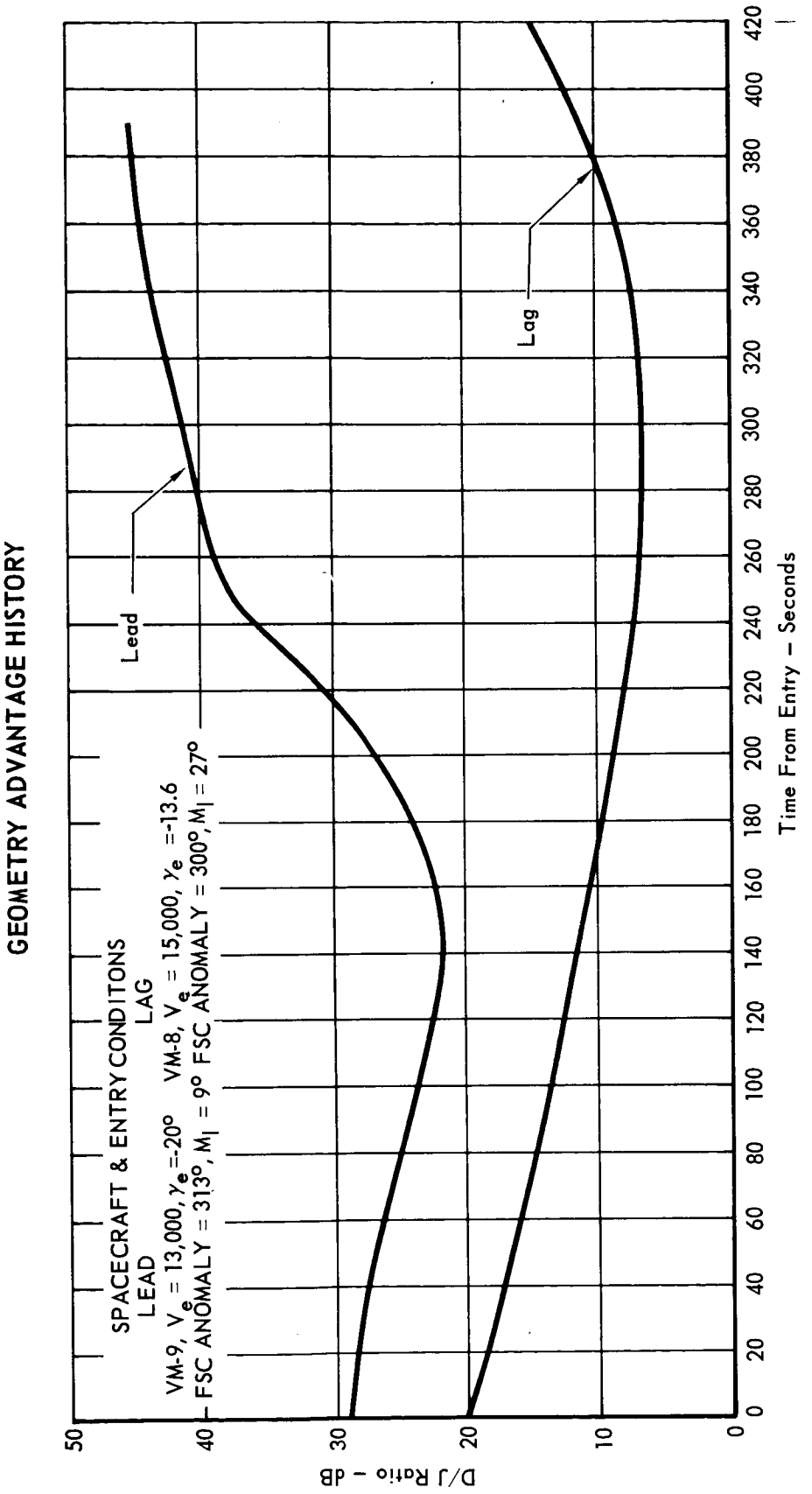
GEOMETRY ADVANTAGE HISTORY
SPACECRAFT & ENTRY CONDITONS
LEAD
VM-9, V_e = 13,000, γ_e=-20° VM-8, V_e = 15,000, γ_e =-13.6
FSC ANOMALY = 313°, M_I = 9° FSC ANOMALY = 300°, M_I = 27°
LAG
Lead
Lag
D/J Ratio – dB
Time From Entry – Seconds
50
40
30
20
10
0
0
20
40
60
80
100
120
140
160
180
200
220
240
260
280
300
320
340
360
380
400
420

Figure 5.5–6

Coherent modulation techniques are approximately 2 to 3 dB more efficient than noncoherent in a non-fading environment. However, several other factors more than negate this efficiency advantage in a multipath environment.

The most critical period of operation for the Capsule Bus link will be immediately after termination of radio blackout during entry. At this time, the strength of the interfering signal received via planet reflection will be strongest due to a disadvantageous attitude, of the capsule. At the same time the receiver must acquire frequency and time synchronization with the signal. The reflection will be offset 3 to 5 kHz in frequency. As it is likely that the reflected signal will contain a strong specular component, there is a possibility that a phase-lock receiver would acquire the reflection instead of the direct signal. For efficiency, the carrier-tracking phase-lock-loop bandwidth of a PSK-PM system would be made as narrow as frequency acquisition and tracking requirements permit. This bandwidth is on the order of 1 kHz. Thus, if the loop acquired the reflected carrier, the direct signal would be well outside the loop passband and hence would be suppressed, preventing acquisition of the desired signal even if it has much greater power. A similar argument also applies to PSK modulation where the receiver phase-lock-loop estimates the carrier phase from the PSK data itself. It is conceivable that anti-interference lock circuits could be designed, but these circuits would add an objectionable amount of complexity and might interfere with the acquisition of the direct signal.

A narrow-band (BT = 1) receiver is approximately 1.7 dB more efficient than a wideband (BT = 5) receiver in a non-fading environment. However, the same arguments as used in the preceding paragraph are applicable; equipment complexity and reacquisition. In a narrow-band (tracking receiver) system the main consideration is the rapidity (and probability) of acquisition immediately after entry blackout when a doppler shift larger than the receiver passband may have occurred. In summary, phase coherent methods such as DPSK and PSK-PM have been ruled out because of the possibility of locking to a strong reflection signal at the critical instant of acquisition after blackout ends. A non-frequency tracking receiver is preferred for reliability and rapidity of acquisition at this critical time. The resulting wideband receiver yields a bandwidth-bit period product which places an FM discriminator at threshold for the highest contemplated bit rate, and below

threshold, (assuming transmitter power is reduced) where degradation is rapid for the lowest bit rates.

These considerations lead to a preference for noncoherent FSK or MFSK modulation. An MFSK system of M=4 would be more efficient, but the battery weight savings would be offset by the additional weight of oscillators. In addition, the receiver would be more complex with a different bit sync regeneration method required. For an M greater than 4, weight savings diminish further. Hence, a preference for the more simple and reliable method leads to binary FSK as the best choice.

The bit synchronizer must recover a timing signal from either the data signal itself or some separate part of the signal designed specifically for this purpose and use this timing signal as a reference in the match filter or data channel portion of the synchronizer.

In the situation where a signal is corrupted by both thermal noise and multipath interference, the thermal noise affects the signal in the same manner as it would in the absence of multipath. The multipath signal can be considered to be additional noise which is partially coherent with the signal. In the VOYAGER situation, the multipath signal and the desired signal seen at the detector output have virtually identical frequencies (generally much less than 1 Hz separation), but a random phase relationship. Therefore, the approach is to distinguish between the two on the basis of phase rather than frequency. This is accomplished by the use of a gate analogous to a range rate in radar applications.

An experimental investigation was performed at McDonnell to determine the effects of multipath interference on bit synchronizer performance. The laboratory system was of a hybrid nature in which the effects of the multipath environment on an envelope detected 2-level, frequency shift keyed (FSK), split-phase signal where simulated by digital computer. By means of digital to analog conversion the video output of the digital computer was passed into bit synchronization equipment for processing. The bit synchronization equipment in this study consisted of a commercially available general purpose bit synchronizer and a special purpose bit synchronizer, designed to give superior performance in the multipath environment as discussed in the previous paragraph.

Preliminary results of this simulation are shown in Figure 5.5-7a together with those from a theoretical analysis of that noise environment

MULTIPATH SIMULATION DATA

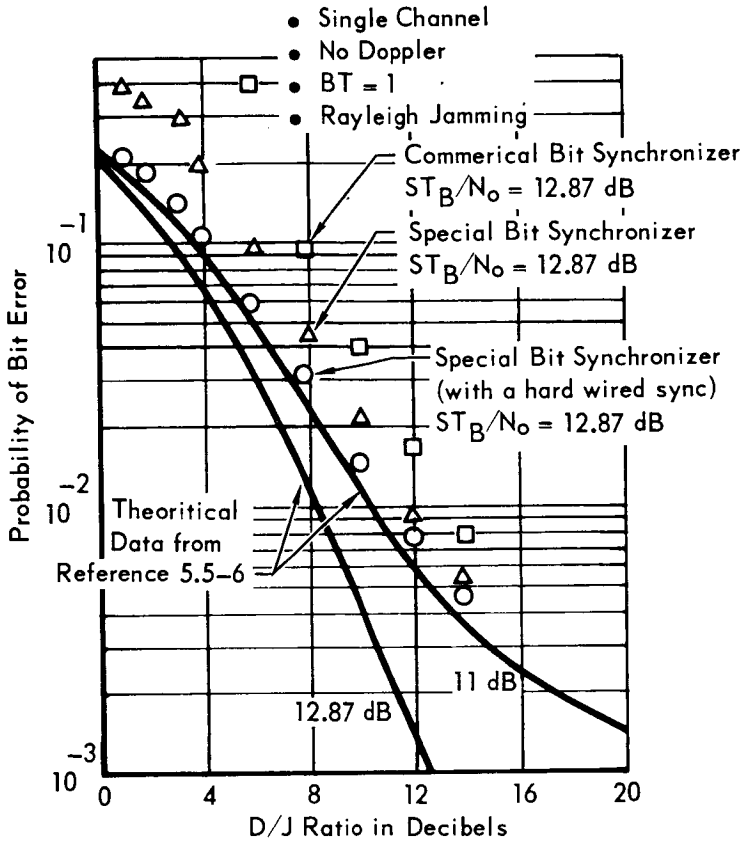

Figure 5.5–7a

A COMPARISON OF APPROACHES

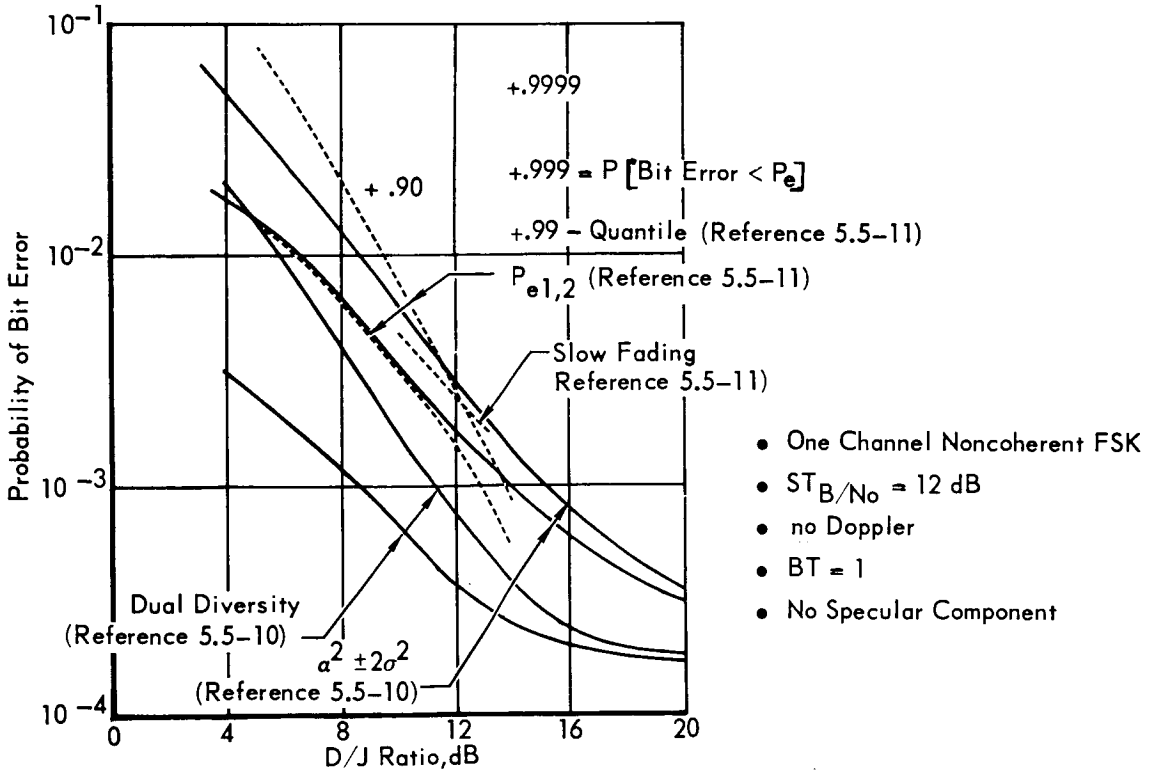

Figure 5.5–7b

from Reference 5.5-6. The theoretical curves are discussed in the Effects of Multipath Interference paragraph. The measured error rate curves are for the cases where a noisy signal fed to both the data channels and the timing circuits and where a noisy signal feeds the data channel with the timing information derived from an identically filtered clean signal.

Three types of diversity are applicable to the relay link; polarization, time and frequency. Space diversity is not applicable because the differential doppler wavelength is excessive. Polarization diversity is not useful because the two signals are dependent and the statistics of the signals are not identical, Reference 5.5-5. Polarization selectivity would be useful if we had prior knowledge of the reflection coefficient history. This knowledge is not available, particularly due to the wide range of possible atmospheres.

Time diversity is not employed per se, as a long time delay is being employed to combat the entry ionization blackout. In order to use this plasma delay as an effective diversity system, the real time bits must be stored and combined with the delayed bits prior to bit detection. Due to the long time delay inherent in the plasma black-out and the associated differential doppler, effective use of time diversity is not possible. A non-optimum usage of the dual delay plasma storage is practical however. Since each bit is transmitted 3 times, except those generated during black-out, the times between these transmissions (50 sec and 100 sec) are sufficiently long that fading can be considered to be independent. After bit decoding on the ground, the 3 bits corresponding to a given information bit may be extracted and a majority decision rule may be used, thus decreasing the resultant effective error probability.

Frequency diversity is an appealing consideration, particularly since an extra transmitter also adds to the reliability of the link in addition to combatting multipath interference.

o Effect of Multipath Interference

Three approaches have been taken to identify the effect of the multipath interference upon the modulation. The first approach is a purely signal strength approach and is adequately documented in References 5.5-5 and 5.5-7. A serious disadvantage to the signal-strength-only analysis is a

lack of direct feeling for the error history, and an in-depth description of the character of the interference upon the modulation technique.

The second approach is an extension of the techniques of References 5.5-8 and 5.5-9 and is documented in Reference 5.5-10. The significant character of the Martian multipath environment may be termed fast fading which results in intersymbol interference. The rate of fading, of the indirect path is classically slow-relative to a bit period; however, the differential path length is great. Thus, the received indirect path signal may change bit state independent of the received direct path signal.

The third, and most sophisticated approach, is documented in Reference 5.5-11. Herein, two channel models are studied. The first assumes that the delay in the indirect path length relative to the data bit is small so that except for producing a phase variation such a delay can be ignored, i.e., a mark-mark situation (P_{e1}).

The second model assumes the delay in the indirect path length relative to the data rate is greater than one bit so that it is reasonable to assume the direct and reflected path transmissions are uncorrelated, i.e., a mark-space situation (P_{e2}). Evaluation of the performance for both channel models bounds the performance of the real channel for the total time that the relay is in operation.

The approaches considered are compared in Figure 5.5-7b.

Figures 5.5-8 and 5.5-9 combined the D/J histories developed in the geometry section with the bit error degradations of this section and result in a bit error history.

The use of diversity conserves approximately one decibel of total battery power. The required transmitter in the frequency diversity case is then 4 dB less than the non-diversity counterpart to achieve the same error rate.

5.5.1.2 Entry Ionization Analysis - The pertinent parameters affecting the flow field prediction of blackout and the resulting telecommunication system degradation have been examined. The analysis included predictions of blackout conditions due to atmospheric gases for the model atmospheres, a worst case sample calculation accounting for the effect of ablation gases, and an estimate of the cost to minimize the blackout times.

Conclusions drawn from this Phase B VOYAGER study on entry blackout are:

- The maximum blackout period is less than 150 seconds; the minimum time

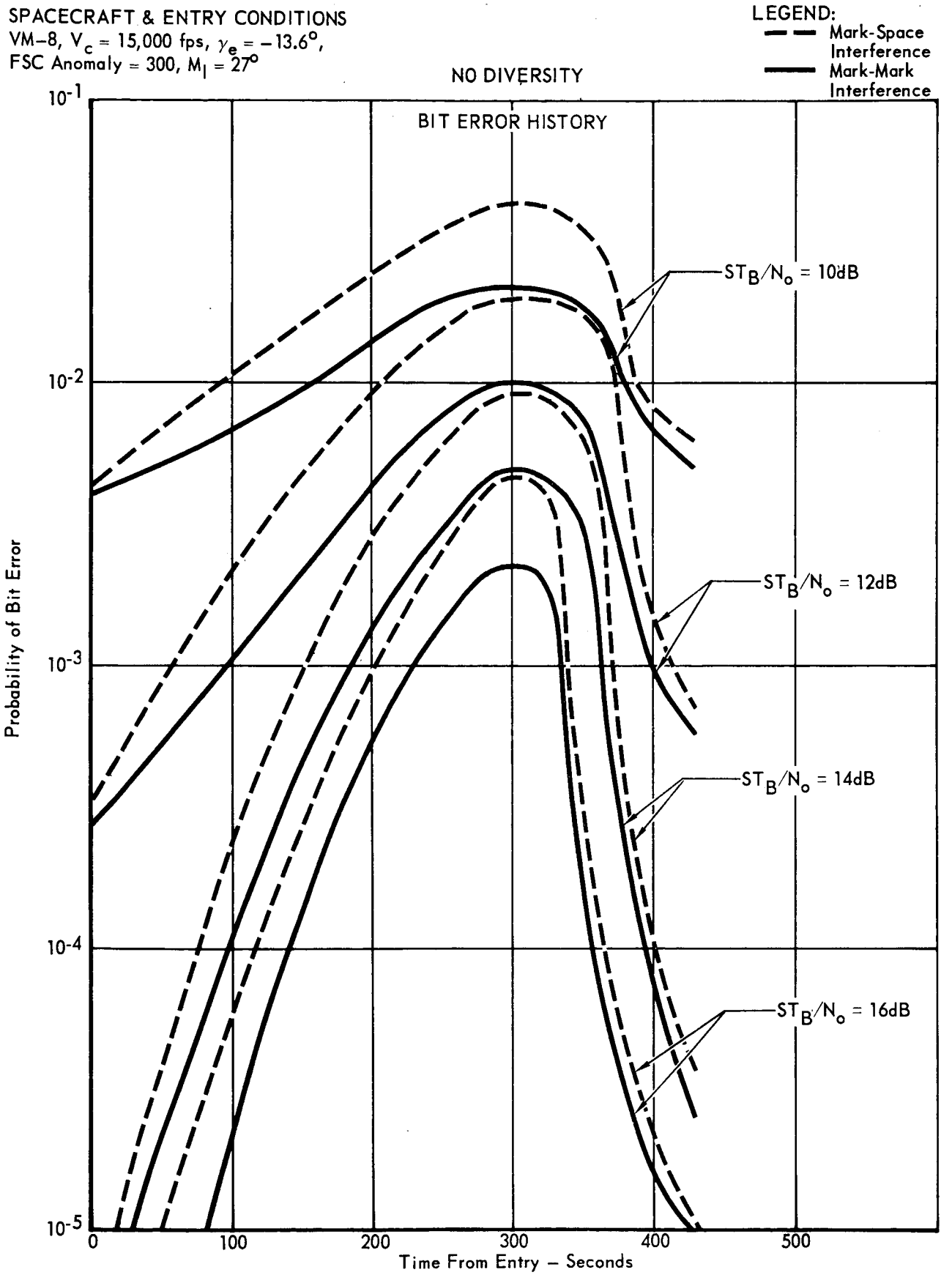
SPACECRAFT & ENTRY CONDITIONS
VM-8, V_c = 15,000 fps, $\gamma_e = -13.6°$,
FSC Anomaly = 300, $M_I = 27°$
NO DIVERSITY
BIT ERROR HISTORY
LEGEND:
Mark-Space Interference
Mark-Mark Interference
ST_B/N_o = 10dB
ST_B/N_o = 12dB
ST_B/N_o = 14dB
ST_B/N_o = 16dB
Probability of Bit Error
10^{-1}
10^{-2}
10^{-3}
10^{-4}
10^{-5}
0
100
200
300
400
500
Time From Entry – Seconds

Figure 5.5–8

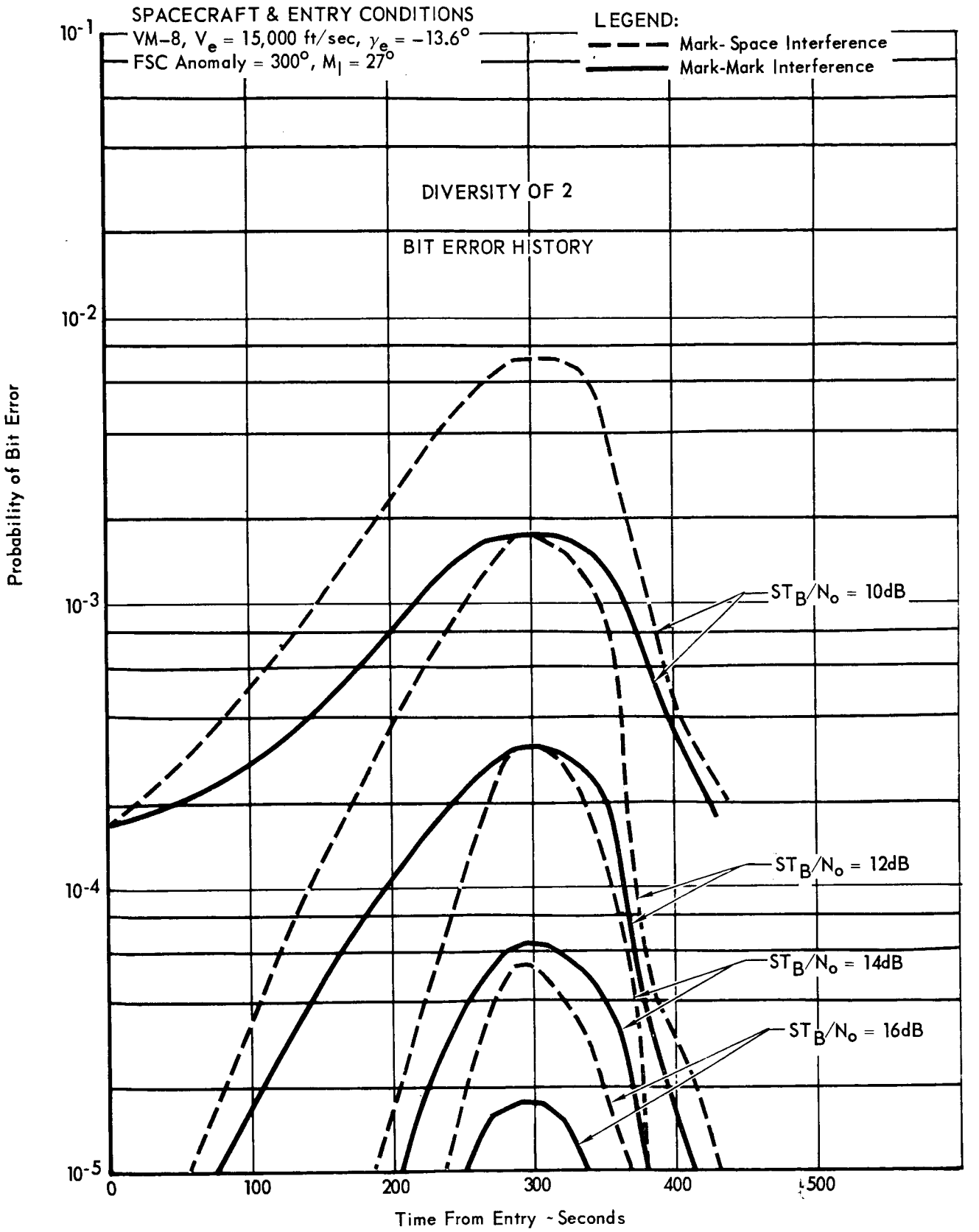
SPACECRAFT & ENTRY CONDITIONS
VM-8, V_e = 15,000 ft/sec, γ_e = -13.6°
FSC Anomaly = 300°, M_l = 27°
LEGEND:
Mark- Space Interference
Mark-Mark Interference
DIVERSITY OF 2
BIT ERROR HISTORY
ST_B/N_o = 10dB
ST_B/N_o = 12dB
ST_B/N_o = 14dB
ST_B/N_o = 16dB
Probability of Bit Error
10^{-1}
10^{-2}
10^{-3}
10^{-4}
10^{-5}
0
100
200
300
400
500
Time From Entry - Seconds

Figure 5.5–9

from end of blackout to impact (without terminal propulsion) is more than 60 seconds.

- o The atmosphere models which contain nitrogen will ionize easily and will cause communications blackout; but atmospheres devoid of nitrogen will cause short black-out periods and then only when the descent is fast and steep.
- o Ablation products will cause blackout at extreme velocities and altitudes and will worsen the blackout caused by atmospheric gases. The metallic ions of the heat shield material cause these high gas ionization levels
- o An S-band telemetry system would experience blackout for shorter times than does a UHF system.
- o Seeding with sulfur hexafluoride in a quantity of less than one percent can cut the ionization in the ablation products considerably.

Martian Atmospheric Blackout - Maximum blackout duration exists between the time of shock formation and the time the vehicle velocity drops below a velocity of about 10,000 ft/sec. The actual times of beginning and ending blackout depend upon the transmitting frequency and the atmospheric composition, which are analyzed in this section. In air, ionization results from the reaction:

$$N + O = (NO+) + (e-)$$

This same reaction exists for Martian atmosphere models in which nitrogen and oxygen are present. But the other model atmospheres depend primarily on the ionizing reactions involving CO^+ and O^+, which require more energy than NO^+ to form; consequently the plasma sheath is less severe for those atmospheres.

The ionization in the wake region is estimated by expanding the Capsule Bus electron concentration from the stagnation density to the free stream density. This is the frozen far wake approximation. Since the collision frequencies are low, the plasma for blunt body entry vehicles is a high pass filter to the transmission waves emanating from the entry vehicle.

Effects of Ablation Products on Wake Conditions - The effect of ablation gases upon the wake ionization is analyzed based on the maximum heating condition - a steep entry into the VM-3 atmosphere listed in Figure 5.5-10. The analysis considers:

- o The heating rate distribution and the resulting total ablation mass loss rate for a typical silicone elastomer ablator.
- o The shock shape and inviscid flow properties on the heat shield.
- o The boundary layer temperature ablation mass fraction, and the equilibrium ion concentration profiles.

WORST CASE CALCULATION CONSIDERATIONS

Entry Conditions		Trajectory Point	
Atmosphere	VM–3	Time	120 seconds
Velocity	15,000 ft/sec	Altitude	200,000 ft
Angle	–20°	Velocity	13,000 ft/sec
Altitude	800,000 ft		

FLOW FIELD GEOMETRY

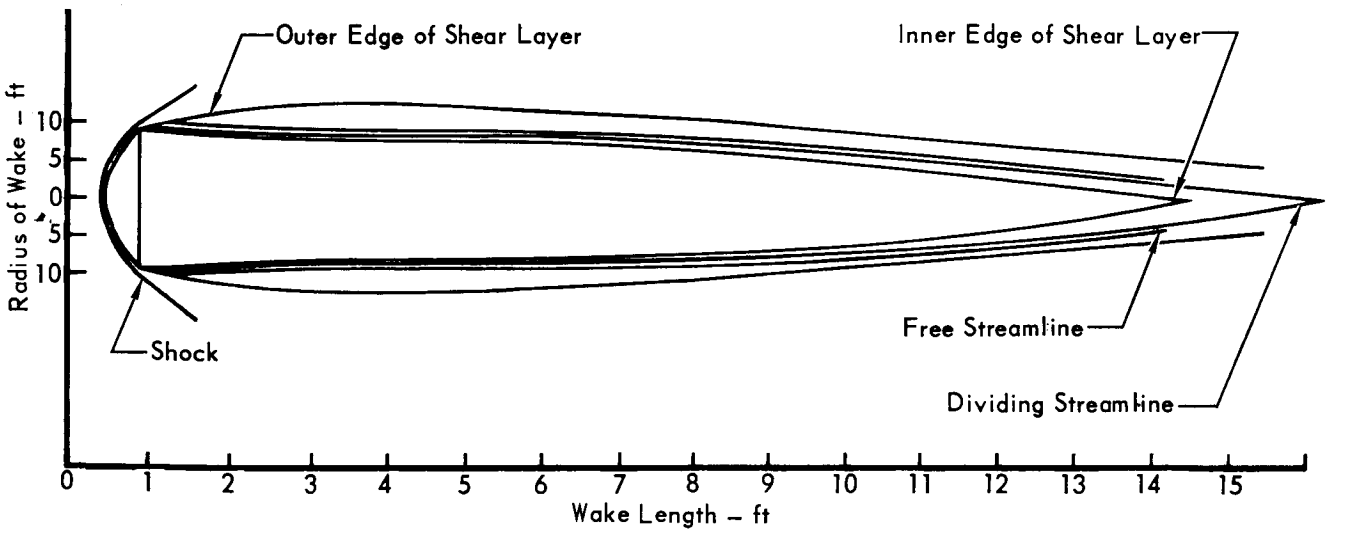

Figure 5.5–10

- o The shear layer location and its density and temperature profiles.
- o The electron concentration in the wake resulting from the boundary layer and shear layer conditions.

The VOYAGER antenna system is mounted on the base of the vehicle. In this position, the antenna experiences minimum heating rates. The transmitted signals are directed into the wake, where they are less likely to be blacked out, as the flow field geometry, Figure 5.5-10 illustrates. The boundary layer gases, which contain the ablation products, expand rapidly as they pass the base of the vehicle and feed the shear layer. It is in the shear layer that ablation products interfere with telemetry communications.

Heating and ablation rate calculations show that peak heating and peak ablation occurs at an altitude of 200,000 feet and a velocity of 13,000 ft/sec and that ablation occurs for about 80 seconds, ceasing at an altitude of about 110,000 feet, for the preferred (GE ESM 1004X) ablator. All of the candidate ablator materials are composed of a silicone elastomer base, so that the ablation rates calculated by a McDonnell computer program for the GE ablator are considered typical.

The inviscid flow field was calculated by a stream tube method (Reference 5.5-12). The shock shape was taken as a spherical bow shock merging into a conical shock. At the base of the vehicle, the entropy layer gases generated by the spherical shock are merged with the boundary layer; therefore, the inviscid flow properties are constant and equal to the properties of a VM-3 atmosphere across a conical oblique shock.

The ablation rate data and the inviscid flow properties were employed to calculate the boundary layer characteristics. The boundary layer properties were calculated for a mixture of ablation and atmospheric gas. Near the wall the ablation concentration and temperature vary widely. The inviscid flow conditions are reached about 1.0 inch from the wall. From the temperature, mass fraction and pressure, the multicomponent equilibrium composition profiles were calculated for some 70 gas species. The composition of the ablation gas was calculated from non-charred (virgin) material compositions taking into account the data on preferential elements loss from MDC S-3 material tests (Reference 5.5-13). The non-charred material and the ablation gas composition for the MDC S-3 and GE ablator as derived from tests are shown in Figure 5.5-11. The aluminum in the GE material, determined the electron concentration in the boundary layer for the conditions used, as seen from the figure.

ABLATOR CONFIGURATION

(% By Weight)

ELEMENT	MDC S-3 MATERIAL		G.E. MATERIAL	
	VIRGIN	ABLATOR GAS	VIRGIN	ABLATOR GAS (EST.)
Silicon	26.82	19.355	37.6	26.65
Carbon	25.63	50.571	38.6	40.64
Hydrogen	5.80	14.705	7.12	19.9
Oxygen	34.802	11.296	23.92	8.55
Magnesium	0.59	.473	–	–
Boron	0.92	0.142	–	–
Aluminum	0.56	0.74	2.76	4.26
Potassium	1.14	0.768	–	–
Calcium	0.058	0.017	–	–
Titanium	4.23	1.933	–	–

BOUNDARY LAYER IONIZATION PROFILES GE ABLATOR

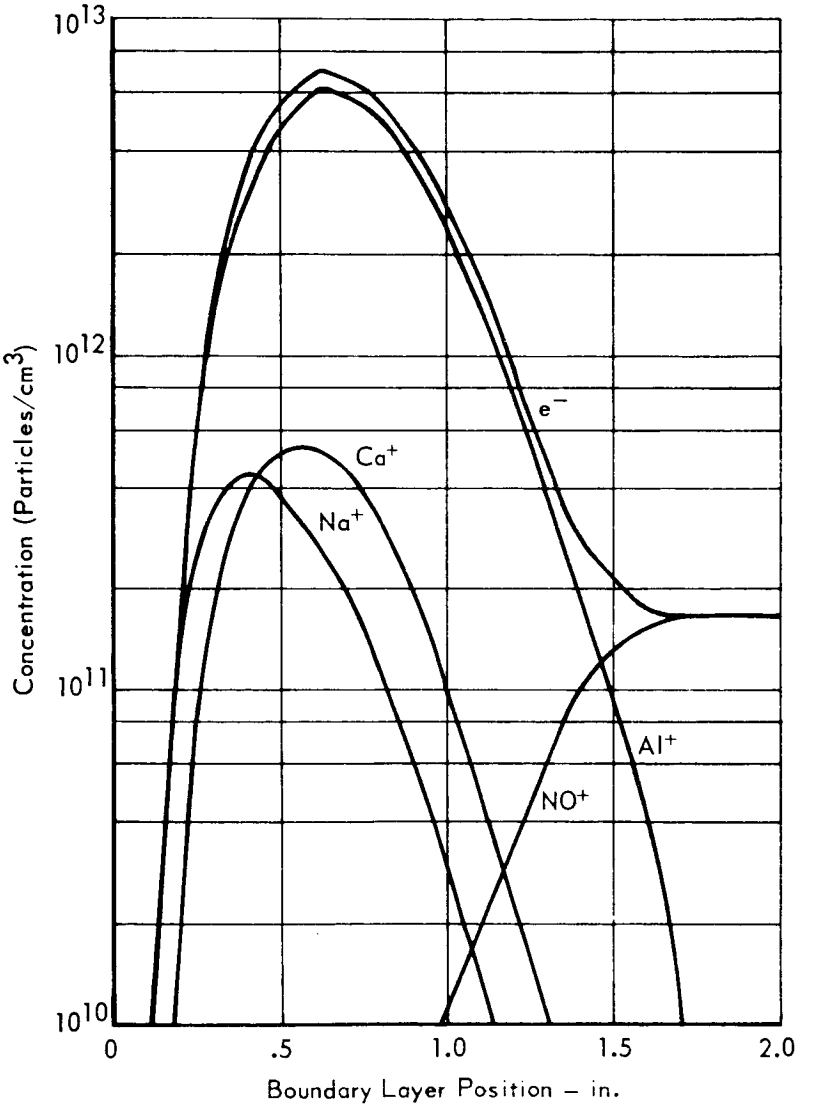

Figure 5.5–11

The next step in the wake flow field analysis was to determine the gas properties in the shear layer. The location of the shear layer was determined by the method of characteristics. The expansion was made from the inviscid flow properties, which were nearly constant from the boundary layer edge to the shock wave. A wake base pressure of 2 lbs/ft^2 was estimated from experimental data on other blunt shapes. The calculated free streamline where the pressure equals the base pressure was used as a reference condition in the shear layer analysis.

The shear layer properties were calculated by the method of Dennison and Baum (Reference 5.5-14). The effect of the recirculating flow was neglected by limiting the boundary layer gases to the shear layer above the dividing streamline. Thus, all the boundary layer gases passed directly into the neck of the wake. The profiles of temperature and density at different stations along the dividing streamline are shown in Figure 5.5-12). The figure shows that neither the density nor the temperature vary appreciably across the shear layer.

The final step is to calculate the plasma properties in the wake. The characteristic reaction lengths indicate that the aluminum recombination reaction in the wake is frozen, because it requires a three body mechanism. On the other hand, the nitric oxide ion, because it is a two body recombination mechanism, is almost in equilibrium. This calculation also shows that equilibrium is a good assumption for the boundary layer.

Since the reaction rate of the principal ion source is frozen, the ionization levels decrease as they pass through the wake due to expansion and diffusion. Figure 5.5-13 gives electron concentration profiles in the boundary layer and at several positions in the wake. The peak electron concentration decreases from 9×10^{12} electrons cm^3 at the capsule base to 3×10^{11} in the neck of the wake. Neglecting the effects of the ablation gases and higher recombination rates for the NO^+ ion, the atmospheric ion concentration minimum is only about 7×10^9 electrons per cm^3.

This detailed wake electron concentration calculation showed that the ablation gases cause a minimum plasma frequency of 4.9 GH_z. This causes blackout for C-band. Neglecting the effect of ablation gases the minimum plasma frequency is only 750 MHz, causing UHF blackout, but not S-band. From this calculation we also see that the frozen far wake approximation predicts a slightly higher plasma frequency (1250 MHz) for the atmospheric gases. The effect of ablation is sufficient to cause blackout for conditions which are not normally blacked out for atmospheric gases, e.g., for the worst case trajectory-atmosphere investigated the ablation products increase the

VOYAGER SHEAR LAYER DENSITY PROFILES

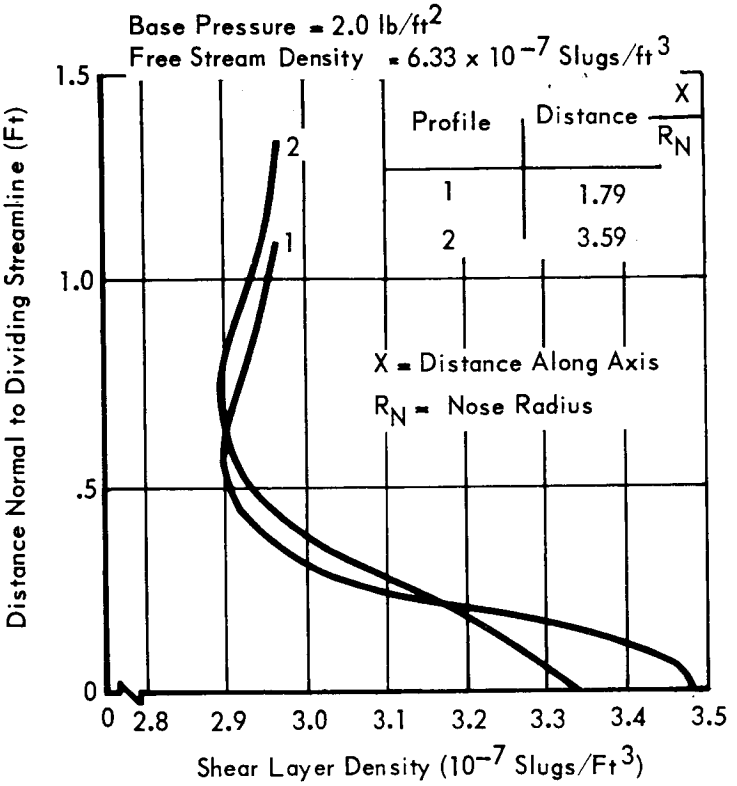

VOYAGER SHEAR LAYER TEMPERATURE PROFILES

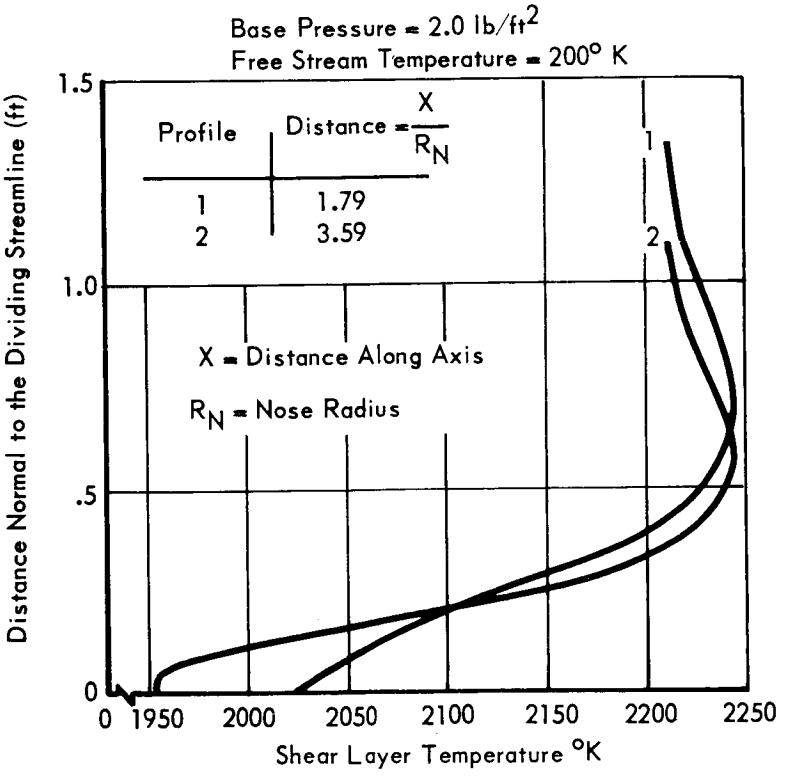

Figure 5.5–12

PLASMA PROFILES IN THE WAKE

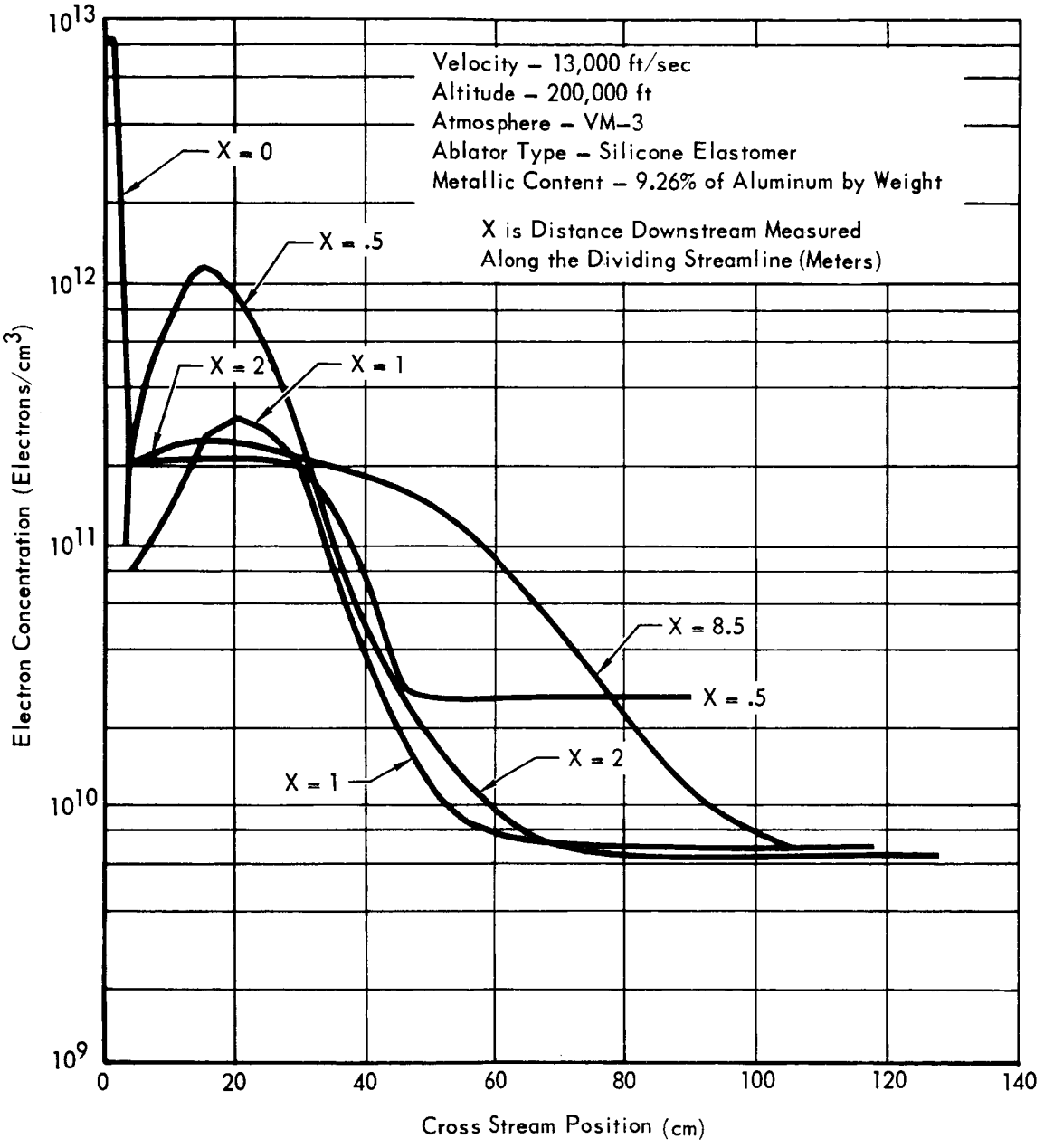

Figure 5.5–13

electron density from 1.7 x 10^{11} electrons/cm^3 to 7 x 10^{12} electrons/cm^3.

Blackout Alleviation - Seeding is a promising technique for reducing the electron concentration in the VOYAGER wake. For the seedants to be effective, they must be delivered to the wake regions of highest electron concentration. When blackout is caused by the ablation products, several seedants can be used. However, when the blackout is due to atmospheric gases, the inviscid flow contains the peak electron concentrations, so seedants are not effective in reducing this ionization.

Experiments were performed to determine the effect of various chemical seedants in reducing electron concentration. Seedants of water and sulfur hexafluoride were evaluated in radio frequency generated plasma of CO_2. The experiment shows that with a seeding of less than 1.0 percent of sulfur hexafluoride (SF_6), the electron concentration was reduced by 40 percent. Increasing the amount of seedant beyond this value does not significantly reduce the electron concentration.

Sulfur hexafluoride scavenges free electrons. This reaction is fast so that the seedant is effective in reducing the electron concentration on the VOYAGER wake even though the recombination reactions are frozen. If only a small reduction in electron concentration is needed to restore communications, seeding can be effective in creating a window through the plasma.

Summary - During the descent stages of the VOYAGER mission, the communications from the CB or the ESP to the FSC will be blacked out for a significant time. The blackout time depends on the Martian atmospheric composition, the initial trajectory conditions, the transmission frequency, and the heat shield material used. A blackout time is predicted for each of the 10 atmospheres, and for each of the four limiting entry trajectories under the following assumptions:

a. Blackout will begin under worst case conditions at the altitude where significant entry heating begins.

b. Blackout will end when the entry vehicle slows to 10,000 fps.

These assumptions give a worst case estimation of the black-out time, tabulated in Figure 5.5-14. The post blackout time is also shown, during which the communications system must re-transmit the blackout data prior to impact. (This time is assumed for the no terminal deceleration case). The maximum blackout time is 145.9 seconds, thus the maximum interleaving delay must be 145.9 seconds. The minimum post-blackout view time is 67 seconds. A 145.9 second delay transmission on the trajectory-atmosphere resulting in the 27.2 second blackout (67 second playback time) would not replay the blackout data. Thus, a "tap" in the delay line is required

BLACKOUT COMPUTATIONS (FROM TRAJECTORIES)

TRAJECTORY IDENTIFICATION	(i) TIME FIRST BEGIN DECREASE VELOCITY	(ii) TIME AT 10 Kfps (SEC)	(iii) TIME OF IMPACT (SEC)	(iv) (i – ii) B.O. TIME (SEC)	(v) (ii – iii) POST B.O. TIME (NO TERMINAL DECELERATION) (SEC)
1. VM–1, 15,000 fps, –20°, 0.3	69.2	139	280	69.8	141
2. VM–1, 15,000 fps, –13.6°, 0.3	109.0	226	444	117.0	218
3. VM–1, 13,000 fps, –20°, 0.3	77.8	144	286	66.2	142
4. VM–1, 13,000 fps, –10.4°, 0.3	163.1	309	553	145.9	244
5. VM–2, 15,000 fps, –20°, 0.3	124.7	152	248.5	27.3	96.5
6. VM–2, 15,000 fps, –13.6°, 0.3	221.4	283	446	61.6	163
7. VM–2, 13,000 fps, –20°, 0.3	136.9	163	255	26.1	92
8. VM–2, 13,000 fps, –10.4°, 0.3	330.4	407	587	76.6	180
9. VM–3, 15,000 fps, –20°, 0.3	66.0	133	310	67.0	177
10. VM–3, 15,000 fps, –13.6°, 0.3	104.3	217	466	112.7	249
11. VM–3, 13,000 fps, –20°, 0.3	74.3	140	316	65.7	176
12. VM–3, 13,000 fps, –10.4°, 0.3	154.9	295	573	140.1	278
13. VM–3, 15,000 fps, –20°, 0.3	121.7	150	269	18.3	119
14. VM–4, 15,000 fps, –13.6°, 0.3	213.8	285	461	71.2	176
15. VM–4, 13,000 fps, –20°, 0.3	133.8	161	277	27.2	116
16. VM–4, 13,000 fps, –10.4°, 0.3	319.3	403	599	83.7	196
17. VM–5, 15,000 fps, –20°, 0.3	61.6	129	343	67.4	214
18. VM–5, 15,000 fps, –13.6°, 0.3	96.2	209	493	112.8	284
19. VM–5, 13,000 fps, –20°, 0.3	69.7	136	348	66.3	212
20. VM–5, 13,000 fps, –10.4°, 0.3	144.0	283	595	139.0	312
21. VM–6, 15,000 fps, –20°, 0.3	112.6	149	302	36.4	153
22. VM–6, 15,000 fps, –13.6°, 0.3	193.2	262	482	68.8	220
23. VM–6, 13,000 fps, –20°, 0.3	124.3	157	308.8	32.7	151.8
24. VM–6, 13,000 fps, –10.4°, 0.3	289.5	372	615	82.5	243
25. VM–7, 15,000 fps, –20°, 0.3	72.6	140	257	67.4	117
26. VM–7, 15,000 fps, –13.6°, 0.3	115.0	234	429	119.0	195
27. VM–7, 13,000 fps, –20°, 0.3	81.6	144	260	62.4	116
28. VM–7, 13,000 fps, –10.4°, 0.3	164.9	307	541	142.1	234
29. VM–8, 15,000 fps, –20°, 0.3	125.4	153	220	27.6	67
30. VM–8, 15,000 fps, –13.6°, 0.3	222.8	288	435	65.2	147
31. VM–8, 13,000 fps, –20°, 0.3	137.7	163	236	25.3	73
32. VM–8, 13,000 fps, –10.4°, 0.3	332.2	412	580	71.8	168
33. VM–9, 15,000 fps, –20°, 0.3	60.2	125	385	64.8	260
34. VM–9, 15,000 fps, –13.6°, 0.3	93.8	200	528	106.2	328
35. VM–9, 13,000 fps, –20°, 0.3	67.9	132	392	64.1	260
36. VM–9, 13,000 fps, –10.4°, 0.3	140.1	272	630	131.9	358
37. VM–10, 15,000 fps, –20°, 0.3	103.8	140	345.8	36.2	205.8
38. VM–10, 15,000 fps, –13.6°, 0.3	173.1	250	515	76.9	265
39. VM–10, 13,000 fps, –20°, 0.3	115.0	150	353	35.0	203
40. VM–10, 13,000 fps, –10.4, 0.3	259.3	355	641	95.7	286

Figure 5.5–14

in order to playback all of the blackout data from all of the forty cases. This "tap" must be at least 27.2 seconds (the minimum blackout period) and at most 67 seconds (the minimum playback time). The design values are then a delay line storage of 150 seconds tapped at 50 seconds. This configuration will insure playing back all of the blackout data from all forty limiting cases.

5.5.2 Telemetry Subsystem - Areas of the telemetry subsystem studied include commutation and instrumentation. Commutation is concerned with data sampling and A/D conversion, while instrumentation is concerned with choosing sensors that successfully monitor the experiments.

Two basic multiplexer approaches were studied: The "hardwired", Mariner-type and the more flexible, stored-program design. The latter approach was selected for the reasons stated in Section 5.5.2.1. Also of concern was the design approach to data formatting. The choice was between the Multiple Access Program, the Look-up Table Program, and the Interlaced Tube Program. The latter was selected.

Instrumentation analysis revealed that off-the-shelf equipment could be used in most applications, with only minor modifications necessary to fulfill the mission constraints.

5.5.2.1 Commutation - The commutator portion of the telemetry subsystem involves data sampling(digital, analog, and bi-level) and analog-to-digital conversion. As used in this section, the term "multiplexing" includes the functional operations of gating and channel sequencing (programming). This section presents a summary of the alternate multiplexing techniques considered for use in the CBS telemetry subsystem, and the analysis used to optimize the gate treeing.

Both whole number and modified pulse-width analog converters were considered. The whole number converter was chosen for reasons of both data source interface and multiplexer programmer simplicity.

Two basic multiplexer configurations were evaluated to determine the best configuration for the CBS telemetry subsystem. Multiplexer configurations similar to previous Mariner telecommunications systems are characterized as hardwired configurations in this study. The alternate configuration studied is the stored-program configuration which uses electrically alterable memory for multiplexer programming. The multiplexer configurations are insensitive to the type of whole-number converter chosen, so the converter design is not a parameter of the study.

Since there are numerous ways of mechanizing each type of configuration, attempts to optimize each configuration were made during the study to achieve maximum trade-off effectiveness. Accomplishing this goal required detailed analyses of analog and digital circuit devices and memory techniques. The evaluation of devices indicated that bipolar integrated circuits (IC's) should be used for all digital applications and hybrid or Metal Oxide Silicon Field

Effect Transistors (MOSFET) IC's for analog (linear) circuits. Core or plated wire memories are preferred for medium-sized storage applications such as the stored programmer memory.

5.5.2.1.1 Multiplexer-Configuration Trade Study - The factors used to compare the hardwire and stored-program multiplexers included reliability, physical properties, versatility, and program management considerations. The failure rate in percent per 1000 hours is used as the measure of reliability in this analysis. Because of its direct effect on the mission probability of success, reliability was assigned the highest relative weighting value of 0.4.

Physical considerations included weight, power requirements and the number of wires required to cross the CB/ESP interface; their relative importance is reflected in an assigned weighting value of 0.3. The methodology employed to compute a single value for system performance including the multiple considerations was as follows:

a. Compute a relative performance value in terms of weight, power, and interface wires.

b. Average the three performances values computed above to achieve a single value.

Versatility was assigned a value weight of 0.2; the two basic considerations were system ability to accept (1) design changes with minimum hardware modification and (2) limited reprogramming prior to separation from the Flight Spacecraft (FSC).

Program management considerations such as cost and development risk are important but not considered applicable to this trade study since neither appears to have an advantage over the other.

A summary chart for the multiplexer configuration analysis is presented in Figure 5.5-15. The stored-program multiplexer configuration is selected.

5.5.2.1.2 Multiplexer Techniques Analysis - Since the multiplexer configuration analysis resulted in the selection of the stored program configuration for the baseline system, the analysis for the hardwired configuration is only summarized briefly, with the major emphasis placed on the stored program configuration.

a. Hardwired Multiplexer - Three multiplexing techniques were evaluated for the hardwired configuration: ring counter, matrix programming and interlaced tube. The ring counter and matrix programming techniques have been used in past systems. The interlaced tube

TRADE STUDY SUMMARY, MULTIPLEXER SELECTION

Functional and Technical Design Requirements: Sampling, ADC and Data Interleaving	MATRIX OF DESIGN APPROACHES		Selected Approach:
	1 – Hardwire	2 – Stored Program	No. 2
Trade Considerations Reliability Weight = 0.4	.32 λ (% 1000 hrs) = 10.24	.4 λ (% 1000 hrs) = 7.48	2 – 1
Physical Considerations Weight = 0.3	.28 Number of Wires = 4 Weight = 3. lbs Power = 4.4 w	.21 Number of Wires = 11 Weight = 4.2 lbs Power = 3.4w	1 – 2
Versatility Weight = 0.2	.16 • Reprogramming involves hardware modifications. • No in-flight programming possible	.2 • Some software reprogramming possible. • Some in-flight programming possible.	2 – 1
Total	0.78	0.81	2

Figure 5.5–15

programming method, a relatively new technique, is described in the next section.

Criteria used for hardwired multiplexer evaluation were reliabilty, physical parameters (size, weight, power, etc.), performance and flexibility, in order of decreasing importance. The analysis indicated that the matrix programmer was best in all categories except performance, where the interlaced tube method provides a somewhat better sample efficiency. The ring counter method ranked lowest in all categories. The matrix programmer was selected for use with the hardwired system.

b. Stored Program Multiplexer - In the stored program configuration the multiplexer programmer is stored program sequencing unit. As a result of an optimization study random-select FET analog gates were selected for use with the stored-program sequencing. Therefore, the difference between the techniques discussed below is confined to memory and channel address logic. The three programming techniques evaluated for the stored program telemetry configuration are multiple access, table look-up and interlaced tube.

c. Multiple-Access Program - The multiple-access programming technique has been used predominately in stored-program decommutator stations and recently has been adopted for the Titan III and Poseidon PCM telemetry systems. This technique is easily implemented and efficent in core utilization. The multiple-access terminology is derived from the need to assess memory two or more times for all subcommutation (i.e., first level subframes require two memory accesses; second-level subframes require three memory accesses, etc.).

One additional flag bit per memory word is required to indicate when the content represents a subframe memory location rather than a channel address. A special memory-position index number is used at the end of each frame to reset the subframe instruction in the appropriate higher-level frame. Some scratchpad is required for storage of the pointers for each rate group. Core memory programming is easily accomplished by listing channel addresses and index number in order of sequence and sampling frequency.

d. Look-Up Table Program - The look-up table program technique is the simplest form of stored-program sequencing in terms of logical

operations but requires a large memory capacity. Programming is achieved simply by listing all channel addresses in order of major frame sequencing, repeating channel numbers as required until the major frame is complete.

Storage capacity is determined by the length of the major frame which is the product of the maximum frame lengths within each commutation level, assuming that all frames within a given subcommutation level are even multiples of the longest frame within that level. If this condition is not met, it is necessary to take the product of all frame lengths within the multiplexing pattern. Under such condition, the major frame length can exceed the time duration of the lowest rate subframe. In any case, memory required to satisfy the SLS multiplexing is extremely large using this technique.

e. Interlaced Tube Program - The interlaced tube programming technique is similar to the multiple-access programming technique described above since it also requires scratchpad and special index instructions. Figure 5.5 -16 is an example of an arbitrary multiplexing format produced by the interlaced tube. The construction simplicity of these formats is clear. For purposes of this description, a major frame represents the total number of samples required to sequence through all data sources and a minor frame is the least number of samples required before a data source is repeated (determined by the highest sampling frequency within the data ensemble).

The interlaced-tube format is constructed by first listing all measurements in groups (tubes) of descending sampling frequency as shown in Figure 5.5 -16. The number of major frame samples, S_{mf}, is determined by:

$$S_{mf} = \sum_{r_{min}}^{r_{max}} N_r \left(\frac{r}{r_{min}}\right)$$

where r = sampling rate for a given rate group

N_r = number of samples in the rth rate group, and

r_{min} = lowest sampling frequency

r_{max} = highest sampling frequency

The number of minor frame samples, S_{pf}, is:

$$S_{pf} = S_{mf} \left(\frac{r_{min}}{r_{max}}\right)$$

The system sample rate in sps is, of course, $S_{pf}\ (r_{max})$. If

INTERLACED TUBE FORMAT EXAMPLE

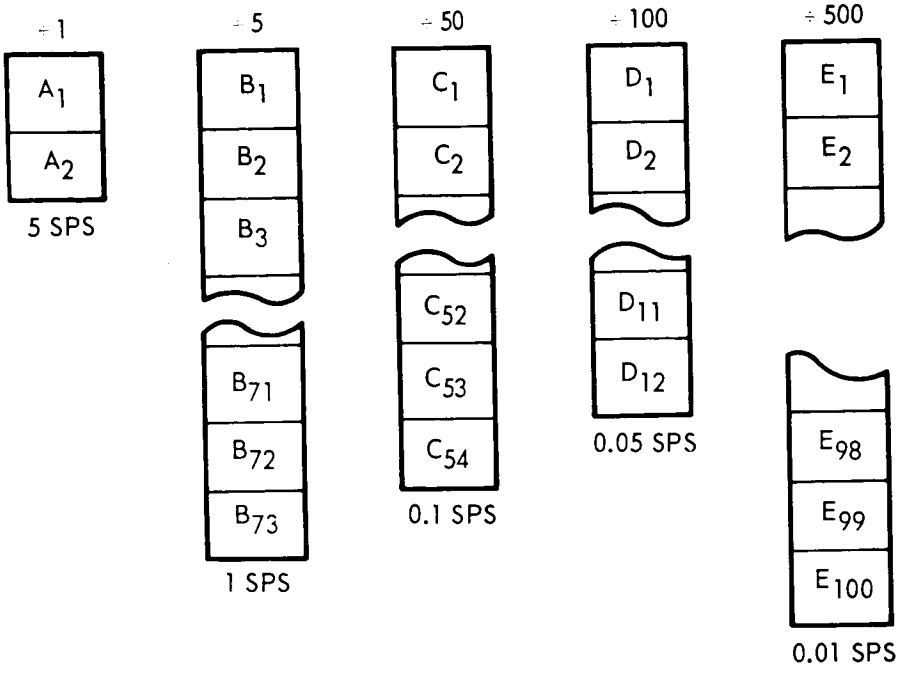

S_{mf} = 9000 Samples/Major Frame

$S_{pf} = \frac{S_{mf}}{500}$ = 18 Samples/Prime Frame

Sample Rate = 18 x 5 = 90 SPS

Frame No. 1	$A_1, A_2, B_1, B_2, B_3, B_4, B_5, B_6, B_7, B_8, B_9, B_{10}, B_{11}, B_{12}, B_{13}, B_{14}, B_{15}, B_{16}$
Frame No. 2	$A_1, A_2, B_{17}, B_{18}, B_{19}, B_{20}, B_{21}, B_{22}, B_{23}, B_{24}, B_{25}, B_{26}, B_{27}, B_{28}, B_{29}, B_{30}, B_{31}, B_{32}$
Frame No. 5	$A_1, A_2, B_{65}, B_{66}, B_{67}, B_{68}, B_{69}, B_{70}, B_{71}, B_{72}, B_{73}, C_1, C_2, C_3, C_4, C_5, C_6, C_7$
Frame No. 6	$A_1, A_2, B_1, B_2, B_3, B_4, B_5, B_6, B_7, B_8, B_9, B_{10}, B_{11}, B_{12}, B_{13}, B_{14}, B_{15}, B_{16}$
Frame No. 500	$A_1, A_2, B_{65}, B_{66}, B_{67}, B_{68}, B_{69}, B_{70}, B_{71}, B_{72}, B_{73}, E_{94}, E_{95}, E_{96}, E_{97}, E_{98}, E_{99}, E_{100}$

Figure 5.5–16

the minor frame is not an integer number of samples, spare channels must be added in any desired combination to meet this requirement. Although this constraint is similar to other multiplexing techniques, it should be noted that the interlaced-tube procedure generally requires fewer spares, resulting in greater sampling efficiency than the other technique.

The channel sequence format produced by the tube method in Figure 5.5-16 is generated as follows:

During the first prime frame, the two 5-sps plus the first sixteen 1-sps channels are sampled. During the second prime frame, the two 5-sps plus pins 17 and 32 of the 1-sps channels are sampled. During the fifth minor frame, the two 5-sps and a last nine pins of the 1-sps plus the first seven pins of the 0.1-sps channels are sampled. The next five prime frames will be identical to the above sequence except that pins 8 through 14 of the 0.1-sps tube will be sampled during the tenth frame. This procedure continues until the five-hundredth prime frame; at this time the last seven pins of the 0.01-sps tube are finally sampled. The sequence then repeats.

5.5.2.1.3 Stored-Program Trade - The results of the stored-program trade study are presented in Figure 5.5-17. The criteria used in the evaluation are physical parameters, reliability, flexibility and performance. Reliability is weighted the heaviest, followed by physical parameters (power and weight), performance and flexibility in that order. The weighting factors used were 0.4, 0.3, 0.2 and 0.1, respectively.

Due to inefficient memory utilization, the look-up table programming technique suffers both a physical and reliability grading. Although the identical logic algorithm can be used for both interlaced-tube and multiple-access techniques, multiple-access does require a few more words in storage (this difference is too small to be observed in the grading numbers).

Because all addresses associated with the higher sampling rate groups are repeated many times in the look-up table memory, programming of software changes become considerably more difficult than with the other techniques. Programming for the multiple-access technique is slightly more complicated because of the extra jump instructions required

TRADE STUDY SUMMARY, HYBRID MULTIPLEXER

CRITERIA	MATRIX OF DESIGN APPROACHES			SELECTION 2
	NO. 1 LOOK-UP TABLE	NO. 2 INTERLACED TUBE	NO. 3 MULTIPLE ACCESS	
Physical Weight – 0.3	.05 Power, 11.5 Watts Weight, 10 lb	.3 Power, 2.4 Watts Weight, 1.5 lb	.3 Power, 2.4 Watts Weight, 1.5 lb	2–3–1
Reliability Index Weight – 0.4	.27 19	.4 28	.4 28	2–3–1
Flexibility Weight – 0.1	.02 Maximum number of software modification to accommodate single measurement change.	.2 Simplest to change	.09 Easy to change. More difficult programming required if cross-strapping is used.	2–3–1
Performance Weight – 0.2	.15 Low sample efficiency unless tube format used.	.2 Good sample efficiency	.1 Low sample efficiency	2–1–3
Total Grading	0.49	1.0	0.89	

Figure 5.5–17

and can become considerably more complicated if super-commutation (cross strapping) is required. Performance is confined to the improved sampling efficiency of the interlaced tube. Look-up table is higher ranking than multiple-access since it is possible to program the look-up table with a tube format; however, programming would be further complicated.

Interlaced-tube programming is selected for the stored program configuration since it is ranked highest under all criteria.

5.5.2.1.4 Commutator Reliability Consideration - Detailed reliability analysis of a commutator design concept was conducted, Reference 5.5-15, and methods were determined by which the reliability can be maximized. The methods consist of incorporation of a combination of multi-channel cooperative and circuit block redundancies. Analysis results are directly applicable to the VOYAGER commutator design concept.

The basis for the analysis was elimination of critical single point failures, improvement of fail-safe design features and maximization of total and partial probability of successful commutator operation.

A generic PCM commutator and encoder design is shown in Figure 5.5-18, which contains the basic elements for operation and handling of high level (HL), low level (LL), bi-level (BL), and digital (D) groups of input data signals. The generic design assumes a standard time division multiplexing method of sampling and gathering input data signals for presentation to a transmitter modulator. All data switches were assumed to be junction field effect transistors (JFET). Similar analysis utilizing metal oxide silicon field effect transistors (MOSFET) could be conducted.

In the analysis, the 120 HL analog data channel group was analyzed and designed as shown in Figure 5.5-18. The reliability of this design was estimated for retrieval of total data, a subgroup (deck) of data channel. A detailed reliability analysis of the generic design was conducted to optimize the design reliability and is shown in Figure 5.5-19 which is the optimum arrangement of data channels which inherently contains multi-channel cooperative redundancy and maximized probability of partial data retrieval.

The basic JFET data switch was assigned a failure rate (f). All other elements were assigned an effective failure rate expressed as

GENERIC PCM COMMUTATOR AND ENCODER BLOCK DIAGRAM

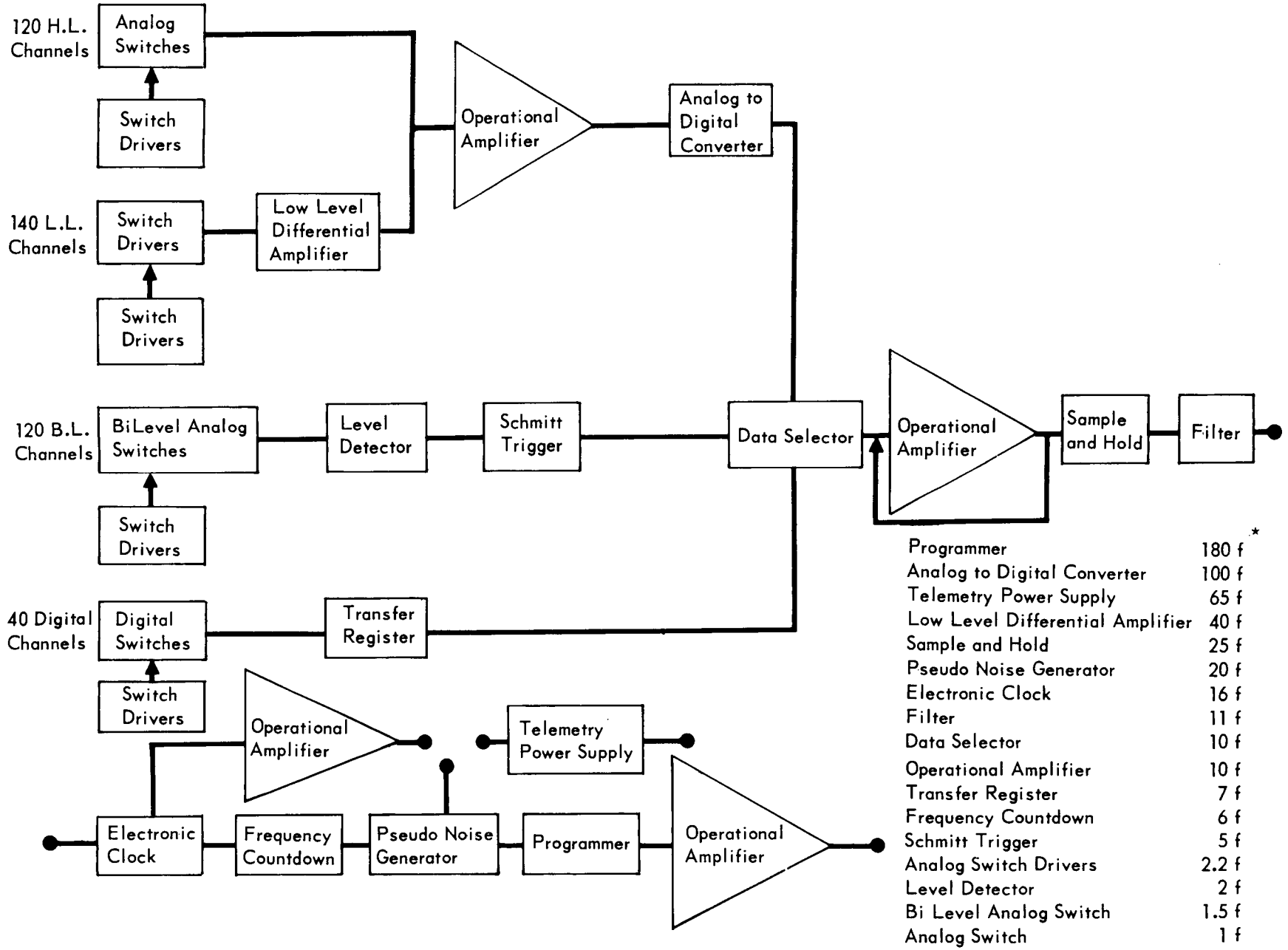

Programmer	180 f *
Analog to Digital Converter	100 f
Telemetry Power Supply	65 f
Low Level Differential Amplifier	40 f
Sample and Hold	25 f
Pseudo Noise Generator	20 f
Electronic Clock	16 f
Filter	11 f
Data Selector	10 f
Operational Amplifier	10 f
Transfer Register	7 f
Frequency Countdown	6 f
Schmitt Trigger	5 f
Analog Switch Drivers	2.2 f
Level Detector	2 f
Bi Level Analog Switch	1.5 f
Analog Switch	1 f

* f = Analog Switch Failure Rate

Figure 5.5-18

HIGH LEVEL ANALOG SIGNAL GROUP

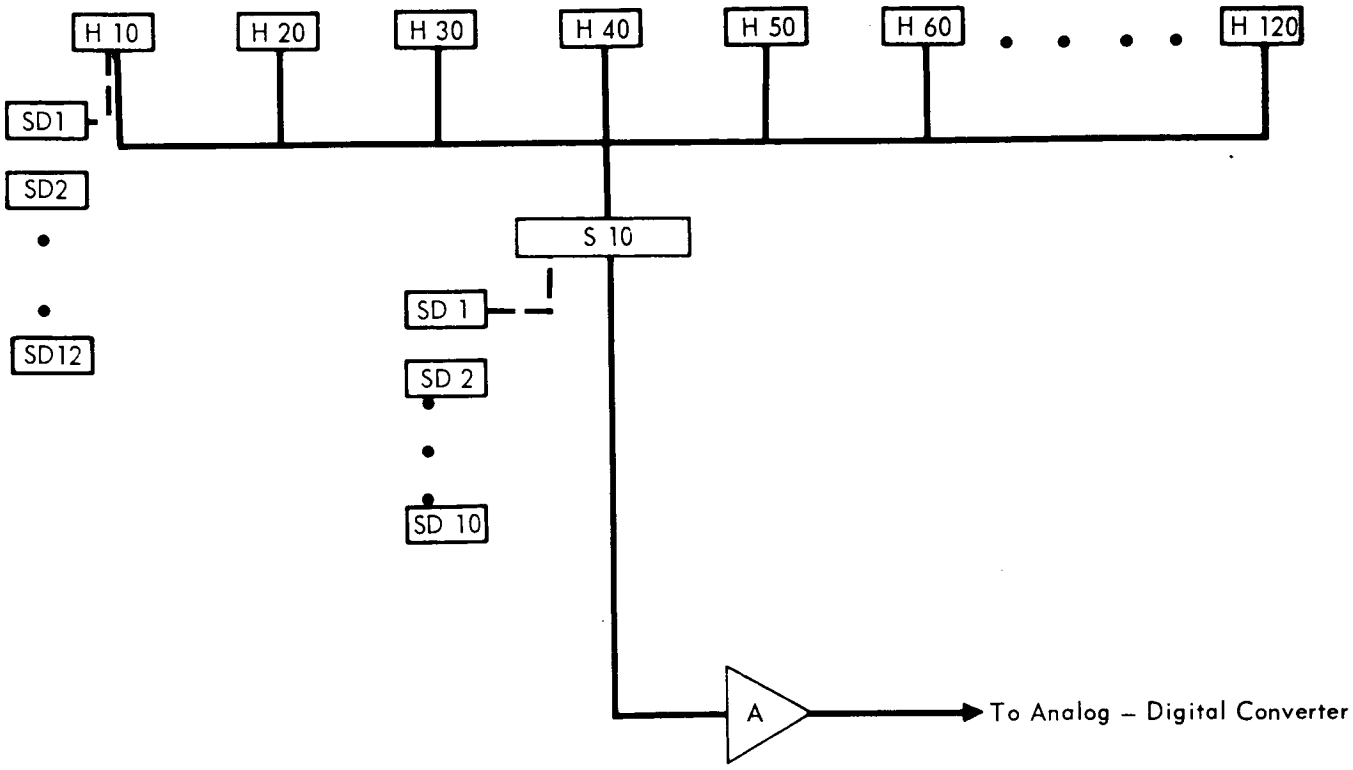

Notes:
1. H10 – First Level Switch Deck (Subgroup) containing 10 Analog Switches.
2. S10 – Second Level Switch Deck containing 10 Analog Switches.
3. SD1 (Switch Driver) Drives all switches in Subgroup H10.
4. Another SD1 drives the first position switch in Deck S10.

Figure 5.5–19

some multiple of (f) for comparative purposes. Different data channel arrangements were analyzed and the comparative reliability was estimated for each arrangement. Results are shown in Figure 5.5 -20.

Limited circuit block redundancy was added in the most critical switching decks, namely decks F5, T5 and S5 in that order, as shown in Figure 5.5 -21. This addition optimizes total data retrieval probability at minimum expense of part increases.

In summary, the reliability of a PCM commutator data channel group has been optimally maximized by incorporation of multichannel cooperative and limited block redundancy and is the recommended design approach for the telemetry commutator. The multichannel cooperative redundancy feature essentially decentralizes the first level of analog data switches for optimum reliability and data switch independence in event of any switch failure. Further decentralization from that showed in Figure 5.5 -22 however, reduces probability of partial and total data channel retrieval for the 120 data channels considered.

5.5.2.2 Instrumentation - The term "Instrumentation Equipment" is used to designate the engineering measurement portion of the telemetry system where data signals are sensed and conditioned to outputs compatible with the PCM encoders. This equipment consists of transducers, signal conditioners, and associated power supplies. Specific feasible equipments that can fulfill VOYAGER peculiar instrumentation requirments are reviewed.

Transducers - The major portion of the CB engineering measurements requiring transducers can be classified in three categories; that is, temperature, pressure and motion.

- o Temperature Measurements - Preliminary requirements for 82 CB and associated subsystem temperature measurements have been established per the Instrumentation List. The temperatures ranges are from a low of -350° F to a high of 3000° F in 13 overlapping spans. Figure 5.5-23 is a table of temperature measurement requirements showing the specific ranges and quantities.

Platinum resistance sensors were selected for the majority of temperature measurements over thermocouples and thermistors for the following reasons:

a. Superior R-T characteristics for wide temperature span. Typical span is 436° F to 1000° F.

HIGH LEVEL ANALOG DATA GROUP RELIABILITY SUMMARY

GENERIC DESIGN	GROUP	SUBGROUP	CHANNEL	REMARKS
10 Channels/Subgroup	235f	204f	78f	
6 Channels/Subgroup	248f	201f	91f	
15 Channels/Subgroup	245f	221f	82f	
8 Channels/Subgroup	238f	201f	82f	
12 Channels/Subgroup	237f	210f	78f	
10 Channels/Subgroup	264f	148f	68f	First level data group divided into independent halves
5 Channels/Subgroup	315f	107f/5 Channels 214f/10 Channels	60f	First level data group divided into independent fourths
5 Channels/Subgroup	271f	65f/5 Channels 130f/10 Channels	34f	Redundant F5 and T5 analog switches switch drivers and programmer sequencers
5 Channels/Subgroup	<235f	< 65f/5 Channels <130f/10 Channels	<34f	Redundant S5 analog switches, switch drivers and programmer sequencers

NOTE: 1. (f) Values for the last three design configurations are cumulative and represent the optimum design approach.

2. As the (f) values are decreased, the reliability is increased exponentially.

3. 1f is equivalent to an analog switch failure rate.

Figure 5.5–20

COMPARISON OF BASIC AND REDUNDANT CIRCUITRY

(a) JFET ANALOG SWITCH AND SWITCH DRIVER

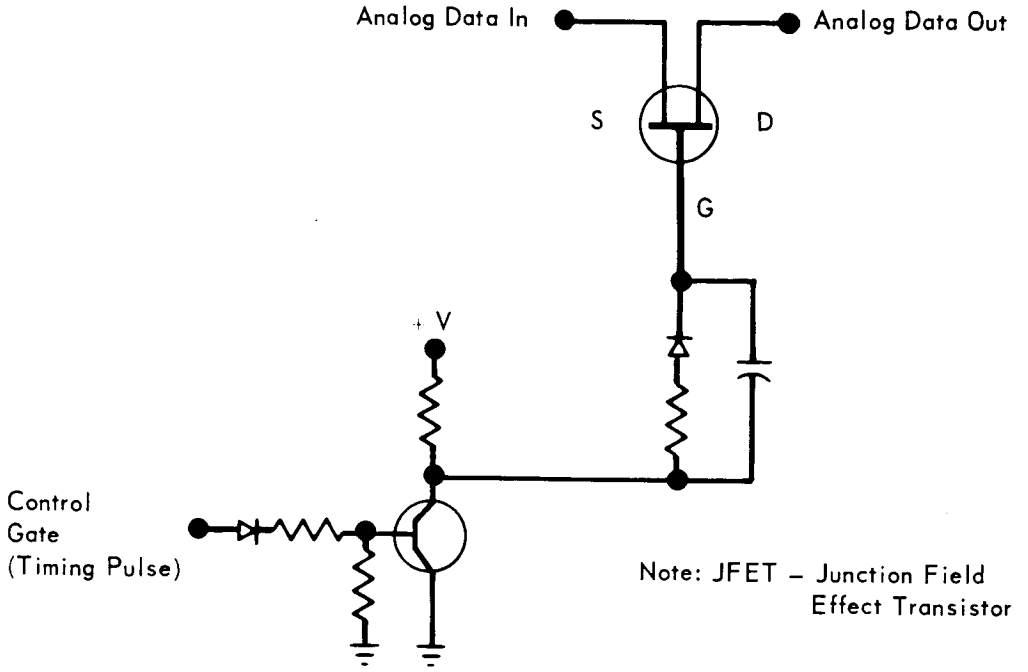

(b) REDUNDANT JFET ANALOG SWITCHES AND REDUNDANT SWITCH DRIVERS

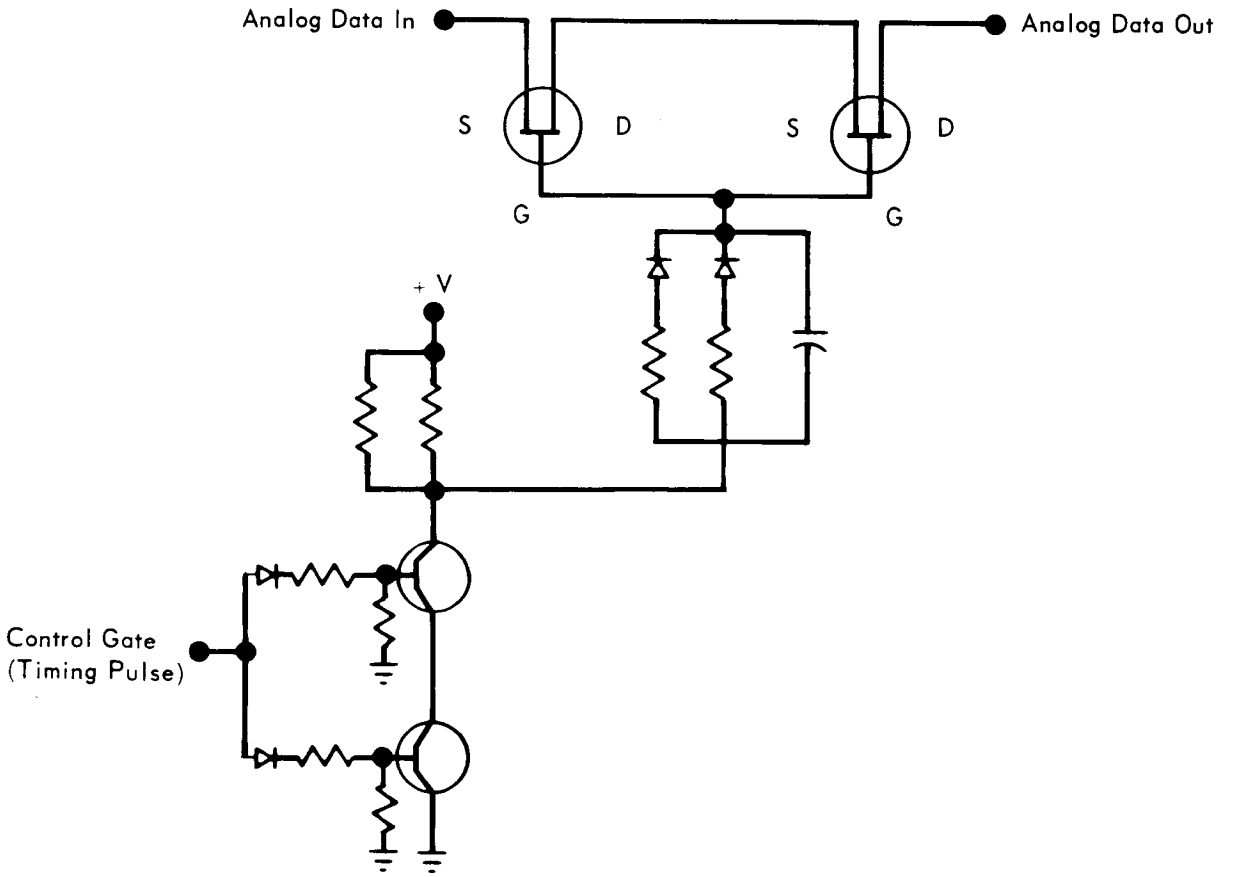

Figure 5.5–21

OPTIMIZED CHANNEL ARRANGEMENT
(120 CHANNELS SPLIT INTO 4 INDEPENDENT GROUPINGS, 5 CHANNELS SUBGROUP)

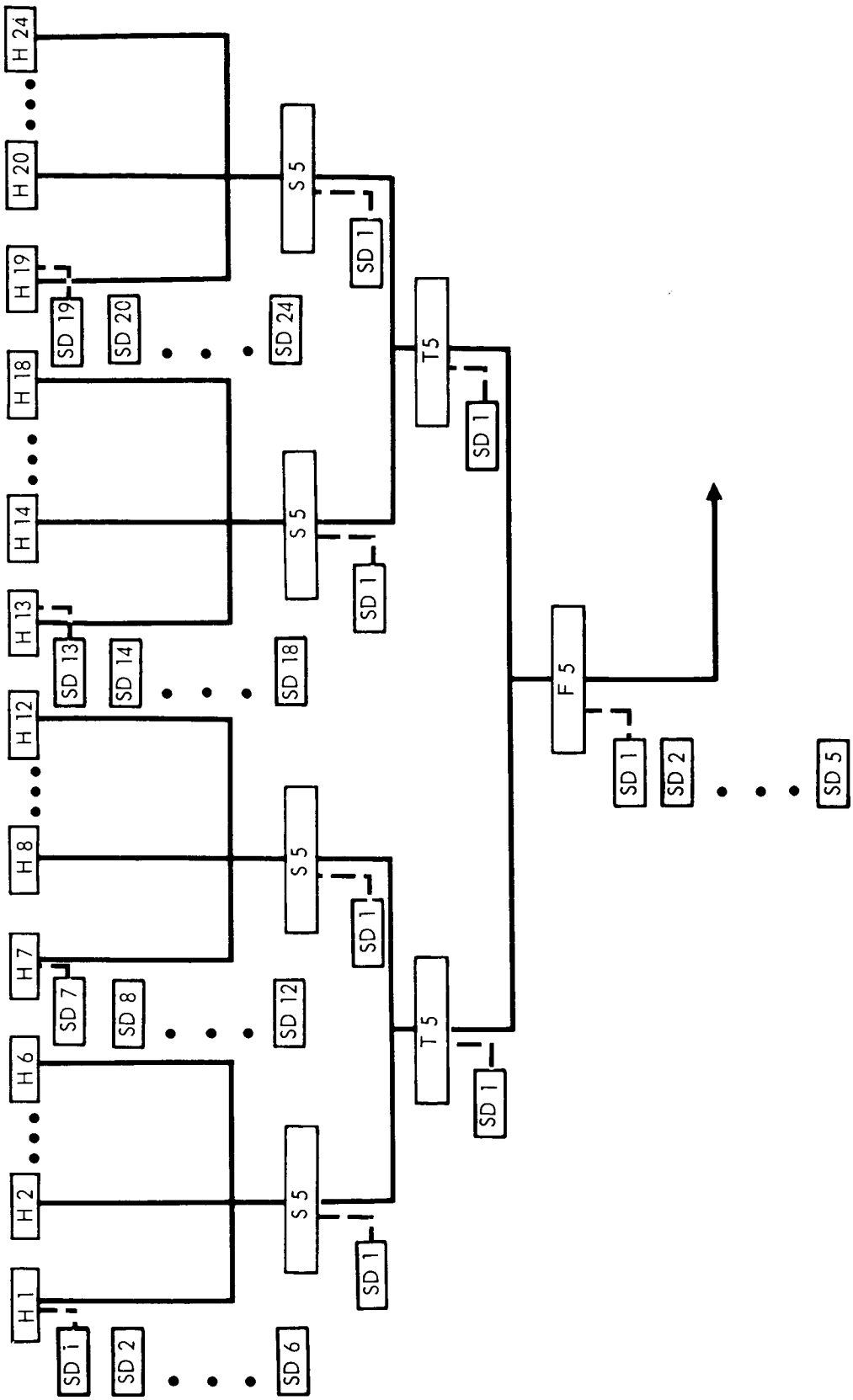

Figure 5.5–22

CB TEMPERATURE MEASUREMENT REQUIREMENTS

TEMPERATURE RANGE	SPAN	NO. MEASUREMENTS
170 to 180°F	10°F	6
Control Temp ± 10°F	20°F	6
50 to 100°F	50°F	1
0 to 120°F	120°F	6
25 to 150°F	125°F	3
−60 to 185°F	245°F	2
−50 to 250°F	300°F	1
−50 to 300°F	350°F	14
−200 to 200°F	400°F	10
−200 to 300°F	500°F	1
−350 to 200°F	550°F	10
−200 to 1000°F	1200°F	16
0 to 3000°F	3000°F	6
	Total	82

Figure 5.5–23

b. Excellent stability of calibration. The interpolation instrument that is used from -182.97° C to 630.5°C on the International Temperature scale is the platinum resistance thermometer.

c. Higher output voltage than thermocouples.

d. Output voltage/degrees exactly as desired over wide temperature limits by adjusting excitation current or bridge design.

e. Reference juncitons not required.

f. Ease of calibration, only a small number of calibration points are required.

Alternate bridge designs were also investigated such as the full bridge, half bridge and the Mariner C single ended configurations. See Figure 5.5-24. The full bridge method is the preferred choice because the common mode noise signals picked up by the lead wires are rejected by the differential amplifier in the low level commutator and lead wire voltage drops errors are minimized.

All the temperature monitoring points are located on equipment, components or structures, requiring surface type temperature sensors that can be attached to variety of surface contours and shapes. Thermistors, platinum resistance thermometers and thermocouples are likely candidates. Platinum resistance thermometers in a conventional Wheatstone bridge arrangement are preferred for the temperature measurements in the ranges between -350°F and 1000°F and with a span over 100°F. Thus, 64 of the 82 temperature measurements are in this category. Six of the remaining measurements range to 3000° F and require thermocouples. The other 12 measurements are narrow ranges for which thermistors were selected.

Computer calculations for typical bridge designs for most of the CB temperature sensors were contributed by Rosemount Engineering Co. and appear in Figure 5.5 -25. The main considerations in the design are minimum power consumption and linear 0-40 mv output using a sensing element R_o value as high as practical without introducing self-heating error. Power consumption is under 2 mw for all ranges shown. Using wire-wound, 5PPM/°C, bridge completion resistors the temperature coefficient effects were calculated and found to be negligible.

The 12 temperature measurements involving ranges of only 10°F and 20°F can best be implemented by a special thermistor and bridge arrangement. Thermistors are well suited to narrow temperature span measurements because

TEMPERATURE MEASUREMENT METHODS

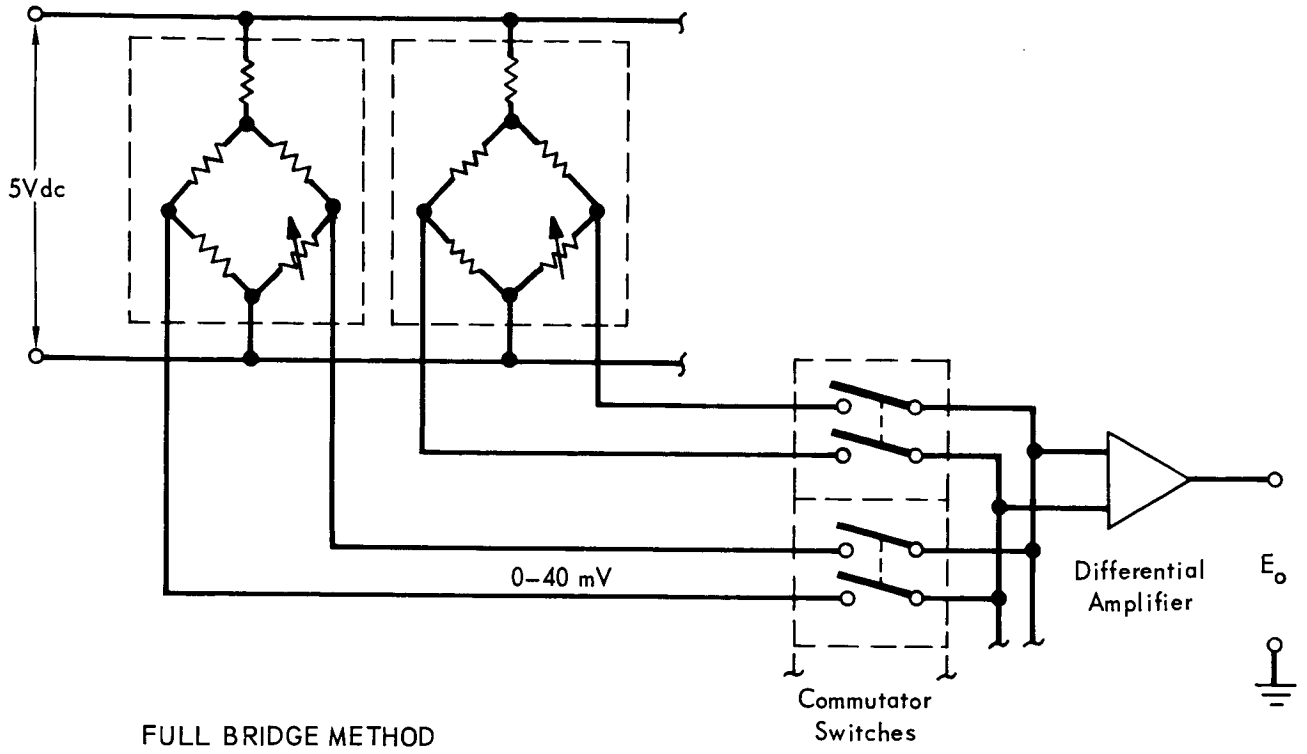

FULL BRIDGE METHOD

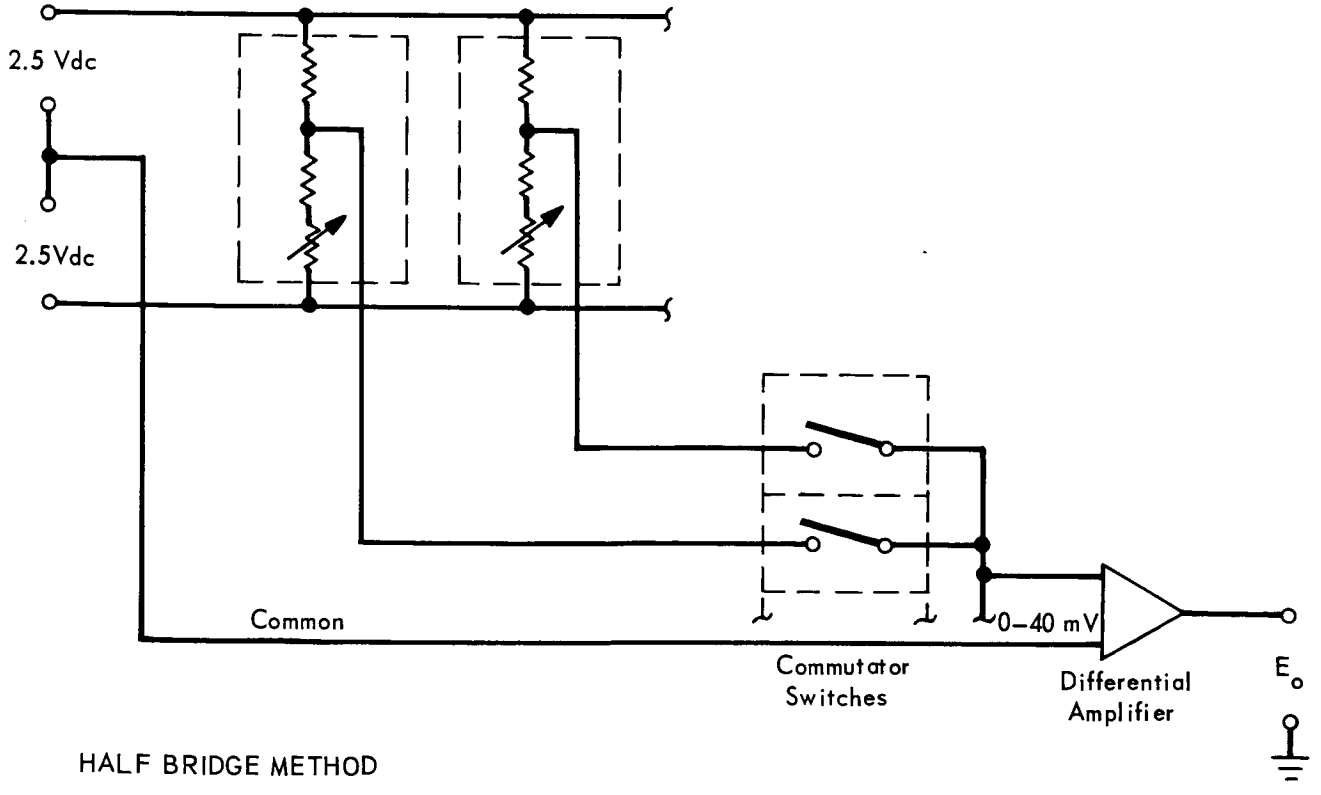

HALF BRIDGE METHOD

Figure 5.5–24

TEMPERATURE SENSOR CALCULATIONS

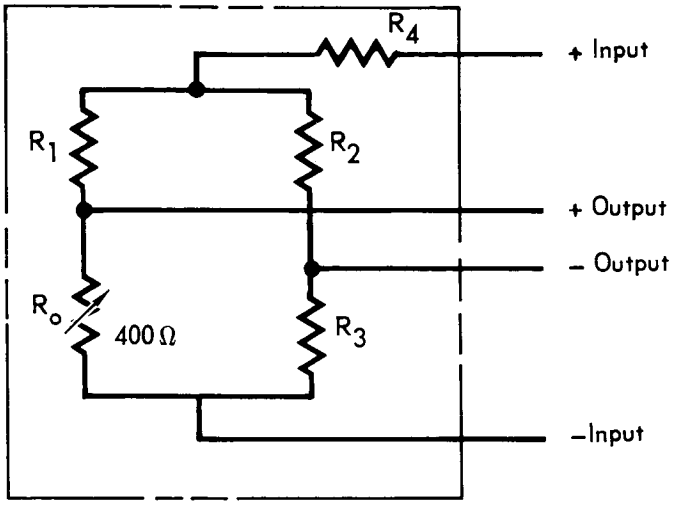

Schematic Diagram

TEMPERATURE RANGES (°F)		BRIDGE RESISTANCE VALUES IN OHMS				POWER REQUIRED	TEMPERATURE COEFFICIENT EFFECTS
		R_3	R_2	R_4	R_1		
1	–200° to + 150°	200	8,380	15,000	7,956	1.3 mW	4.62×10^{-7} Volts
2	–50° to + 200°	300	9,361	7,500	10,201	1.99 mW	6.08×10^{-7} Volts
3	–50° to + 300°	300	10,030	12,000	10,930	1.44 mW	4.62×10^{-7} Volts
4	–350 to + 200°	50	12,508	25,000	11,862	0.8 mW	3.72×10^{-7} Volts
5	–200 to + 200°	200	8,613	17,500	8,177	1.14 mW	4.91×10^{-7} Volts

Input Required: 5 Volts

Output 0–40 mV

Figure 5.5–25

of their large dR/dT characteristics. Three metal sheathed thermocouple combinations for the six heat shield measurements were considered for the high temperature heatshield measurements. These are:

a. Columbium (Cb) sheath - tungsten (W) 5% rhenium (Re) vs tungsten (W) 26% Re thermoelements - magnesium oxide(MgO) insulator for use to 3000°F

b. Molybdenum (Mo) sheath -- W5Re/W26Re thermoelements - (BeO) insulator for use to 4000° F

c. Platinum (Pt) 20% Rhodium (Rh) - Pt/Pt 10 Rh thermoelement - MgO insulator for use to 3000° F.

All of these combinations have been used successfully by McDonnell for high temperature measurements on the ASSET and 122Y Boost-Glide Re-entry Vehicles. The preferred choice for the VOYAGER Aeroshell is the Cb - W5Re/W26Re thermocouple. The tungsten thermoelements have a higher output than the platinum thermoelements and the columbium sheath is more practical for fabrication and installation than molydbenum.

o Pressure Measurements - Thirty-six pressure measurements are presently required to monitor CB subsystem equipment pressures and Aeroshell mold line pressures (see CB Instrumentation List). The specific pressure ranges required and number of measurements applicable to each range are summarized below:

PRESSURE MEASUREMENT REQUIRMENTS

PRESSURE RANGE	NO. MEASUREMENTS
0 to 0.5 psia	1
0 to 5 psia	17
0 to 500 psia	5
0 to 1500 psia	4
0 to 4500 psia	2
Total	29

Six types of pressure transducers were considered as potentially capable of meeting the VOYAGER requirements. The types are potentiometric, bonded strain gage, unbonded strain gage, variable reluctance, capacitive, and LVTD type. Of these the potentiometric type is the preferred for all the pressure measurements except the 0 to 0.5 psia range for the following reasons:

a. Lowest power consumption for 5V output (.25 mW)
b. No amplifier required
c. Simplicity and reliability
d. Suitable for all ranges except 0 to 0.5 psia
e. Lowest weight
f. Relative low cost

A variable reluctance unit was selected for the 0 to 0.5 psia range because of previous successful experience with this type low pressure unit on the ASSET , 122Y and Gemini programs.

Signal Conditioners - The required CB signal conditioning includes DC current monitors, pyrotechnic current plus detectors and RCS thrust valve monitors. This section discusses the technical requirements and alternatives for mechanization of these monitoring systems.

- o Current Monitoring - Nineteen DC current measurements are presently required in the CB power, thermal control and radar subsystems. The ranges vary from 0-2A to 0-25A. The two methods considered for monitoring DC current were calibrated shunts with amplification by the telemetry low level DC amplifier and individual magnetic amplifiers for each measurement. The shunt method results in large savings in weight and overall power consumption. The disadvantage of this method is that accuracies are poor near the zero point. To a smaller degree, this is also true of the magnetic amplifiers. Shunt monitoring is capable of meeting the accuracy requirements and will be used for all the current measurements except the battery charge current measurement. For this measurement where greater accuracy and circuit isolation is required a magnetic amplifier type circuit will be used. The weight and power savings of using shunts as compared to individual magnetic amplifiers is approximately 5.6 lbs and 7 watts.
- o Pyrotechnic Current Pulse Detector - The detection of a firing current pulse is required for each of 57 squib cartridges in the pyrotechnic subsystem. Safety considerations prevent a hard wire connection to the pyrotechnic firing circuits. The current pulse can be monitored by a current transformer with a hole through it for the return leg of the squib circuit to pass through. Detecting a current pulse is a less complex problem than monitoring current, since the current pulse is dynamic in nature. This eliminates the need for magnetic amplifiers and other associated circuitry

necessary for DC current monitoring.

Figure 5.5-26 is a block diagram of a current pulse detector. The pulse transformer is fabricated from a toroid in such a manner that a single turn of the pyrotechnic lead wire is sufficient for pulse detection. The pulse, upon amplification, then provides an impedance match between the transformer and the level detector.

The level detector is adjusted so that spike amplitude and spike energy are combined to give the necessary bi-level signal to make the telemetry flip-flop change states. The flip-flop retains this information until sampled by the commutator.

- o Solenoid Poppet Valve Monitoring - Monitoring of the eight RCS solenoid valves is required during dry system in-flight checkout and in-flight operation. An investigation was made to determine feasible monitoring equipment. The system requirements of the poppet monitor are twofold: (1) to indicate movement of a poppet valve energized by a solenoid, and (2) to indicate the return to the normal off state of the valve. Thus, a bi-level output is required.

The problem of monitoring a poppet valve inside a solenoid valve is most easily accomplished by monitoring the current through the solenoid coil. This method is feasible due to the relationship between the inductance (L) and resistance (R) of the coil and the variance in magnetic field strength about the coil when the poppet valve first moves. This variance in field strength is due to the change in L based on the variable reluctance principle.

The equivalent circuit of the solenoid may be represented by an inductance and a series resistor. As a DC voltage is applied to the coil, the current rises exponentially with a time constant L/R. When the current reaches the solenoid pull-in level, the armature (poppet) displacement generates a back EMF which momentarily opposes the flow of current. This opposition of current flow is noted as a short negative slope in the current waveform. A change in the rising slope constant (L/R) due to the change in L is also noted and is shown in Figure 5.5-27 along with the negative slope due to poppet valve movement.

Two methods of detecting this negative-going portion of the current waveform were suggested by the engineering department of Electro-optical Systems, Inc., as possible solutions to the monitoring problem. The two block diagrams and waveforms relative to these systems are shown in Figures 5.5-28 and -29.

CURRENT PULSE DETECTOR

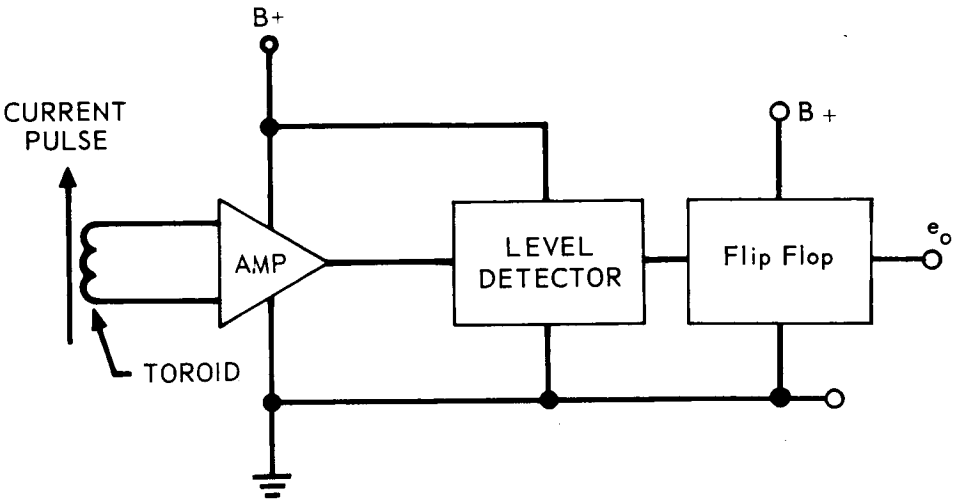

Figure 5.5–26

POPPET VALVE CURRENT WAVEFORM

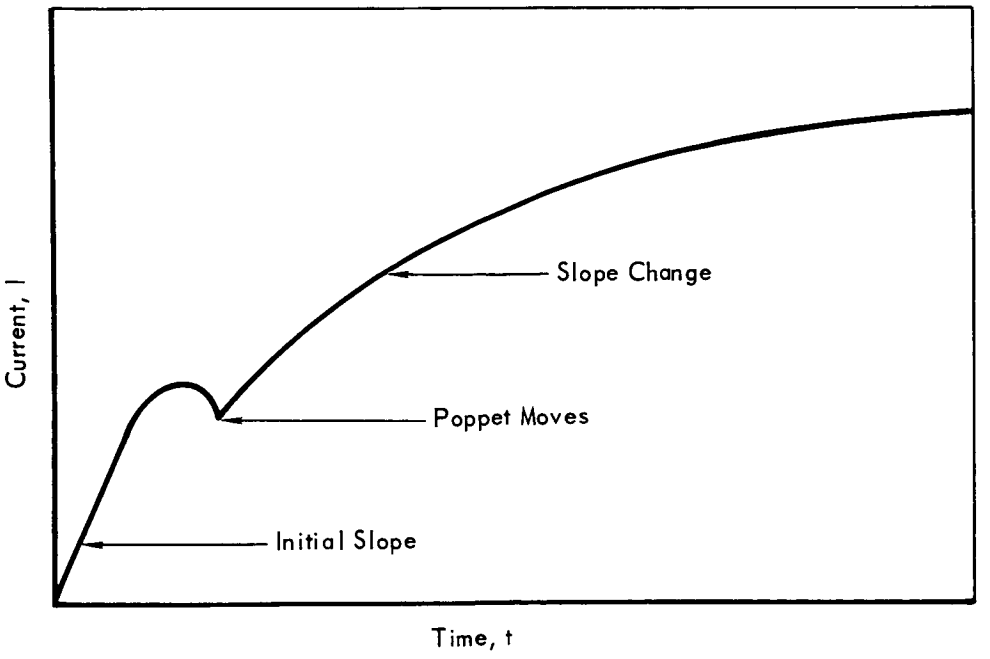

Figure 5.5–27

POPPET VALVE MONITOR, METHOD I

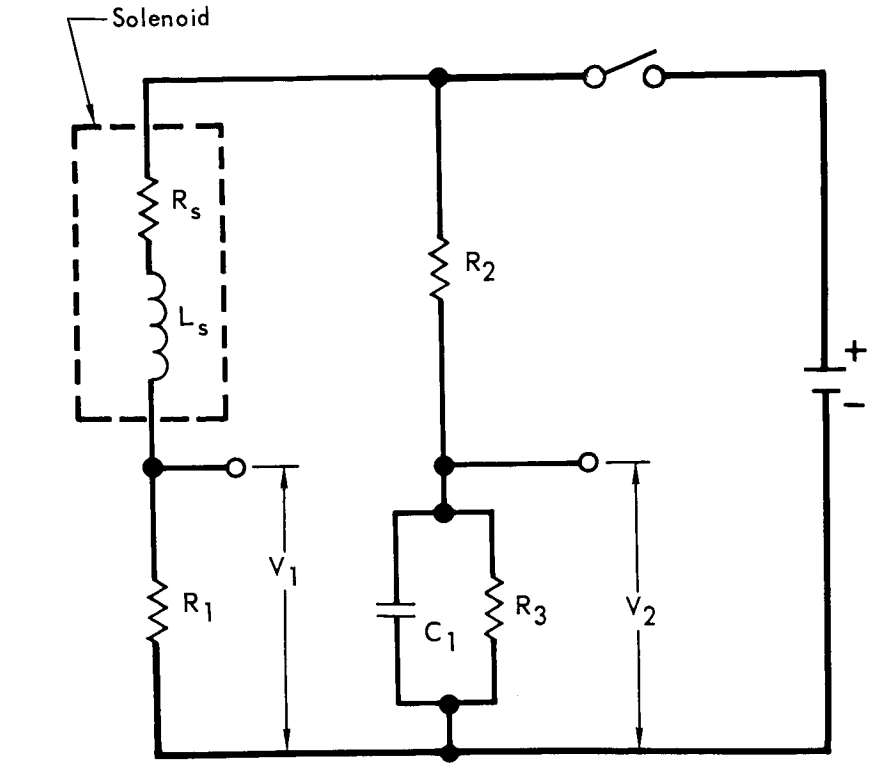

$$\frac{R_s}{R_1} = \frac{R_2}{R_3}$$

$$\frac{L_s}{R_1} = R_2 C_1$$

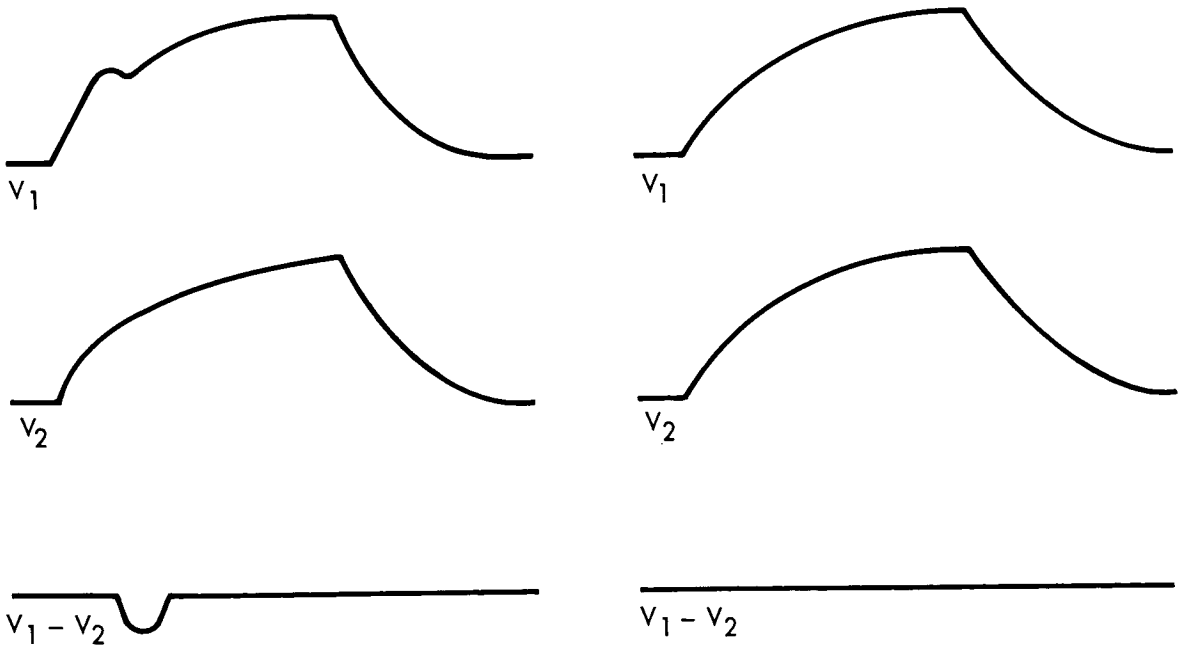

(a) Solenoid Operating Properly

(b) Armature is Not Free to Move

Figure 5.5–28

POPPET VALVE MONITOR, METHOD II

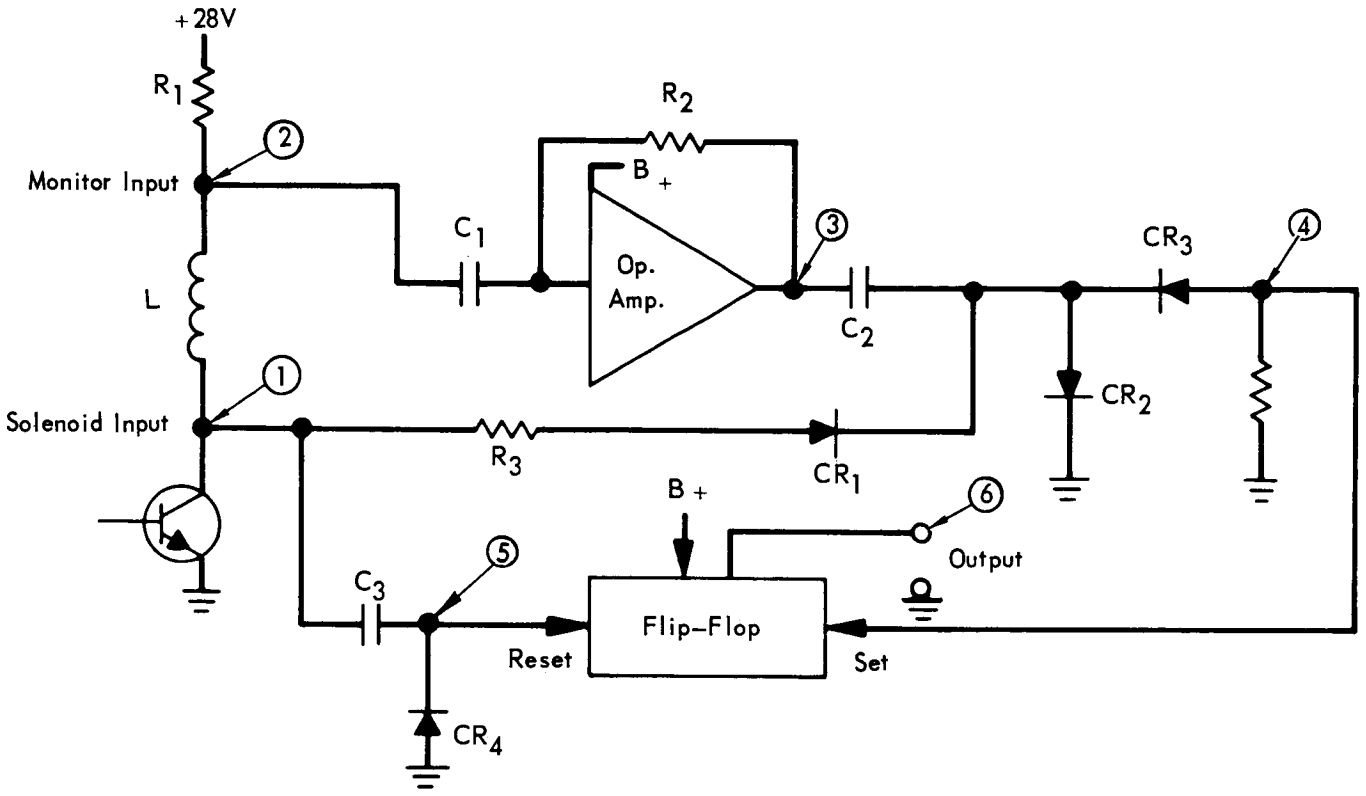

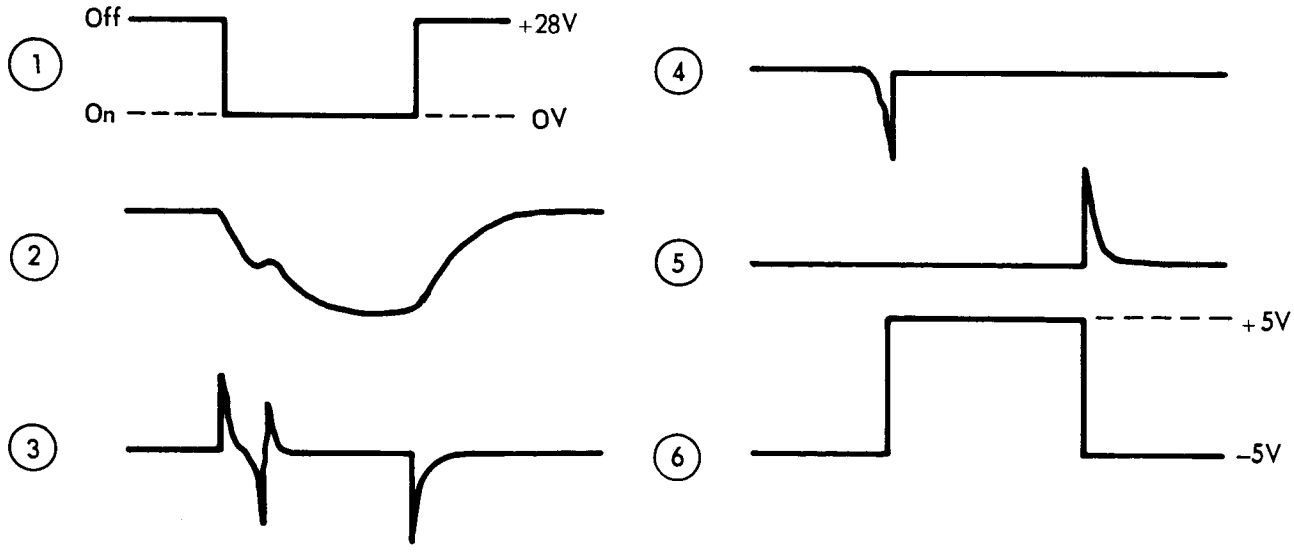

Figure 5.5–29

Figure 5.5-28 shows a system which detects the back EMF by generating a wave from the switching voltage which is equal to the voltage across the current monitoring resistor when the armature is prevented from moving. If the output is taken as the difference between the two voltages, it will be directly proportional to the back EMF. Therefore, if the armature is prevented from moving the output will be zero. The disadvantage of this method is that it is difficult to maintain a balanced output because of solenoid resistance variations with temperature.

Figure 5.5-29 shows a block diagram of the preferred method of monitoring the current waveform. Using this method, the current waveform is differentiated to measure the slope directly. This measurement is then summed with the solenoid transistor switching logic to obtain the desired output at the flip-flop. The current waveform developed across R_1 is differentiated by C_1, R_2, and the operational amplifier. The differentiated signal is referenced to ground with diode CR_2. Since the required signal is a negative going pulse, diode CR_3 cuts off the unwanted positive pulses. During solenoid turn-off, CR_1 shorts CR_2 so that the negative signal pulse due to solenoid switch-off is blocked and does not allow erroneous change of the flip-flop. The signal at point 4 is then a single negative going pulse only when solenoid pull-in occurs. This pulse is used to set the flip-flop. The reset is provided by a positive-going pulse when the solenoid is switched off.

5.5.3 Radio Subsystem - It was concluded that the CB radio subsystem will operate in a satisfactory manner within the mission constraints. System noise temperature, diversity combining method and CB to ESP signal compatibility were among the factors considered in the design of this subsystem.

5.5.3.1 Receiver System Noise Temperature - The receiving noise temperature used in the link power budget is $555^{\circ}\ ^{+25}_{-80}$ °K. This derivation is summarized herein.

The antenna temperature is determine by noise sources within the beam of the spacecraft relay link receiving antenna. The principal sources are galactic noise and Martian surface radiation. The worst case occurs when the beam is completely filled by the planet. This may occur under certain trajectory and landing site conditions. Therefore the worst case of 283°K is used for the link calculations.

For the quiet Sun conditions in 1973-75, the average incremental receiver noise is estimated at 2°K. Solar noise is therefore ignored. During the 1977-79 noisy Sun years this will not be the case (Reference 5.5-16) and solar noise will be a factor.

- o Receiver Noise Temperature - The receiver RF preamplifier utilizes a state-of-the-art, low noise silicon transistor with a noise figure of less than 3 dB (290°K).
- o Receiving System Noise Temperature - A line plus diplexer loss of 1.5 dB between the antenna and preamplifier input is predicted. Assuming an ambient temperature of 50°C, and an antenna temperature of 283°C, the receiving system noise temperature is 555°K. The tolerances were estimated based on previous experience.

5.5.3.2 Receiver Diversity Combining Method - The CBS to FSC communications link employs frequency diversity to combat multipath degradation. The two diversity channels must be properly combined to realize the diversity improvement. The combiner may be either a predetection or a post detection device.

- o Post Detection Combining - Post detection combining is simple. Furthermore, theory predicts (Reference 5.5-17) that an equal gain square-law post-detection combiner essentially is optimum for this environment
- o Predetection Combining - Predetection combining is more complex than post-detection combining because the received signal must be multiplied by a function of itself. This necessitates complex measurement circuitry.

5.5.3.3 CB - ESP Signal Compatibility - The CB and ESP carriers are separated by 1.3 MHz, and the CBS-FSC receiver input bandwidth is greater than 4 MHz (because of stability requirement in filter design). It is unavoidable that the ESP and CB radio signals will simultaneously enter the ESP receiver front end and on to the mixer. The significant cross products are, however, outside the IF band and therefore no cross talk between CB and ESP signals will be detected. A 30 MHz crystal bandpass filter is incorporated at the IF input. The filter has a 60 KHz bandwidth and a selectivity ratio of 3 which would attenuate the adjacent ESP frequency (1.3 MHz away) by at least 60 dB. Therefore the CB receiver IF AGC is not affected by the ESP signal.

5.5.3.4 Receiver Gain Stability Requirement - Since equal gain dual frequency diversity is employed, the effect of gain variations between the two receivers was briefly investigated.

No analysis was found which answers this question for a Rician fading signal input. When the interference is Rayleigh, the difference between the single channel (zero receiver gain in one channel) and dual channel (both receivers with equal gain) links is approximately 4 dB, Reference 5.5-17. This is based on a bit error probability of 10^{-3} when the signal-to-interference ratio is 9 dB.

An analysis based on a simplified non-fading model predicted a loss in link performance of 0.3 dB when the differential receiver gain is 3 dB. These receiver mismatch margins are within the capabilities of the preferred design.

5.5.3.5 Dynamic Range - The dynamic range of the CB FSK receiver is determined by the AGC and RF power handling capability of the receiver. The AGC will provide a 100 dB dynamic range, i.e., from the threshold signal level -123 dBm to -23 dBm. When the RF input is above -23 dBm, the RF preamplifier will saturate and it will act as a limiter. In the limiting condition the receiver continues to process the FSK signal without deterioration of signal characteristics since both noise and interference is insignificant during this condition (CB physically close to the FSC).

The power handling capability of the low noise transistor, however, is limited to approximately +20 dBm. When the input level is above +20 dBm, the transistor may be damaged due to high junction temperature. When the CB Radio Subsystem is activated at time of separation, the CB receiver would be confronted with high RF power which may exceed the danger level of +20 dBm. Calculations indicate that, if the CB Radio Subsystem is activated after separation when the Capsule Bus is greater than 2 meters away from the spacecraft, the maximum RF input to the receiver

is less than +20 dBm. Hence, safe operation can be maintained by inserting a short delay in transmitter turn-on at separation. An alternative design is to design the receiver front end to withstand up to one watt of CW power by incorporating a Varacter limiter. The penalty here is increase of the receiver noise figure by 0.5 dB.

5.5.3.6 Receiver IF/LO Configuration - Two IF channels are required in the CBS frequency diversity receiver. The preferred configuration uses a common local oscillator frequency that lies midway between the two operating frequencies. This configuration offers the following advantages:

- o Identical IF amplifiers facilitate gain matching between the two diversity receivers.
- o Identical LO/IF design reduces cost.
- o Standard 30 MHz IF frequency simplifies test equipment set-up and test procedure.

In this configuration, one receiver is operating on the image frequency of the other. Consequently interferences would occur if no preselectors are used. The frequency diplexer, however, serves as a means of channeling the diversity signal power from the antenna into the diversity receivers as well as providing frequency isolation. The diplexer can provide at least 60 dB isolation between channels, which is more than sufficient to avoid interchannel crosstalk.

5.5.4 Antenna Subsystem - Performance characteristics of the CB antenna subsystem will satisfy the requirements for adequate signal margin during normal operation from separation until at least 5 minutes after landing. The following discussion presents the analyses and rationale which lead to the selected characteristics and configurations for the CB- and FSC-mounted antennas.

5.5.4.1 Transmitting Antenna Requirements - The antenna radiation pattern requirements for descent and entry have been developed in Section 5.5.1.3 from a number of trajectories analyzed for the multipath calculations. A gaussian pattern, shown in Figure 5.5-5, was assumed in the analysis and it was shown that this pattern has desirable characteristics for a multipath environment. In this section, the pattern requirements for the remainder of the mission are discussed. After the total requirement has been developed, the alternate approaches taken in the selection of an antenna configuration and the results of a radiation pattern study are discussed. An Archimedes spiral above a cavity was the selected approach.

Separation Through De-Orbit - At FSC/CB separation the CB moves along a path aligned with the FSC longitudinal (+Z) axis to a position at least 1000 feet from the FSC. At this time the -Z axis of the CB is nearly aligned with the +Z axis of the FSC. The CB then performs a roll maneuver followed by a pitch maneuver to attain the de-orbit attitude. The magnitude of the pitch maneuver ranges from 40 degrees to 80 degrees depending on the de-orbit anomaly. The view to the FSC will therefore remain within the hemisphere centered on the roll (-Z) axis of the CB. The gaussian pattern will provide coverage at the 80 degree view angles and the relatively short range will provide adequate link margin.

Orbital Descent and Entry - In Section 5.5.1.1 the geometric constraints imposed by multipath considerations on the relative positions of the CB and the orbiting FSC at entry were discussed. The view angle requirements were established and were limited to the hemisphere centered on the roll axis. The advantage of shaping the pattern at angles greater than 50 degrees off the roll axis were discussed and it was shown that a rapid decrease in gain with angle was desirable. A gaussian shaped pattern was therefore assumed in the analysis and is a realistic requirement.

Terminal Descent - For the two multipath entry trajectories studied, the CB to FSC view angles at the time of parachute deployment are within 14 degrees of the roll axis. The CB roll axis will be nearly aligned with the local vertical during this phase except for high wind gust conditions. The wind gust effects on the CB to FSC view angles have not been explored in detail. The view angle in the VM-9 trajectory analyzed is 12 degrees from the roll axis and the symmetrical antenna pattern provides 15 dB of range margin at this angle. A wind gust would effectively shift the pattern and considering the range margin available, a large angular rotation of the pattern could be tolerated.

Post Landing - For post landed operation, the major factor influencing the pattern are the 34 degree maximum ground slope and the maximum 5 degree additional slope induced by the impact attenuators material after crushing. The worst case view angles occur when the total 39 degrees of roll axis tilt is normal to the orbital plane. The FSC has been constrained to be at least 34 degrees above the local horizon at the time of landing and a 5 minute post landed minimum viewing period is required.

An analysis was performed to determine the communications time lost with the unfavorable orientation of the gaussian radiation pattern caused by the maximum slope and crush angles. The orientation of the pattern with respect to the orbital plane was analyzed and the time lost under these conditions was calculated.

The probability of landing on 34 deg. slopes is considered to be low. In addition, the worst case slope directional bearing is normal to the orbital plane and the probability of landing on a 34 deg. slope with this bearing is even lower. The percent of the possible slope bearing orientations for which adequate antenna gain is not available at all times was calculated. For the worst case view angles to the FSC (34 deg elevation), 40% of the possible slope bearings will not provide adequate gain. However, the FSC does move into the higher gain portion of the pattern during its orbit. The communications time lost was calculated based on the angular rate of the FSC at periapsis (.047 deg/sec) for the large orbit (4900 x 23,400 KM). The maximum time list is 4.7 minutes which is considered an acceptable condition considering the probability of this situation existing.

Antenna Pattern Study - The analysis presented in Section 5.5.1.3 made use of the CB antenna pattern shaping to mitigate the effects of multipath. A broad pattern with sharp rolloff outside the required beamwidth is desired. The pattern was assumed gaussian, centered on the -Z axis of the CB, with a 90° beamwidth in all planes containing the -Z axis. It was shown that such a pattern did satisfy the multipath constraints. As shown above, such a pattern also provides adequate coverage when variations of CB attitude are considered. Therefore, a test program has been conducted to achieve the desired pattern with a realizable antenna. The test program goals were to identify the antenna which best meets the following requirements.

- o Circular polarization
- o Low axial ratio within the beamwidth
- o 90° beamwidth
- o Approximate gaussian pattern
- o Low backlobes
- o Approximately 20% beamwidth

Three major types of antennas were investigated; conical spirals, flat equiangular spirals and cavity backed Archiemedes spirals. Testing was at one-third scale, with various configurations of each antenna type considered. The general results may be summarized as follows:

- o The conical spiral which satisfies the pattern requirements would be too large at UHF.
- o The flat equiangular spiral of reasonable dimensions provides an axial ratio which is too large.
- o An Archimedes spiral mounted above a cavity (some separation between cavity and spiral) provided the best total radiation characteristics.

Figure 5.5-30 presents the measured pattern of the Archimedes spiral, with the analytical gaussian pattern shown for comparison, and illustrates a conic section 55° off axis, showing a variation of approximately 1.5 dB. This coverage satisfies the CB transmitting antenna requirements. Pertinent characteristics of the antenna selected are as follows:

- o 3 dB beamwidth - 95°
- o Gain at 70° off axis - 7.5 dB below maximum
- o Rolloff between 70° and 90° - 0.73 dB per degree
- o On axis axial ratio - <1 dB
- o Backlobe level - 26 dB below maximum

5.5.4.2 Spacecraft Mounted Equipment - Pattern coverage requirements for the FSC-mounted CB receiving antenna are governed by FSC attitude, possible CB dynamics after separation, landing site selection and post landed view time constraints. Antenna gain requirements are constrained by other link gains and losses, to limit the CB Radio Subsystem power consumption and weight. The antenna pattern is required to be at least 180° x 45°, based on the above. Maximum antenna gain possible for the coverage required is 7.15 dB, less efficiency effects.

Antenna Pattern Analysis - Thirty-four possible separation through entry dynamic cases were considered. In each case the cone and clock angles from the Sun/Canopus oriented FSC to the CB were calculated for three possible orbit orientations. Also, the two bounding entry through landing cases were considered. It was found that the clock and cone angles during entry partially retraced the bounds established by the dynamics before entry. Post landed requirements were established by assuming coverage until the FSC is 30° above landing site local horizontal. Maximum post landed requirements occur with a 360° anomaly landing. Figure 5.5-31 shows the effects of the dynamics and post landed coverage requirements for two orbit inclinations and a morning terminator landing. The required FSC mounted antenna coverage is seen to be approximately 165° x 10°. Taking account of possible FSC attitude variations, out of plane entry, and variations of de-orbit date, increases the required coverage to approximately 180° x 45°. Figure 5.5-32 shows that

ANTENNA PATTERN

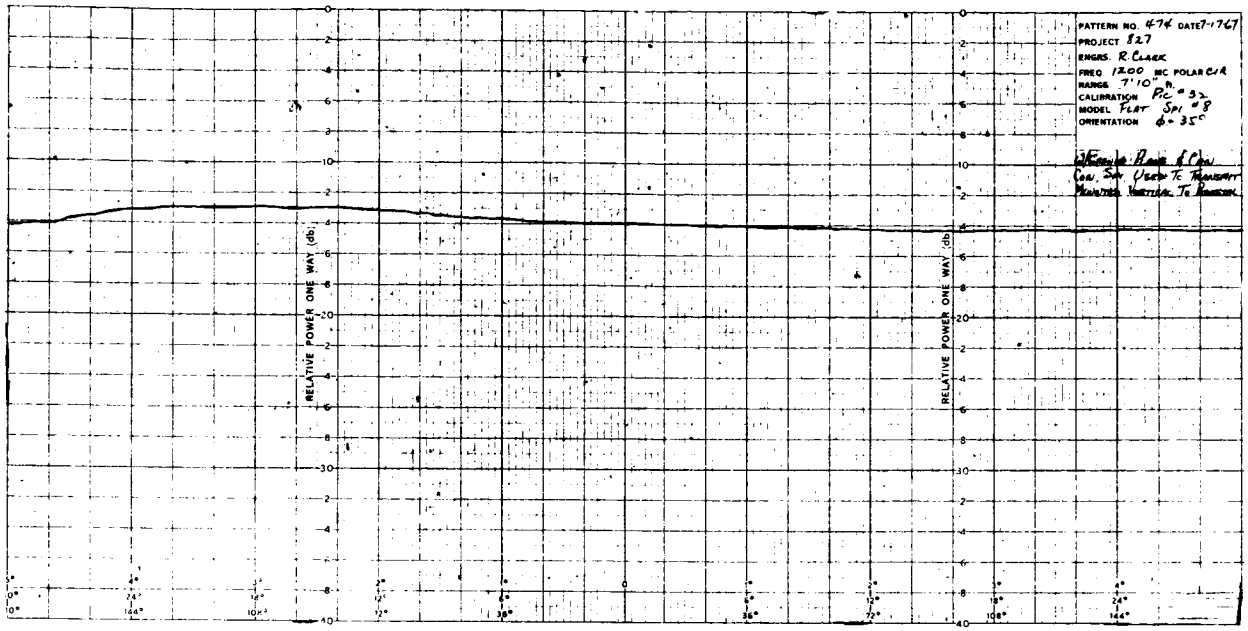

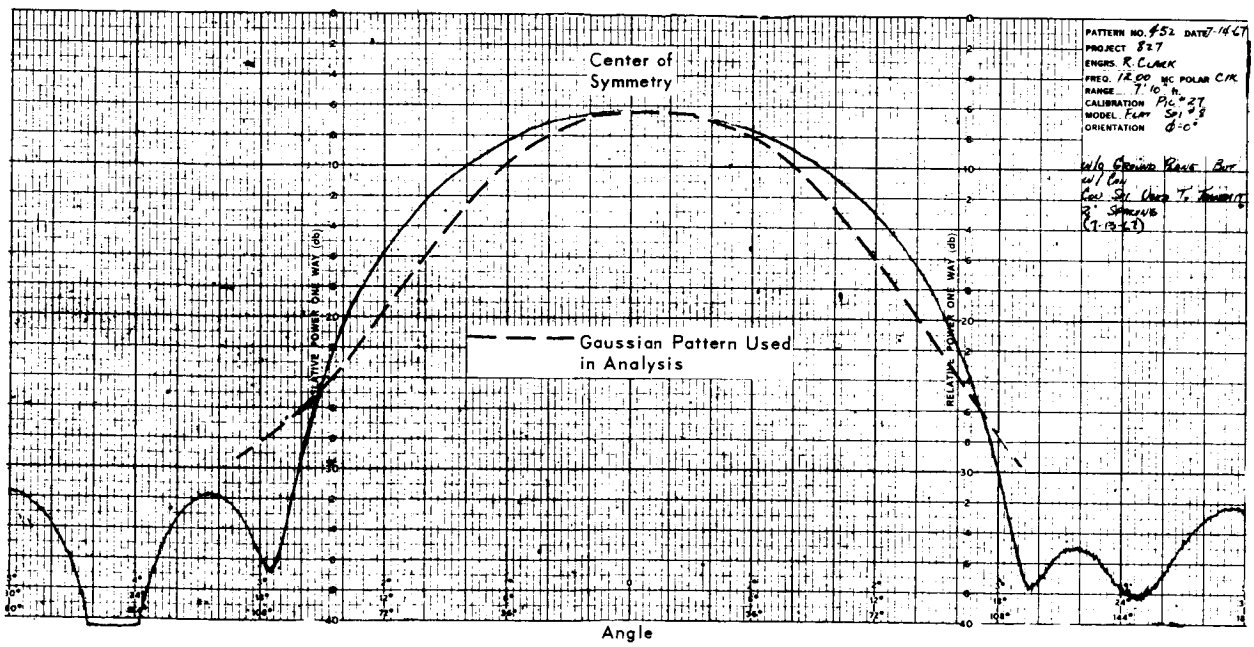

Figure 5.5–30

CAPSULE BUS RECEIVING ANTENNA VIEW ANGLE REQUIREMENTS
LANDING NEAR MORNING TERMINATOR
(20 MARCH 1974)

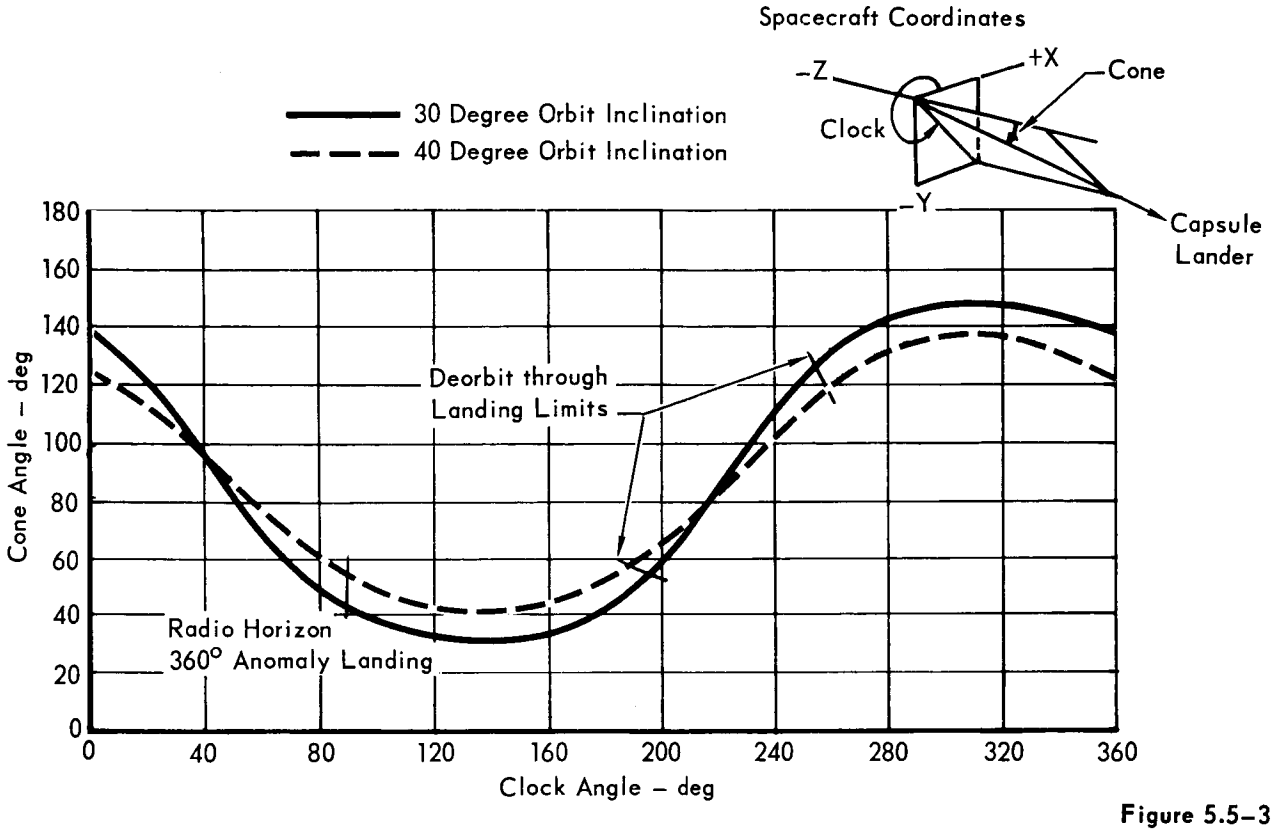

Figure 5.5–31

CAPSULE BUS RECEIVING ANTENNA VIEW ANGLE REQUIREMENTS
LANDING NEAR EVENING TERMINATOR
(3 FEBRUARY 1974)

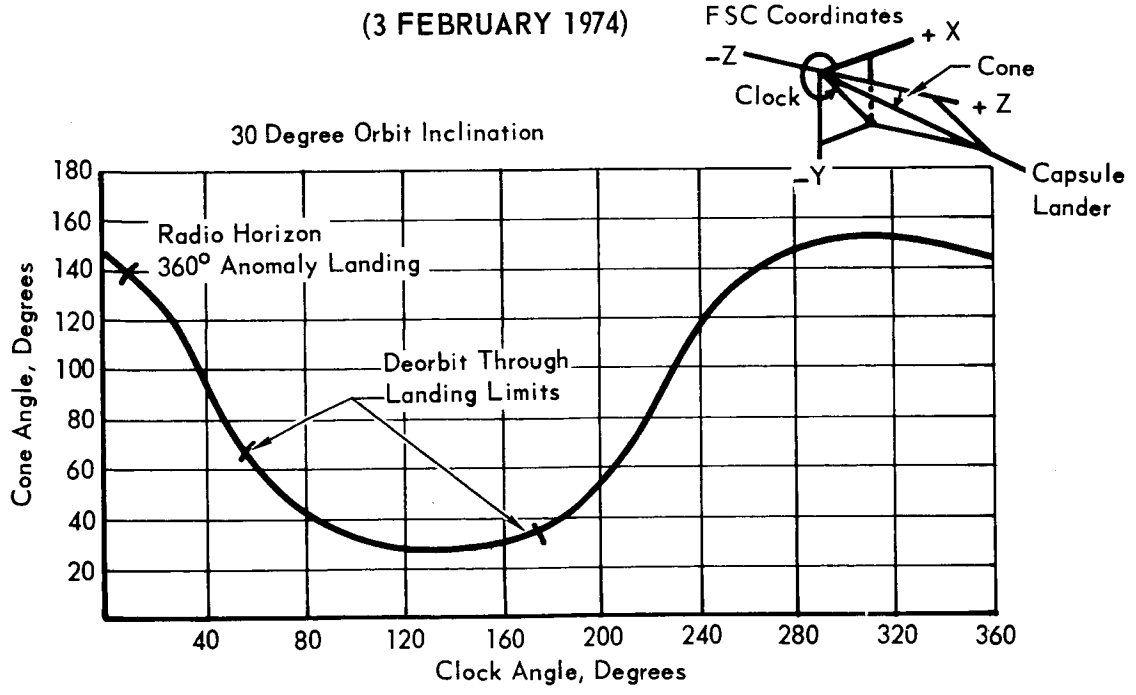

Figure 5.5–32

the same magnitude of coverage is required for an evening terminator landing, but the antenna pattern should be oriented differently in the FSC coordinate system. If both the morning and evening landings are covered by a single pattern, the required coverage is approximately 280° x 45°. The maximum gain available from a 280° x 45° antenna pattern is 5.23 dB. The maximum gain available from from a 180° x 45° pattern is 7.15 dB. If the FSC mounted antenna is pointed on the basis of approximate landing site, the higher gain pattern may be employed. For the morning landing conditions shown, the antenna pattern should be pointed in the directions: clock angle 200°, cone angle 65°. For the evening landing shown, the angles are: clock 45°, cone 80°. Both directions are approximately perpendicular to FSC coordinate radius vector described by a cone angle of 50° and a clock angle of 320°. Thus, an antenna subsystem with a pattern perpendicular to the above radius vector may be rotated about the vector to provide coverage for all cases considered. If mechanical rotation is not employed, the total pattern coverage must be obtained through the use of a lower gain antenna pattern or antenna switching. Any method employed must use circularly polarized antennas due to relative attitude variations between the FSC and CB. Also, the required coverage precludes the use of a fixed CB receiving antenna located within the SC adapter section.

Alternatives - Two basic approaches are considered to satisfy the FSC mounted CB data receiving antenna coverage requirements. First, employ a fixed 280° x 45° pattern, and second, employ a steerable 180° x 45° pattern. Two implementations of the steerable pattern are considered. Figure 5.5-33 summarizes the pertinent features of each approach, using antenna configurations which provide the closest approximation to the desired patterns.

Selection - As shown all approaches employ antennas mounted on the FSC. This placement is the only possible choice for the body mounted switching array, considering the FSC geometry and the required line-of-sight variations. Mast mounted antennas attached to the FSC may be deployed before CB separation, providing time for telemetry monitoring and backup commands in case of malfunction. A mast mounted antenna stowed in the Capsule Adapter could not be deployed until after CB separation, with the attendant time delay in status verification.

The RF switched array pattern coverage is limited to two discrete sectors. More complete coverage requires more antennas and switches. Either mast mounted approach provides total coverage of 360° in one plane. Therefore, mast mounted antennas are selected.

COMPARISON OF CANDIDATES FOR CB RECEIVING ANTENNA

CANDIDATE APPROACHES

	1	2	3	REMARKS
IMPLEMENTATION	Two each, two element arrays. Mounted on Flight Spacecraft RF Switches activate selected array for morning or evening landing	Single antenna, mounted on mast extending from Flight Spacecraft. No mast rotation	Array mounted on mast extending from Flight Spacecraft. Mast rotated to point array for morning or evening landing.	Approach 1 provides coverage in two fixed sectors. Approach 3 may have continuous resolution if update is desired.
PATTERN COVERAGE, GAIN	160° x 48° Instantaneous 280° x 48° Total Maximum gain, 7.4dB	360° x 45° Maximum gain, 4.15 dB	180° x 48° Instantaneous 280° x 48° total Maximum gain, 6.85dB	Approach 2 requires increased transmitter power for same performance level.
COMPLEXITY	Mechanically simple, but constrains other external structure to provide clear field of view. Also, requires RF switches. Requires non-real time command.	Requires mast extension mechanism	Requires mast extension mechanism. Mast rotation requires non-real time command.	RF switches not desirable. Mast extension improves field of view capabilities.
CONFIGURATION	Two arrays. Two crossed slot antennas per array.	Single bicone	Two dimensional bicone array.	
SIZE, WEIGHT	4800 cu. in. 6 lb. plus RF switches	1430 cu. in. 3 lb. plus mast and mechanism.	4400 cu. in. (envelope) 6 lb. plus mast and mechanism.	Weight advantage of single bicone offset by increased weight in CB radio subsystem.

Figure 5.5-33

The mechanically steered array is only slightly more complex than the fixed, low gain antenna due to mast rotation capability, while providing higher gain. Four circularly polarized biconical antennas arrayed as shown in Figure 5.5-34, provide the antenna coverage required. The calculated element and array patterns are shown in Figure 5.5-35.

FLIGHT SPACECRAFT MOUNTED CAPSULE BUS RECEIVING ANTENNA ARRAY ORIENTATION

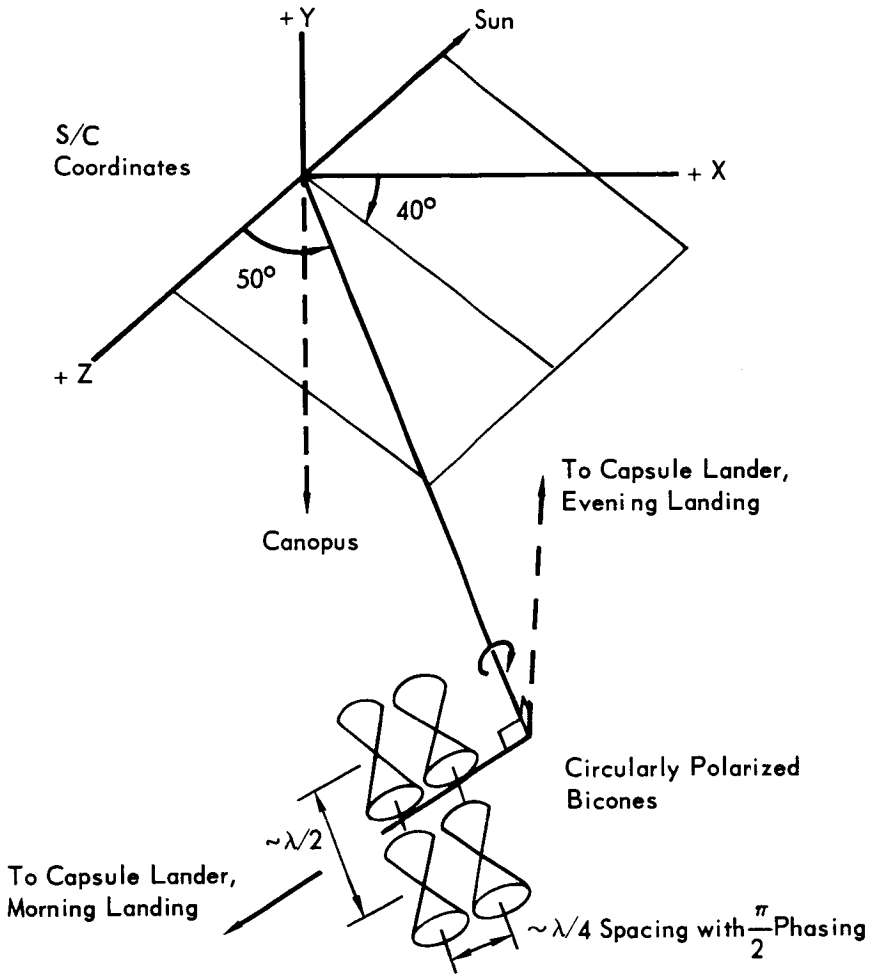

Figure 5.5–34

CALCULATED CAPSULE BUS RECEIVING ANTENNA ARRAY PATTERNS

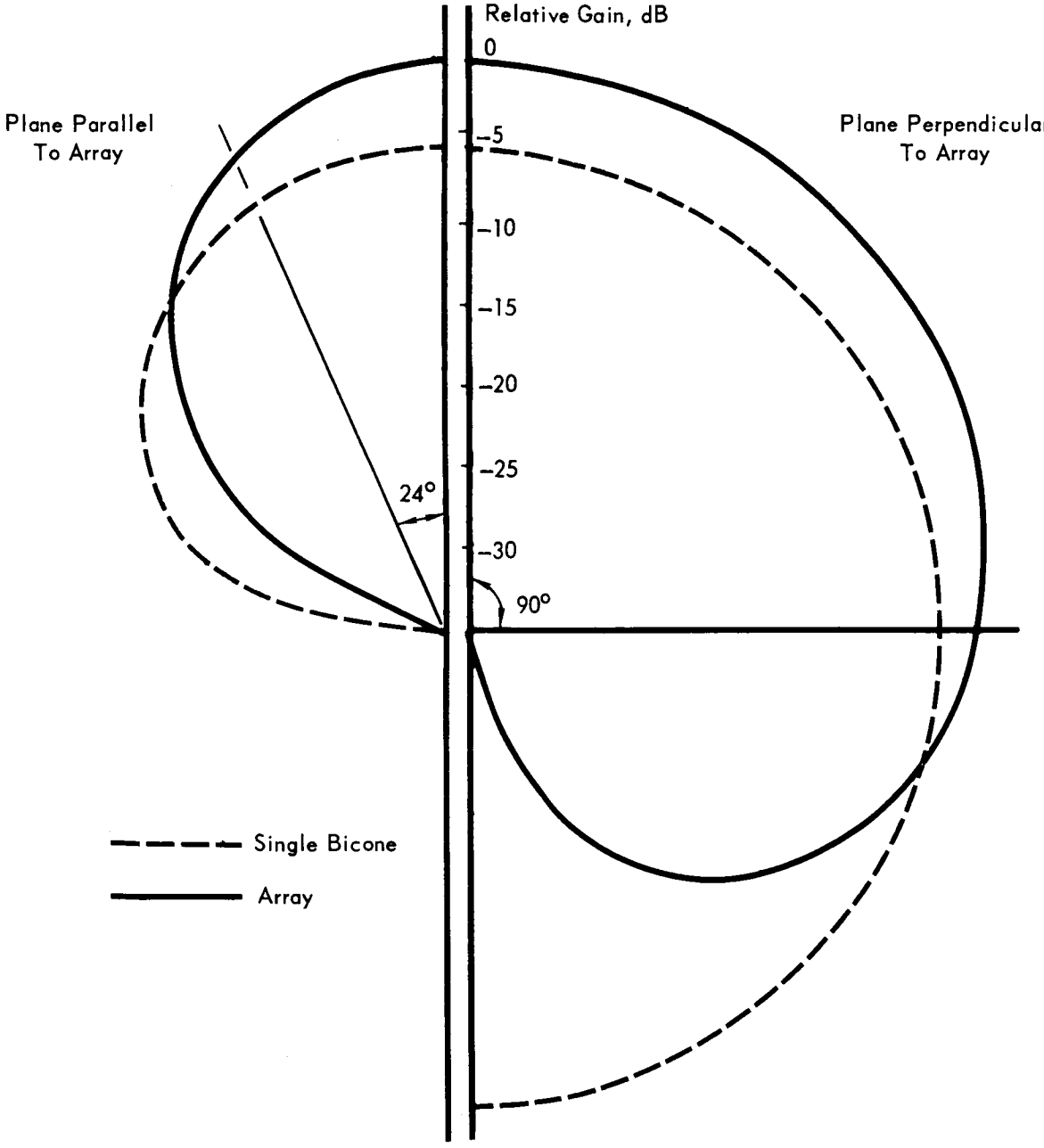

Figure 5.5–35

5.5.5 Data Storage Subsystem - Storage is required in the Capsule Bus telecommunications system because of shock induced ionization. Atmospheric data gathered during communications blackout is stored in the Capsule Bus for delayed transmission after the blackout period ends. The blackout period will be a maximum of a 150 seconds Requirements and trade offs in this area are discussed in detail below.

5.5.5.1 Configuration Trade - Two storage configurations were considered. One utilized external commands from the S&T or external sensors (such as an accelerometer) to steer the input data to a data store immediately prior to blackout. The store is read out after blackout prior to touchdown, with the stored data interleaved or multiplexed with real time data. This configuration was recommended for a hard landing probe (Reference 5.5-16). However, in that study an extremely short time period between end of blackout and landing was anticipated. Therefore stored data was transmitted at a faster rate than it was accumulated. The quantity of real time data transmitted after blackout was reduced to accommodate the stored data transmission.

For VOYAGER, the time between end of blackout and touchdown will be greater than the blackout period. Furthermore, the real time data rate requirement after blackout does not decrease. Thus a tapped delay line storage configuration, has been selected. While reliability was the major consideration in this analysis, the availability of redundant bits obtained by transmitting the stored data throughout the entire operation (separation to touchdown) can provide additional protection against multipath interference. The correlation between fading between two points in time separated by the delay store time (150 seconds) is normally expected to be quite small. (See Section 5.5.1.1) Therefore, redundant bits may be identified on the ground and used in connection with additional redundant bits obtained via the Entry Science Package to implement a majority decision logarithm in the MDE. In the absence of the Entry Science Package, the Spacecraft relay receiver AGC, monitored via telementry, may be used to provide a selection criteria.

The preferred configuration incorporates a dual delay storage. This figure includes the Entry Science Package interconnection as recommended in Section 5.5.6.

5.5.5.2 Functional & Technical Requirements - The CB Storage Subsystem requires 50 second and 150 second storage devices operating as delay lines. Required

performance and characteristics are listed below:

- o Input data - NRZ data at a bit rate of 910 BPS.
- o Output data - NRZ data
    - o Input data delayed 50 seconds
    - o Input data delayed 150 seconds

  Input and both outputs must be synchronized on a bit by bit basis
- o Total storage requirements ------(150 seconds) (910 BPS)
  = 136,500 bits
- o Delay Time Tolerance - No tolerance can be allowed, i.e. - the storage capacity must be unvariant for all conditions (temperature, variation of memory parameters with time, etc).
- o Meet environmental requirements including sterilization temperature and radiation
- o Weight, volume and power should be minimized without compromising reliability.
- o The selected storage devices should be state of the art, preferably with flight proven history.

5.5.5.2.1 Candidate Storage Devices - Because of the large requirement of 136,500 bits of storage, semiconductor devices are not considered. Although many storage techniques have large packing densities (resulting in low weight and volume), the only techniques considered suitable for VOYAGER are magnetic core memories, plated wire memories and magnetic tape memories. The magnetic core memories may be organized as 2, 3 or 2-1/2 dimensional. The magnetic tape memories may be coplaner (reel to reel), coaxial (reel to reel) or endless loop.

- o Magnetic Core Memories - Magnetic core memories consist of individual discrete toroidal magnetic cores strung on conductive wires to form planar arrays. The wires threading the cores supply the selection of the desired core as well as the capability for writing into and reading out of the particular core.

  There are three major core memory organization arrangements; these are referred to as multidimensional (2D, 3D, and 2-1/2D). The first of these, the 2D memory, is characterized by the simplest conductor threading pattern. A pair of orthogonal wire sets are threaded through the cores so that a core encloses every crossing point of the wires. These wire

sets are commonly referred to as the X and Y wires. The 2D memory is also known as a word organized memory since all of the bits in a single word are included in a single row of cores within the core plans. Thus all memory is included in the X and Y dimension, giving rise to the 2-dimensional designation. All of the selection logic is supplied by the associated electronic circuitry and thus the 2D memory requires more electronics than the other two types. The advantage of the 2D system lies in its comparatively high operating speed. This is brought about by the minimization of the inductive and capacitive effects since only the minimum of two conductors per core are necessary. Also, speed is advantageously affected by the higher, non-coincident drive currents that are utilized.

The 3D memory is characterized by a larger number of conductors threading each core and distinctively different from the 2D memory in that each bit in a particular word lies within a separate core plane of X,Y dimension. The number of bits required in the data word then dictates the number of planes required in the Z axis direction. Hence, the designation of 3D or 3-dimensional organization is appropriate.

The 2-1/2D organization attempts to combine the best features of both the 2D and 3D memories. Essentially the 2-1/2D uses a coincident current read which is similar to the 3D and a linear select write system found in the 2D memory. The coincident current read provides a level of logic decoding within the core matrix itself, thus reducing cost of external electronic decoding, while the linear select write provides high drive currents for fast core switching. In addition, the word capacity is normally doubled by the expedient of doubling the number of core planes with only a small increase in the associated electronics. This is accomplished by the use of a phasing technique for one dimension of drive current.

The selection of a particular type of core memory is based on volume, weight and power vs total bit capacity. The 3D memory is the best choice as it requires much less power and weight than the other two organizations.

- Magnetic Tape Recorders - Tape recorders are well known storage mediums in spacecraft applications. The amount of storage required for this

application calls for an endless loop type of recorder.

- o Plated Wire Memories - A more recent development than the magnetic core memory is the planted wire memory. The basic memory element consists of an elemental segment of plated magnetic material surrounding a conductive wire. A continuous wire plating process results in a continuum of these memory elements along the length of the wire. During the manufacturing process, a polarizing magnetic field is established so that the magnetic domains are lined up circumferentially around the wire substrate. Thus, the magnetic film may be easily magnetized in either rotative direction circumferentially, however, a not so easily magnetized component may be produced longitudinally along the length of the wire.

  The plated wires are arranged in parallel in a single plane and another set of parallel wires, without a magnetic coating, are interwoven orthogonally. Information is read into the magnetic film by applying currents of proper direction and amplitude to the orthogonal wire sets. Readout is accomplished by applying current to only the noncoated wire, while the coated wire provides the second function of acting as an output sense windings. The memory plane is thus similar to a 2D or word organized memory utilizing magnetic cores.

- o Comparison of The Three Candidate Storage Devices - Both the 3D core and plated wire memories are ideally matched to the delay storage requirements of synchronous read and write operation and a non-variant and predictable delay line. The endless loop magnetic tape can not meet these requirements due to the jitter characteristics. A disadvantage of the plated wire memory is its sensitivity to shock and vibration that would tend to disqualify it from space applications at this time pending further development. It is therefore concluded that a magnetic core storage is ideally suited for the CB storage subsystem. Figure 5.5-36 presents a summary of the parameters associated with each memory type considering the requirements listed under functional and technical requirements.

5.5.6 Interconnection with Entry Science Package - During the early mission(s) the Capsule Bus will carry an Entry Science Package which contains a separate telemetry subsystem operating in a separate UHF data link via the spacecraft. The Entry Science Package operates simultaneously with the Capsule Bus during the last ten minutes prior to touchdown, when the critical entry and landing

CANDIDATE STORAGE DEVICES

MEMORY TYPE	SIZE (cu in)	WEIGHT (lb)	POWER (watts)	PROBLEMS OF MEETING PHYSICAL ENVIRONMENT	ABILITY TO WITHSTAND STERILIZATION	CHOICE
3D Core Storage	400	6	10	Space Qualified	No Problems Foreseen	1
Plated Wire Storage	300	4	5	Not Space Qualified (Still Under Development)	Status Unknown	2
Endless Loop Tape Storage	500	7	2	Space Qualified	Tape and Lubrication Materials Under Development	3

Figure 5.5–36

phases take place. It is concluded that a significant gain in reliability can be achieved during the final descent phase by parallel transmission of CB data over the ESP link. The increase in bit rate for the ESP link is insignificant due to the high rate television data carried on that link.

Conversely, all low rate ESP data may be transmitted in parallel over the CB link. This increases the required data rate by approximately 50%, leading to a corresponding increase in the CB transmitter power or decrease in link margin. The link has been sized to accommodate this additional data (Section 5.5.1) in order to take advantage of this functional redundancy for the ESP low rate experiments.

The data path through the CB link allows operational flexibility for the start-up of the ESP link. This may be useful since the low-rate ESP data is significant from the start of the entry mode, while entry television is not required until much lower altitudes.

5.5.6.1 Configuration Trade Study - A trade study was performed on several CB/ESP telemetry configurations to determine the most desirable degree of integration of the two telemetry subsystems. This trade study is summarized in the following paragraphs.

Design Approaches - Three alternate CB/ESP telemetry signal flow configurations were considered. The first configuration, Alternate 1, assumes no interface between the CB and ESP telemetry subsystems, i.e., autonomous CB and ESP telemetry subsystems. Alternate 2 provides a partial integration of the CB and ESP telemetry subsystems. The third configuration provides a high degree of integration. Abbreviated flow diagrams of the three alternate configurations are depicted in Figures 5.5-37, 38 and 39 respectively.

In the Alternate 1 configuration, each subsystem has its own programmer. Since alternates 2 and 3 are integrated, either a single, common programmer located in the CB or dual programmers may be used in these configurations. In the latter configuration the CB programmer must provide the sync for the ESP unit.

Alternate 1 configuration allows complete standardization of the CB (no CB/ESP interface). Deletion of the ESP in post '73 missions then has no effect upon the CB. In Alternates 2 and 3 the CB is affected by deletion of the ESP because of the data paths between the two telemetry subsystems. Since the primary CB telemetry data path, including delay store, is contained within the CB, dele-

SIMPLIFIED CB/EP DHS CONFIGURATION (ALTERNATE 1)

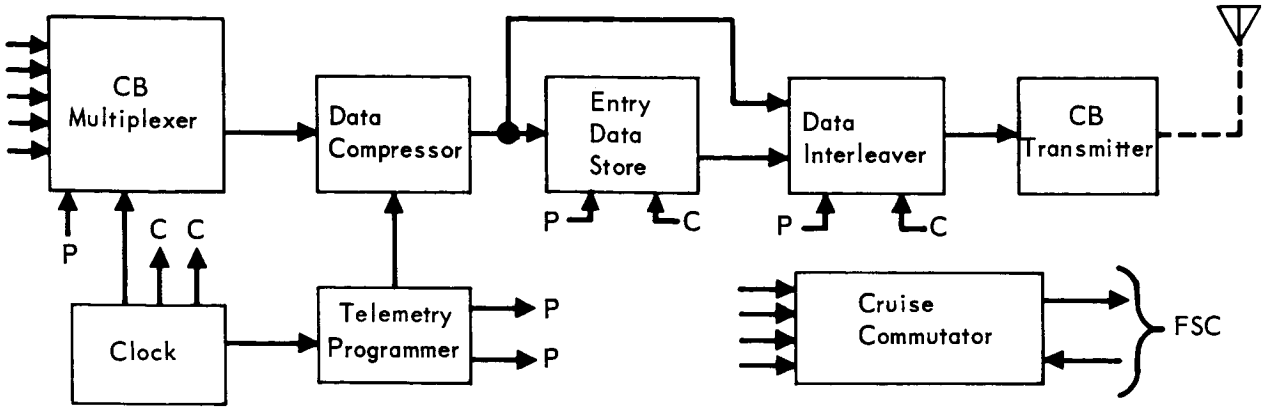

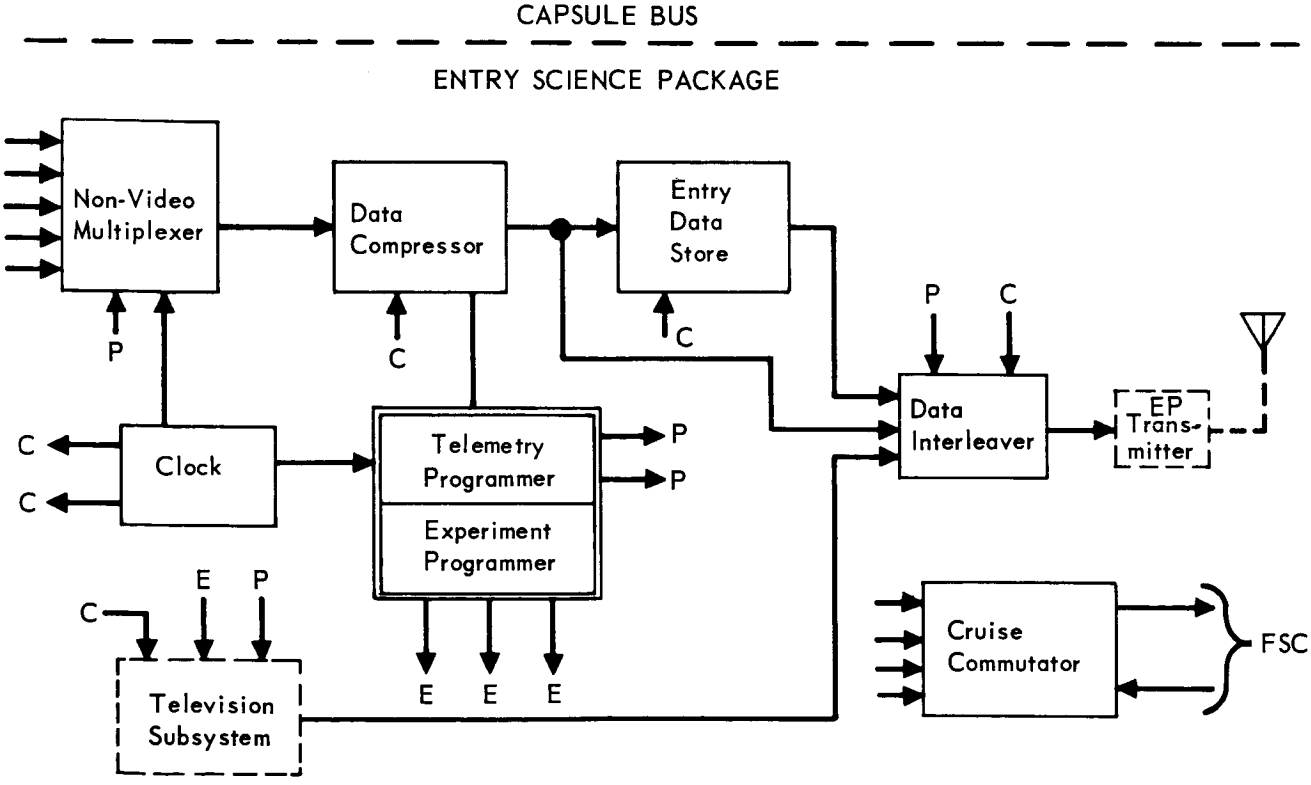

Figure 5.5–37

SIMPLIFIED CB/EP DHS CONFIGURATION (ALTERNATE 2)

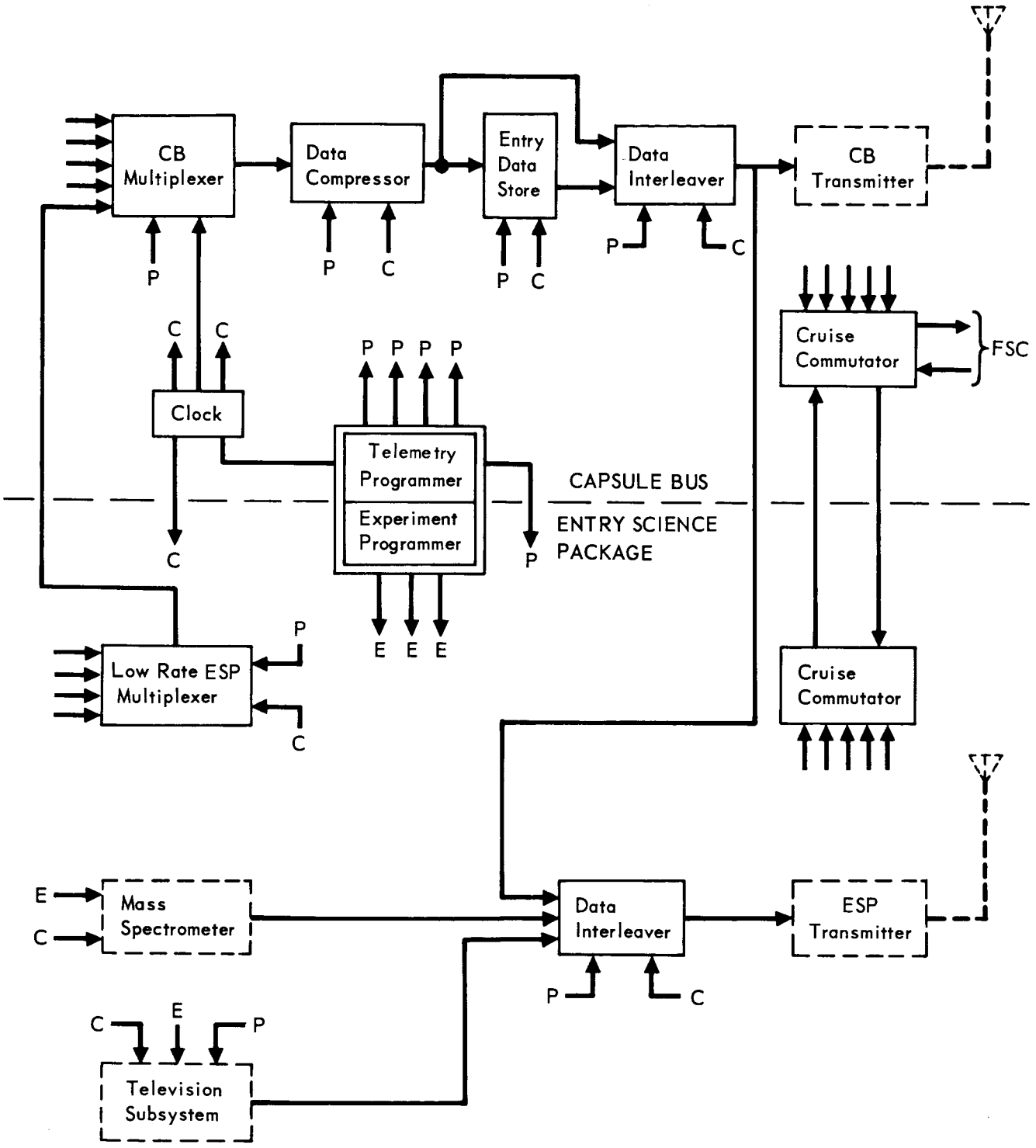

Figure 5.5–38

SIMPLIFIED CB/EP DHS CONFIGURATION (ALTERNATE 3)

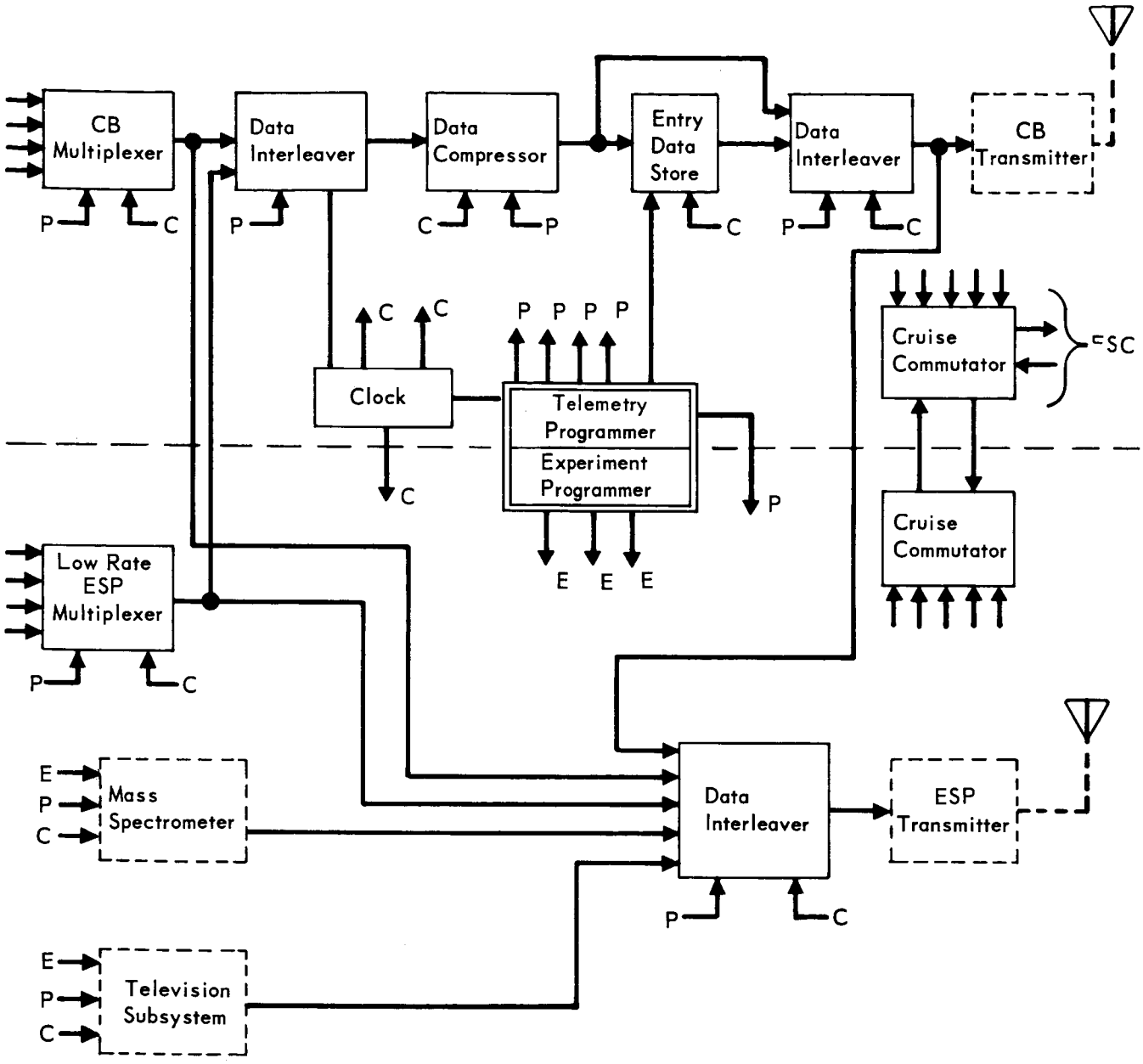

Figure 5.5–39

tion of the ESP only severs the redundant data paths. The CB is then standardized except for the deletion of the ESP interface cables and connections.

In alternates 2 and 3 the CB transmitter is sized for both the CB and ESP low-rate data. When the ESP is deleted, this 50% overcapacity is available for growth.

Selection Factors - Factors used to evaluate the alternate configurations are: probability of mission success, subsystem performance, versatility and program management aspects. The weighting associated with each of these four factors is presented in the following paragraphs.

Mission success for the CB/ESP telemetry subsystem can be defined in terms of the percentage of total data which can be successfully acquired, processed and delivered to the transmitters or FSC support system. Of the many factors which can affect mission success, reliability was considered the most significant. Reliability considerations include probability of component survival, graceful degradation capabilities and alternate functional path availability. Reliability was assigned the highest weighting coefficient of all comparison factors; 0.45.

The most important factors in subsystem performance include weight, power and data transmission rate requirements. These factors were assigned a combined weighting coefficient of 0.3.

The major versatility design considerations include the ease of accommodating changing requirements (both intra-mission and inter-mission), and the ability to assist other subsystems in performance of their assigned tasks. Versatility was assigned a weighting coefficient of 0.15.

Evaluation - In the evaluation of the candidate configurations, both the CB and ESP telemetry subsystems were considered simultaneously. Each composite (CB/ESP) configuration was graded according to its ability to satisfy each criterion presented in the previous section, and the grades weighted by the appropriate factors presented above. The weighted grades for each configuration are then summed to indicate configuration preference.

The evaluation of the reliability of the candidate configurations is based on the probability that a specified quantity and type of data can be successfully delivered to a user subsystem. This probability in turn is determined using the results of detailed reliability analyses of the candidate systems. In the evaluation the CB engineering data was weighted highest. ESP low rate measurements were rated slightly less important than the CB data because some atmospheric data can

be obtained by the CB. Although the entry television data is significant, it si rated less important than the CB engineering data and ESP low-rated measurements. The lowest weighting coefficient was assigned to mass spectrometer data because the SLS may provide some back-up capability for this experiment.

The reliability analysis indicates that the alternate functional path configurations do not offer the highest probability of successful data acquisition. However, the integrated systems provide better graceful degradation characteristics, resulting in higher overall reliability evaluation, since probability successful data acquisition and graceful degradation were weighted equally in the evaluation.

The physical characteristics of the candidate approaches is given in Figure 5.5-40. By assigning ralative value weightings to a compositive value for subsystem performance was derived. Included in the weight considerations is the inherent reduncancy which minimizes the need for more weight to eliminate single-point failures.

Some versatility has been provided in all of the candidate configurations by a stored program control which permits limited modification during in-flight checkout. The more complex systems have greater versatility because the alternate functional path capability results in a greater chance to find and initiate by command alternate data paths in the event of an in-flight preseparation failure. Perhaps the most important versatility aspect provided in the interlaced CB/ESP system is the reduction of RF multi-path interference through use of frequency diversity techniques.

Cost differences between configuration should be slight. None of the candidate configurations involve high risk items. However, the more complex systems will be slightly more expensive to produce and have a somewhat greater possibility of schedule slippage.

The use of a common programmer located in the Capsule Bus or separate programmers for the CB and ESP were considered separately. Separate programmers for the CB and ESP, with CB programmer sync provided to the ESP unit, were selected because of the greater reliability provided and fewer interfaces required. Fewer interfaces facilitate the standardization of the CB for future mission in which the ESP is not included. These factors outweigh the small increase in power

CB/EP DHS PHYSICAL CHARACTERISTICS TRADE STUDY

DHS PHYSICAL CHARACTERISTICS	MATRIX OF DESIGN APPROACHES				
	Alternate 1	Alternate 2 Common Programmer	Alternate 2 Dual Programmer	Alternate 3 Common Programmer	Alternate 3 Dual Programmer
Power Requirement Weighting = 0.4	12.7 W 0.32	11.0 W 0.39	13.6 W 0.30	10.3 W 0.40	13.4 W 0.31
Weight – 0.25	22.2 lb 0.20	18.0 lb 0.25	22.0 lb 0.20	20.1 lb 0.22	24.3 lb 0.19
Inherent Redundancy Weighting = 0.45	0 0	0.5 0.08	0.6 0.09	0.9 0.14	1.0 0.15
Transmission Rates CB Low Rate Weight = 0.05	119 bps 0.04	105 bps 0.05	105 bps 0.05	112 bps 0.05	112 bps 0.05
CB High Rate Weight = 0.05	1428 bps 0.05	1575 bps 0.05	1575 bps 0.05	1568 bps 0.05	1568 bps 0.05
ESP Rate = 0.1	51K bps 0.1	54K bps 0.09	54K bps 0.09	53,424 bps 0.1	53,424 bps 0.1
Total Value	0.71	0.91	0.78	0.96	0.85

Figure 5.5–40

and weight relative to the total CBS/ESP power-weight requirements.

Selected Configuration - Separate programmers for the CB and ESP, with CB programmer sync provided to the ESP unit, were selected because of the greater reliability provided and fewer interfaces required. The comparative evaluation of candidate configurations with separate programmers is summarized in the comparison matrix of Figure 5.5-41. Alternate 3 was selected as the preferred functional configuration.

The preferred approach includes an entry data store in the ESP in addition to the entry data store in the Capsule Bus. Thus an alternate path for data accumulated during blackout is provided, (See Section 5.5.1.4) and loss of blackout data due to catastrophic failure of an entry data store is precluded. Dual time delay storage is used in the baseline system instead of the single delay assumed in the trade study. However, the validity and conclusions of the trade study are unaffected by these enhancements.

5.5.6.2 Interleaving - Figure 5.5-42 shows the equipment required to interleave the CBS and ESP data. The purpose of this analysis is to determine what type(s) of data interleaving will be most satisfactory from a synchronization viewpoint.

Three types of interleaving will be considered: Frame, word, and bit interleaving. Frame interleaving uses the simplest logic at the receiver to de-interleave the data stream, requiring only the sensing of the frame sync word in consecutive bits to steer the data frame to the correct location for decoding. It will normally require storage prior to interleaving for the bit streams not being gated.

Bit interleaving doesn't require storage prior to interleaving, but the de-interleaving logic is generally more complex. The "one-one" case is degenerate, i.e., the de-interleaving logic is trivial; but the general case of n bits of one bit stream to m bits of the other requires the search for the respective frame sync words to take place over non-consecutive bits of the data stream. Given that at least one of the frame sync words is in the decommutation shift register, the shift register length, L, is defined between

$$\left\{(x/n)-1\right\}\ (m+n)\ +n \leq L \leq \left(\frac{x}{n}\right)(m+n);\quad (x/n \geq y/m)$$

(where x is the sync word length in n data stream and y is the m sync word), to guarantee a long enough shift register to find either sync word.

CB/ESP TELEMETRY COMPARISON MATRIX

FUNCTIONAL AND TECHNICAL DESIGN REQUIREMENTS	MATRIX OF DESIGN APPROACHES			SELECTION
	ALTERNATE 1	ALTERNATE 2	ALTERNATE 3	
Accepts signals from Engineering and scientific sensing devices; samples, processes and formats data for transmission.	Autonomous Systems 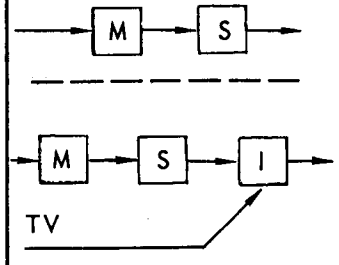	Partially Integrated Systems 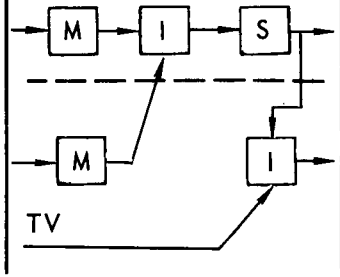	Fully Integrated System 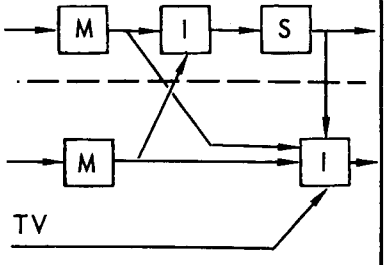	Select Alternate 3
	Legend: I – Interleaver, M – Multiplexer, S – Storage			
Reliability	0.50 0.24	0.76 0.36	0.95 0.45	3–2–1
System Performance	0.71 0.24	0.78 0.275	0.85 0.30	3–2–1
Versatility	0.10	0.13	0.15	3–2–1
Management	0.10	0.085	0.075	1–2–3
	0.69	0.85	0.975	

Figure 5.5–41

TELECOMMUNICATIONS EQUIPMENTS – DESCENT PHASES

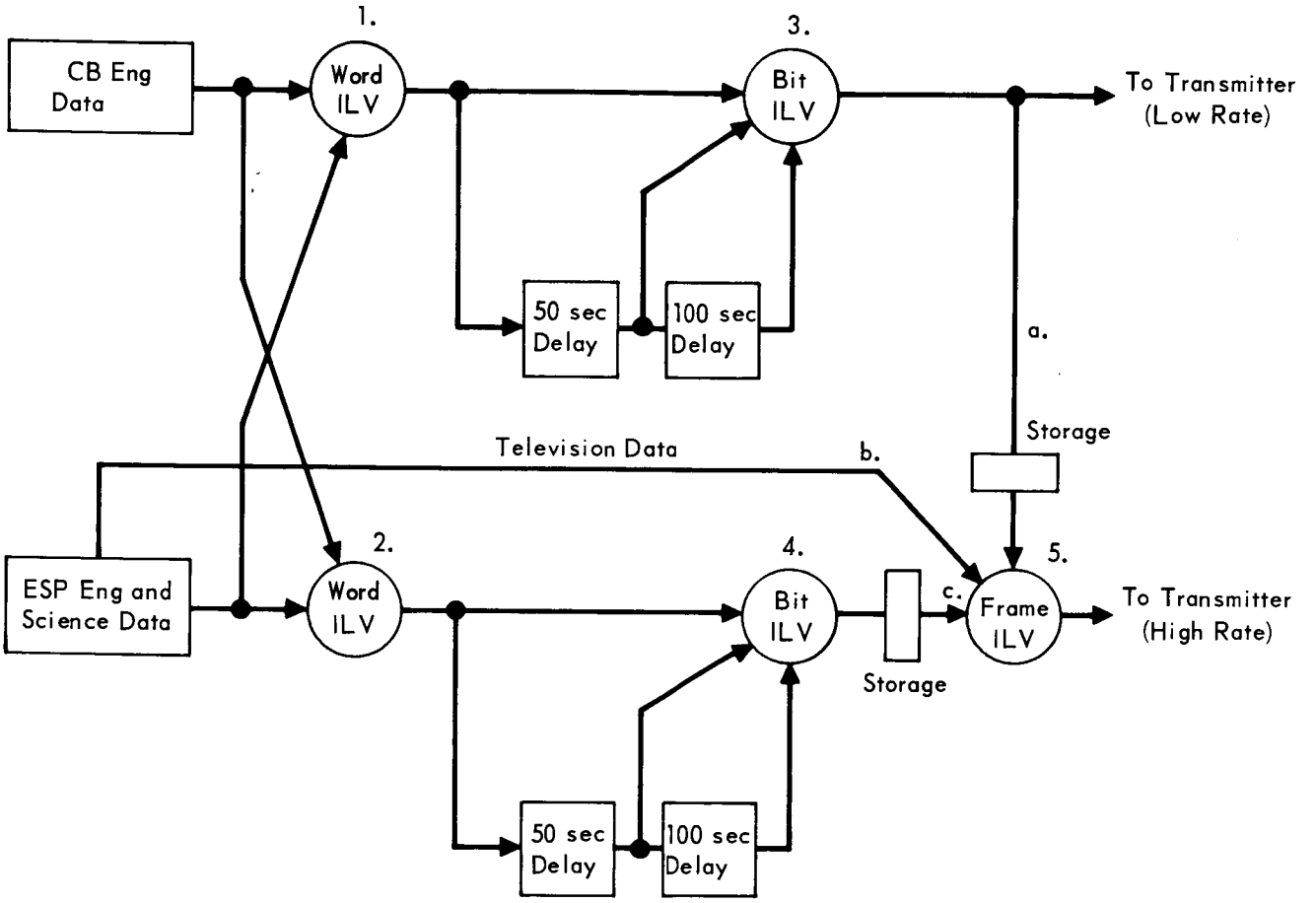

Figure 5.5–42

Word interleaving requires some storage for the bit streams not being gated, but not nearly as much as for frame interleaving. The logic requirements for de-interleaving are much the same as for bit interleaving; frame sync must always be searched for in non-consecutive bits of the data stream.

Interleavers 3 and 4 of Figure 5.5-41 are designated bit interleavers because the data is in the ratio 1:1:1; in fact the data streams are identical except for relative timing delays. Interleavers 1 and 2 may be either bit or word interleavers dependent upon the commutation formats. Interleaver 5 is shown as a frame interleaver because the relative data rates of the three data streams is $(a = c)/b \approx 1/200$, which would cause the shift register lengths (and associated logic) for either the bit or word types to be excessive.

The designation frame interleaver covers several variations. One variation is to have definite locations within the television frame for data from data streams a and c. A second approach is to identify data from all streams with adequate address bits for de-interleaving purposes. Still another approach is to interleave complete frames of data from each bit stream. The first approach would not add any bits to the data stream (and therefore does not increase the transmission rate), but will be inflexible to future changes in the system. The second will provide great flexibility for the future at the cost of the address bits, but will not create any problems on frame sync or timing, as the third approach will. The first approach is the preferable one.

5.5.7 Use of Data Compression - The preferred telemetry subsystem described in Part A does not include data compression. Preliminary investigations indicate the desirability for further study leading to a possible incorporation of form of data compression, to circumvent aliasing errors.

Data compression utilization on the CBS and on portions of ESP data streams would not be included to reduce communications rates but to enhance subsystem performance by providing a higher tolerance to the effects of uncertain environmental factors. System design and operation is as follows: A typical instrumentation list defines the sample rate requirements based on expected vehicle performance in an assumed environment. If these sample rate requirements are underestimated, significant measurement errors may be introduced; on the other hand if the sample rate requirements are adequate, sampling at higher rates would result in unnecessary data transmission.

The CBS multiplexer sampling rates would be increased to about ten times the required rate. The data compressor will accept this data, separate those samples which would have been provided by a lower-speed multiplexer, and output them without modification. In addition, an appropriate compression algorithm (for example, a First-Order Interpolation) will be applied to the remaining samples. If the original sample rate requirements are adequate, the compressor will produce no additional data; if the slow speed sampling becomes inadequate, the compressor will store additional samples of excessively active channels for subsequent transmission. By increasing the communication link capability about 10%, the data compressor output frame format would include all required data samples, followed by an additional 10% of compressed data samples. For example, if the required sample rate were 100 sps, (samples per second) the compressor output would be 110 sps (the first 100 time slots being the required samples and the last 10 containing any excess samples produced by the compression algorithm). Thus, if the highest sample rate per channel required were 1 sps, at least ten channels could be adaptively increased to 2 sps; similarly one channel activity is not excessive, even greater adaptivity can be expected.

The calculated data compressor failure rate is about 2.81%/1000 hours, based on the parts count for existing ground data compressors capable of performing similar operations. Obviously, this reliability figure can vary as a function of the compressed data store (buffer) capacity but it is not likely to become a poor risk item. If the multiplexer is designed to operate at both the required sample rates and an order of magnitude faster, the data compressor could be by-passed by ground command any time prior to Capsule Bus separation.

REFERENCES

5.5-1 FCC Rules and Regulations Vol. II, Part 2, Frequency Allocations, May 1966 (Revised), pp 32-37.

5.5-2 Private Communication with D. Schweizer, Department 613-1 of SRSD Philco-Ford at L.A.R.S. Cape Kennedy.

5.5-3 R. M. Goldstein and W. F. Gillmore: Radar Observations of Mars, Science, Vol. 141, pp 1171-1172, 20 September 1963

5.5-4 R. B. Dyce: Recent Arecibo Observations of Mars and Jupiter, Radio Science, Vol. 69D, pp 1628-1629, December 1965.

5.5-5 Selected Studies of VHF/UHF Communications for Planetary (Mars/Venus) Relay Links, Final Report, prepared by Astro-Electronics Division, Defense Electronic Products, Radio Corporation of America, Princeton, New Jersey, under Contract No. NAS 2-3772, AED R-3091; 15 January 1967

5.5-6 G. Schoreder: Noncoherent Binary FSK in Slow Fading, McDonnell Douglas Corporation; I.O.M. 413-AT-70820, 10 August 1967

5.5-7 A. B. Glenn and G. Lieberman: Effect of Propagation Fading and Antenna Fluctuations on Communication Systems in a Jamming Environment, IRE Transactions on Communications Systems, March 1962.

5.5-8 G. L. Turin: Error Probabilities for Binary Symmetric Ideal Reception Through Nonselective Slow Fading and Noise, Proc. of IRE, September 1958.

5.5-9 W. C. Lindsey: Error Probabilities for Rician Fading Multichannel Reception of Binary and N-ary Signals, IEEE Transactions on Information Theory, October 1964, pp 339-350.

5.5-10 C. A. Hinrichs: Martian Entry Fading, McDonnell Douglas Corporation, VN-11.2.1-4 (DELS), 29 April 1967.

5.5-11 L. Schuchman: Wideband Detection of MFSK Transmission in a Two-Path/ Multipath Channel, Philco Ford TM 119, 14 July 1967

5.5-12 J. C. South: Program Description of Appropriate Solution for Supersonic Flow Past Blunt Bodies with Sharp Sonic Corners, Langley Working Paper NWP-240, 12 July 1966.

5.5-13 C. D. Joerger, H. J. Fivel, G. G. Grose, J. F. Fox: The Effect of Ablative Products on Gemini Reentry Communications, Final Report Contract No. NASw-1209, April 1966.

5.5-14 M. R. Denison and E. Baum: Compressible Free Sheer Layer with Finite Initial Thickness, AIAA Journal, February 1963.

5.5-15 VOYAGER Technical Memo 4.1-19 (LQ), 5 July 1967.

5.5-16 A Feasibility Study of an Experiment for Determining the Properties of the Atmosphere, Vol. 3, Book 1, AVCO Corporation, 1 September 1966.

5.5-17 W. C. Lindsey: Error Probabilities for Rician Multichannel Reception of Binary and N-ary Signals, IEEE Transactions of Information Theory, October 1964.

5.6 POWER SUBSYSTEM - The power subsystem provides electrical power during periods of the interplanetary cruise when Flight Spacecraft power is unavailable, during the descent to the surface of Mars, and during the period of post-landed Capsule Bus operation. For 1973, the preferred subsystem uses manually activated silver-zinc batteries for the main electronic loads and automatically activated silver-zinc batteries for high current loads such as solenoids and pyrotechnics. Both have been demonstrated to be heat sterilizable. Each subsystem will provide voltage regulators internally in order to prevent a single failure from affecting the whole capsule. The power subsystem must provide 1700 watt-hours during the Capsule Bus mission which is based on a 6 hour de-orbit time. Peak power output is estimated to be 1550 watts; weight is estimated to be 107 lb.

5.6.1 Requirements - The electrical energy which must be provided for Capsule Bus equipment operation is strongly dependent upon the de-orbit time. The electrical power requirements of the Capsule Bus equipment are shown in Figure 5.6-1. This is the maximum amount of energy required from the main Capsule Bus battery for the normal mission profile selected for the McDonnell design. The total energy required from the Capsule Bus power source is shown in Figure 5.6-2. A power profile showing the power levels which must be provided from the power subsystem is shown in Figure 5.6-3.

5.6.2 Alternate Approaches and Selection - Candidate power sources for providing the electrical power and energy requirements of the Capsule Bus include the following:

a. Manually activated AgZn batteries for the electronic equipment loads and automatically activated batteries for the high current descent engine solenoid and valve loads.
b. Automatically activated AgZn batteries capable of providing both the equipment and high current loads.
c. Silver cadmium batteries for the electronics equipment and automatically activated AgZn batteries for the high current loads.
d. Nickel cadmium batteries for the electronics equipment and automatically activated AgZn batteries for the high current loads.
e. Hydrazine powered turbine-alternator unit for the electronics and automatically activated AgZn batteries for the high current loads.
f. Hydrazine powered turbine-alternator unit sized to provide all of the requirements.

CAPSULE BUS BASELINE MISSION ELECTRICAL POWER REQUIREMENTS

EQUIPMENT	LAUNCH AND MIDCOURSE CORRECTION (3 HR)		CRUISE		PRE-SEPARATION (1.0 HR)		ORBITAL DESCENT (6 HR)		ENTRY (10 MIN)		TERMINAL DE-CELERATION (1.5 MIN)		POST LANDER PERIOD (10 MIN)	
	Watts	WH	Watts	WH	Watts	WH	Watts	WH	Watts	WH	Watts	WH	Watts	WH
PART A														
Telecommunications							30	2.5	30	5	30	0.8	30	5
Radio Subsystem					30	4.5	30	180	30	5	30	0.8	30	5
Telemetry Subsystem														
Telemetry Equipment	1.5	4.5	1.5	*	5	0.8	5	30	5	0.9	5	0.1	5	0.9
Instrumentation Equipment	3	9	3	*	21	3.5	21	126	21	3.5	21	0.6	21	3.5
Data Storage Subsystem							7	1.6	7	1.2	7	0.1	7	1.2
Command Decoder	1.4	0.5	1.4											
Radar Subsystem														
Landing Radar														
Antenna Assembly									59	9.6	59	1.5		
Electronics Assembly									86	13.9	86	2.2		
Radar Altimeter														
Electronics									40	1.83	40	1		
Guidance and Control Subsystem														
Inertial Measurement Unit			–		45	45	45	270	45	7.5	45	1.2		
Guidance and Control Computer			–		61	61	61	22.0	61	10.2	61	1.5		
Power Supply			–		24	24	24	144	24	4	24	0.6		
Sequencer and Timer			–		14	14	14	84	14	2.4	14	0.4	14	2.4
Thermal Control Heaters			85				65	390						
Power Subsystem														
Battery Charger			8											
Converter Regulator			25											
Power Switching and Logic Unit	2	6	2	*	2	2.0	2	12.0	2	0.4	2	0.1	2	0.4
Line and Diode Losses (6%)	0.5	1.2	7.6		12.1	9.3	18.2	76	25.5	3.9	25.5	0.7	6.6	1.1
Totals	8.4	21.2	133.5		214.1	164.1	322.2	1338.1	449.5	69.3	449.5	11.6	115.6	19.5
Sterilization Canister Equipment														
Cruise Commutator	0.8	2.4	0.8	*										
Instrumentation Equipment	2.1	6.3	2.1	*										
Dual Battery Charger			5	*										
Dual Separation Programmer														
Thermal Control Heaters	3	18	3	*										
Line and Diode Losses (6%)	0.6	1.6	0.6											
TOTALS	6.5	28.3	11.5											
PART B														
Pyrotechnics and Solenoids														
Pyrotechnic Initiators							360							
Attitude Control Thruster Drivers							128	3.5	128	0.3				
Descent Engine Throttle Valves											642	16.1		
Descent Engine Valve Solenoids											360	9.0		
Line and Diode Losses (8%)							39.1	0.28	10.2	0.02	80	2.0		
Totals							527.1	3.78	138.2	0.32	1082	27.1		

* Continuous Operation

Figure 5.6–1

CAPSULE BUS ELECTRICAL ENERGY REQUIREMENT VS ORBITAL DESCENT TIME

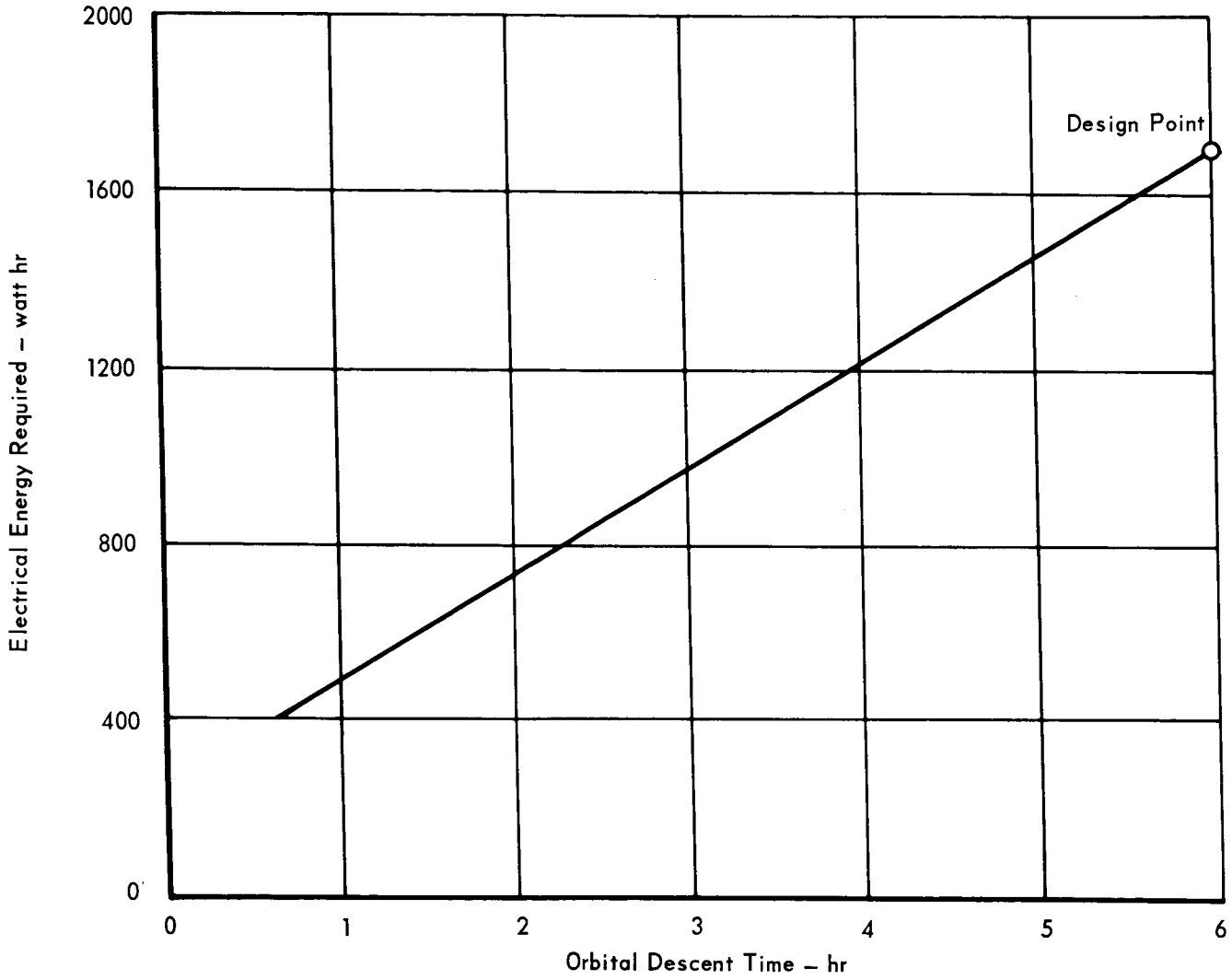

Figure 5.6–2

CAPSULE BUS BASELINE MISSION ELECTRICAL POWER PROFILE

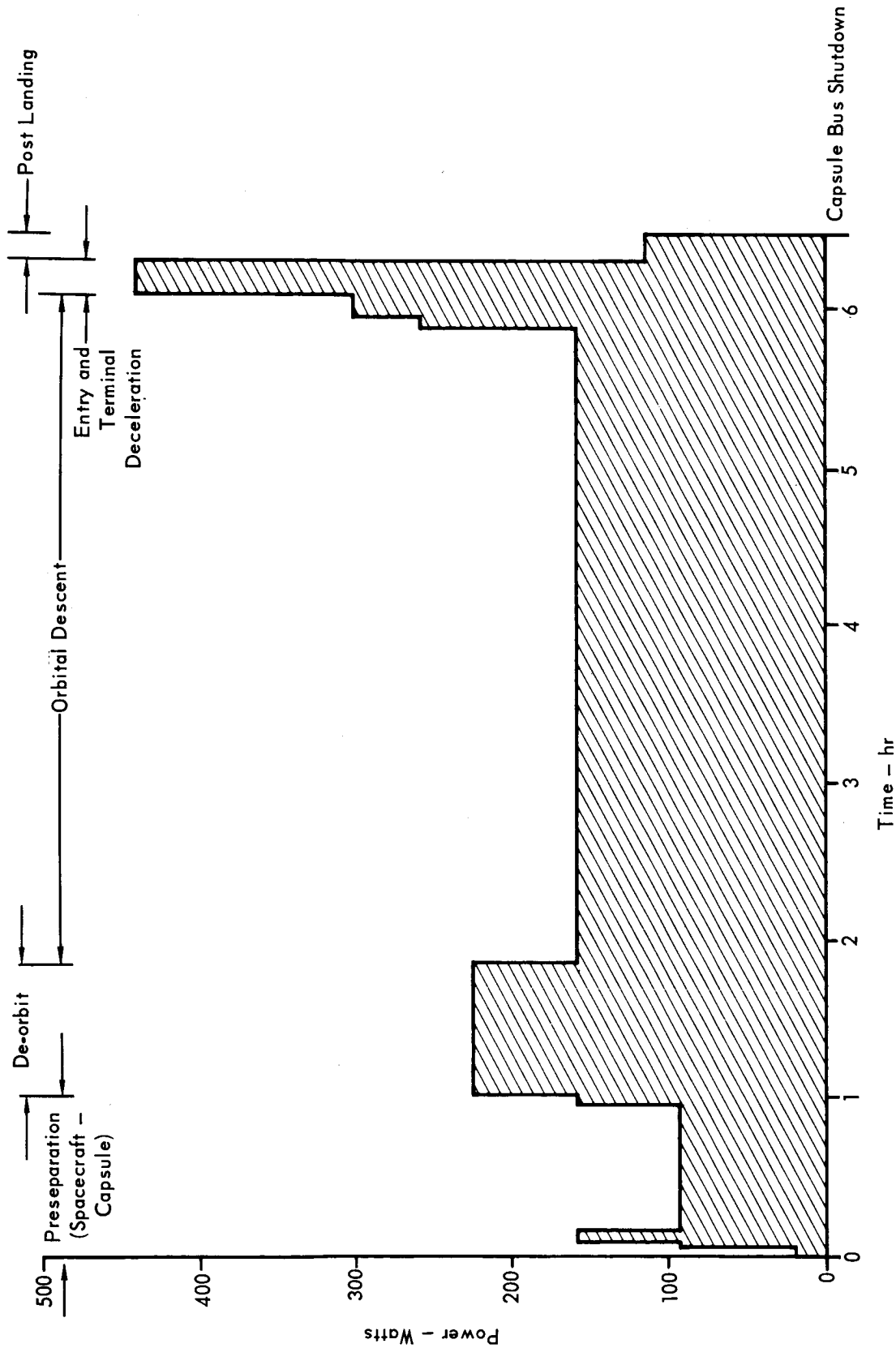

Figure 5.6–3

The weights of power sources designed to meet the Capsule Bus requirements are shown in Figure 5.6-4 plotted against the required de-orbit time. Characteristics of these sources are shown in Figure 5.6-5. Of these, the manually activated AgZn battery was the lightest of the battery systems to meet the Capsule Bus requirements. The use of a hydrazine powered turbine alternator unit offers the lightest weight approach but contributes to contamination of the Martian surface.

5.6.2.1 Automatically Activated Batteries for High Current Loads - The alternative that uses manually activated AgZn batteries for the electronics loads and automatically activated AgZn batteries for high current terminal propulsion solenoid and valve loads, being the lightest battery system, was selected as the preferred approach. Providing all of the requirements from a single manually activated battery was rejected because it would require discharge of the battery at about the one hour rate after removal of 90% of the battery capacity. This would necessarily make the battery a thin plate design and would result in a low energy density. The use of automatically activated batteries for providing the high current loads of the terminal descent engine solenoids and servovalves also allows their use for initiating pyrotechnics in the Capsule Bus without significantly affecting the high-current battery size. This approach eliminates the need for capacitor discharge circuits in the Capsule Bus, which would weigh 12.5 pounds. The development of heat sterilizable, automatically activated batteries has been carried to the point that heat sterilization of the battery without the battery activator has been demonstrated for a 120 hour period. This work was carried out by the Electric Storage Battery Co.. Four battery packs of twenty one 0.75 ampere-hour cells each were subjected to the heat sterilization environment at 135 degrees centigrade for 120 hours. The batteries were then pressure checked and activated. All batteries gave expected performance at the Ag_2O level.

Heat sterilizable gas generators for automatically activated batteries have been developed by Unidynamics, a division of the Universal Match Co. These devices have demonstrated the capability of surviving $300^{\circ}F$ for 168 hours with no appreciable effect on its characteristics.

The battery activator has not been subjected to heat sterilization. A tube type activator made of stainless steel or copper with silver diaphragms, has been proposed by the Electric Storage Battery Co. for this application. The development of such a battery activator is not considered to be a major development problem.

CANDIDATE CAPSULE BUS ELECTRICAL POWER SOURCES

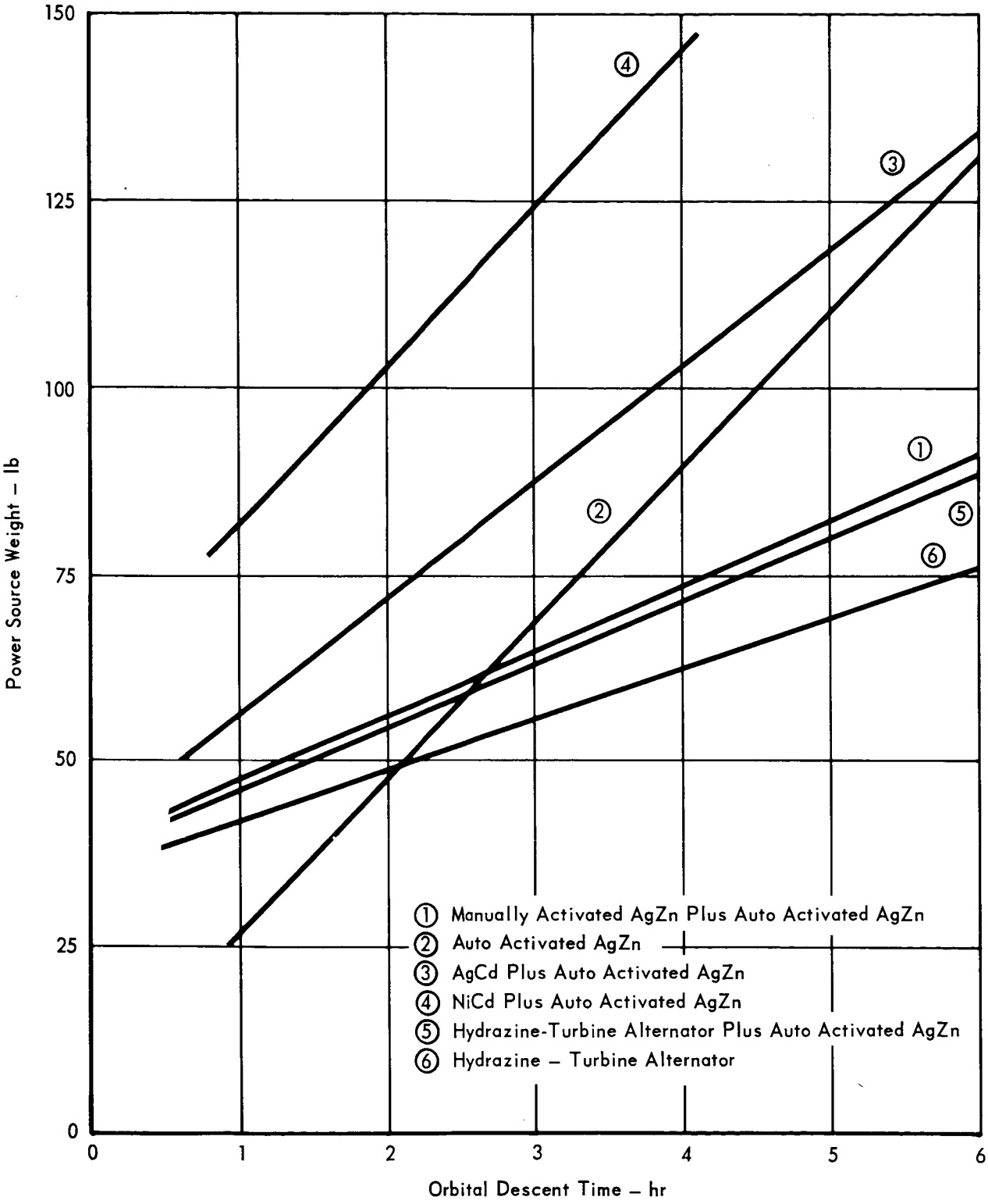

Figure 5.6–4

COMPARISON OF POWER SOURCES FOR THE CAPSULE BUS

PARAMETER \ POWER SOURCE	MANUALLY ACTIVATED AgZn BATTERY	AUTOMATICALLY ACTIVATED AgZn BATTERY	SILVER CADMIUM BATTERY	NICKEL CADMIUM BATTERY	HYDRAZINE POWERED TURBINE ALTERNATOR
Watt Hours/lb	25	13	16	10	4.0 (1000 watt hours)
Watt Hours/cu in.	1.7	1.0	1.7	1.3	1.3
Watts/lb	6–7	20–30	8–9	10–12	40 (600 watt unit)
Voltage Regulation	1.3 to 1.86 volts/cell	1.4 to 1.6 volts/cell	0.9 to 1.4 volts/cell	1.0 to 1.4 volts/cell	28 Vdc ± 1%
Storage Life	1 yr	3 yr	2 yr	5 yr	> 1 yr
Heat Sterilizable	Yes	Yes	Yes	Yes	Yes
Cost	Low	Low	Low	Low	High
Surface Contamination	No	No	No	No	Yes

Figure 5.6–5

5.6.2.2 Sealed Battery Energy Density and Wet Stand Condition - Review of development work on sealed, sterilizable, long wetlife, AgZn batteries indicates that significant advances have been made in this technology. The design and performance parameters used for sizing the Capsule Bus main battery are conservatively estimated on the basis of accomplishments of three battery development programs. These are: (1) a program conducted by the Electric Storage Battery Company to develop a battery using an organic separator material, (2) a program conducted by the Eagle Picher Company to develop a battery using an organic separator material, and (3) a program conducted by the Douglas Astropower Laboratory of the McDonnell Douglas Corporation to develop a battery using an inorganic separator material. All of these development programs have shown promising results. Cells of all three types have been heat sterilized at 135°C for approximately one sterilization period and have given satisfactory performance afterward. The design parameters of the cells which were subjected to heat sterilization testing are shown in Figure 5.6-6. A summary of the heat sterilization and wet stand tests is shown in Figure 5.6-7. Performance curves for these cells are shown in Figure 5.6-8. This figure also includes a curve for the Douglas Astropower cells, utilizing new separator materials, DE(F), which give significantly higher performance capability. Testing of cells using these separators is now in process at Douglas Astropower. These test results provide evidence of sterilizability of AgZn batteries. The energy density achieved in these test cells indicates that 20 to 30 watt hours per pound is achievable with discharge rates in the range of C/4 on small cells. Battery energy densities of 25 to 35 watt hours per pound therefore would be achievable on large capacity batteries in the range of 60 ampere-hours. A conservative figure of 25 watt-hours per pound was assumed for the Capsule Bus battery. This allows some weight contingency in the battery which may be used in solving the remaining development problems.

The Electrical Power Subsystem preferred design is described in Section 7. In that section, it is pointed out that charge/discharge cycling of the battery prior to heat sterilization is not presently planned. This is because of the limitations on the cell being developed by the Electric Storage Battery Co. This requirement stems from the possibility of zinc metal remaining in the negative plate causing excessive hydrogen pressure in the cells. This limitation is considered to be a major restriction on the sterilization and prelaunch operation because no battery performance checks are possible prior to terminal Flight Capsule sterilization. Discovery that the battery does not give satisfactory performance

DESIGN PARAMETERS OF STERILIZABLE CELLS TESTED

MANUFACTURER / DESIGN PARAMETERS	ESB MODEL 334	EAGLE PICHER	DOUGLAS ASTROPOWER
Capacity	40 amp hr	8 amp hr	2 amp hr
Separator	5-RA1-116	4 Pernion -307	Inorganic - Z (8)
Cell Case	Polyphenylene oxide	Polypropolene	Polyphenylene oxide
Type of cell	Sealed	Sealed - pressure relief	Sealed
Battery Case	-	Magnesium-sealed	-
Cells/Battery	-	6	-
No. of Cells Tested	7	12	16
Operating Temp	80°F	75°F	77°F

Figure 5.6-6

SUMMARY OF STERILIZABLE AgZn CELL AND BATTERY TESTS

MANUFACTURER / PERFORMANCE	ESB MODEL 334	EAGLE PICHER CO		DOUGLAS ASTROPOWER
		BATTERY NO. 1	BATTERY NO. 2	
Sterilization Environment	135°C-120 hr-1 cycle	145°C-36 hr-3 cycles		145°C-36 hr-3 cycles
Wet Stand Time	-	10 months	10 months	5 months-4 cells, 3 months-4 cells, 2 months-4 cells, 1 month-4 cells
Wet Stand Condition	-	Discharged	Charged	Charged
Discharge Rate	4 hr rate to 1.3 v/cell then 8 hr rate to 1.3 v/cell	4 hr rate to 1.25 v/cell	4 hr rate to 1.25 v/cell	7 hr rate for 1 hr then 2.7 hr rate to 1.0 v/cell
Energy Density	31.5 wh/lb	30 wh/lb	38 wh/lb	20.5 wh/lb*
Cycle Life Following Wet Stand (100% Depth)	-	2	16	2+

*Projected for optimized battery design

Figure 5.6-7

PLATEAU VOLTAGE OF STERILIZABLE AgZn CELLS

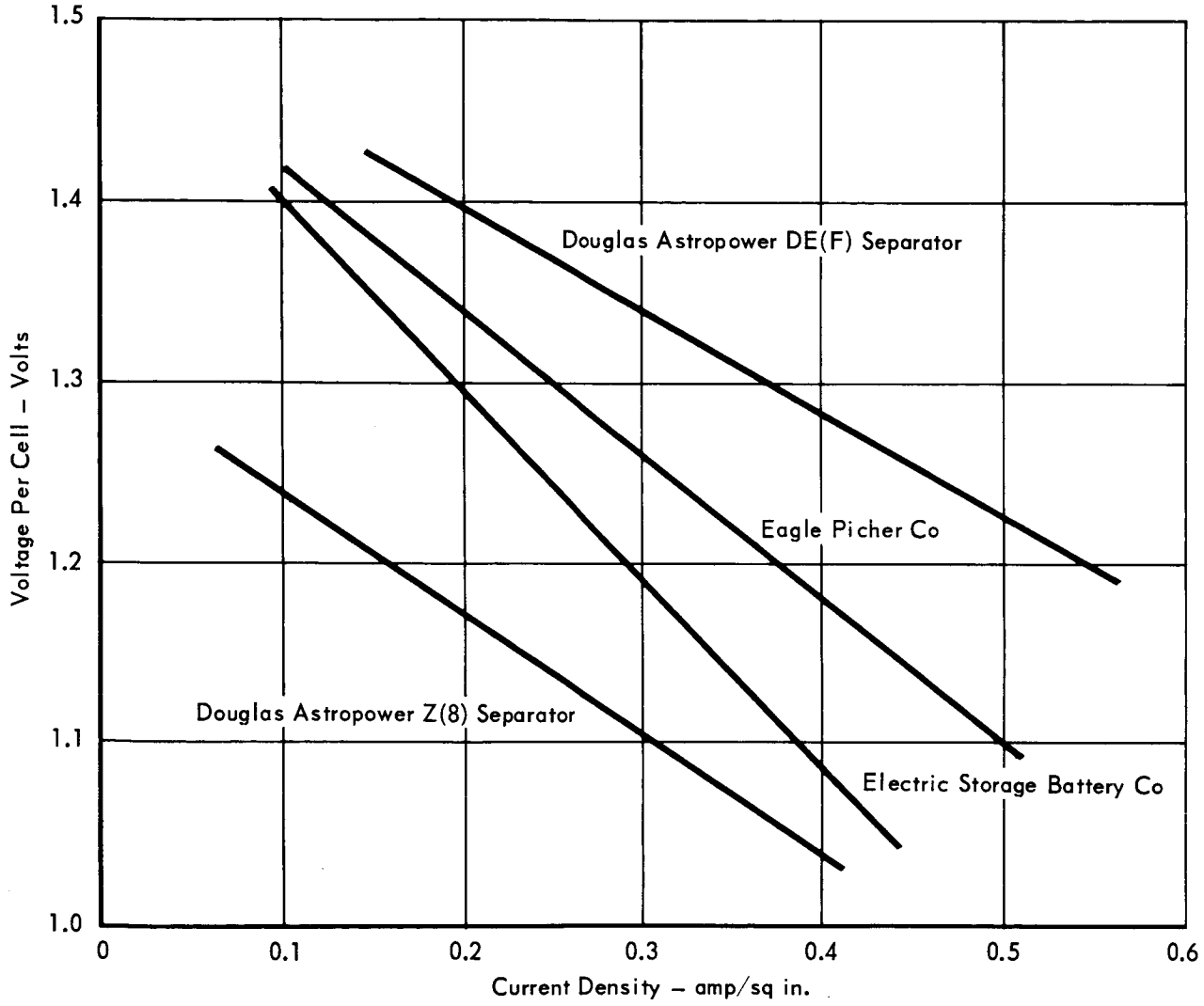

Figure 5.6–8

will require that the Flight Capsule be subjected to a second cycle of terminal heat sterilization with a new battery. Work performed on the Eagle Picher battery by the General Electric Co. demonstrated that this battery can survive the heat sterilization after charge/discharge cycling. Depending on future development in this area, this restriction may be removed at a later time; however, the present design concept is constrained to assume battery sterilization prior to formation charge.

An alternate approach to sealed AgZn battery wet heat sterilization is to be investigated by McDonnell under contract to NASA Marshall Space Flight Center. This work is to be accomplished under Contract NAS 8-31114. The objective of this work is to demonstrate dry heat sterilization of the battery pack, and filling and sealing of the cells in a sterile environment. This work may offer an alternate approach to wet heat sterilization although presently the approach does not meet the constraints of JPL SE003BB002-2A21, "1973 VOYAGER Capsule Systems Constraints and Requirements Document, Revision 2". This approach would require cooling of the battery during Flight Capsule terminal heat sterilization and decontamination of the battery case by ETO.

Only the quivalent of one cycle (120 hours) of heat sterilization at the Type Approval test temperature of 135°C has been demonstrated. The capability of these systems to survive longer periods at the Type Approval temperature is now known at this time and will require further testing. It is presently planned for the flight batteries to be installed at the launch facility prior to Flight Capsule terminal sterilization; the design of the Capsule Bus will allow easy access to the battery locations. Failure of equipment during or after terminal heat sterilization, necessitating a second heat sterilization cycle, may result in battery replacement depending upon what further battery development and testing indicates.

Selection of the preferred approach to battery storage during the cruise phase of the mission requires additional wet stand testing on AgZn cells. Eagle picher cells assembled into 6 cell batteries were tested by the General Electric Company. Eagle-Picher Batteries of Figure 5.6-8 survived a 10 month wet stand period after sterilization and, then, were cycled. The battery stored in a discharged condition yielded 98% of its initial capacity after the wet stand period, and has survived 11 additional cycles to date. The battery stored in a charged condition, after replacing the capacity loss, delivered 75% of its initial capacity after the wet stand period but failed to accept a charge after the second discharge.

Analysis of the cell indicates that failure was due to dehydration of the electrolyte caused by loss of hermetic seal. Increased electrolytec concentration is believed to have resulted in accelerated oxidation of the separator. These tests indicate that a battery of this construction on long wet stand in a discharged condition has a high probability of survival. Testing is considered desirable, however, to compare cell degradation in a charged open circuit condition, discharged condition, and stand on float charge.

Maintaining the Capsule Bus battery on continuous charge during cruise was selected as the preferred approach for the following reasons:

a. It is a lighter weight approach than open circuit charged stand since the battery need not be oversized to allow a 4% to 12% per month expected loss of capacity.

b. It is preferred over stand in a discharged condition since the battery is independent of the battery charger insofar as partial mission success is concerned.

c. Internal power must be provided within the capsule bus during periods when FSC power is not available to the FC. This power is required for cruise commutator and command decoder operation.

d. The power used for the battery charger operating in the float mode (1.87 volts per cell) is dissipated as heat in the CB, serving the same purpose as electrical heaters.

Battery Charger Selection - A two step float charge method of battery charging was selected, based upon work performed by NASA Goddard Spaceflight Center on this type of charger in tests of long cycle life AgZn batteries. This type of charger appears to offer a reduction in the cell degradation processes of zinc dendrite penetration of the cell separator and silver migration through the separator.

5.6.2.3 Power Switching - Provisions for turning on and off power to the CB subsystem was assigned to the electrical power subsystem PS&L, to minimize cabling weight within the CB and to allow maximum versatility in utilizing existing cabling for late design modifications on the 1973 mission equipment and design modifications which might be required on the 1975 and later vehicles. Location of these switching functions as well as secondary power distribution busses in the secondary PS&L units provide minimum cabling weight and maximum versatility.

5.6.3 Interfaces - The electrical Power Subsystem has interfaces with all other subsystems in the Capsule Bus, (CB), the Flight Spacecraft (FSC), the Surface

Laboratory (SL), and the Entry Science Package. The trade studies required to properly define these interfaces are the following:

a. Comparison of alternate power grounding approaches within the Flight Capsule.

b. Comparison of alternate methods of providing redundancy for the Capsule Bus main battery.

c. Comparison of alternate approaches to providing power to the Capsule Bus electronic equipment (unregulated battery voltage, regulated dc power, regulated ac power).

5.6.3.1 Comparison of Power Grounding Approaches - The three alternatives available for the design of the primary power return ground reference system are presented in Figure 5.6-9, where (A), (B), and (C) are defined as follows:

Concept (A) - A dc-dc converter/regulator is used to regulate the raw dc power delivered by the FSC, and to provide electrical isolation between the Flight Spacecraft and FC primary power systems. The FC primary power system return is referenced by a single connection to the SL central ground point (CGP).

Concept (B) - Regulated power is provided by the Flight Spacecraft to the FC. During flight the FC primary power system retains the reference provided by the Flight Spacecraft. Upon switching to internal power, the FC power return system will switch its ground reference from the Flight Spacecraft fo the SL central ground point.

Concept (C) - Same as Concept (A) except that the primary power return is referenced to structure by a connection within the CB, the SL, and the ESP.

Figure 5.6-10 presents the trade-offs between these three alternate approaches, and evaluates the alternatives in the light of each trade-off as follows:

From the standpoint of this trade-off, the approach is

0 - Unacceptable

1 - To be avoided, if possible

2 - Acceptable as a compromise

3 - Preferred

On the basis of this evaluation, the (A) approach has been adopted for the CB primary power system. The (B) approach is considered to be a feasible alternative; however, it requires that the power from the Flight Spacecraft be within the same voltage limits as that of the Flight Capsule batteries. The (C) approach must be discarded due to its ability to generate and propagate electro-

THREE PRIMARY POWER GROUND REFERENCE DESIGN CONCEPTS

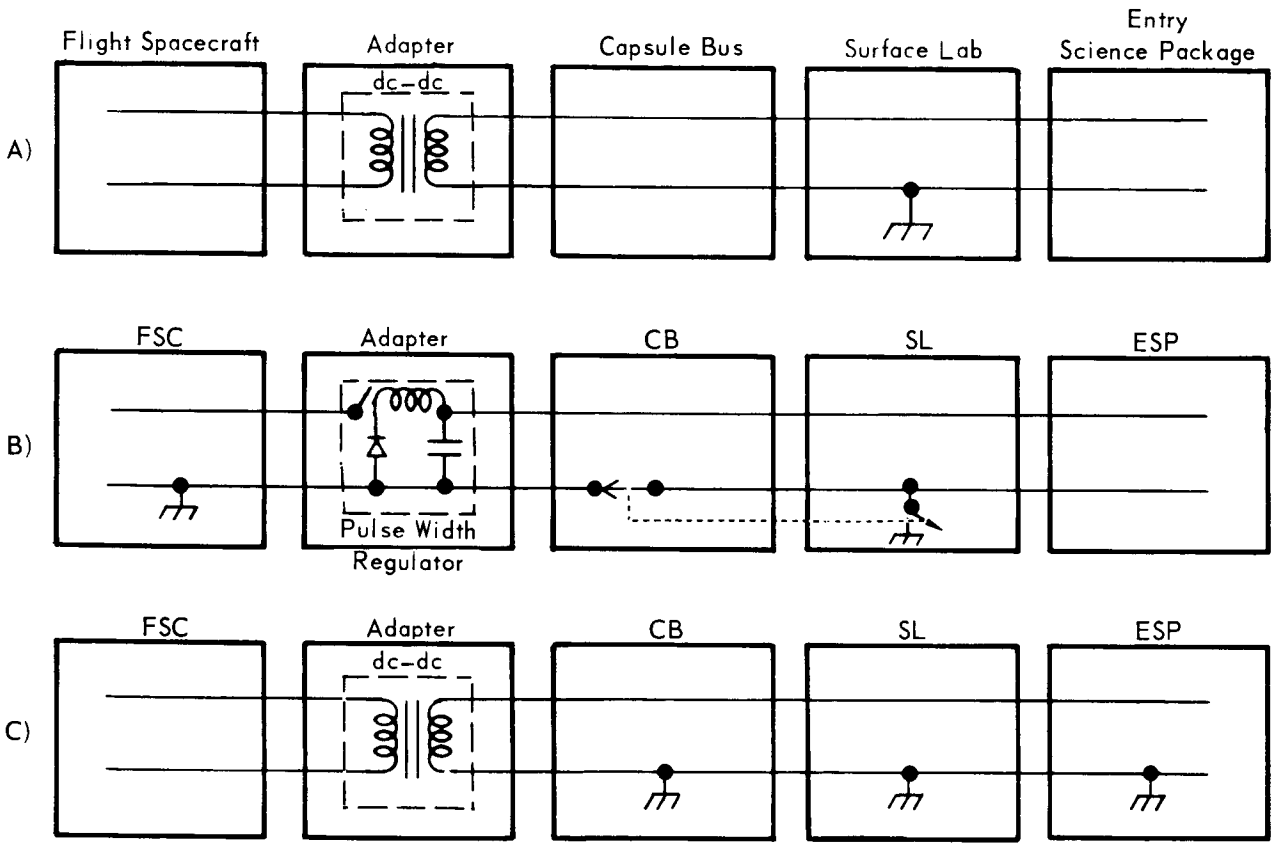

Figure 5.6–9

COMPARISON OF FC GROUNDING APPROACHES

	ALTERNATIVE APPROACHES		
Trade-offs (Primary Power System)	A	B	C
Reliability of Ground Reference System	2	1	3
Design Flexibility – Grounding	2	2	3
Design Flexibility – General Electrical/Electronic	3	2	1
Number of Electrical/Electronic Components Required	2	3	2
Redundant Equipment Required	2	3	2
Redundant Wiring Required	2	2	3
CB/SL/ESP Interface Complexity	3	2	3
SC/FC Interface Complexity	2	2	2
Power Switching Functions	3	1	2
EMI From Ground Loops	3	3	0
EMI From Shared Return and/or Reference Paths	3	3	0
Totals	27	24	21

Figure 5.6–10

magnetic interference (EMI).

5.6.3.2 Capsule Bus Main Battery Redundancy - The two approaches considered for providing redundant battery capacity to the Capsule Bus are:

1. providing this redundancy within the Capsule Bus, and
2. providing this redundancy from the Surface Laboratory.

The second approach was selected. Standardization of the Capsule Bus is not affected because later missions will utilize a long term power source. Projected later mission requirements indicate that sufficient power and energy will be available from the Surface Laboratory to act as a backup for the Capsule Bus battery. The weight and reliabilities of the two approaches were compared. The use of three batteries in the Capsule Bus with one being redundant results in an overall weight of 104 pounds of wet batteries and battery chargers in the Capsule Bus, while the preferred approach results in only 67 pounds, thereby resulting in a weight saving of 37 pounds. The reliabilities of these two approaches are 0.9808 for the first approach and 0.984 for the preferred approach. The use of the Surface Laboratory batteries to provide redundancy to the Capsule Bus does not appreciably affect the SL power subsystem reliability. The Capsule Bus and Surface Laboratory power subsystems are mutually independent and self-supporting in their primary operating modes. Only in the event of a failure of the Capsule Bus main battery would the Capsule Bus become dependent upon the Surface Laboratory.

5.6.3.3 Type of Power Distribution - Alternate approaches to distributing power to the Capsule Bus equipment during descent are:

(1) providing unregulated power from the main battery to the Capsule Bus equipment with a voltage regulation of 23 to 33.5 volts DC,

(2) the use of a central regulator in the power subsystem providing an output voltage regulated to within 1%,

(3) the use of a central inverter in the power subsystem providing a square wave ac output with a voltage regulation in the range of 1%, and

(4) the use of a central power supply in the power subsystem to provide the particular outputs required by the Capsule Bus equipment.

The primary advantage of the first approach, which was selected for use in the Capsule Bus, is that no catastrophic failure mode exists which can terminate the entire mission. In this approach each Capsule Bus subsystem contains a power supply which provides the precise voltage required for that subsystem. An additional advantage of this approach is that it provides maximum flexibility in

that many design modifications can be made within a subsystem which do not affect the power subsystem design.

The use of a central regulator within the power subsystem requires the use of block redundancy. This redundancy does not eliminate the possibility of a failure of the redundant regulator because it is subjected to the same environmental conditions as the primary regulator. Also, this approach does not eliminate the need for transformer coupled power supplies in the Capsule Bus subsystems, which are necessary for signil and power ground isolation as well as for conversion to voltage levels required for subsystem equipment operation. It does, in some cases, eliminate the need for regulator equipment in the subsystems. The overall weight of this approach does not indicate a reduction over the selected approach. This approach is not considered as attractive an alternate approaches as (3).

Approach (3) is considered the most attractive alternate to the selected approach. Here the use of a central inverter in the power subsystem does eliminate the need for inversion in the subsystem power supplies and some weight saving may be afforded. An exact weight comparison requires detailed knowledge of the outputs required from the subsystem power supply. The approach does require block redundancy and switching to replace the primary inverter. In addition, the short rise and fall time of the square wave creates a broad spectrum of interference which is difficult to remove from susceptible circuits.

Approach (4) is not an attractive approach. Circuit redundancy within the power supply would be used instead of block redundancy with necessary complex switching. The wiring weight is increased because of multiple voltage distribution. This approach requires considerable integration to preclude subsystem design from including superfluous power conditioning and to acquire early, accurate definitions of all subsystem power requirements. Any deficiency of the early definitions yields an inadequate or delayed conditioner design due to the inflexibility of this method after completion of the hardware design.

5.7 SEQUENCING AND TIMING - The subsystem which governs the on-board automatic control of the sequencing and timing functions of the Capsule Bus (CB) is of primary importance in maintaining meaningful operation throughout the periods out of contact with the Earth. This subsystem, denoted the Sequencer Subsystem, is divided into two functional component units:

a. Sequencer and Timer (S&T) - Furnishes timing references and automatic sequential control of supporting subsystems during the CB operational mission, and

b. Inflight Test Programmer (TP) - Furnishes timing and sequencing required for exercising the SL subsystems as required for checkout of landed mission readiness.

Since the in-flight test philosophy and the rationale and analysis of the Test Programmer are discussed in Section 4.9, only the Sequencer and Timer analysis and selection are presented here.

5.7.1 Requirements and Constraints - The requirements and constraints which have influenced the design of the S&T are those of mission, system and subsystem effects upon the S&T, as shown in Figure 5.7-1.

5.7.1.1 Primary Constraints - The requirement that the CB be entirely on-board sequenced subsequently requires a device to control all post-separation CB functions from a stored memory sequence. This on-board sequencing controller must contain an alterable (electrically reprogrammable) memory using updates through the Flight Spacecraft (FSC) command link. Self-test capability is included in the CB S&T to minimize the time and electrical energy required to perform inflight checkout.

5.7.1.2 Secondary Constraints - The size of the S&T memory is determined by the maximum duration and resolution of time delays, the number of different time-based marks or functions required by the CB subsystems and the allowance for redundancy and growth capability. A number of different discrete stimuli are needed by the CB subsystems. The number of S&T outputs includes an allowance for redundancy and growth capability. The S&T size and weight limitations are similar to those throughout the CB; however, the requirement for minimum power applies especially to the S&T and similar equipment which are ON continuously. Also, the S&T must endure the peak full-charge battery voltage when first activated on the essentially unloaded bus, and the lower voltage primary power input when the unregulated bus is depressed under full load.

The S&T must operate in the temperature, vibration, and other environments throughout the VOYAGER mission (per Reference 5.7-1) within the constraints of the

TABULATION OF SEQUENCER & TIMER (S&T) DESIGN REQUIREMENTS AND CONSTRAINTS

REQUIREMENT OR CONSTRAINT	REASON
1. Stored Memory Sequence	CB must be entirely on-board sequenced.
2. Memory Alterable in Flight (vis FSC).	To enable post-launch mission modifications by Earth command (prior to de-orbit).
3. Built-in Self-test	To verify proper operation after cruise-storage, in a shortest in-flight checkout period.
4. Size of Memory	Number of different time marks required to sequence CB subsystems.
5. Number of Outputs	Number of different discrete stimuli required by CB subsystems.
6. Size Limitation on S&T Packaging	Capsule configuration requires minimum size electronics package
7. Weight Limitation	Capability of launch vehicle for interplanetary mission requires lightest possible equipment.
8. Input Power Constraints	Must consume minimum power to conserve battery weight, must operate with fluctuating voltage levels.
9. Withstand Temperature Vibration, etc. Environments	VOYAGER Mission subjects equipment to severe environment

Abbreviations: S & T: Sequencer & Timer
FSC: Flight Spacecraft
CB: Capsule Bus

Figure 5.7–1

FC structure and thermal control subsystems. The S&T memory storage must be designed to withstand the high temperature, shock and electromagnetic radiation environments.

5.7.1.3 Operational Requirements - The S&T will supply the following classes of outputs which the CB subsystems require:

a. Discrete (Bilevel or Pulse) - Switching time-based control of subsystem operation (ON/OFF, START/STOP or Mode Selection),

b. Data Word (Train of digital data pulses) - Proportional information transferred to the using subsystem from the S&T,

c. Reference Frequency - Cyclic clock or synchronizing periodic reference signals for subsystem timing.

These requirements form the basis for the corresponding memory and output sizing constraints. The CB S&T interface diagram, shown in Figure 5.7-2, summarizes the CB subsystem interface constraints placed upon the S&T.

a. Inputs

- o Primary Power - 23 to 35 VDC
- o Sensors - Start commands from CB sensors/subsystems
- o Command Link - Real-time and/or non-real-time signals to provide Earth updates or backup commands

b. Outputs

- o Discrete Outputs - ON/OFF, START/STOP, Mode Commands

to Guidance and Control	(7)
To Electrical Power	(16)
To Propulsion	(14)
To Pyrotechnic	(12)
To Radar Subsystems	(3)
To Telemetry	(4)

- o Digital Data - Fixed or timing data words

To Guidance and Control	(10)
To Telemetry	(1) plus memory readout, as required

- o Reference Frequencies

To Guidance and Control

To Telemetry

5.7.1.4 S&T Functional Requirements - The resulting S&T functional definition is based upon the preceding requirements.

CB S & T INTERFACE DIAGRAM

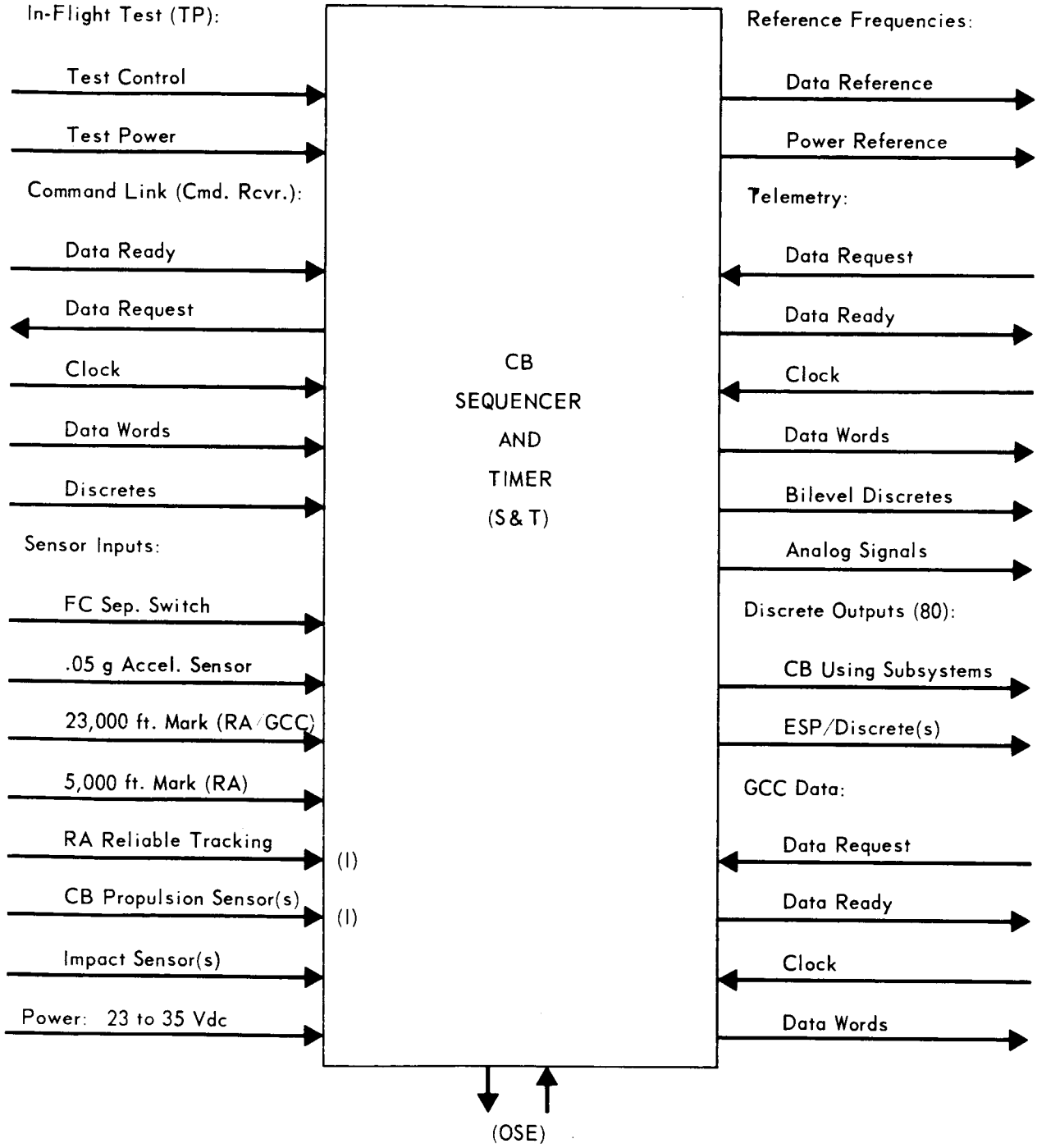

Figure 5.7–2

a. Accept, decode and store non-real-time (delayed) commands from the Command Decoder.

b. Time the delayed period from the corresponding "START" signal (based on these commands and on internally generated timing clock).

c. Activate the appropriate discrete output when this delay period has elapsed. Transfer the desired stored data word (command) to this subsystem upon request from a using subsystem.

d. Generate reference clock frequencies for use by interfacing subsystems.

Figure 5.7-3 shows the Functional Block Diagram of the CB S&T to accomplish these functions, and the interconnections and inter-relationships of the functions themselves.

5.7.2 Alternate Approaches and Selection - A study of the timing and memory techniques was performed to evaluate alternate implementation approaches.

5.7.2.1 Timing Technique - The two methods which were considered to implement the "Count Down Time Delay" function in Figure 5.7-3 are the decrementing and incrementing timing techniques. In general, data words stored in the memory represent time-to-go-to-output following receipt of the appropriate sensor input signal. There are two ways of determining when to enable each output. The first way is decrementing (subtracting a pulse from) the stored word periodically after the sensor input is received and enabling the output when the word represents zero time-to-go. The second way is incrementing (adding a pulse to) a master time word, whose value is initially zero, periodically and comparing it to the stored word. When the words are equal, the output is enabled.

Operational Differences - In a destructive read-out (DRO) memory, decrementing requires the stored word to be read from the memory periodically, decremented, and be written into the memory. The stored word is therefore changed at intervals equal to the time represented by its least significant bit. Incrementing requires the stored word to be read from the memory and then be restored in it without change. The read/write operation must be performed at intervals equal to the time represented by the least significant bit of the stored word. Therefore, the decrementing and incrementing methods are equal in the number of read/write operations required.

In this case, where time-data words with two different accuracies (resolutions) are stored and counted, incrementing is more complex. Incrementing is complicated by the need for one master time word with the greater accuracy represented by its least significant bit (LSB) and for another master time word with the lesser accuracy represented by its least significant bit. Only by using binary coded

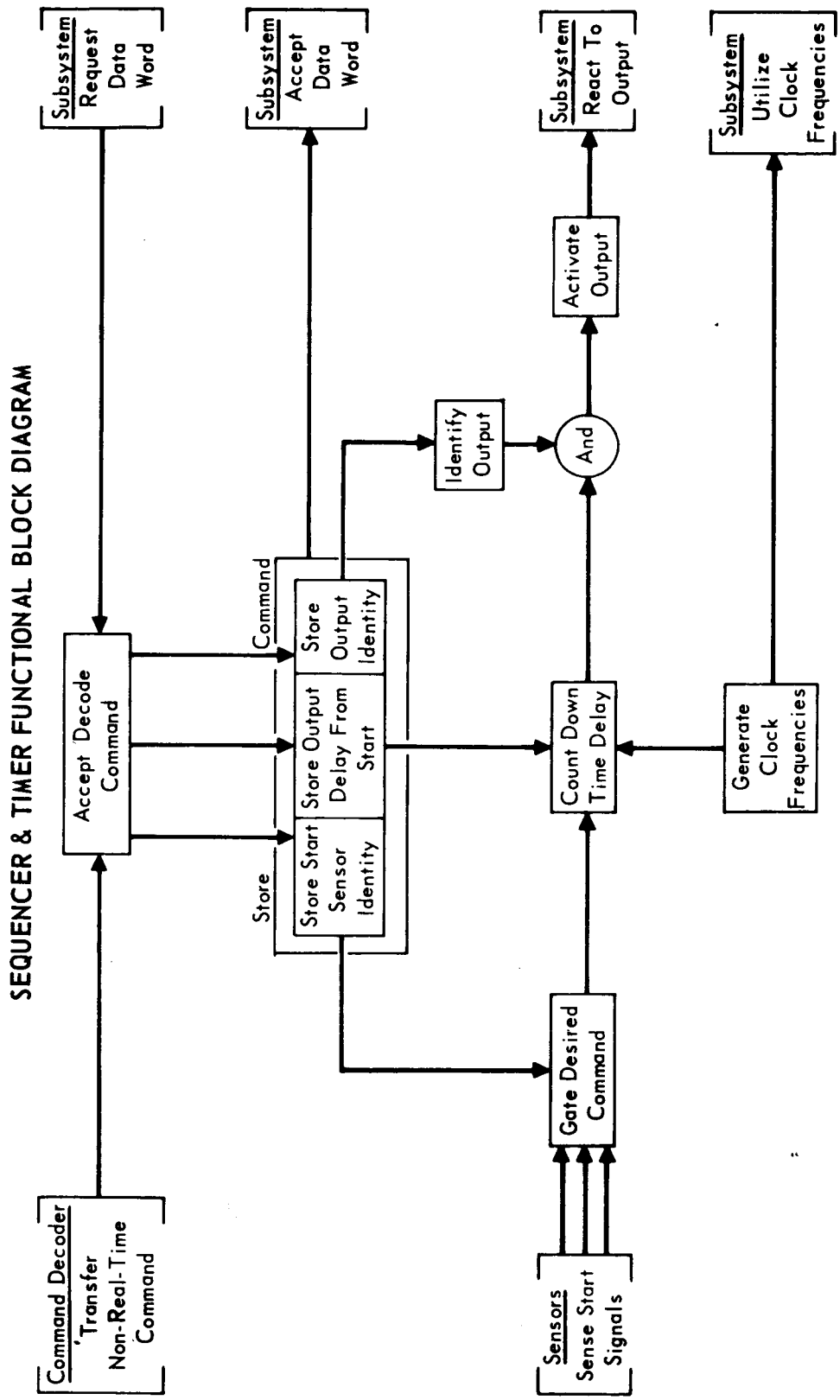
SEQUENCER & TIMER FUNCTIONAL BLOCK DIAGRAM
Subsystem Request Data Word
Subsystem Accept Data Word
Subsystem React To Output
Subsystem Utilize Clock Frequencies
Activate Output
Identify Output
And
Command
Store
Store Output Identity
Store Output Delay From Start
Store Start Sensor Identity
Accept Decode Command
Count Down Time Delay
Generate Clock Frequencies
Gate Desired Command
Command Decoder Transfer Non-Real-Time Command
Sensors Sense Start Signals

Figure 5.7-3

decimal (BCD) coding for the stored words would one master word be required. However, BCD coding would require longer words and the resulting BCD incrementer would be more complex. Therefore, two master time words are required for the simpler of the two incrementing methods.

Since there are eight sensor inputs which activate the same number of independent groups of time functions, either 8 sets of two master time words each are required, or one set of two master time words are required with the following method.

The one set of two master time words are incremented following receipt of the first sensor input. The stored words associated with the first sensor are periodically compared to the appropriate master time word. Upon receipt of the second input, the stored words associated with it are modified by adding the existing master time to them and then comparing them to the master time words. The third through eighth groups of stored words are likewise modified upon receipt of their sensor inputs. Of course, all of the master time words must be stored in the non-volatile memory to prevent their loss during power interruptions. The master time words are then similar to the stored words in the decrementing method since they must be read from the memory, incremented instead of decremented, and be written into the memory.

Effect of Failure - In the decrementing method, a malfunction during the read/write affects only one time function. In the incrementing method, a malfunction during the read/write of a master time word affects all the time functions associated with it.

Method Selection - The comparative characteristics of the preceding timing methods, summarized as follows, show the clear superiority of the decrementing over the incrementing method of timing applied to a destructive read-out non-volatile memory.

Characteristic	Decrementing	Incrementing (2 master time words)	Incrementing (16 master time words)
Read/write operations	All data words periodically	2 master time words periodically and most of data words once	16 master time words periodically
Read only	None	All data words periodically	All data words periodically
Read/write failure effect	One time function	All time functions associated with the master time word	All time functions associated with the master time word

Characteristic	Decrementing	Incrementing (2 master time words)	Incrementing (16 master time words)
Complexity	Simplest	Most complex	Second most complex
Implementation	Easiest	Most difficult	Second most difficult
Easiest to increase capacity	Easiest	Second most difficult	Most difficult
Accuracy	Most accurate (least operations per second	Second most accurate	Least accurate (because of more operations per second)

5.7.2.2 Memory Technique - The function "store/readout command" on the CB S&T Functional Block Diagram (Figure 5.7-3) involves the selection of the proper data storage or memory technique. The selection of memory techniques evolves directly into the corresponding choice of hardware devices for digital data storage. Since a detailed discussion of the trade-off study of such storage devices is already included in the Telecommunication Data Storage Selection of Section 5.5.5, only a summary of the rationale as applies to the CB S&T is repeated here.

a. Functional Requirements
   - o Capacity - 3072 bits (128 words of 24 bits each)
   - o Input from command link - Serial data streams
   - o Output to telemetry - Periodic serial data stream at 500 to 800 bps.
   - o Output to others - Serial data stream at 10^4 to 10^5 bps.

b. Technical Requirements
   - o Maximize reliability
   - o Minimize weight
   - o Minimize size
   - o Minimize volume
   - o Meet environmental requirements including sterilization temperatures, shock, and radiation.

c. Candidate Memories - The requirement that the S&T retain the stored digital data words during the 30 week power off transit phase, and that these words be updateable by the command link before separation, necessitates a non-volatile memory with a capacity sufficient to store and manage the required data words. The volatile semiconductor memory and the larger capacity dynamic magnetic memories are not considered for the CB S&T data storage. The following types of non-volatile memories have been considered.

- o Magnetic Shift Registers - Magnetic Shift Registers (MSR) such as were used in the Gemini Electronic Timer offer wide temperature range, large operating margins, high noise immunity, low power, and high output voltage. Their disadvantages are speed (10 microseconds per shift) and size (120 cubic inches for 82 words of 16 bits). Each 16 bit MSR requires a shift current generator, transfer switch and write amplifier. The serial output allows simple serial arithmetic circuits.
- o Core Memory - Random access, coincident current, core memories, with a cycle time of 2 microseconds are available. A wide temperature range ferrite core stack can be used to eliminate the necessity for an oven to control stack temperature. The access circuitry of coincident current core memories is relatively simple and when a matrix selection technique is used, the circuit component count can be kept low compared to other types of memories. Also in the random access mode, a word can be selected from the entire store in a fixed time (access time) which is independent of its location in the stack. The comparatively high output levels of core memories enable the use of sense amplifiers of relatively low gain-bandwidth product thereby providing high reliability and high immunity to noise. The standard core memory described above can be operated as a non-volatile memory by incorporation of a power shut down sequencer. The additional advantages of cores lie mainly in their ready availability, known characteristics, and high degree of uniformity.
- o Non-Destructive Read Out (NDRO) Memories - Memories that fall into this category are thin film, drum, twistor, plated wire, and multi-aperture devices (MAD). Magnetic drum or tape memories of the low bit densities required for the S&T would provide excellent NDRO storage but size, weight, and power requirements would be excessive. Disadvantages of drum and tape memories are the susceptibilities to both thermal and mechanical shock impulses and the requirement for a warm-up time after initial power turn-on. Another disadvantage is the access time which is of the order of milliseconds. Thin film, twistor and plated wire memories are presently in the stage of advance development. They have a comparatively low output level and low signal-to-noise ratio and thereby requires complex high gain-bandwidth amplifiers. The multi-aperture device (MAD) memories have many of the characteristics of core memories. Power requirements for a MAD memory are lower

than core memories because consecutive interrogate cycles can be performed without the requirement to restore data, but access circuits would be more complex.

a. Memory Selection - Because of its advantages, the destructive read-out coincident current magnetic core memory has been selected as the S&T storage device. Again summarizing the results of the Data Storage study of Section 5.5.5 as pertaining to a memory applicable to the CB S&T (about 3,000 bits), the following requirements were considered with the corresponding choices resulting.

b. Meets functional requirements - magnetic core.

c. Reliability - magnetic core or semiconductor.

d. Power - magnetic core.

e. Weight - magnetic core or semiconductor.

f. Volume - magnetic core or semiconductor.

g. Environment - magnetic core.

h. Cost - magnetic core.

i. Selected approach - magnetic core.

An example S&T Memory Schematic Block Diagram is shown in Figure 5.7-4. This is the 3-D coincident current implementation of a magnetic core memory requiring the same total number of X and Y drivers as the sum of the core "dimensions" of the memory stack while the sense amplifiers and inhibit driver are each the same in number as the bit lengths of the data word.

5.7.3 Selected Approach - The alternates studied and the major factors involved in the selected techniques are summarized in Figure 5.7-5. The configuration of the CB S&T which complies with the preceding requirements and selections is as follows:

a. Coincident current magnetic core memory.

b. Decrementing memory word timing technique.

c. Memory Size - 128 words, 24 bits each, reprogrammable in flight.

d. Estimated probability of 1973 mission success - .9932

e. Size - 10 in. x 6 in. x 6 in.

f. Weight - 13 pounds

g. Power consumption - 14 watts (23 to 35 VDC primary power)

h. Reference frequency outputs - 1 Hz to 40 KHz, $\pm$ .01% accuracy

i. Digital word outputs - up to 16 bits/word at 500 to 40,000 bps.

j. Discrete command outputs - 80 discrete outputs, delayed in time up to 8 hours from any of 8 selected input occurance, $\pm$ 1 to .05 sec timing accuracy.

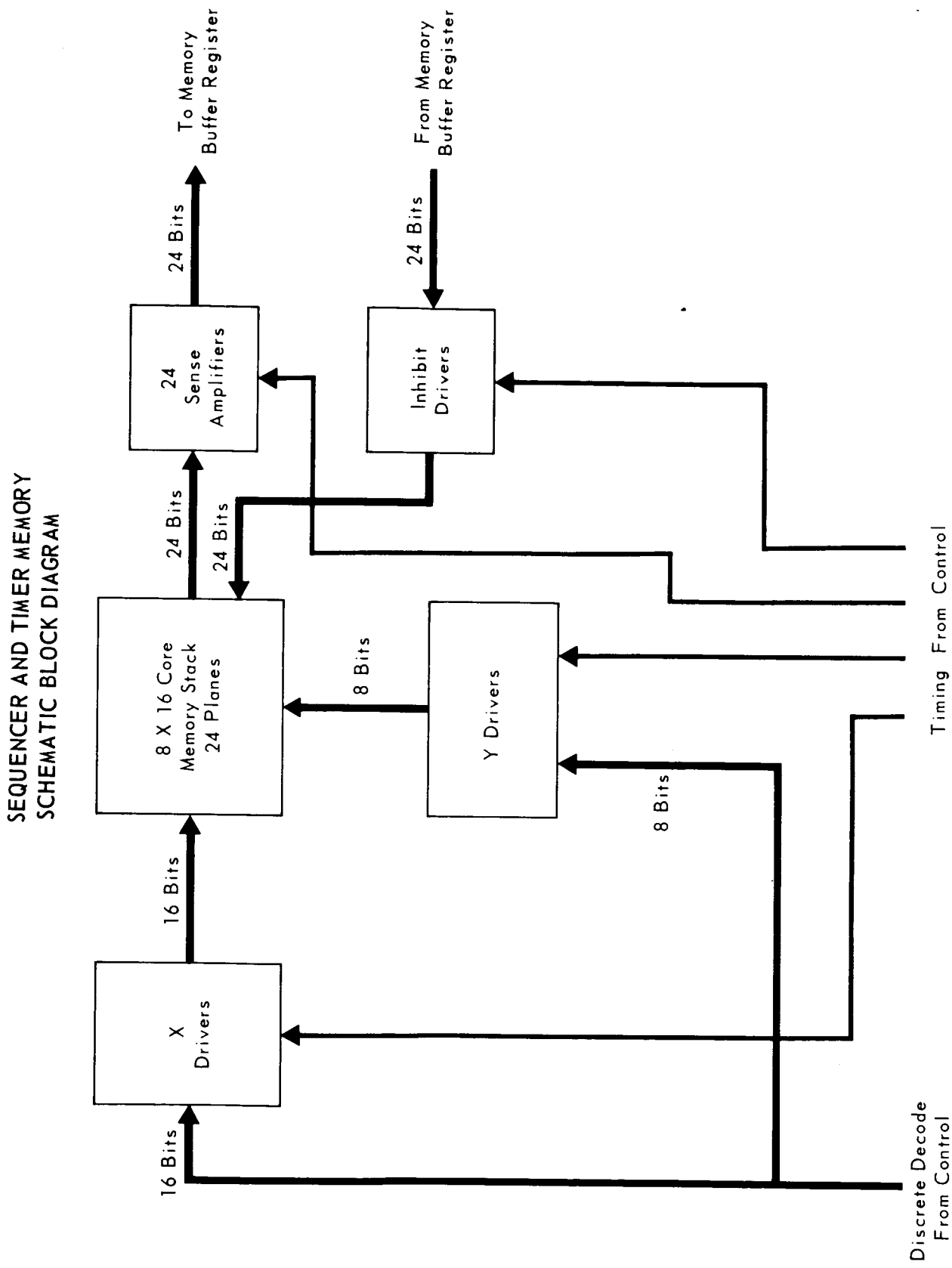
SEQUENCER AND TIMER MEMORY
SCHEMATIC BLOCK DIAGRAM
To Memory
Buffer Register
From Memory
Buffer Register
24 Bits
24 Bits
24
Sense
Amplifiers
Inhibit
Drivers
24 Bits
24 Bits
8 X 16 Core
Memory Stack
24 Planes
8 Bits
Y Drivers
Timing From Control
16 Bits
8 Bits
X
Drivers
16 Bits
Discrete Decode
From Control

Figure 5.7–4

SEQUENCER AND TIMER (S&T) TRADE STUDY SUMMARY

S&T ELEMENT	ALTERNATE TECHNIQUES	MERITS OF SELECTED APPROACH
Memory Storage Technique	**Magnetic Core**	Non-volatile memory
	Magnetic tape/drum	Less complex
	Semiconductor devices	More reliability, smaller, lighter and consumes less power
	Advanced static magnetic devices	Survives VOYAGER environment/ sterilization
		Lower development cost
		Better development status
Timing Technique	**Decrementing Method**	Sufficient speed and accuracy
	Incrementing Method	Less complex
		More reliable
		Easier design implementation
		Best increased capacity ability
		Greater flight experience

[ ] Selected Technique

Figure 5.7–5

5.7.3.1 Design Points - The CB S&T design concept is based upon the selected implementation approaches to the subsystem requirements. The required outputs to CB subsystems are detailed as follows:

Discrete Outputs - The CB subsystems currently require 56 discrete commands subsequent to one of 8 possible mission "marks"; these discrete outputs are desired at a time of up to 8 hours after a given "mark" with an accuracy $\pm$ 1 second. A more accurate time sequence is also required for delays up to 30 minutes after the "mark" with an accuracy of $\pm$ 0.05 second. These discrete output requirements are based upon the sequence of operational events for the typical 1973 mission, shown in Figure 5.7-6. The input stimuli and the required S&T reactions for this mission may be summarized as follows:

a. Power ON (S&T activation)
b. Update Memory (S&T verifies memory upon telemetry request)
c. "Prepare for Separation" command (an "ARM" command, resulting in 16 discrete outputs.)
d. "Start Separation Sequence" (a "FIRE" command resulting in 3 S&T output).
e. Sensed FSC/CB Separation (successive discrete, 18 outputs from the S&T)
f. Sense .05 g CB Deceleration (4 S&T sequential outputs).
g. 23,000 foot mark (12 outputs are sequenced)
h. 5,000 foot mark (5 outputs are required from S&T)
i. Sense Touchdown (6 S&T discrete outputs result)
j. Radar Altimeter (RA) Reliable Tracking Signal (an inhibit signal to prevent 0-7-1 S&T backup output from occurring).

Digital Data Words - The S&T must also supply digital words to the CB subsystems for the 1973 mission previously described.

a. Guidance Control Computer - (10 words, up to 16 bits each)

De-orbit Roll #1 (magnitude and polarity)
De-orbit Pitch (magnitude and polarity)
De-orbit Roll #2 (magnitude and polarity)
De-orbit Thrust Magnitude
Entry Roll #1 (magnitude and polarity)
Entry Pitch (magnitude and polarity)
Entry Roll #2 (magnitude and polarity)
Velocity Profile Data Word #1
Velocity Profile Data Word #2
Velocity Profile Data Word #3

CB SEQUENCER AND TIMER (S & T) SEQUENCE OF EVENTS FOR A TYPICAL 1973 MISSION

INTERFACE DESIGNATION	S & T INPUT (I)/OUTPUT (O)	SOURCE	S & T DESTINATION	BACKUP	MISSION TIME	S & T TIME
I-1	Apply Power to CB S & T	FS CC & S	CB Pwr	MOS	T_{12} – 228 Min	(Warmup)
I-2	Update CB S & T Parameters (via Cmd Rcvr.) (Up to 128 words)	MOS	CB S & T	–	T_{12} – 225 Min.	(Update)
O-1	Verify CB Parameters (via. T/M) (128 words)	CB S & T	MOS	–	T_{12} – 195 Min	(Verify)
I-3	Receive "Prepare FC for Separation" Cmd (Cmd Rcvr)	MOS	CB S & T	–	T_{12} – 70 Min.	T_a
O-3-1	Switch CB & ESP to Internal Power	CB S & T	CB & ESP Pwr	MOS	T_{12} – 65 Min.	+ 5 Min.
O-3-2	Activate CB TM (Checkout Mode)	CB S & T	CB TM (Pwr)	MOS	T_{12} – 64 Min	+ 6 Min
O-3-3	Activate CB GCS (IMU)	CB S & T	CB GCS (Pwr)	MOS	T_{12} – 63 Min	+ 7 Min
O-3-4	Activate CB GCC	CB S & T	CB GCC (Pwr)	MOS	T_{12} – 62 Min	+ 8 Min
O-3-5	Transfer GCS Data Words (10)	CB S & T	CB GCC	MOS	T_{12} – 61 Min	+ 9 Min
O-3-6	Turn GFF GCC	CB S & T	CB GCC (Pwr)	MOS	T_{12} – 60 Min	+ 10 Min
O-3-7	Activate Squib Battery No. 1	CB S & T	CB Pwr	MOS	T_{12} – 59 Min	+ 11 Min
O-3-8	Activate Squib Battery No. 2	CB S & T	CB Pwr	MOS	T_{12} – 58 Min	+ 12 Min
O-3-9	Activate Squib Battery No. 3	CB S & T	CB Pwr	MOS	T_{12} – 57 Min	+ 13 Min
O-3-10	Switch ESP/SL/CB Cruise Commutators to CB TM Control Mode	CB S & T	ESP/SL/CB CC	MOS	T_{12} – 56 Min	+ 14 Min
O-3-11	Switch Canister to Internal Power	CB S & T	CN Pwr	MOS	T_{12} – 10 Min	+ 60 Min
O-3-12	Turn On Low Rate UHF Transmitter	CB S & T	CB TM (Pwr)	MOS	T_{12} – 9 Min	+ 61 Min
O-3-13 (Repeat O-3-4)	Activate CB GCC	CB S & T	CB GCS (Pwr)	MOS	T_{12} – 8 Min	+ 62 Min
O-3-14	Switch CB TM to De-Orbit Mode	CB S & T	CB TM	–	T_{12} – 6 Min	+ 64 Min
I-4	Start Separation Sequence (Cmd Rcvr to CC & S)	FS CC & S	CB S & T	MOS	T_{12} – 5 Min	T_b
O-4-1	Initiate GCC Separation Routine	CB S & T	CB GCS	MOS	T_{12} – 30 Sec	+ 5.5 Min
I-5	Enable CB S & T Separation Command	CN DP	CB S & T	–	T_{12} – 15 Min	T_c
O-5-1	Enable CB RCS	CB S & T	CB RCS	–	T_{12} – 5 Sec	+ 10 Min
O-5-2	Separate FC from FS	CB S & T	CB GCS	–		+ 15 Sec
I-6	Verify FS–FC Separation	FC Sep Sw	CB S & T	–	T_{12} +	T_d
O-6-1	Terminate RCS Separation Firing	CB S & T	CB GCS	–	T_{12} + 1 Sec	+ 1 Sec
O-6-2	Initiate De-Orbit Attitude Maneuver Sequence	CB S & T	CB GCC	–	T_{12} + 25 Sec	+ 25 Sec
O-6-3	Initiate De-Orbit Velocity Routine	CB S & T	CB GCC	–	T_{12} + 15 Min	+ 15 Min
O-6-4	Arm CB De-Orbit Motor	CB S & T	CB Prop (Pyro)	–	T_{13} – 5 Sec	+ 19 Min, 5.5 Sec
O-6-5	Ignite CB De-Orbit Motor	CB S & T	CB Prop (Pyro)	–	T_{13} +	+ 20 Min
O-6-6	Arm De-Orbit Motor Thrust Termination	CB S & T	CB Prop (Pyro)	–	T_{13} + 0–31 Sec	+ 20 Min, 31 Sec
O-6-7	Terminate CB De-Orbit Thrust Motor (Backup)	CB GCC	CB Prop	CB S & T	T_{13} + 0–32 Sec	+ 20 Min, 32 Sec
O-6-8	Arm Motor Case Release Mechanism	CB S & T	CB Prop (Pyro)	–	T_{13} + 35 Sec	+ 20 Min, 35 Sec
O-6-9	Release De-Orbit Motor	CB S & T	CB Prop (Pyro)	–	T_{13} + 40 Sec	+ 20 Min, 40 Sec
O-6-10	Separate De-Orbit Motor (Backup)	CB Pyro	CB Prop (Pyro)	CB S & T	T_{13} + 40.1 Sec	+ 20 Min, 40.1 Sec
O-6-11	Initiate Entry Attitude Maneuver Sequence	CB S & T	CB GCC	–	T_{13} + 2 Min	+ 22 Min
O-6-12	Start Coast Roll	CB S & T	CB GCC	–	T_{13} + 15 Min	+ 35 Min
O-6-13 (Repeat	Turn Off GCC	CB S & T	CB GCC (Pyro)	–	T_{13} + 16 Min	+ 36 Min

Figure 5.7-6

0-3-6)						
0-6-14 (Repeat 0-3-4)	Activate GCC	CB S & T	CB GCC (Pyro)	–	T_{14} – 8 Min	+ 5 Hr 52 Min
0-6-15	Initiate GCC Acceleration Routine	CB S & T	CB GCC	–	T_{14} – 7 Min	+ 5 Hr, 53 Min
0-6-16	Turn on CB Radar Altimeter	CB S & T	CB RA (Pwr)	–	T_{14} – 6 Min	+ 5 Hr, 54 Min
0-6-17	Turn on ESP	CB S & T	ESP Pwr	–	T_{14} – 5 Min	+ 5 Hr, 55 Min
0-6-18	Switch CB TM to Entry Mode	CB S & T	CB TM	–	T_{14}	+ 6 Hr
1-7	Sense .05 g CB Deceleration	CB GCC	CB S & T	–	T_{15}	T_e
0-7-1	Turn on Landing Radar (Backup)*	CB RA	CB LR (Pwr)	CB S & T*	T_{15} + 30 Sec	+ 30 Sec
0-7-2	Arm TPS Valves Pressurant	CB S & T	CB Prop (Pyro)	–	T_{15} + 49 Sec	+ 49 Sec
0-7-3	Fire TPS Pressurant Isolation Valves	CB S & T	CB Prop (Pyro)	–	T_{15} + 50 Sec	+ 50 Sec
0-7-4	Fire TPS Propellant Isolation Valves	CB S & T	CB Prop (Pyro)	–	T_{15} + 55 Sec	+ 55 Sec
1-8	23,000 Foot Mark	CB RA	CB S & T	CB GCS	T_{19} – .5 Sec	T_f
0-8-1	Shutdown CB RCS	CB S & T	CB Pyro (RCS)	–	T_{19} – .2 Sec	+ .3 Sec
0-8-2	Enable CB Aerodecelerator Deployment	CB S & T	CB Pyro	–	T_{19} – .1 Sec	+ .4 Sec
0-8-3	Deploy CB Aerodecelerator	CB S & T	CB Pyro	–	T_{19}	+ .5 Sec
0-8-4	Arm CB Aeroshell Separation Mech	CB S & T	CB Pyro	–	T_{20} – 1 Sec	+ 11 Sec
0-8-5	Initiate GCC Descent Control Mode	CB S & T	CB GCC	–	T_{20} – 1 Sec	+ 11 Sec
0-8-6	Start RA Hold-off Signal	CB S & T	CB RA	–	T_{20} – 1 Sec	+ 11 Sec
0-8-7	Switch CB & ESP TM to Terminal Deceleration Mode	CB S & T	CB/ESP TM	–	T_{20} – .5 Sec	+ 11.5 Sec
0-8-8	Release CB Aeroshell (Electrical)	CB S & T	CB Pyro	–	T_{20} – .2 Sec	+ 11.8 Sec
0-8-9	Release CB Aeroshell (Mechanical)	CB S & T	CB Pyro	–	T_{20} – .1 Sec	+ 11.9 Sec
0-8-10	Separate CB Aeroshell	CB S & T	CB Pyro	–	T_{20}	+ 12 Sec
0-8-11	End RA Hold-off Signal	CB S & T	CB RA	–	T_{20} + 4 Sec	+ 16 Sec
0-8-12	Arm Aerodecelerator Release	CB S & T	CB Pyro	–	T_{20} + 35 Sec	+ 47 Sec
1-9	5,000 Foot Mark	CB RA	CB S & T	–	T_{21} – .5 Sec	T_g
0-9-1	Ignite Terminal Propulsion Motors (Backup)	CB GCC	CB Prop	CB S & T	T_{21}	+ .5 Sec
0-9-2	Release Aerodecelerator from CB (Backup)	CB Prop Sensors	CB Pyro	CB S & T	T_{21} + .5 Sec	+ 1 Sec
0-9-3	Throttle Down Terminal Thrust to .8 g	CB GCC	CB Prop	CB S & T	T_{21} + .5 Sec	+ 1 Sec
0-9-4	Separate Aerodecelerator from CB	CB S & T	CB Pyro	–	T_{21} + .6 Sec	+ 1.1 Sec
0-9-5	LR Search/Track Enable Command	CB S & T	CB LR	–	T_{21} + 2 Sec	+ 2.5 Sec
1-10	Sense Touchdown	CB IS	CB S & T	SL IS	T_{26}	T_h
0-10-1	Touchdown Time Backup (Shutdown LR, RA, GCS, Propulsion)	CB IS	CB Pwr	CB S & T	T_{26}	T_h
0-10-2	Arm CB Stabilizer Legs	CB S & T	CB Pyro	–	T_{26} + 5 Sec	+ 5 Sec
0-10-3	Release CB Stabilizer Legs	CB S & T	CB Pyro	–	T_{26} + 6 Sec	+ 6 Sec
0-10-4	Extend CB Stabilizer Legs	CB S & T	CB Pyro	–	T_{26} + 8 Sec	+ 8 Sec
0-10-5	Shutdown CB (Transfer Residual Power)	CB S & T	CB Pwr	–	T_{26} + 10 Min	+ 10 Min
0-10-6	Shutdown ESP	CB S & T	ESP Pwr	–	T_{26} + 10 Min	+ 10 Min
1-11	RA Reliable Tracking Signal	CB RA	CB S & T	–	(During RA Tracking)	

*Conditional backup – inhibited if RA "Reliable Tracking Signal" is present.

†Conditional reaction – if release has been accomplished.

Notes:

CB	Capsule Bus
CC	Cruise Commutator
CC & S	Central Computer & Sequencer
CMD	Command
CN	Canister (Sterilization)
DP	Dual Programmer
ESP	Entry Science Package
FSC	Flight Spacecraft
GCS	Guidance Control Computer
GCS	Guidance Control Subsystem
IMU	Inertial Measurement Unit
IS	Impact Sensor (Landing)
LR	Landing Radar
MOS	Mission Operations Systems
PROP	Propulsion
PWR	Power (Electrical)
PYRO	Pyrotechnic
RA	Radar Altimeter
RCS	Reaction Control Subsystems
RCVR	Receiver
S & T	Sequencer & Timer
SL	Surface Laboratory
TM	Telemetry
TPS	Terminal Prop. Subsystem

Times:

T_{12}	Separation (CB/FSC): T_b
T_{13}	De-Orbit: T_d + 20 min
T_{14}	Predicted (S & T) Entry: T_d + (1 to 6) hr
T_{15}	Sensed .05g Entry: T_e
T_{19}	Aerodecelerator Deployed: T_f + .5 sec
T_{20}	Aeroshell Separation: T_f + 12 sec
T_{21}	TPS Ignition: T_g + .5 sec
T_{26}	Touchdown: T_h

5.7-19-2

b. Telemetry Subsystem - (required each minute or as requested)

Data Stream Time - tag (up to 9 hours, ± 1 sec. resolution)

Reference Frequencies - The CB subsystems require the following clock frequencies:

a. 1 KHz ± .01% for telemetry synchronization reference.

b. 38.4 KHz ± .01% for guidance gyro inverter synchronization.

5.7.3.2 Functional Elements - The S&T consists of the following functional elements, connected as shown on the schematic block diagram of Figure 5.7-7: Memory, memory buffer register, decrementor and zero detector, timing and control, master oscillator, converter-regulator and power detector, and the required interface units (digital data, telemetry, command link, input sensor, reference frequency and discrete output). With these elements being standard or flight proven in design concept, the CB S&T will perform the required functions within the constraining technical requirements analyzed herein.

SL SEQUENCER AND TIMER SCHEMATIC BLOCK DIAGRAM

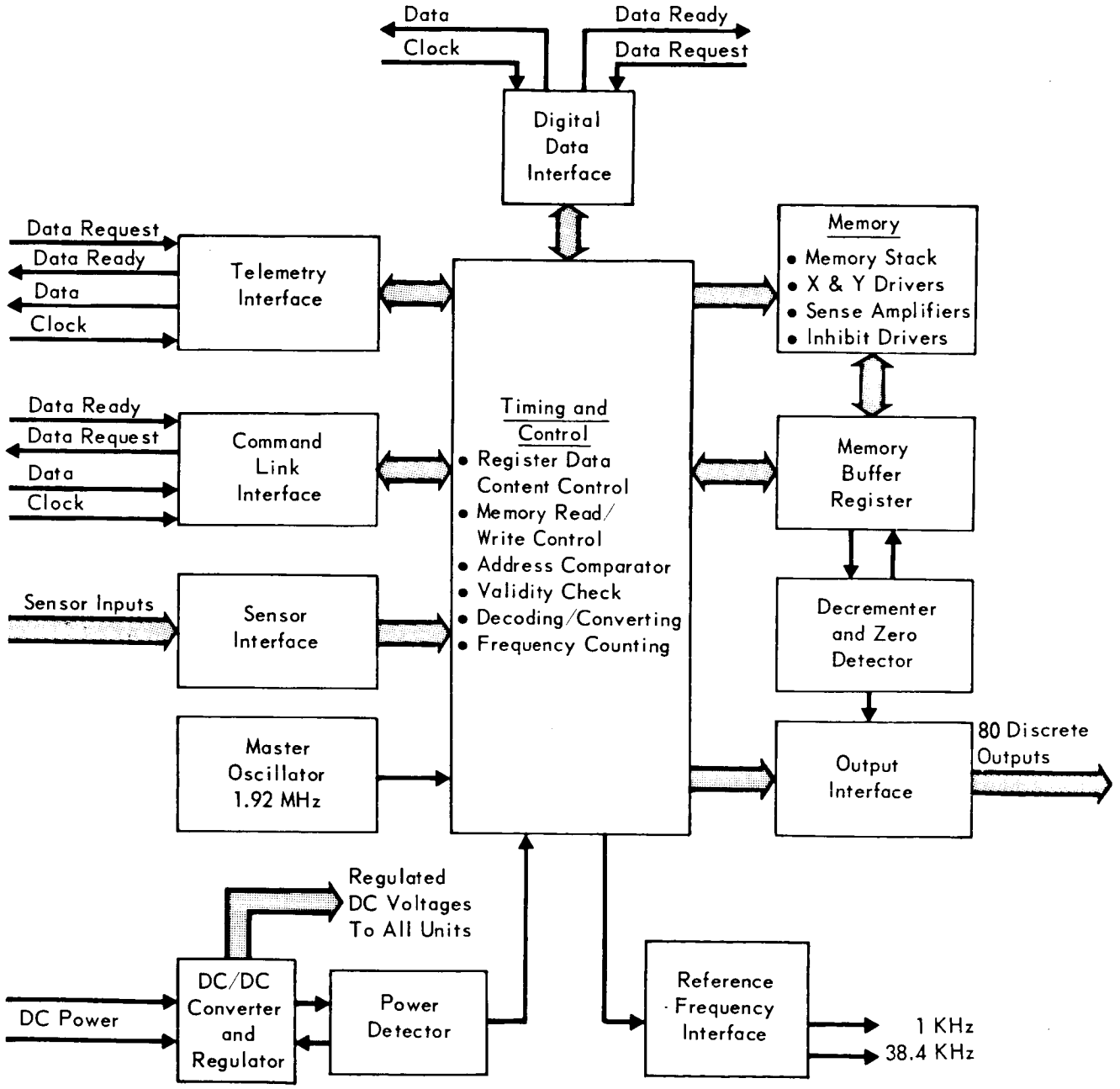

Figure 5.7–7

REFERENCE

5.7-1: McDonnell Report E191, "1973 VOYAGER Flight Capsule Equipment Environmental Sepcification for Preliminary Design", revised 15 May 1967.

5.8 GUIDANCE AND CONTROL SUBSYSTEM - The Guidance and Control Subsystem (GCS) contains instruments and electronics needed to guide the Capsule Bus from separation to touchdown on the Martian surface. This trade study was performed to compare candidate configurations for the GCS and to select the best approach for use in the VOYAGER Capsule Bus.

5.8.1 Scope - This study defines and compares candidate equipment concepts and selects a preferred configuration for the attitude reference and the support electronics. Subsystem performance dynamics are discussed in Part C, Section 9.0 (orbit phase), and in Sections 2.3.6 (entry) and 2.3.7 (terminal descent). The functional description of the GCS preferred concept is given in Part C, Section 9.0.

Evaluation of the candidates is limited to comparison of the Inertial Measurement Unit (IMU) packages and the control electronics packages.

5.8.2 Summary - Two possible IMU concepts are considered in this study: strapped-down and gimballed. Each of these IMU concepts was combined with an analog and a digital control electronics to form four candidate configurations. These are:

I Strapped-down IMU with analog control electronics

II Strapped-down IMU with digital control electronics

III Gimballed IMU with analog control electronics

IV Gimballed IMU with digital control electronics

Figure 5.8-1 presents a summary of the characteristics of the four configurations.

The candidates that utilize a gimballed IMU were eliminated because of the low reliability of the platform. The mechanical complexity of the IMU also contributes to the sterilization sensitivity. A gimballed IMU that can satisfy the sterilization requirements is not in development, whereas, Honeywell Incorporated (Aero Division) and Bell Aerosystems have developed sterilizable inertial sensors for strapped-down applications, under JPL contracts.

A strapped-down IMU can be implemented with either digital or analog control electronics. Analog control electronics can be designed that will satisfy all mission requirements. A slight performance penalty results from the impracticability of incorporating a scheme for minimizing gyro coning errors. The analog circuitry presents a potential sterilization problem due to the tight tolerances required. Also, analog systems are inherently inflexible devices. A digital implementation is very flexible and has growth potential that insures standardization of the GCS throughout the VOYAGER Program. Digital flexibility through

GUIDANCE AND CONTROL SUBSYSTEM EQUIPMENT TRADE SUMMARY CHART

	SELECTED CONFIGURATION			
SELECTION CRITERIA	I STRAPDOWN IMU ANALOG ELECTRONICS	II STRAPDOWN IMU DIGITAL ELECTRONICS	III GIMBALLED IMU ANALOG ELECTRONICS	IV GIMBALLED IMU DIGITAL ELECTRONICS
Probability of Mission Success	Simplest candidate, high reliability.	High reliability. Key mission profile parameters may be changed in flight.	Lowest reliability due to mechanical complexity and use of linear circuits. Not feasible to add significant redundancy to single IMU.	Also has low reliability.
	Limited rate and attitude capability makes strapdown system more susceptible to unexpected wind and gust disturbances.		High rate capability and wide attitude limits of gimballed platform make it least sensitive of all candidates to wind and gust disturbances.	
System Performance	Pointing error less than 1.74 degrees per axis at de-orbit (3 sigma).	Less than 0.87 degrees (3 sigma).	Less than 0.87 degrees (3 sigma)	Less than 0.87 degrees (3 sigma)
	Reference frame drift rate during limit cycle is greater than 1 degree per hour by coning drift error.	1 degree per hour plus drift due to coning.	1 degree per hour (3 sigma)	1 degree per hour (3 sigma)
	Smallest size, least weight and power.	12 percent larger 20 percent more power and weight than I.	30 percent larger 25 percent more power and weight than I.	25 percent larger 20 percent more power 25 percent more weight than I.
Development Risk	Strapdown gyros used on Ranger, Surveyor, Mariner and Lunar Orbiter.	Digital strapdown guidance system used on PRIME vehicle.	Two axis platform used on classified space program.	Used on Gemini with analog autopilot.
	Sterilizable inertial components in development.	Digital autopilot used on BGRV		Similar concept developed for BGRV.
	Potential sterilization problem with analog electronics.	Minimum sterilization induced problems.	Platform bearings, slip rings, and inertial sensors suitable for sterilization must be developed.	Suitable platform must be developed.
Versatility	Analog electronics are inherently inflexible – changes in mission profile necessitate changes in circuitry.	Most flexible concept – both changes in mission profile and attitude freedom can be accommodated by changes to computer software.	Analog electronics are inherently inflexible.	High flexibility – software can accommodate changes in mission profile but range of attitude freedom is fixed.
Cost	Mission changes after development will significantly increase cost.	Least uncertainty in cost estimate of this approach.	Sterilizable platform development will be expensive.	Sterilizable platform development will be expensive.
	Lowest initial cost.			Highest initial cost.

Figure 5.8-1

software reprogramming increases confidence in meeting the GCS development schedule by allowing changes in mission profiles without last minute redesign and requalification of the control electronics.

The strapped-down IMU with digital control electronics is the best design approach and has been selected for the capsule GCS.

5.8.3 Functional and Technical Requirements - The GCS generates stabilization and guidance commands for the VOYAGER Capsule Bus throughout its mission. To accomplish this, the GCS must fulfill the performance and functional requirements listed in Figure 5.8-2. These requirements emanate from explicit JPL constraints, are derived from JPL constraints on other subsystems, or are imposed by other subsystems.

5.8.3.1 Reduction of the Requirements to a Functional Schematic - The mission requirements dictate the GCS functional relationships, internally and externally, with the reaction control subsystem (RCS), sequencer and timer (S&T), landing radar subsystem (LRS), de-orbit engine subsystem, and the descent engine subsystem.

An attitude reference is required and must be maintained accurately ($\pm 0.86°$ -3 sigma) through de-orbit and coarsely ($\pm 15°$) down to entry. The subsystem must be capable of accepting desired Capsule Bus attitude information and generating RCS control commands to acquire and maintain these attitudes. Rate stabilization is necessary; however, thruster logic derived (pseudo) rate stabilization may be employed during times when no forces are acting on the Bus other than the RCS. Actual body rates must be measured and used for rate stabilization when external forces are present; i.e., during de-orbit thrusting and entry.

To meet the axial de-orbit velocity error constraint, a velocity meter (i.e., axial accelerometer with integrated output and velocity comparison) must be used to command de-orbit engine cut-off. Uncertainties in de-orbit engine impulse preclude the use of a simpler timed thrust scheme. Lateral velocity dispersions caused by thrust misalignments are not large enough to warrant use of lateral accelerometers for correction.

The attitude of the Capsule Lander is controlled by differential throttling of the canted descent engines. By virtue of the proportional control and the external forces on the Lander, body angular rates must be measured and utilized for rate stabilization. After Aeroshell and aerodynamic decelerator separations,

GUIDANCE AND CONTROL SUBSYSTEM FUNCTIONAL AND PERFORMANCE REQUIREMENTS

MISSION PHASE	FUNCTIONAL REQUIREMENTS	PERFORMANCE REQUIREMENTS
Pre-Separation	1. Calibrate 2. Alignment transfer	1. None 2. Flight capsule reference to flight spacecraft axes – ±0.3 degree (3 sigma) – spacecraft axes to inertial reference alignment – ±10 mrad (3 sigma) design goal ±20 mrad (3 sigma) maximum
Separation	1. Maintain inertial reference	1. Pre-separation reference
Coast to De-Orbit	1. Maintain inertial reference 2. Generate commands to damp separation disturbances and maneuver to de-orbit attitude	1. Pre-separation reference 2. Attitude deadband – ±2 deg maneuver rate 1 – 3 deg/sec 300 meter separation required prior to de-orbit engine activation (30 min max)
De-Orbit	1. Maintain inertial reference 2. Maintain de-orbit attitude against thrust disturbances 3. Measure longitudinal velocity change and issue thrust terminate discrete	1. Pre-separation reference 2. Attitude deadband – ±0.25 deg capsule bus attitude error – (each axis) ±15 mrad (3 sigma) design goal ±30 mrad (3 sigma) maximum 3. Error in incremental velocity ±0.75% (3 sigma)
Orbital Descent	1. Generate commands to orient capsule bus to, and maintain pitch and yaw entry attitude 2. Generate commands to slow roll capsule bus for thermal control	1. Attitude error at entry ±15 deg (3 sigma) attitude deadband – ±2 deg 2. 3–4 Revolutions/hr
Entry	1. Generate rate stabilization commands about pitch, roll, and yaw axes 2. Terminate control at aerodynamic decelerator deployment 3. Align reference frame to wind reference velocity vector while on aerodynamic decelerator.	1. Maximum rate – 3 deg/sec 2. None 3. Attitude reference alignment – ±20 deg pitch and yaw.
Aeroshell and Aerodynamic decelerator Separation	1. Maintain alignment of reference frame	1. Velocity vector reference in pitch and yaw – roll reference is arbitrary
Terminal Descent	1. Generate commands to damp separation disturbances and control capsule bus attitude for radar acquisition 2. Generate lateral steering commands and rate stabilization 3. Control thrust to velocity vs range profile 4. Generate commands to maintain attitude during constant velocity descent 5. Generate thrust termination discrete	1. Align to velocity vector reference frame in pitch and yaw; roll attitude is arbitrary 2. Landing radar velocity information utilized 3. Landing radar velocity and range utilized 4. Attitude – 0.5 degree 5. Range – 10 feet

Figure 5.8–2

the GCS must be capable of computing the Lander angle of attack and orienting the Lander to the zero angle of attack, to allow LRS acquisition. Velocity and range information from the LRS are accepted and attitude steering and thrust control signals are generated to control the Lander through the low-thrust portion of the descent and to conform to the descent velocity/range profile down to descent engine cutoff.

The GCS must be capable of accepting from the sequencer and timer, command attitude data words prior to separation and mission timing and event discretes throughout the mission.

All of the GCS functional requirements lead to the functional schematic shown in Figure 5.8-3. This figure is the base upon which the GCS was designed.

5.8.3.2 Instrumentation - The functional schematic may be instrumented through two approaches; a limited attitude inertial reference, or an all-attitude inertial reference. Limited attitude guidance systems are so-called because the vehicle attitude must be constrained in one or more axes. The vehicle attitude is computed relative to a command body attitude and must be maintained very near to the command attitude to preserve reference accuracy. This requirement is satisfied by slaving the stabilization and control loop to the inertial attitude error signal. Maneuvering is accomplished by torquing the inertial body reference with stored or computed rate commands. All-attitude concepts are those in which the attitude reference is maintained regardless of vehicle attitude. In the all-attitude inertial configuration, the vehicle attitude is computed relative to a known nonrotating inertial reference. Maneuvers are effected by attitude offset commands relating the inertial reference to the desired body attitude.

5.8.4 Guidance and Control Subsystem Candidates - Four potential GCS configurations were chosen for study. These configurations are:

I Strapped-down IMU with analog control electronics

II Strapped-down IMU with digital control electronics

III Gimballed IMU with analog control electronics

IV Gimballed IMU with digital control electronics

Configuration I is a limited attitude concept with an IMU similar to those of the Ranger, Surveyor, and Mariner Spacecraft. The GCS mechanization is similar to that of Surveyor. This concept was chosen for study because of its simplicity

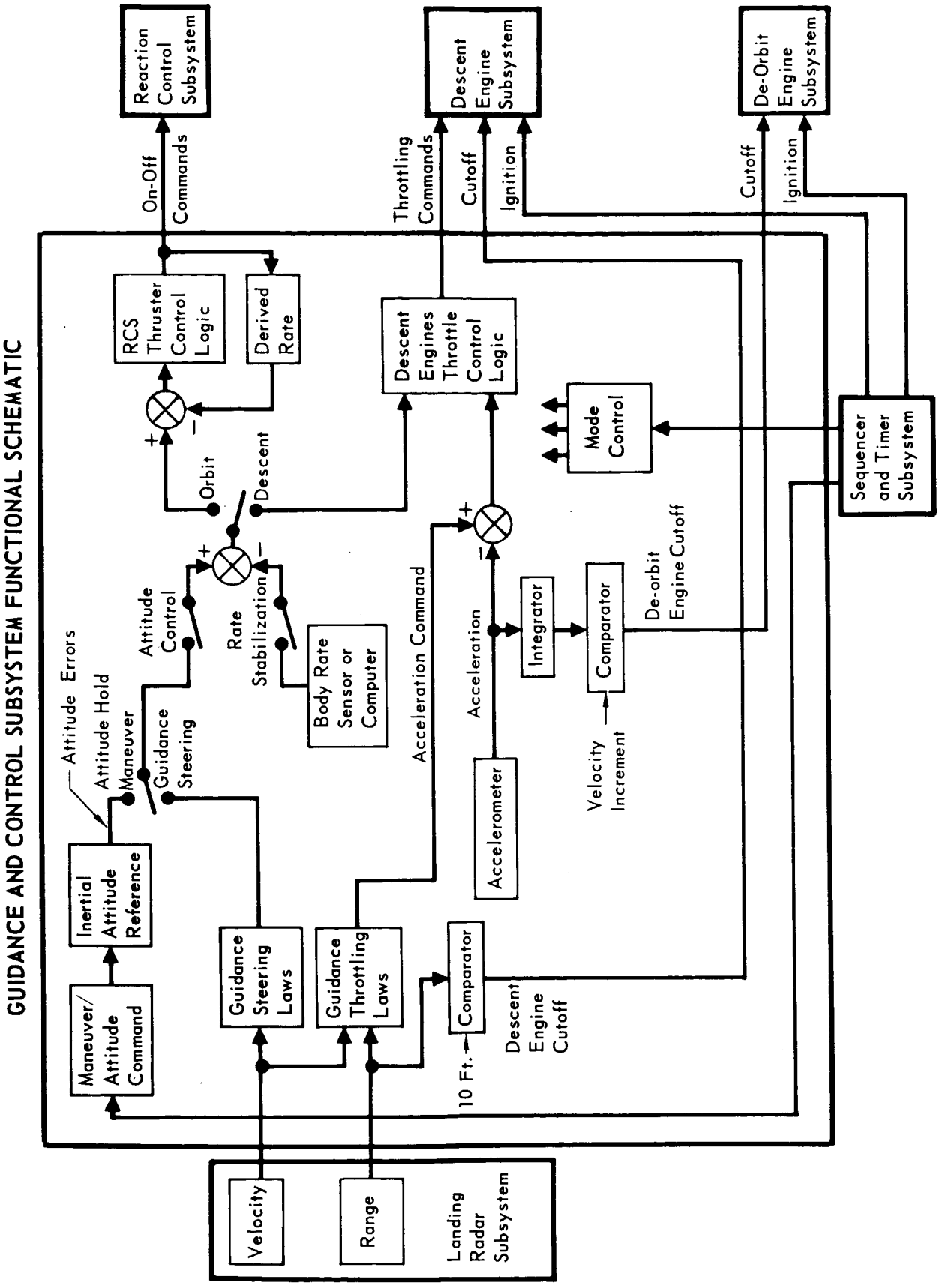
GUIDANCE AND CONTROL SUBSYSTEM FUNCTIONAL SCHEMATIC
Reaction Control Subsystem
Descent Engine Subsystem
De-Orbit Engine Subsystem
On-Off Commands
Throttling Commands
Cutoff
Ignition
Cutoff
Ignition
RCS Thruster Control Logic
Derived Rate
Descent Engines Throttle Control Logic
Mode Control
Sequencer and Timer Subsystem
Orbit
Descent
Attitude Control
Rate Stabilization
Body Rate Sensor or Computer
Acceleration Command
Acceleration
Integrator
Comparator
De-orbit Engine Cutoff
Attitude Errors
Attitude Hold
Maneuver
Guidance Steering
Velocity Increment
Accelerometer
Inertial Attitude Reference
Maneuver/ Attitude Command
Guidance Steering Laws
Guidance Throttling Laws
Comparator
10 Ft.
Descent Engine Cutoff
Velocity
Range
Landing Radar Subsystem

Figure 5.8–3

and past usage. Configuration II is a digital version of Configuration I employing a general purpose Digital Control Electronics (or Guidance and Control Computer) that can be all or limited attitude, depending on computer size and speed. This configuration is more complex than the first but was chosen for study because it is more versatile and has the potential of growth without circuit redevelopment or requalification.

Configurations III and IV are all-attitude, gimballed IMU concepts with analog and digital control systems. These systems were chosen because of their capability of absorbing high vehicle angular rates while maintaining an accurate inertial reference, and the ease with which another gimbal system (e.g., antenna positioning device) may be slaved to the IMU gimbals.

5.8.4.1 Configuration I - Strapped-down IMU with Analog Control Electronics - Configuration I is a limited attitude GCS system that consists of a strapped-down IMU and analog control electronics. Figure 5.8-4 defines the system and shows its functional organization.

Strapped-down IMU - The IMU consists of three single degree of freedom rate integrating gyros and one axial (Z-axis) analog rebalanced pendulous accelerometer. The gyros are operated uncaged during inertial attitude hold and during maneuvers. Maneuver commands are fed into the gyro torquers. Gyro outputs provide attitude error signals. When the gyros are caged, their outputs are proportional to true body rates.

Analog Control Electronics - The control electronics implements the stabilization and control functional requirements. Body rates, measured by the caged rate integrating gyros, are integrated to approximate the attitude errors during mission phases where attitude control and measured rate are required. To constrain errors introduced by analog integrator drift, use of this dual mode circuitry must be limited to short time intervals, i.e., de-orbit thrust, entry, Aeroshell and aerodynamic decelerator separation, and terminal descent. During long mission phases requiring attitude hold, the gyros are operated open loop and the outputs (integrated body rate) are used as the inertial body reference. Integrated rate used to approximate inertial body attitude introduces coning errors that can accumulate during limit cycle operation. Caged IMU gyros can supply

CONFIGURATION I – FUNCTIONAL DIAGRAM – STRAPPED DOWN IMU WITH ANALOG CONTROL ELECTRONICS

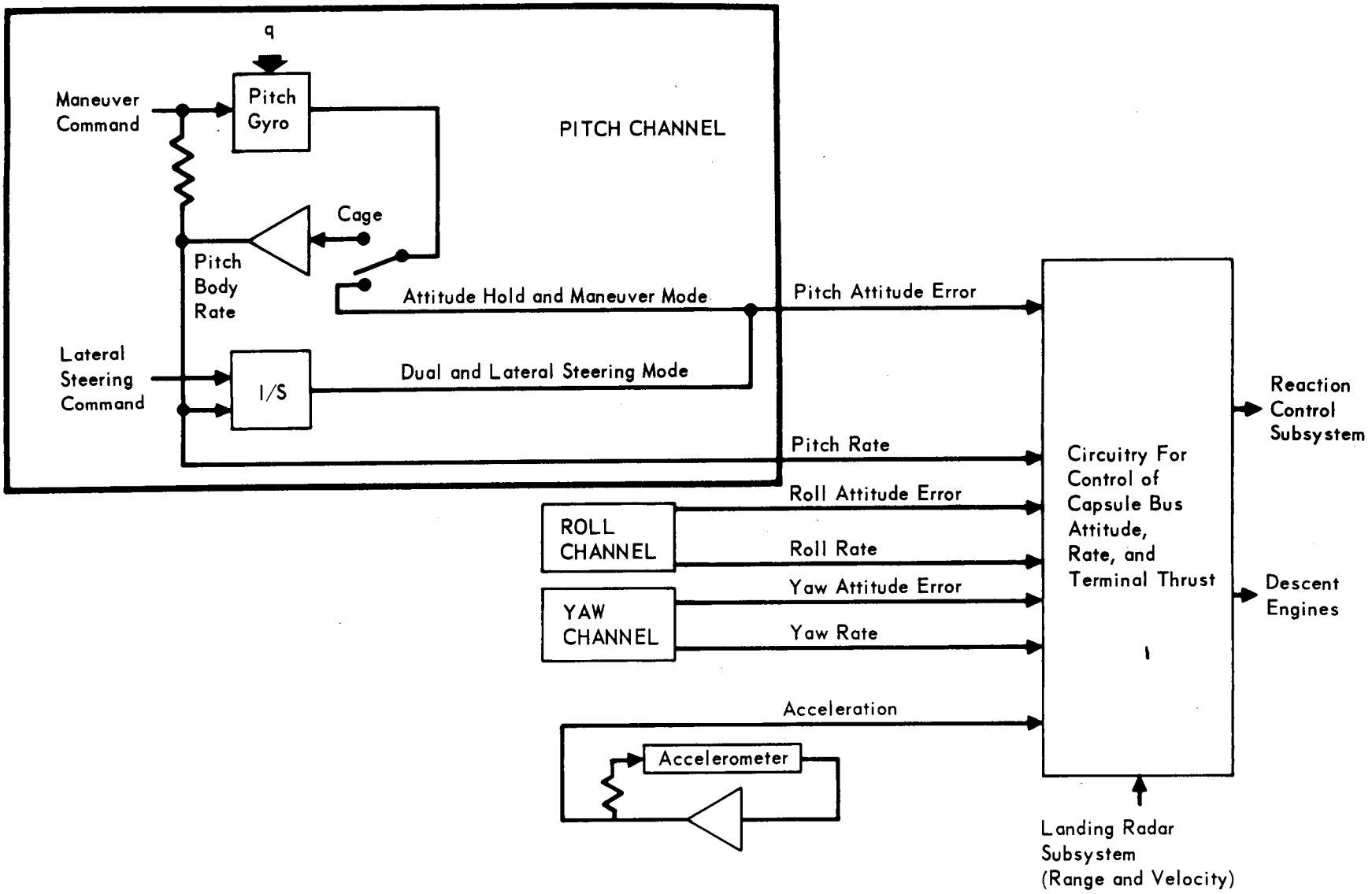

Figure 5.8–4

rate stabilization signals directly. Derived rate reaction jet logic is used for stabilization when the gyros are operated in the open loop attitude mode.

The accelerometer provides stabilization for the thrust control loop. Incremental velocity, calculated from acceleration, is compared to the de-orbit velocity to be gained to provide a de-orbit engine cutoff discrete.

The landing radar normal and lateral (X and Y) velocity signals are mixed with body rate and integrated to provide the Lander lateral steering signals during descent. The landing radar range signal programs the descent engine thrust command. When the range reaches 10 feet a terminal propulsion engine cutoff command is issued.

5.8.4.2 Configuration II - Strapped-down IMU with Digital Control Electronics - Configuration II is an expanded digital version of Configuration I. The system consists of a strapped-down IMU and a digital computer. Figure 5.8-5 is a functional schematic of the system.

Strapped-down IMU - The IMU consists of three pulse rebalanced, single degree of freedom, rate integrating gyros and an axially mounted, pulse rebalanced, pendulous accelerometer. The outputs of the package are pulses corresponding to rebalance torque pulses for each of the components. The pulses from the gyros are indications of the rotational increments that the body has turned about each axis and in the case of the accelerometer, represent velocity increments along the roll axis.

Digital Control Electronics - The control electronics for this configuration digitally performs the same guidance and control functions as the analog electronics of Configuration I. The attitude reference can be maintained more accurately because the integrals of linearized Euler rates are used in place of the integrals of body rates for approximating vehicle attitudes. During the long orbital coast period, four to six hours, the majority of the computer input/output circuitry can be de-energized and only that portion of the input/output circuitry required to control the RCS thrusters will remain active. Derived rate will be used in this mode of operation (true body rate is used at all other times). This deactivation feature conserves CB battery power.

5.8.4.3 Configuration III - Gimballed IMU with Analog Control Electronics - Configuration III is an all attitude GCS concept that consists of three packages: a gimballed IMU, rate gyro package, and analog control electronics. Figure 5.8-6 shows the functional schematic of these packages.

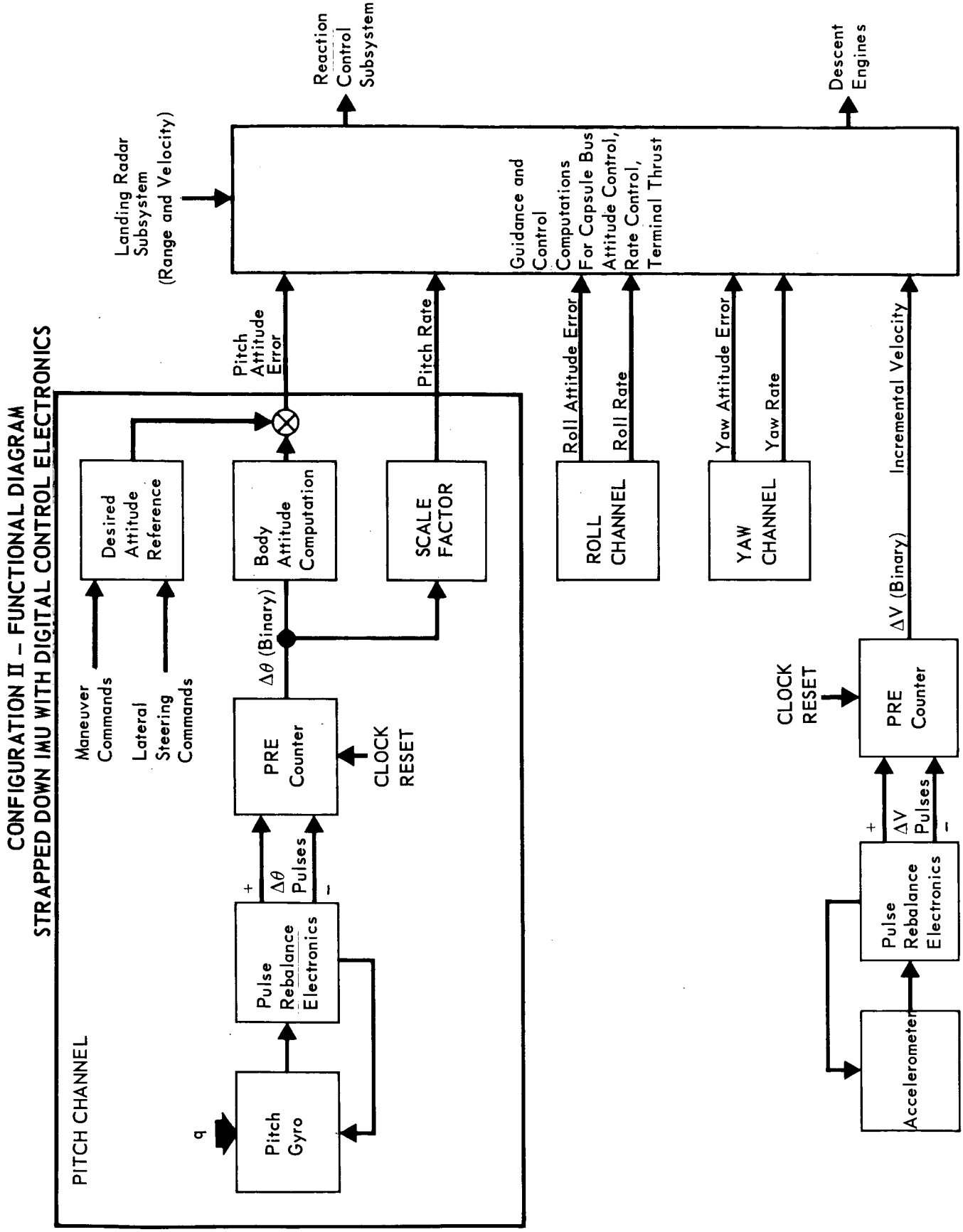
CONFIGURATION II – FUNCTIONAL DIAGRAM
STRAPPED DOWN IMU WITH DIGITAL CONTROL ELECTRONICS
PITCH CHANNEL
Pitch Gyro
q
Pulse Rebalance Electronics
+
Δθ Pulses
–
PRE Counter
CLOCK RESET
Δθ (Binary)
Maneuver Commands
Lateral Steering Commands
Desired Attitude Reference
Body Attitude Computation
SCALE FACTOR
Pitch Attitude Error
Pitch Rate
Landing Radar Subsystem (Range and Velocity)
Guidance and Control Computations For Capsule Bus Attitude Control, Rate Control, Terminal Thrust
Reaction Control Subsystem
Descent Engines
ROLL CHANNEL
Roll Attitude Error
Roll Rate
YAW CHANNEL
Yaw Attitude Error
Yaw Rate
Accelerometer
Pulse Rebalance Electronics
+
ΔV Pulses
–
PRE Counter
CLOCK RESET
ΔV (Binary)
Incremental Velocity

Figure 5.8–5

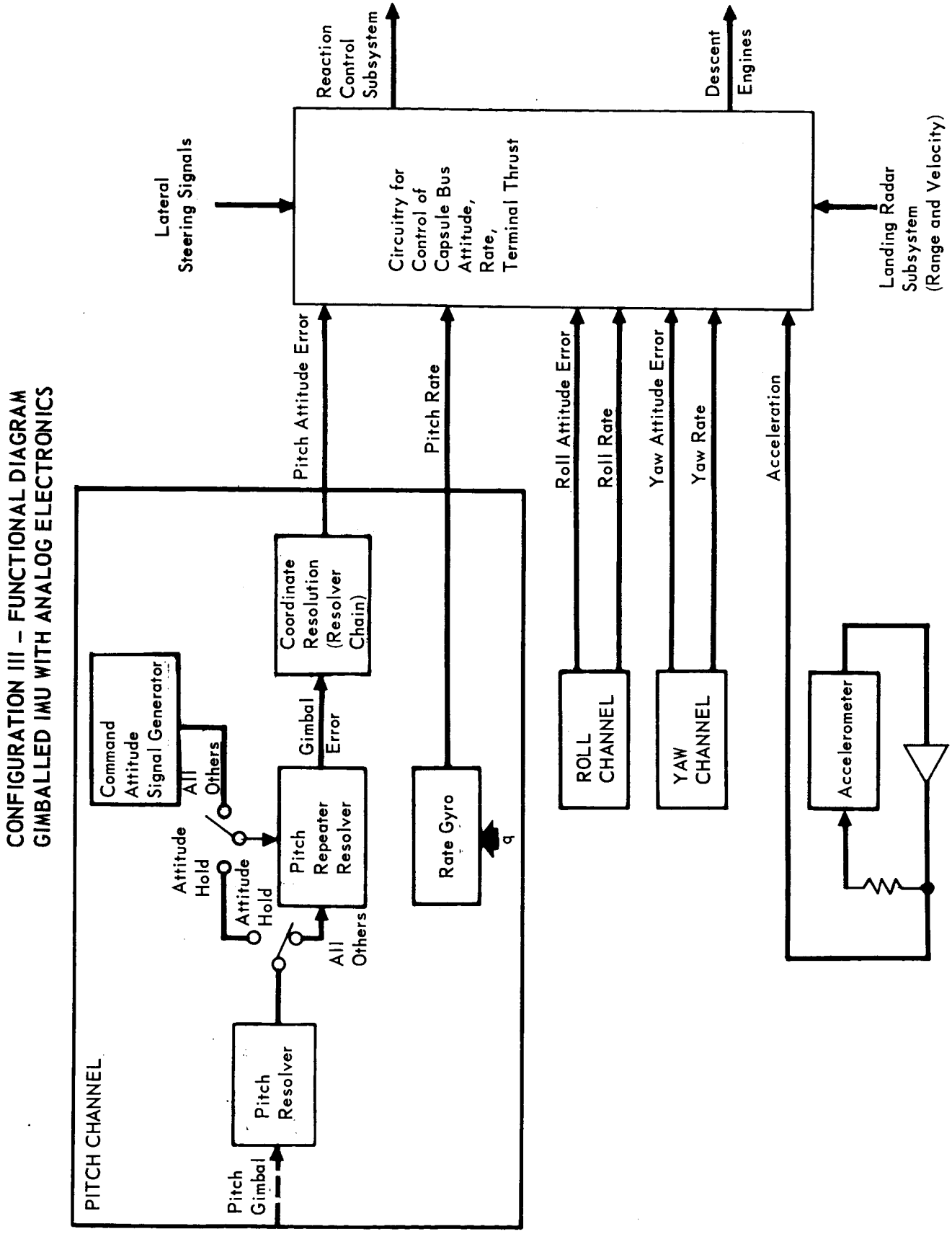
CONFIGURATION III – FUNCTIONAL DIAGRAM
GIMBALLED IMU WITH ANALOG ELECTRONICS
Lateral Steering Signals
Circuitry for Control of Capsule Bus Attitude, Rate, Terminal Thrust
Reaction Control Subsystem
Descent Engines
Landing Radar Subsystem (Range and Velocity)
Pitch Attitude Error
Pitch Rate
Roll Attitude Error
Roll Rate
Yaw Attitude Error
Yaw Rate
Acceleration
PITCH CHANNEL
Pitch Gimbal
Pitch Resolver
Command Attitude Signal Generator
All Others
Attitude Hold
Attitude Hold
Pitch Repeater Resolver
All Others
Gimbal Error
Coordinate Resolution (Resolver Chain)
Rate Gyro
q
ROLL CHANNEL
YAW CHANNEL
Accelerometer

Figure 5.8–6

Gimballed IMU - The IMU consists of three single degree of freedom rate integrating gyros mounted on the inner gimbal. The gimbal assembly consists of four gimbals (1st - pitch, 2nd - inner roll, 3rd - yaw, 4th - outer roll), associated servo-motors, resolvers, electronics and readout resolvers. A roll axis force rebalanced accelerometer is included within the platform case.

The vehicle inertial attitude reference is represented by the gimbal angles sensed by resolvers mounted on the 1st, 3rd, and 4th gimbal shafts. Two additional resolvers transform gimbal error signals to body coordinates.

Rate Gyro Package - This package consists of three body mounted rate gyros that are used to supply body rate information to the control electronics for rate stabilization.

Analog Control Electronics - As shown in Figure 5.8-6, each gimbal angle is subtracted from a commanded angle in a gimbal angle repeater resolver. The difference of the two signals is the gimbal error. This error is transformed into body coordinates through the platform resolver chain and applied to the attitude channel of the control electronics. The system is put into an attitude hold mode by uncoupling the repeater resolver and thus fixing the command angle to that stored in the repeater resolver at the instant of de-coupling. Rate stabilization is accomplished by summing the attitude error with measured body rates from the rate gyros. During the orbital descent period, the rate gyros are de-energized and derived rate is used for stabilization. During radar guidance steering, the landing radar velocity signals normal to the vehicle roll axis are normalized and summed with the rate gyro signals to drive analog integrators. The signals are then employed by the descent engine thrusters logic to steer the vehicle. The landing radar range output and the Z-axis velocity are used to control the vehicle to the descent velocity versus range profile. The accelerometer output is summed with the velocity command to provide stabilization of the thrust control loop. If, for any reason, the radar signals are lost, the GCS will go into an inertial attitude hold mode and command a constant deceleration. At a range equal to 10 feet, a descent engine cutoff command is issued.

5.8.4.4 Configuration IV - Gimballed IMU with Digital Control Electronics - Configuration IV is an all-attitude GCS concept that is a digitized version of Configuration III. It consists of three packages, a gimballed IMU, rate gyro package, and digital control electronics. Figure 5.8-7 is a functional schematic of this GCS concept.

CONFIGURATION IV – FUNCTIONAL DIAGRAM – GIMBALLED IMU WITH DIGITAL CONTROL ELECTRONICS

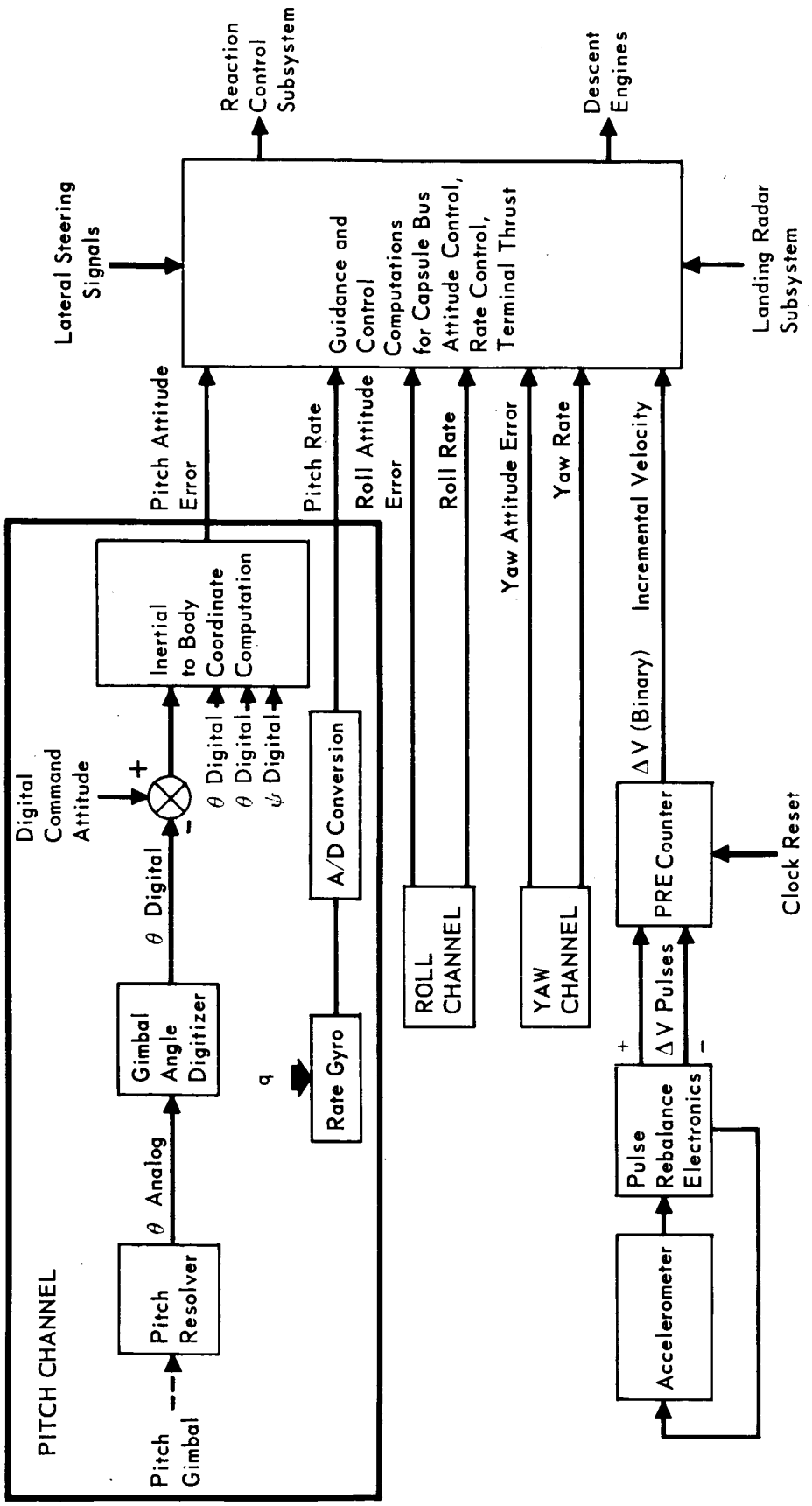

Figure 5.8–7

Gimballed IMU - The IMU consists of three single degree of freedom rate integrating gyros, an accelerometer, and a gimbal assembly identical, except for the absence of the resolver chain, to that of Configuration III.

Rate Gyro Package - This package contains three analog rate gyros identical to those of Configuration III.

Digital Control Electronics - The inputs to the control electronics are the IMU gimbal readout resolver signals, accelerometer signals, rate gyro rate signals, landing radar velocity and range signals, and sequencer and timer discretes and data words. The control electronics operates on these inputs to digitally perform all functions of the analog control electronics of Configuration III.

5.8.5 Evaluation of Candidate Subsystems - Figure 5.8-8 presents the design characteristics of the candidate GCS versus the VOYAGER Capsule functional and technical requirements. While all of the candidate systems can meet the functional and performance requirements established in Section 5.8.3, their physical characteristics differ considerably. The four candidate configurations are placed in two main groups - strapped-down IMU's and gimballed IMU's. Each of the main groups are further broken down into analog and digital control electronics mechanizations. In order to simplify the comparison of the candidates the comparison is presented in two stages; strapped-down versus gimballed IMU, and digital versus analog control electronics.

5.8.5.1 Gimballed versus Strapped-down IMU - The two IMU concepts are functionally identical. The inertial attitude reference is maintained mechanically by the gimbals in the gimballed IMU and electronically in the strapped-down system. The comparison of the two is, therefore, a comparison of mechanical complexity with electronic complexity.

Reliability - The strapped-down IMU mean-time-between-failure (MTBF) is three to seven times the gimballed IMU MTBF. Reliability of rotating mechanical joints and assemblies is a problem which is avoided in a strapped-down system. Elimination of slip rings also provides significant reliability improvement.

Redundancy - For improved reliability redundancy may be advisable in the IMU. Redundancy in a strapped-down IMU consists of duplication of sensors. An example is the addition of a fourth gyro in forming the skewed redundant gyro concept. If additional inertial components are added to a gimballed IMU, the inner element

GUIDANCE AND CONTROL SUBSYSTEM CANDIDATE COMPARISON MATRIX

COMPARISON FACTORS	STRAPPED-DOWN IMU CONCEPTS						GIMBALLED IMU CONCEPTS							
	I. ANALOG CONTROL ELECTRONICS			II. DIGITAL CONTROL ELECTRONICS			III. ANALOG CONTROL ELECTRONICS				IV. DIGITAL CONTROL ELECTRONICS			
Reliability (Estimated MTBF Range)	IMU 3,500– 8,000 Hr. Electronics 8,000–12,000 Hr. Total 2,430– 4,810 Hr.			IMU 3,500– 8,000 Hr. Electronics 7,500–10,000 Hr. Total 2,390– 4,450 Hr.			Rate Gyros 3,000– 6,000 Hr. IMU 500– 1,500 Hr Electronics 8,000–12,000 Hr. Total 407– 1,090 Hr.				Rate Gyros 3,000– 6,000 Hr. IMU 500– 1,500 Hr. Electronics 7,500–10,000 Hr. Total 405– 1,070 Hr.			
Redundancy	Incorporated by duplication of inertial components; e.g., 4 skewed gyro IMU.			Incorporated by duplication of inertial components; e.g., 4 skewed gyro IMU.			Not feasible to implement with a single IMU – duplication of IMU needed for useful redundancy.				Not feasible to implement with a single IMU – duplication of IMU needed for useful redundancy.			
Constraints to meet Voyager requirements	Cannot maintain attitude reference after aero decelerator deployment – attitude errors must be kept small to de-orbit.			Limited attitude configuration cannot maintain attitude reference after aerodecelerator deployment and attitude errors must be kept small to de-orbit. No constraints with an all-attitude configuration.			None.				None.			
Interface Simplicity	Sequencer and timer, radar, telecommunications, are digital interfaces, therefore, interface is complex; descent engines are analog.			Simple interface with digital subsystems.			Complex interfaces with digital subsystems.				Simple interfaces with digital subsystems.			
	IMU	ELECTRONICS	TOTAL	IMU	ELECTRONICS*	TOTAL	IMU	RATE GYROS	ELEC-TRONICS	TOTAL	IMU	RATE GYROS	ELEC-TRONICS	TOTAL
Size – Cu.In.	390	400	790	390	460–500	850–890	550	65	450	1065	550	65	400	1015
Weight – Lb.	17	13	30	17	15–19	32–36	19	3	16	38	19	3	15	37
Power – W	55	45	100	55	50–75	105–130	55	12	60	127	55	12	55	122
Energy – W-Hr.			320	*Varies with capability		330–350				340				340

Functional and Performance Capability	Meets maximum attitude reference accuracy requirement at de-orbit. Reference frame drift equals gyro drift plus coning error.	Meets design goal attitude accuracy at de-orbit. Reference frame drift equals gyro drift.	Meets design goal requirements. Reference frame drift equals gyro drift.	Meets design goal requirements. Reference frame drift equals gyro drift.
Sterilization	Sterilizable inertial sensors in development under JPL contracts; however, tight tolerances required for analog circuitry are difficult to maintain through high temperature sterilization cycles.	Minimum sterilization problems. Sterilizable inertial sensors in development under JPL contracts; wide tolerances allowed on digital circuitry decreases high temperature sensitivity.	Potential problem with IMU lubricants, bearings, and slip-rings when subjected to sterilization cycles. Tight tolerances required with analog circuits are potential problem.	Potential problem with IMU lubricants, bearings, and slip-rings. Wide tolerances allowed with digital circuitry enhances electronics sterilization qualification.
Experience	Used on Surveyor. Strapped down gyros used on Mariner, Ranger, Lunar Orbiter, Agena.	Used on PRIME-digital autopilot developed for BRGV.	Two axis system used on classified program.	Used on BGRV. Gemini with analog autopilot.
Development Status	Sterilizable inertial components in development under JPL contract, Honeywell GG334S gyro and Bell VII accelerometer, circuit sterilization studies in process at JPL.	Sterilizable inertial components in development, memory and circuitry sterilization studies in process at JPL.	No sterilizable inertial platform in development.	No sterilizable inertial platform in development.
Flexibility	Inherently inflexible. Change in mission profile requires control electronics change and possible requalification.	Very flexible. Mission changes require no hardware changes, only software.	Analog electronics. Inherently inflexible; hardware redesign and requalification may result from mission changes.	Very flexible. Only software changes required for mission changes.
Growth Potential	Low. New requirements will necessitate redesign and probable requalification of electronics.	High. Only software changes necessary to accommodate new requirements; with proper electronics sizing, concept is capable of growth from limited attitude to all attitude reference with no hardware change.	Low. New requirements will necessitate redesign and probable requalification.	High. Only software change necessary for new requirements. Attitude reference is fixed.
Cost	Mission changes may increase cost and development time if redesign is necessary.	Cost and schedules can be accurately estimated at beginning of program. Very little cost increase if mission requirements change.	Sterilizable platform development will be expensive.	Sterilizable platform development will be expensive.

Figure 5.8-8

S-8-15-2

becomes more massive and increases the stresses on the gimbal bearings and torque motors. Larger and more power consuming gimbal structures and motors would be required to accommodate these stresses. The torque motors, bearings, slip rings, and resolvers are an integral part of the IMU and also require redundant components. No simple way of providing redundancy for all of these components has been devised, outside of complete IMU redundancy.

Size, Weight and Power - The gimballed is 10 percent heavier than the strapped-down. Power consumtpion is the same for the two approaches. The strapped-down IMU is smaller in size because of the improved packaging efficiency that can be achieved. An additional disadvantage of the gimballed system is the shape restrictions that result from the clearance requirements of the rotating gimbals. These constrain the gimballed IMU to assume a spherical or cylindrical shape, whereas the strapped-down configuration provides more packaging freedom.

Functional and Performance Capability - Both of the IMU configurations can meet the functional and performance requirements. The gimballed IMU is inherently an all-attitude concept, which is not necessarily a requirement for VOYAGER. The strapped-down concept can be designed as either a limited attitude or an all-attitude inertial reference.

Development Risk - The mechanical complexity of the gimballed IMU poses a potential sterilization problem. Bearing and slip ring corrosion may result from evaporation of the lubricants and outgassing of other components when subjected to high temperatures. Development of a sterilizable gimballed IMU for VOYAGER type application has apparently not been attempted, whereas, strapped-down inertial component sterilization has been the subject of several studies under JPL contracts. Honeywell Aero has demonstrated that the production GG159 gyro can be sterilized with minor modifications. These modifications are incorporated in a special version, the GG334S, that is presently in test at JPL. Bell Aerosystems is developing sterilizable accelerometers (Bell VII) and expects to deliver hardware in 1969. Strapped-down IMU's have been used in most long lived space vehicles to date; e.g., Mariner, Ranger, Lunar Orbiter, Surveyor. Where gimballed platforms were employed, the mission duration and requirements were not compatible with the VOYAGER mission, e.g., Gemini.

5.8.5.2 Analog versus Digital Electronics - Analog implementation of GCS electronics is characterized by a large number of simple circuits arranged in specialized functional groups one for each of the VOYAGER GCS functions. In contrast, digital implementation is complex, but capable of satisfying all of the required GCS functions with a single basic mechanization. The comparison of the characteristics of the two concepts are discussed below.

Size, Weight, Power Reliability - the size, weight, power and reliability of the two concepts are nearly equal.

Functional and Performance Capability - The analog strapped-down system has a higher reference frame drift than a digital system because it is more susceptable to coning errors. Coning effects are inherent in a gyro when it is subjected to motions, such as occur during limit cycle attitude control, that cause its input axis to inscribe a cone in space. This effect is a rotational input to the gyro caused by the non-commutativity of the Euler angles. In an analog system, Euler angles are approximated by the integrals of body rates, whereas, a computer can calculate the exact attitude error by integrating the true Euler rate equations. Coning error due to a ± 2 degree attitude deadband prevents the analog system from satisfying the de-orbit error constraint of 0.87 degrees (design goal). This constraint can be met if the deadband is reduced to ± 0.5 degrees. Figure 5.8-9 shows how attitude uncertainty grows with time. Coning error accounts for most of the increased drift of an analog attitude reference over a digital reference.

Flexibility - Analog control electronics are tailored to fit given functional and performance requirements which must be fixed prior to hardware design and development. A change in the requirements will necessitate a change in the hardware and a possible requalification of the system. Analog mechanization of the control functions is therefore, an inflexible system. Digital implementation, to the contrary, results in a very flexible system. With properly designed electronics, only software changes are required to meet different mission profiles or changes in the functional requirements.

An illustration of the flexibility of digital electronics is the manner in which a landing radar requirement was fulfilled. During the aerodynamic decelerator portion of entry, it is necessary to process body rate information through an appropriate computation to align the attitude reference to the wind referenced velocity

DRIFT REDUCTION BY USE OF DIGITAL ELECTRONICS

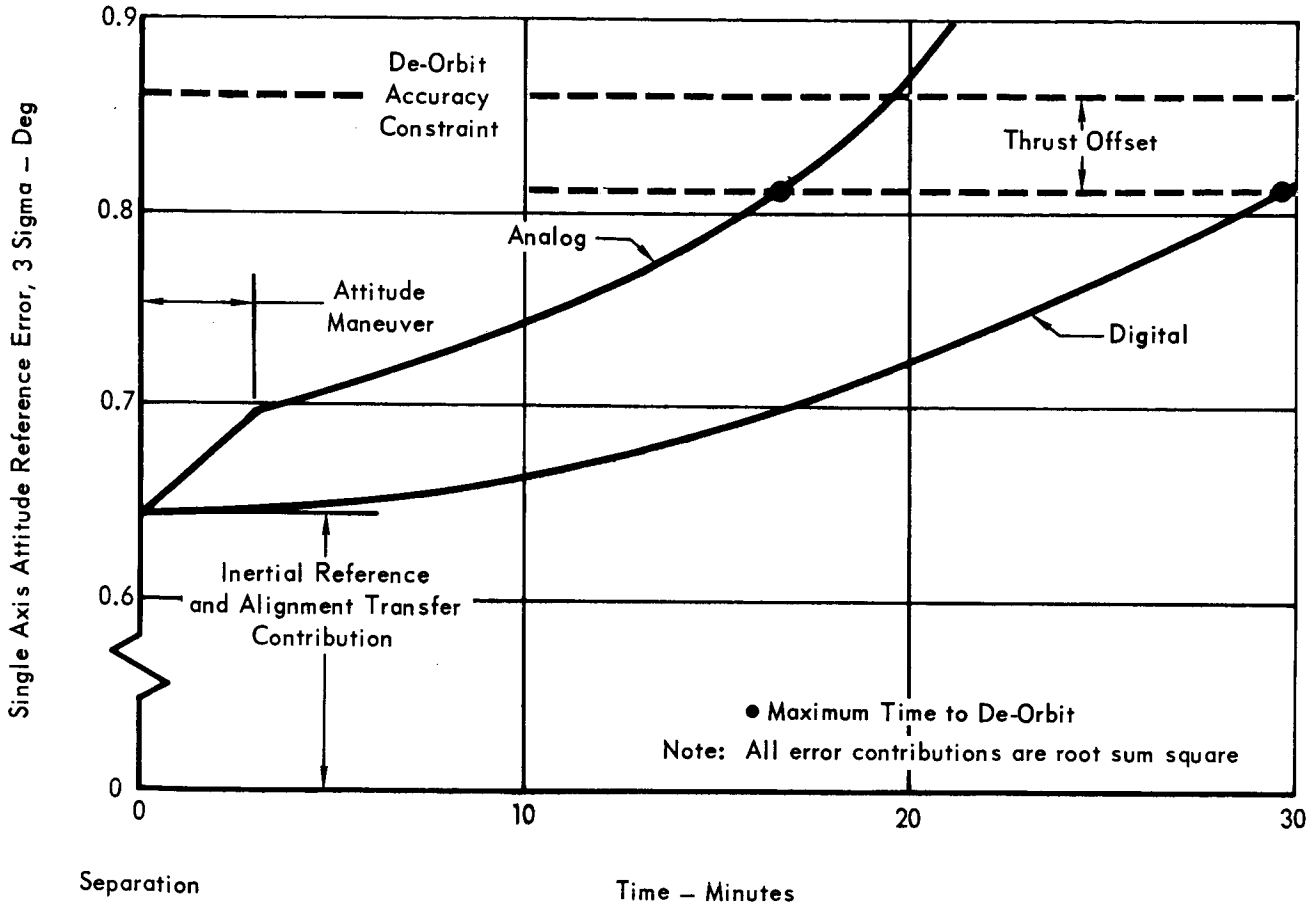

Figure 5.8–9

vector in order to ensure radar acquisition. The digital GCS permitted the implementation of this function with only a minimal increase in memory allocation. To mechanize this same function in an analog system, it required a minimum of six multipliers, six switches, two summing amplifiers, and an order of magnitude increase in the dynamic range of the integrators.

Growth Potential - Analog control electronics, because of their inflexibility, have very little growth potential. Sufficient instruction repertory and reserve speed and memory capacity of a digital computer can be selected, at very little cost in size, weight, or power, so that confidence in meeting future VOYAGER mission requirements can be established.

5.8.6 Recommended Design Approach - The configurations employing gimballed IMU's were eliminated by the low reliability of the platform. The high development risk resulting from the sensitivity to sterilization and lack of suitable hardware designs was also a major contributor to the gimballed IMU's elimination. Therefore, a strapped-down IMU is the approach to be used on the VOYAGER GCS. The electronics for the GCS can be either digital or analog. There is a performance penalty if an analog system is used; however, it is not considered to be significant enough to eliminate the analog approach as a candidate. The major trade areas of the two approaches are versatility and standardization. The requirements for later missions are indefinite at this date. A simple change in mission profile, such as revision of the terminal range versus velocity profile, could require significant hardware changes in an analog system. The inability of an analog system to accommodate mission changes without hardware changes, and probable environmental requalification, means that the mission profile must be frozen at the start of hardware development or run the risk of schedule slippage. To freeze the profile at the beginning of development would mean that the knowledge gained in the following years must be ignored. Digital systems, because of their versatility, ensure confidence in meeting a development schedule and, because the mission profile is implemented by software, a standardized digital system with sufficient reserve capacity can be designed with assurance that it will meet the mission requirements that exist in 1979. The strapped-down IMU with digital control electronics is the selected VOYAGER GCS configuration.

5.8.6.1 Details of the Design Selection Matrix - Figure 5.8-10 is a design selection matrix of the candidate subsystems. The selection criteria are weighted in order of importance. The factors that contribute to each criterion are also weighted in the same manner. These factors are discussed within the body of Section 5.8.5. Each candidate was assigned a utility value of 0 to 1.0 to establish the degree to which it complies with the selection factors. The score of a particular design was found by multiplying the criterion weight, the factor weight and the utility value and totaling the results. The matrix indicates that the strapped-down IMU with digital electronics configuration is considerably better than its closest competitors and illustrates the selection of this GCS implementation for VOYAGER.

5.8.6.2 Selection Criteria and Factors - Probability of Mission Success - Criterion Weight: 0.35 - The factors contributing to the probability of mission success are:

a. Reliability
b. Redundancy
c. Interface Simplicity
d. Constraints on Other Systems

The most important factor is reliability of the GCS subsystem. This factor was assigned a weight of 0.7. The other three factors are estimated to be of equal importance in selecting the design of the GCS and are assigned weighted values of 0.1 each.

System Performance - Criterion weight: 0.20 - The factors contributing to system performance are:

a. Size
b. Weight
c. Energy
d. Functional and Performance Capability

Power consumed by the GCS was not considered in the selection because the total energy consumed by the GCS throughout the mission is considered to be a more relevant factor. The capability of the GCS to meet the functional and performance requirements is judged to be the most important factor and was assigned a weight of 0.5. The weight and energy requirements were determined to be of equal importance and assigned a weight of 0.2 each. Size was assigned a weight of 0.1.

DESIGN SELECTION MATRIX

SELECTION CRITERIA	WEIGHT (C)	CRITERION FACTORS	WEIGHT (F)	I. STRAPDOWN IMU WITH ANALOG ELECTRONICS		II. STRAPDOWN IMU WITH DIGITAL ELECTRONICS		III. GIMBALLED IMU WITH ANALOG ELECTRONICS		IV. GIMBALLED IMU WITH DIGITAL ELECTRONICS	
				UTILITY FACTOR (U)	WEIGHTED SCORE (C) (F) (U)	UTILITY FACTOR (U)	WEIGHTED SCORE (C) (F) (U)	UTILITY FACTOR (U)	WEIGHTED SCORE (C) (F) (U)	UTILITY FACTOR (U)	WEIGHTED SCORE (C) (F) (U)
Probability of Mission Success	.35	Reliability	.7	1.0	.245	0.9	.220	0.2	.049	0.2	.049
		Redundancy	.1	1.0	.035	1.0	.035	0	0	0	0
		Interface Simplicity	.1	0.2	.007	1.0	.035	0.2	.007	1.0	.035
		Constraints on System	.1	0.6	.021	0.8	.028	1.0	.035	1.0	.035
System Performance	.2	Size	.1	1.0	.020	0.9	.018	0.7	.014	0.8	.016
		Weight	.2	1.0	.040	0.8	.032	0.8	.032	0.8	.032
		Energy	.2	1.0	.040	0.9	.036	0.9	.036	0.9	.036
		Function and Performance Capability	.5	0.7	.070	1.0	.100	1.0	.100	1.0	.100
Development Risk	.15	Sterilization	.5	0.7	.053	1.0	.075	0.3	.023	0.3	.023
		Experience	.1	1.0	.015	0.5	.007	0.5	.007	0.5	.007
		Development Status	.4	1.0	.060	1.0	.060	0	0	0	0
Versatility	.15	Flexibility	.7	0	0	1.0	.105	0	0	1.0	.105
		Growth Potential	.3	0	0	1.0	.045	0	0	1.0	.045
Cost	.1		1.0	1.0	.100	1.0	.100	0.8	.080	0.8	.080
Weighted Score					.706		.896		.383		.563

Figure 5.8–10

Development Risk - Criterion weight: 0.2 - The factors contributing to development risk are:

a. Sterilization

b. Experience

c. Development Status

Sterilization and development status are difficult to differentiate between. Hardware that can meet the functional and performance requirements of the VOYAGER GCS has been developed for all of the candidate configurations. However, development of hardware that is capable of withstanding the sterilization environment has not been accomplished in all cases.

The present status of development is considered to be of slightly less importance than the ease with which sterilizable components that will meet the VOYAGER mission requirements can be developed. Sterilization was assigned a weight of 0.5 and a development status - 0.4. Experience was assigned a weight 0.1.

Versatility - Criterion weight: 0.15 - The factors of GCS versatility are:

a. Flexibility

b. Growth Potential

Flexibility is of primary importance for this study, since the probability of requirements changing after equipment design is greater than the probability that the performance requirements will increase. Flexibility was assigned a weight of 0.7 and growth potential 0.3.

Candidate Configuration Utility Factors - The configurations were assigned a utility factor for each of the criterion factors. The candidate configuration whose characteristics best satisfy the criterion was given the utility factor of 1.0. The degree that the other candidates measured up to the best configuration was assessed and a relative estimate made of their utility factor.

5.9 RADAR - The general approach used to select the preferred VOYAGER Capsule Lander radar subsystem configuration was:

a. Determine the radar requirements for each alternate landing concept.
b. Establish radar subsystem alternatives for each landing concept.
c. Combine alternate radar subsystems that apply to several landing system concepts.
d. Request technical information from interested vendors asking for specific designs for these radar subsystem alternatives.

The chain of activities is shown in Figure 5.9-1. These included computer simulations and parametric studies, evaluation of vendor supplied data, and definition of a preferred radar subsystem for the selected landing concept. During these activities the existing Lunar Module (LM) landing radar was used as a reference point.

Potential radar subsystem problems are discussed in Section 5.9.1. Then, in Section 5.9.2 the requirements for the various landing system configurations are combined, and vendor responses are presented. In Section 5.9.3 the requirements for the preferred Capsule Lander radar altimeter and landing radar concepts are presented. The landing radar selection and performance are given in Sections 5.9.4 and 5.9.5, respectively. The radar altimeter selection and performance are given in Sections 5.9.6 and 5.9.7.

5.9.1 Potential Problems and Alternatives - Potential radar subsystem problems and possible solutions are discussed as they appeared at the beginning of this study. The problems are mostly associated with the use of a single radar to make all measurements required for landing. Figure 5.9-2 is presented to define the radar terminology.

5.9.1.1 Attitude - Lander attitude affects the point at which radar acquisition occurs via the variation in received power with beam slant range and incidence angle. The lander pitch angle profile will be influenced by the atmospheric model, deceleration techniques employed, entry conditions, and wind model. The radar must acquire before the thrust axis can be aligned with the velocity vector. At that time, the mean pitch attitude will be determined by the aerodynamic velocity vector, and steady state winds will have no effect. However, staging transients, wind gusts, and vehicle aerodynamic characteristics will cause oscillations about this mean pitch angle. One approach to improve the radar acquisition probability is to increase the radar transmitter power and/or receiver sensitivity. Alter-

PHASE B STUDY ACTIVITIES

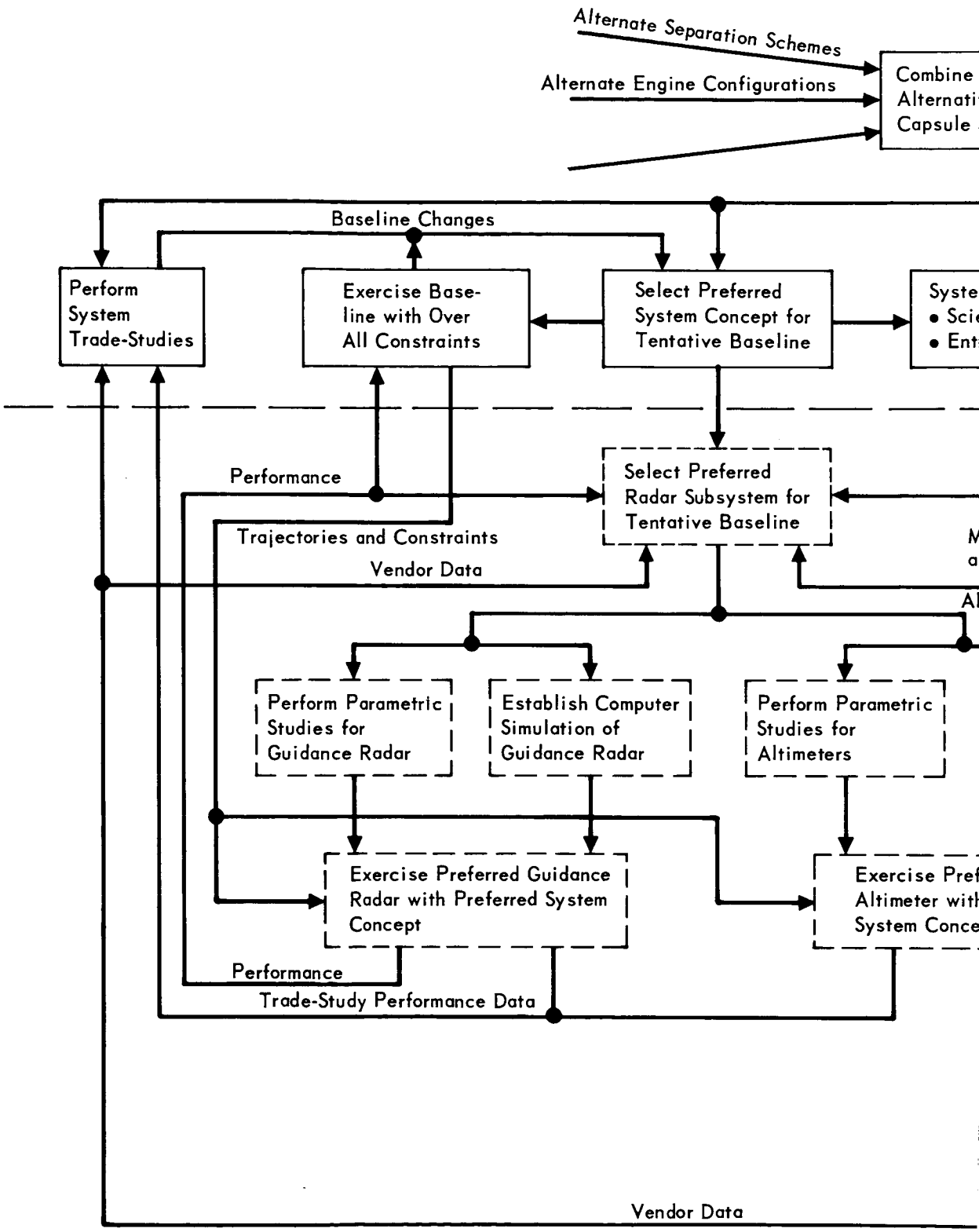

Figure 5.9–1

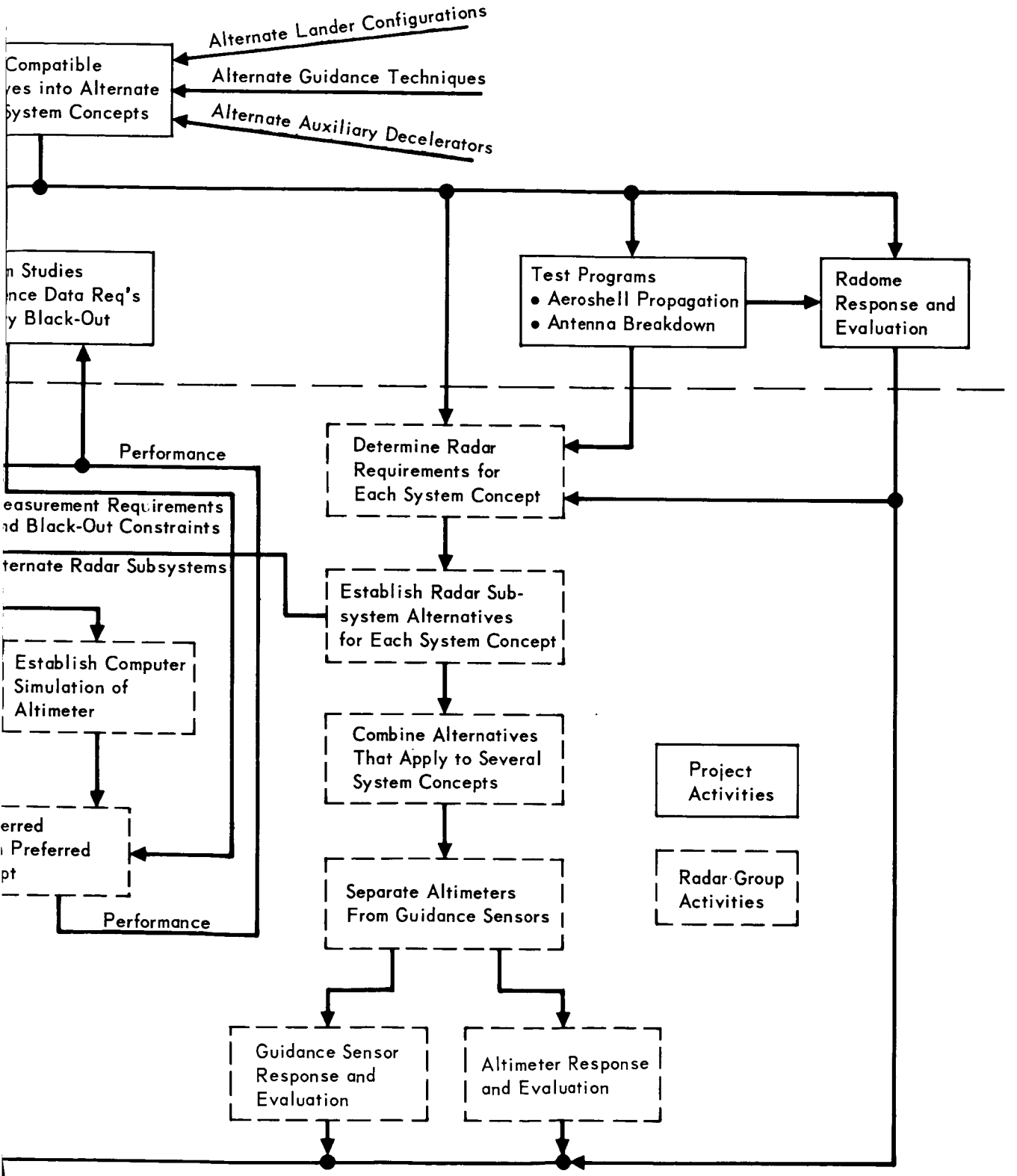
Alternate Lander Configurations
Alternate Guidance Techniques
Alternate Auxiliary Decelerators
Compatible
es into Alternate
System Concepts
n Studies
nce Data Req's
y Black-Out
Test Programs
• Aeroshell Propagation
• Antenna Breakdown
Radome
Response and
Evaluation
Performance
Determine Radar
Requirements for
Each System Concept
easurement Requirements
id Black-Out Constraints
ternate Radar Subsystems
Establish Radar Sub-
system Alternatives
for Each System Concept
Establish Computer
Simulation of
Altimeter
Combine Alternatives
That Apply to Several
System Concepts
erred
Preferred
pt
Performance
Separate Altimeters
From Guidance Sensors
Project
Activities
Radar Group
Activities
Guidance Sensor
Response and
Evaluation
Altimeter Response
and Evaluation

DEFINITION OF RADAR TERMINOLOGY

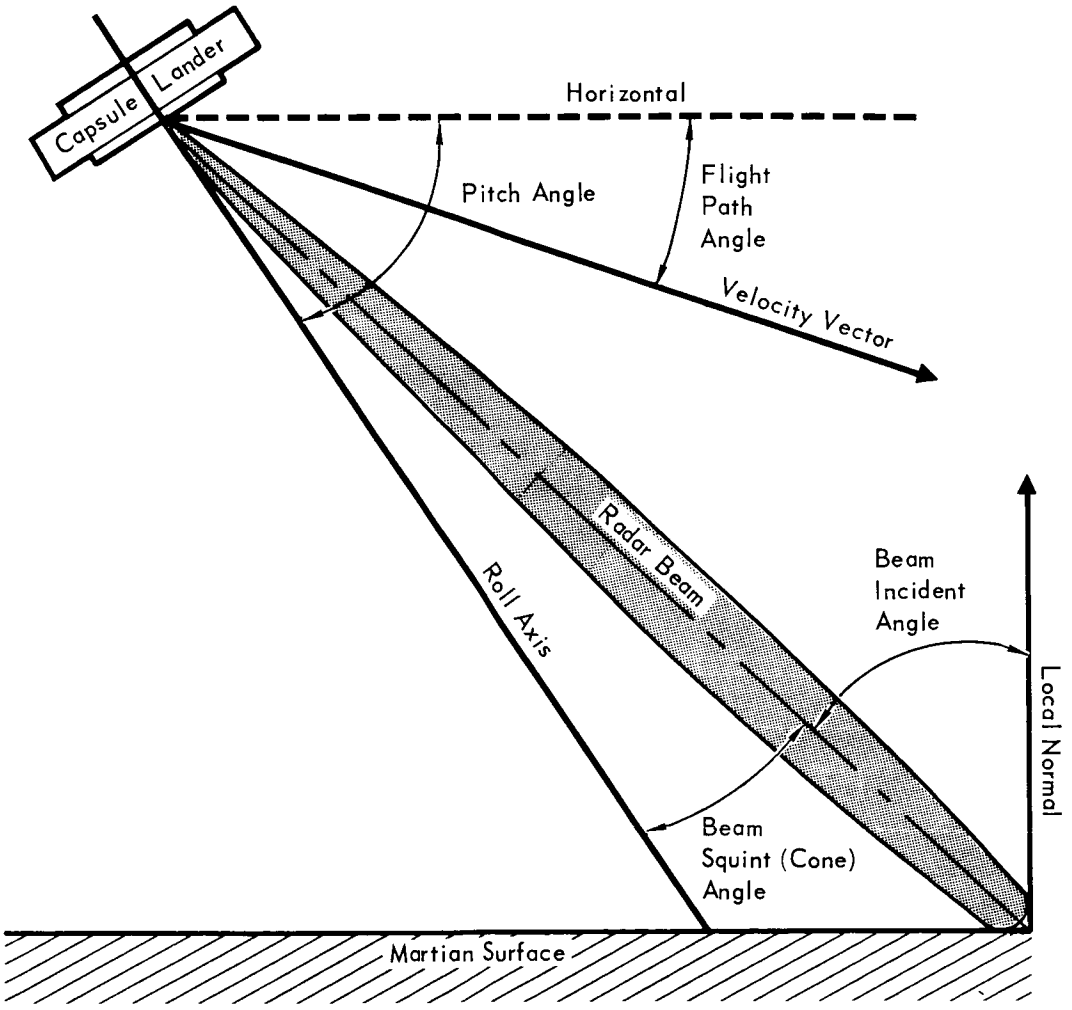

Figure 5.9–2

nately or in combination, the radar beam incident angles can be improved. The trajectory can be verticalized by early use of rockets or auxiliary aerodynamic decelerators (in which case other provisions must be made to trigger these devices). Also, radar beam incident angles can be minimized by proper implementation of the beam configuration. If lander roll position control is available, the radar beam group can be tilted away from the vehicle roll axis toward the vertical. If a preferred roll position is not available, the number of radar beams can be increased to assure that at least three have a favorable incident angle. A direct extension of these techniques would employ single or multiple beam scanning.

With a steady state wind, the roll axis will not be aligned with the velocity vector after radar acquisition, so a pitch maneuver is required. If the direction of the wind is such as to require a more shallow pitch angle, radar break lock on one or more velocity beams may occur. The same techniques may be employed to avoid breaking lock during velocity vector alignment. In addition, attitude rate limiting can be used to reduce the pitch angle transient during this maneuver.

5.9.1.2 Attitude Rates - Lander attitude rates will induce rates on the various radar measurement parameters (e.g., slant range and velocity). Although the signal-to-noise ratio may be sufficient for signal detection and acquisition in the static case, excessive rates may prevent tracking. The point at which break lock occurs depends primarily upon signal-to-noise ratio, signal bandwidth, and tracking point. The signal parameters determine tracker loop gain, and, consequently tracking rate capability. Generally, higher pitch and yaw rates are tolerable with lower altitudes and smaller incident angles.

Prior to velocity vector alignment, wind gusts, vehicle aerodynamic characteristics, and staging transients influence attitude perturbations. These perturbations depend on the particular terminal descent concept and landing mode. Pitch perturbations with large rates and amplitudes are expected with auxiliary aerodynamic decelerators, especially at separation. During the initial Aeroshell only deceleration phase, similar but lower amplitude pitch oscillations are anticipated. After the radar has established track and the velocity vector alignment maneuver has been initiated, the ensuring induced rates during the maneuver can also result in break lock.

The radar tracking capability can be maximized by increasing transmitter power and/or receiver sensitivity, increasing loop gains, or selecting tracking filter bandwidths consistent with the expected rate-induced tracking errors.

In addition, steps may be taken to improve the radar beam incident angles as discussed in Section 5.9.1.1. At a given altitude, smaller incident angles will result in higher signal-to-noise ratios and loop gains which will provide greater rate tracking capability. For slant range tracking, smaller beam incident angles reduce the range rate sensitivity to pitch rates. Also, rate limiting may be employed by the Guidance and Control Subsystem to control attitude rates during the velocity vector alignment maneuver.

5.9.1.3 Acquisition Time - Signal acquisition requirements will be determined by the terminal descent concept. In order to detect the received signal and establish track, the radar must search over a predetermined uncertainty interval for each tracked parameter. The terminal descent concept will influence the time available for searching, the size of the uncertainty interval, and the trajectory point at which acquisition must be completed.

In general, the time required for the radar to complete acquisition will decrease with decreasing altitude, beam incident angle, and velocity. These conditions result in increased signal-to-noise ratio, thereby allowing increased search rates for the same probability of detection. In addition, they result in a smaller range and velocity uncertainty interval to be searched.

Several design techniques are available to minimize the acquisition time. The search interval may be optimized with respect to the uncertainty interval, and may be updated during descent via auxiliary marks. A simultaneous searching process could be employed at the expense of increased complexity. The search rate could be optimized with respect to the anticipated signal-to-noise ratios. Alternately, detection could be accomplished in a static manner, by merely waiting for the dynamic signal parameter to fall into a predetermined interval (one or more detection bins).

The acquisition time available to the radar and the uncertainty interval to be searched may be minimized by proper implementation of the terminal descent concept and sequence. Auxiliary deceleration devices combined with delaying the point at which radar operation is required will minimize the uncertainty interval and maximize the signal-to-noise ratio. Careful control of event sequencing will maximize the time available for searching.

5.9.1.4 Aeroshell Lock-On - There is the possibility that the Aeroshell will remain within the field of view of the radar after separation and interfere with radar operation.

Reflections from the back side of the Aeroshell have been estimated for a model Aeroshell which included ring support structure, but did not include internally mounted equipment. The resultant radar cross section for X-band is shown in Figure 5.9-3. The narrow tail-on spike ($\theta = 0°$) has approximately the same amplitude at L-band but is slightly wider. This tail-on spike is primarily due to the combined reflections from the ring structure and nose cap flange. The spikes at angles 20 degrees from the roll axis are due to the normal reflections from the shallow angle conical ring stiffeners, and are 10 dB lower than shown at L-band. The spikes at 30 degrees are due to reflections from the inner side of the Aeroshell. Again, they are 10 dB lower than shown for L-band.

The radar cross section for angles between zero and 30 degrees is the same for both L-band and X-band. This reflection is primarily from the spherical nose cap but fluctuates above and below 6.5 square meters as the reflections from the ring structure combine in and out of phase. Alternatives for eliminating or reducing the possible interference caused by Aeroshell reflections after separation are:

- Employ separation techniques where the Aeroshell falls behind the lander.
- Control auxiliary aerodynamic decelerator size and deployment time, Aeroshell/lander separation time, and aerodynamic decelerator release time, so as to result in the maximum separation distance between the Aeroshell and lander when radar operation is required.
- Actively control Aeroshell (with flaps or jets), or lander trajectories, to produce large separation angles when radar operation is required.
- Reduce reflections from back of the Aeroshell by choice of mechanical design and/or the use of radar absorbing material.
- Make the radar able to discriminate between the reflection from the Aeroshell and the surface on the basis of range or velocity.

5.9.1.5 Aeroshell/Radome Propagation Effects - Most landing concepts require that some radar measurement be made while within the Aeroshell. Ablative Aeroshell propagation tests show that the transmission losses are quite high after charring. For example, the two way losses at X-band are 10 dB at normal incidence for some charred ablation materials. Several materials were tested and it became evident that those landing concepts employing velocity sensing through the Aeroshell (at high operating frequencies to get the narrow beams) would probably require a non-ablative radome.

X-BAND AEROSHELL RADAR CROSS SECTION ESTIMATE

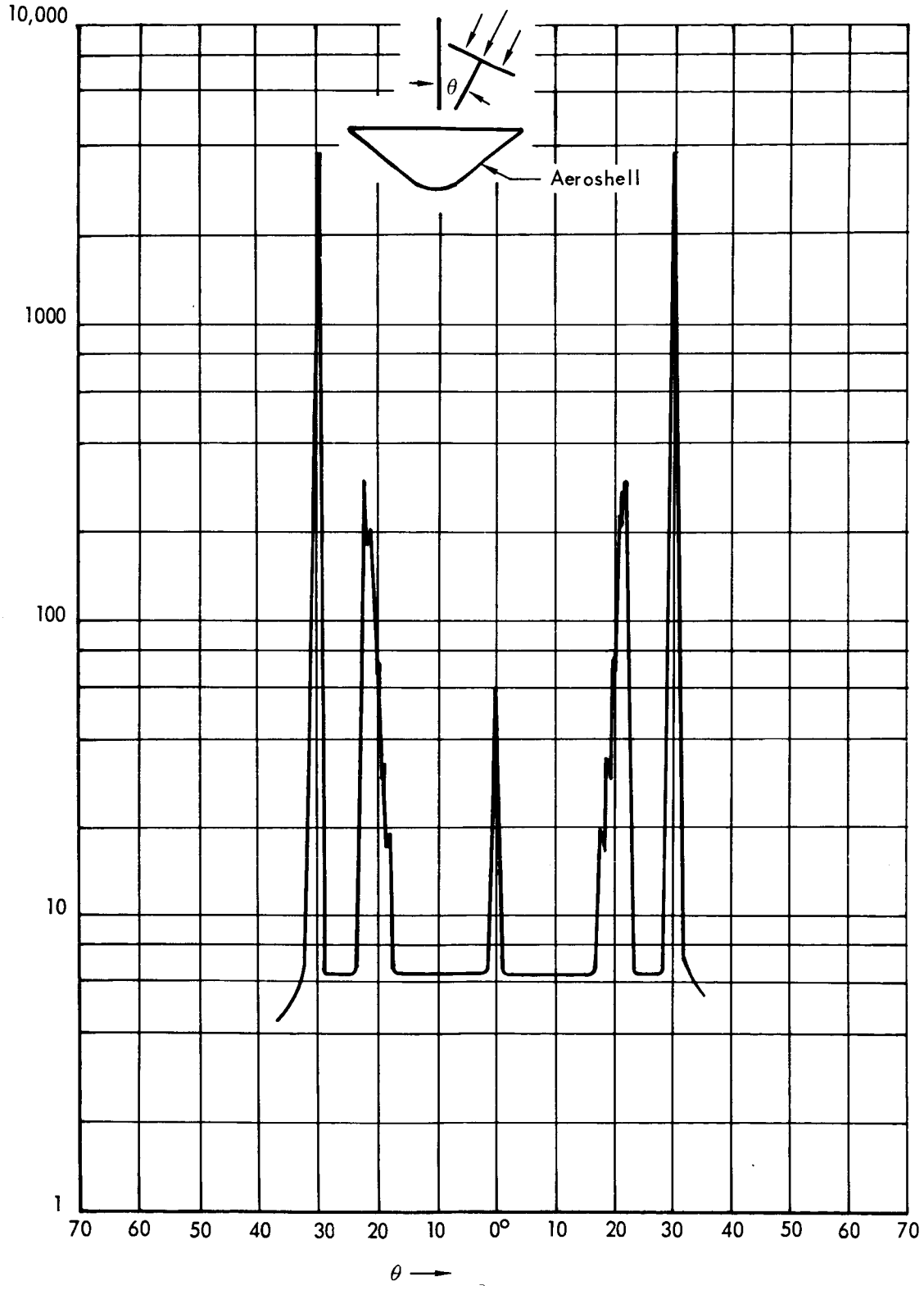

Figure 5.9-3

Vendors were contacted to determine the status of a non-ablative radome development. Responses show that none have built a radome of the required size to withstand the expected heating loads. One proposed radome technique looks promising for satisfying the physical and electrical requirements. However, development is required to prove its feasibility.

The electrical requirements were severe in terms of the allowed reflections, because McDonnell had been looking at CW velocity sensors of the type used on LM and Surveyor. However, contacted radome vendors indicated they could meet the reflection requirements, and the LM radar manufacturer indicated they could operate with these reflections, within the predicted levels of radome vibration. It was evident that considerable testing would be required in Phase D to assure that the radome and radar were compatible.

Later, additional modulation schemes were investigated for the velocity sensor to provide some range discrimination against radome reflections (Reference Sections 5.9.2.2 and 5.9.4.2).

In summary, it appeared that alternate solutions for solving the potential Aeroshell/radome reflection problem were as follows:

- Develop a radome for use with an existing CW velocity sensor (such as used on LM and Surveyor) for those concepts requiring range and velocity sensing prior to Aeroshell separation.
- Develop a new landing radar, capable of operating through an ablative Aeroshell, if range and velocity sensing is required prior to Aeroshell separation.
- Choose a landing concept that requires only altitude measurements prior to high altitude separation of the Aeroshell. (Altitude measurements are best made with an altimeter operating at L-band frequencies where losses through a charred ablative heat shield are not severe.)

5.9.1.6 Plume Damage and Interference - The radar antenna, if mounted on the base of the lander near the terminal descent rocket engines, could suffer from the effects of plume damage and propagation interference.

Plume Damage - Effects of pressure, thermal damage and contamination must be considered which are principally a function of:

- Entry
- Separation technique
- Terminal propulsion configuration

A propulsive (rather than aerodynamic) terminal decelerator that is initiated prior to Aeroshell release would add to entry heating. However, due to Aeroshell protection and the relatively short period of thrust, this heat input would be small.

A fire-in-the-hole separation technique would give rise to increased pressure, heating and contamination over alternate separation techniques, but pressure and contamination levels are not expected to be significant. The descent engines would be used to back the lander out of the Aeroshell which would result in an intense but short thermal pulse. Using conservative heating rates, the temperature rise of the LM antenna during fire-in-the-hole separation was calculated to be 30 degrees F for a multiple engine configuration.

A multi-nozzle engine configuration for the Terminal Propulsion Subsystem introduces exhaust recirculation or backflow, which occurs when the highly expanded exhaust jets from adjacent rocket nozzles impinge on one another. This reverse flow causes an elevated pressure within the nozzle cluster and gives rise to base heating. Single engine configurations would not have recirculation; pressure and contamination would be lower than for the multiple engine configuration and heat transfer would be by radiation only.

The effect of any antenna contamination will be to attenuate and reflect the transmit and receive signals. Attenuation of the signals will affect all types of radars equally. Antenna deposits will cause reflections and increase antenna VSWR. Therefore, systems using a common transmit/receive antenna will be affected to a greater degree. Contamination would be greater with a solid propellant motor.

Propagation Interference - Propagation through a rocket exhaust plume can cause RF reflection, beam bending, phase shifts, and attenuation. The principal factors determining the degree of interference (besides transmitting frequency) are electron density, electron collision frequency, and plasma thickness. These are functions of engine configuration, including plume/antenna geometry, size and fuel.

Multiple terminal descent engine configurations have several engines placed around the radar antenna, which increases the probability of plume interference with one or more of the radar beams. Single engine configurations with split antennas would not require propagation through the exhaust plume and would cause less propagation interference. Variation of engine size within the range of those considered for VOYAGER will not appreciably alter propagation interference estimates. Solid propellant exhaust is expected to have higher electron densities than liquid

propellant exhaust, resulting in greater propagation effects.

5.9.2 Radar Alternatives - The radar requirements resulting from variations in the landing concept were categorized, and submitted to qualified vendors.

5.9.2.1 Combination of Radar Requirements - For system trade studies, it was necessary to determine quantitatively the impact of different landing concepts on the radar subsystem, and vice versa. The major radar alternatives are combined with the major landing concept alternatives in Figure 5.9-4. Radar requirements are shown bounded by dashed lines in the figure.

The bold lines indicate a preferred landing concept and possible radar subsystem. Detailed radar requirements for this basic radar concept and for variations to the basic concept were derived. Each variation corresponds to one of the other alternatives shown by faint lines in Figure 5.9-4. The requirements for the altimeter and the landing radar, along with the variations, were distributed to qualified vendors.

5.9.2.2 Proposed Landing Radars - Characteristics of the radars proposed to meet the "basic" requirements are shown in Figure 5.9-5. Figure 5.9-6 presents the proposed modifications to satisfy requirements imposed by variations in the basic requirements. The following are of particular importance:

- No preferred roll - Lack of a preferred roll position results in only a moderate change to the proposed systems with the exception of the ICW/FM-CW radar. It is felt that this radar would also have relatively few modifications if a two position antenna is avoided.
- Range measurement to 30,000 ft - A requirement for a slant range measurement at an altitude of 30,000 ft requires extensive modification to the basic proposed systems. The increased transmitter power requirements of the ICW and J_2 FM-CW radars would probably preclude the use of a solid state transmitter.

5.9.3 Requirements Resulting from Selection of Preferred Landing Concept - Major trade studies with inputs from all subsystems have resulted in a preferred landing concept.

5.9.3.1 Landing Sequence - Principal events in this concept are:

- Entry with three axis rate damping from .05g with fixed roll attitude.
- Parachute deployment at 23,000 feet altitude. No active attitude control.
- Aeroshell separation 12 seconds (16,000 to 19,000 feet altitude) after parachute deployment using a differential drag technique.

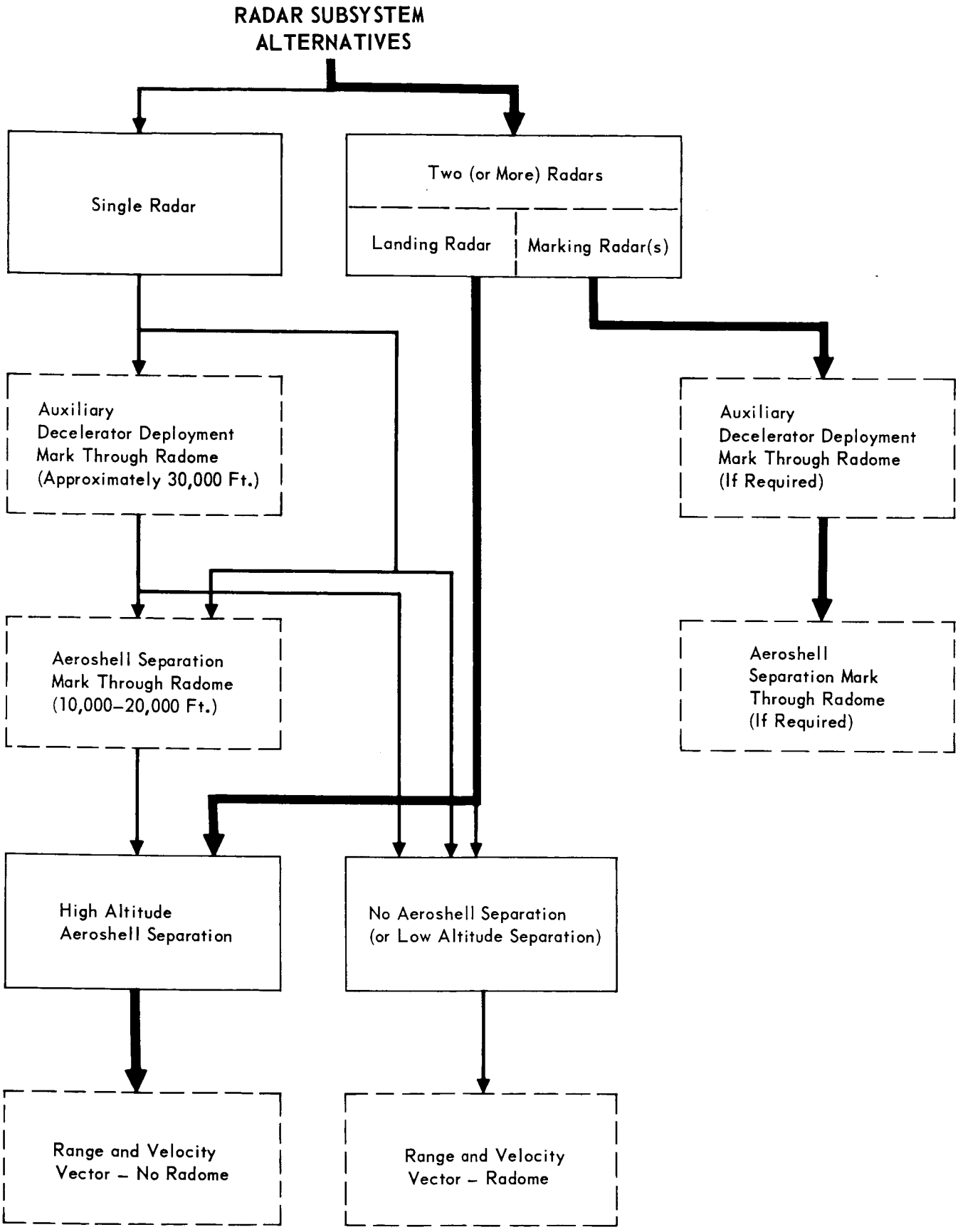
RADAR SUBSYSTEM ALTERNATIVES
Single Radar
Two (or More) Radars
Landing Radar
Marking Radar(s)
Auxiliary Decelerator Deployment Mark Through Radome (Approximately 30,000 Ft.)
Auxiliary Decelerator Deployment Mark Through Radome (If Required)
Aeroshell Separation Mark Through Radome (10,000–20,000 Ft.)
Aeroshell Separation Mark Through Radome (If Required)
High Altitude Aeroshell Separation
No Aeroshell Separation (or Low Altitude Separation)
Range and Velocity Vector – No Radome
Range and Velocity Vector – Radome

Figure 5.9–4

BASIC SYSTEM CHARACTERISTICS

SOURCE	TRANSMITTER			ANTENNA		RECEIVER/ SIGNAL PROCESSING	SIZE	WEIGHT	POWER
	FREQ	POWER	MODULATION	BEAM CONFIGURATION	TYPE				
Ryan (CW/FM–CW)	Range – 9.58 GHz Velocity – 10.51 GHz	Range – 175 mW Velocity – 200 mW	Range – linear sawtooth FM–CW 8 MHz and 40 MHz deviation Velocity – CW	Range – one beam along role axis Velocity – three beams, rectangular footprint with group centerline 20.38° off role axis	Planar array – separate transmit and receive antenna	Zero IF, quadrature pairs used to determine velocity sense	1.6 ft^3	29 lb	65 W
LFE (ICW)	9.6 GHz	5 mW	ICW PRF – 20 to 250 KHz	Three beams, "V" footprint with one beam along role axis and two beams 20° off	Dielectric lens	Heterodyne	3.64 ft^3	30 lb	100 W
Sperry (J_2 FM–CW)	Range – 9.58 GHz Velocity – 10.51 GHz	Range – 200 mW Velocity – 150 mW	Range – sinusoidal FM–CW, two modulation frequencies, both a function of range Velocity – sinusoidal FM–CW, single modulation frequency a function of range	Range and roll axis (z) velocity – one beam along role axis Lateral velocity – three beams equally spaced 28° off the role axis	Strip line planar array	Heterodyne, utilizes second side-band for information, varies modulation frequency to maximize second side-band	0.52 ft^3	29 lb	42 W
Autonetics (ICW/FM–CW)	13.3 GHz	350 mW	ICW – 30 k ft to 700 ft Sinusoidal FM–CW – 700 ft to touchdown	Range – one beam along role axis Velocity – four beams equally spaced 10° off role axis	Dielectric lens	Heterodyne in ICW mode; second side-band with zero IF range channel in FM–CW mode	2.4 ft^3	29.5 lb	53.5 W

Figure 5.9–5

REQUIRED MODIFICATIONS vs. CONCEPT

SOURCE	TRANSMITTER			ANTENNA		RECEIVER SIGNAL PROCESSING	SIZE	WEIGHT	POWER	CONDITIONS
	FREQUENCY	POWER	MODULATION	BEAM CONFIGURATION	TYPE					
Ryan		Range – 350 mW	Linear triangular FM–CW	Change beam configuration; increase range receive gain to 30.5 dB, split antenna for better isolation		Decrease in range accuracy to 3% above 10 k ft and 2% below 10 k ft, increase range acquisition time to 10 sec, add range frequency tracker	2 ft^3	31.5 lb	78 w	Range measurement required from 30 k ft through an ablative aeroshell
LFE		2.5 W								
Sperry		Increase (by 23 dB)								
Autonetics				Two position antenna, select beam with good return		Add selection logic				
Ryan						Increase preamplifier roll-off				Velocity measurement through a radome
LFE		7.9 mW								
Sperry		Increase (by 2 dB)								
Autonetics										
Ryan				Increase (gain) size of beam 3 receive antenna by two, split antenna for better isolation						Velocity measurement through an ablative aeroshell
LFE		31.5 mW								
Sperry		Increase (by 8 dB)								
Autonetics										

Figure 5.9–6

REQUIRED MODIFICATIONS vs. CONCEPT (Continued)

SOURCE	TRANSMITTER			ANTENNA		RECEIVER SIGNAL PROCESSING	SIZE	WEIGHT	POWER	CONDITIONS
	FREQUENCY	POWER	MODULATION	BEAM CONFIGURATION	TYPE					
Ryan						Range tracker would not follow rates of 10°/sec				No decelerator
LFE		40 mW (increase of 9 dB)								
Speery				Two position antenna (by either electrical or mechanical means)		Discriminate against ambiguities				
Autonetics				Two position antenna (by adding a second cluster of five feeds in the lens antenna and the associated switching)						
Ryan				Change beam configuration to that of Figure 5.9.4.4-1 (less one velocity beam)			Estimated 2 cu.ft.	Estimated 30 lb.		No preferred roll position
LFE		28 mW (increase of 7.5 dB,								
Sperry		Increase by 14 dB								
Autonetics				Antenna modification with considerable increase in weight and complexity						
Ryan			Linear triangular FM-CW	Change beam configuration; up range receive gain to 30.5 dB		Decrease in range accuracy to 3% above 10 k ft and 2% below 10 k ft, increase range acquisition time to 10 sec, add range frequency tracker		29.5 lb		Range measurement required to 30 k ft through a radome
LFE		634 mW (increase of 21 dB)								
Sperry		Increase (by 17 dB)	Lower modulation frequencies (or add mode switching)							
Autonetics				Two position antenna, select beam with good return		Add selection logic				

Figure 5.9-6(Continued)

- Terminal engines ignited at 5000 ft. Inertial hold control initiated. Lander released from the parachute approximately 0.5 seconds after engine ignition.
- Lateral velocity control initiated within six five seconds after ignition and thrust axis controlled to the velocity vector. Roll orientation is held constant but not in a preferred attitude.
- Intersection of the preprogrammed deceleration profile and subsequent deceleration to the constant velocity descent phase.
- Constant velocity command initiation at a velocity of 10 ft/sec which occurs at a slant range of approximately 50 ft. Inertial hold control initiated.

Primary radar subsystem requirements then become:

- Parachute deployment mark through the Aeroshell at 23,000 ft. altitude.
- Engine ignition mark at 5000 ft altitude.
- Velocity vector information prior to six seconds after engine ignition. Slant range information at approximately the same time. Continuing velocity vector and slant range information down to 10 ft/sec and 10 ft. (lateral velocity data needed only to 50 ft. altitude.)

In addition, continuous altitude information from approximately 200,000 feet is desired for entry science data correlation.

5.9.3.2 Requirements - Slant range measurement at relatively high altitudes and shallow pitch angles presents a particularly difficult problem to a landing type radar (velocity vector and slant range outputs). These problems are covered in Sections 5.9.2.2 and 5.9.5. On the other hand altitude measurement is relatively simple in concept and implementation for a pulse radar. This is covered in more detail in Section 5.9.6 and Section 5.9.7. For these reasons two radars are preferred with the following utilization:

Radar Altimeter

- Parachute deployment mark
- Engine ignition mark
- Entry science data
- Landing radar range measurement backup

Landing Radar

- Velocity vector measurement
- Slant range measurement

The preferred landing concept coupled with a utilization of two radars results in a nearly optimum environment for the radar subsystem. This concept, indicated by the bold path of Figure 5.9-4 results in the following performance requirements for the landing radar:

- An auxiliary aerodynamic decelerator is used to slow and verticalize trajectories. Worst case landing radar acquisition conditions become:

  VM-7 with 220 fps tail wind

  Pitch angle - 56 degrees

  Altitude - 5000 ft.

  Velocity - 406 ft/sec

  VM-10 with 120 fps tail wind

  Pitch angle - 70 degrees

  Altitude - 5000 ft.

  Velocity - 167 ft/sec

  20 degrees of pitch angle are due to Guidance and Control alignment uncertainty at parachute release.

- Aeroshell separation occurs prior to required landing radar operation. Its operation through a radome is not required.
- Landing radar acquisition time of 4 seconds is required.
- Worst case misalignment of the lander roll axis and Martian referenced velocity vector at initiation of velocity vector control is:

	Pitch Angle	Velocity Vector Angle (to horizonal)
VM-8 with wind	87°	41.7°
VM-10 with wind	90°	44°

(These pitch angles do not include attitude stabilization errors which would be less than 20 degrees. See Section 2.3.7)

This misalignment will result in transients during the velocity vector alignment maneuver, and the indicated, Martian referenced, velocity vector angles will approximate the shallowest attitude alignment during landing radar operation.

- Attitude control during landing radar operation is:

  a. Roll orientation - No preferred position

  b. Roll rates - Negligible

  c. Pitch and Yaw Errors - < 20 degree before radar acquisition, negligible afterward

d. Pitch and Yaw Rates - Negligible under steady state conditions.
Less than 15 deg/sec while maneuvering

- Minimum range requirement - 10 feet
- Minimum velocity requirement - 10 ft/sec.

5.9.4 Landing Radar Selection - In this section the landing radar alternatives, which were shown in Section 5.9.3 to apply for the preferred landing concept, are evaluated. The selection criteria are developed, the selection is made, and various modifications are proposed.

5.9.4.1 Selection Criteria - The selection criteria and weighting factors used to evaluate the landing radar alternatives are given in Section 5.0.

The criteria must be related to factors pertinent to the radar design. The landing radar alternatives were judged according to the following factors as related to this criteria:

- Probability of Mission Success (.35)
  - Simplicity of Concept (.40)
  - Independence of range and velocity measurements (.30)
  - Vulnerability to spurious signals (.30)
- System Performance (.20)
  - Quality of data beyond minimum requirements (1.00)
- Development Risk (.20)
  - Similarity to existing equipment (.50)
  - Need for state-of-the-art improvement (.50)
- Versatility (.15)
  - Adaptability to changes in landing concept (1.00)
- Cost (.10)
  - Similarity to existing equipment (.50)
  - Need for state-of-the-art improvement (.50)

The weighting used for each of the design factors is indicated for each criterion.

5.9.4.2. Landing Radar Evaluation - Major differences in the proposed landing radars are in the antenna, transmitter modulation technique, and receiver signal processing. In evaluating the radar, the antenna is considered independently. The transmitter modulation and receiver signal processing are considered together in terms of how they affect independence of range and velocity measurements, efficiency, ambiguity suppression, accuracy, vulnerability to spurious signals and simplicity. Finally, the proposed approaches are compared to existing equipment and rated using the previously established criteria.

Antenna - Two types of antennas are proposed, the dielectric lens and the phased array. Both weigh about the same. The lens is a simpler design and would, therefore, simplify development of an electronically positioned beam (if this were required). The array has less volume (particularly the strip line array) and lends itself to flush mounting. Either is functionally adequate.

Independence of Range and Velocity Measurement - Velocity compensation of the range beam is required in the CW/FM-CW radar. Loss of velocity information causes gross inaccuracies in the range measurement.

The J_2 FM-CW, ICW and ICW/FM-CW radars all require range information for mechanization of both velocity and range measurements. Without range information, the J_2 FM-CW radar would have range holes where neither range nor velocity information could be obtained. The ICW and ICW/FM-CW radars vary pulse repetition frequency with range (PRF ranging) from acquisition down to approximately 1000 ft. At the lower altitudes the ICW radar fixes the pulse repetition frequency (PRF) and changes receiver gating to allow sufficient signal return; the ICW/FM-CW radar changes modes to FM-CW. Both the ICW and ICW/FM-CW radars could incorporate relatively simple logic to allow velocity measurement in the event of range failure at the higher altitudes; changes in mode or receiver gating could be switched by a backup altimeter mark or conceivably by a velocity mark.

Efficiency - CW and FM-CW modulation techniques use a 100% duty cycle. CW and linear sawtooth FM-CW techniques utilize all of this energy (less approximately 0.5 dB with the FM-CW due to flyback) in signal processing. Sinusodial FM-CW techniques extracting second sideband information can minimize loss in signal processing to approximately 6 dB by varying modulation frequency to maximize the information in this second sideband. Usable received signal will fall off at approximately 20 dB/decade if the modulating frequency is fixed (as it must be at low altitudes to avoid excessively high modulation frequencies). ICW maintains a 50% duty cycle down to low altitudes (approximately 1000 ft) by PRF ranging. Below this the PRF is fixed and the duty cycle decreases.

Range/Velocity Ambiguity Suppression - The addition of modulation to the transmitter output creates potential range/velocity ambiguities. The CW/FM-CW radar with no modulation for velocity measurement and sawtooth linear frequency modulation for range measurement does not have this problem over the range of positive dopplers encountered with all landing trajectories. The J_2 FM-CW radar with modulation frequency varied to maximize return and the ICW/FM-CW radars with PRF ranging all run into range/velocity ambiguity problems at higher ranges and

velocities. These ranges and velocities will not be encountered with the selected landing concept but adaptability to changes in the landing concept for later missions would be curtailed. For later missions and larger payloads, the higher Mach numbers may preclude the use of auxiliary aerodynamic decelerators for separation. Separation might be required up to altitudes of approximately 15000 feet with accompanying slant ranges of up to 21000 feet and velocities above 700 ft/sec. This would cause ambiguity problems for all three of these radars.

Range Accuracy - The width of the transmitter signal spectrum is limited by the modulating frequency of the low deviation J_2 FM-CW radars and the PRF of the fifty percent duty cycle, ICW radars. Because of range ambiguities, these are limited to 50 KHz at 5000 ft altitude. With linear FM/CW, the width of the transmitted frequency spectrum can be controlled independent of modulation frequency. Wide frequency deviations are easily obtained with no range ambiguity problems. Consequently, range accuracy is inherently better with comparable signal-to-noise ratios.

Vulnerability to Spurious Signal - All of the proposed radars provide some discrimination against unwanted near range and low velocity returns. During the final phase of the mission these discrimination techniques will receive their most stringent test. Potential interference during this critical phase could arise from thermal noise, carrier leakage or vibration induced modulation of this carrier leakage. In this case carrier leakage is meant to include the unmodulated second sideband in the J_2 FM-CW and ICW/FM-CW radars.

A closer look at this portion of flight is shown in Figure 5.9-7. Usable received power (Pr) from the Martian surface is shown for the roll axis beam (solid line) and the off axis beams (dashed lines) for a vertical trajectory. Carrier leakage (P_L) was estimated for single transmit/receive antennas by assuming an antenna VSWR of 1.05 and determining transmitter reflection back into the receiver. The CW/FM-CW system uses separate transmit and receive antennas and a transmit/receive isolation of 60 dB was assumed.

If this reflected signal is now considered to be vibration modulated, it assumes the character of a return with velocity and range (except for ICW where no range interference is generated). A modulation sideband corresponding to a velocity of approximately 15 ft/sec was used for comparison. This velocity corresponds to a different vibration frequency for different systems but is approximately 300 cps. A velocity of 15 ft/sec would normally be encountered at an altitude of approximately 100 ft on the terminal descent profile. This assumed sideband (P_{LS})

MARTIAN SURFACE RETURN (P_R), REPRESENTATIVE LEAKAGE MARKS (P_L) AND COMPARATIVE LEAKAGE SIDEBANDS (P_{LS}) VERSUS RANGE FOR VERTICAL FLIGHT

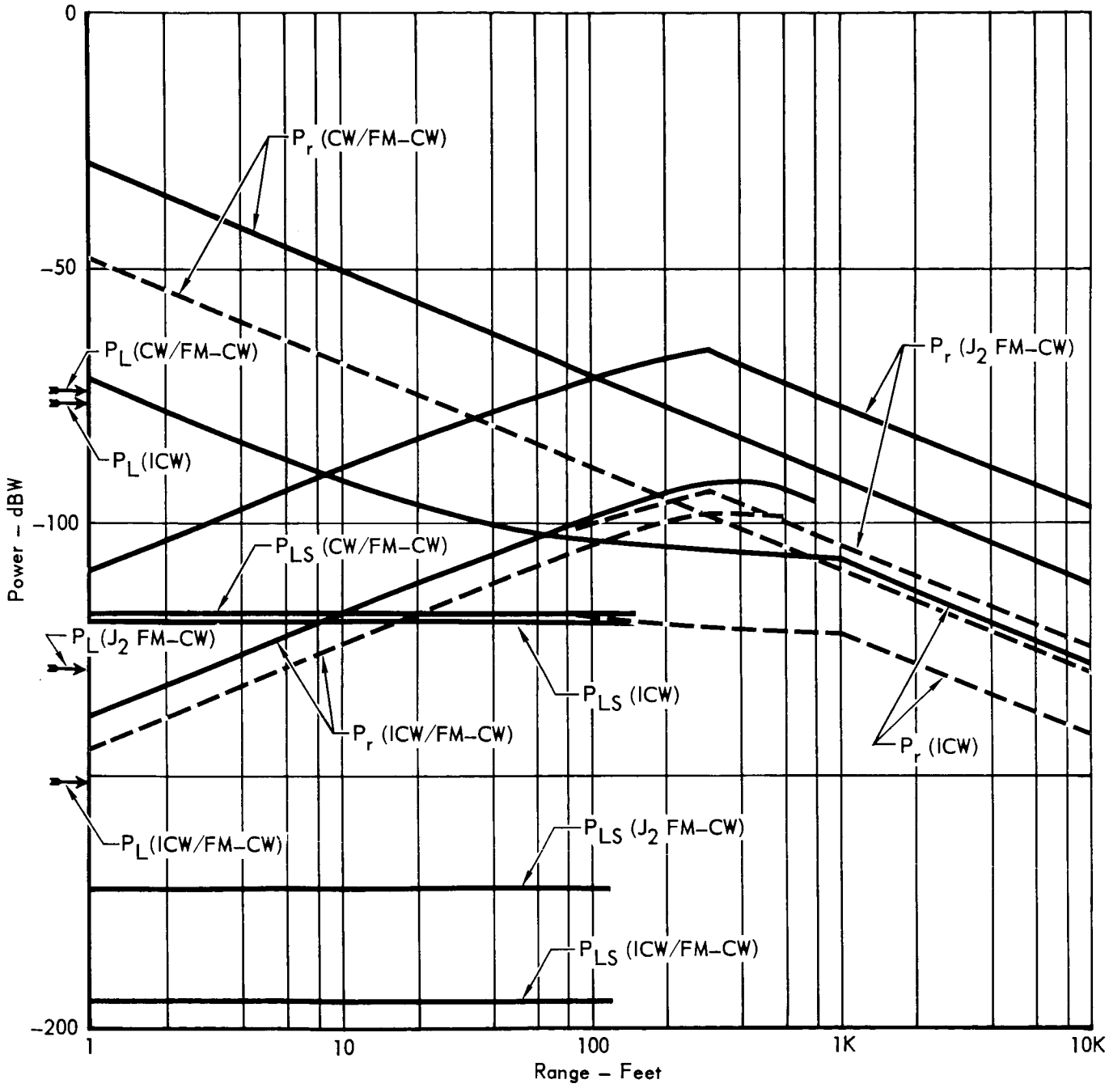

Figure 5.9–7

must be down 42 dB from the carrier leakage to equal the worst (ICW off-axis beam) surface return signal strength at an altitude of 100 feet. Using this 42 dB figure, relative ability of the various systems to discriminate against vibration induced interference is compared. Where ICW performance is marginal, it is generally acceptable for the other techniques. This received signal to interference ratio (both carrier leakage and its vibration induced sidebands) will decrease for J_2 FM/CW techniques with decreasing range because of the reduced received power in the J_2 sideband as range decreases. Performance gets better for CW/FM-CW because power is increasing with decreasing range. This is a rather simple approach to showing that range modulation does not necessarily increase the ability of the radar to discriminate against near range targets. As an examination of waveform ambiguity diagrams will show, large transmitted signal bandwidths are required to gain appreciable advantage in this respect. The additional ability to discriminate against near range targets with range modulation is a function of the range resolution capability of the waveform.

The CW/FM-CW homodyne receiver should do a good job of removing carrier leakage at a price of increased thermal noise at low frequencies as shown in Figure 5.9-8. Direct carrier leakage in the ICM and ICW/FM-CW (velocity beam) radars will have an additional attenuation by a carrier elimination filter (CEF) (something in excess of 45 dB is required by the ICW radar). A CEF is not mentioned in the J_2 FM-CW concept but one could certainly be incorporated. The CW/FM-CW radar uses a 6 dB/octave preamp roll-off and similar characteristics could be implicit in the carrier elimination filter used in the ICW and ICW/FM-CW radars. This uses knowledge of the descent profile and attenuates low frequency vibration induced interference along with the stronger low frequency surface return.

Simplicity - The ICW radar in concept is among the simplest proposed. Variation of receiver gating is required at approximately 1000 ft.

The ICW/FM-CW radar requires two modulators, two range trackers and mode switching. The ICW/FM-CW radar is considered most complex and on a part count basis is expected to have the poorest reliability.

The J_2 FM-CW radar uses multiple modulation frequencies that vary as a function of range. The radar in concept appears less reliable than the ICW and CW/FM-CW radars.

The CW/FM-CW radar uses a homodyne receiver with dual (in-phase and quadrature) channels for velocity sense detection (both the ICW and the ICW/FM-CW radars

MARTIAN SURFACE RETURN (P_R) AND THERMAL NOISE (N_T) VERSUS RANGE FOR VERTICAL FLIGHT

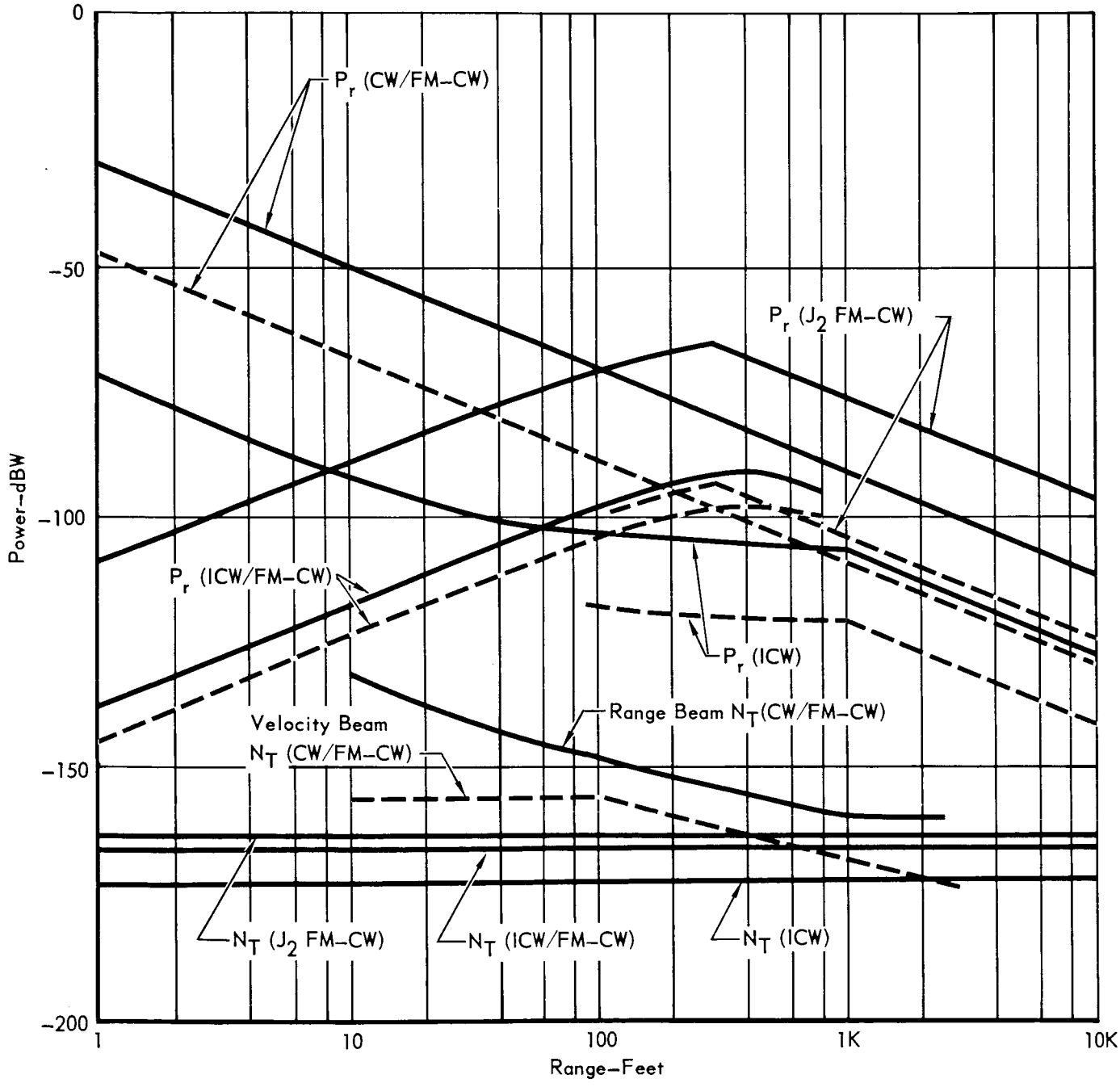

Figure 5.9-8

go to in-phase and quadrature channels for implementation of their carrier elimination filters). Simplicity of concept and implementation approaches that of the ICW radar.

Similarity to existing equipment - The J_2 FM-CW and ICW radars have evolved from airborne altimeter and airborne doppler navigation radars. Both would require a complete design and development cycle. The proposed radars are not identifiable with any existing radar.

The ICW/FM-CW radar is preceeded by a series of hardware oriented studies. A radar built to anticipated VOYAGER needs is now being breadboarded. A complete design and development cycle would be required. The proposed radar is not identifiable with any existing radar.

The CW/FM-CW radar is an established design based on the LM and Surveyor radars. It is identifiable with the LM radar except for the modifications delineated in Section 5.9.4.5.

Relative Rating - As a guide in arriving at a relative rating of the proposed radars a numerical evaluation was performed using the previously established criteria.

Little need for beyond state-of-art hardware was indicated, so the radars are ranked nearly equal in this respect, with some consideration given to the solid state transmitters.

Results of the rating are given in Figure 5.9-9. Ratings for each factor are from .1 to 1.0 with 1.0 high.

5.9.4.3 Reliability Improvement Considerations - Velocity measurement is the most critical function performed by the landing radar and contributes directly to successful landing. Range measurement is also performed but is less critical because the radar altimeter is available for back-up.

Several methods were studied to improve the success probability of velocity sensing. Among the possibilities are: (1) provide two velocity sensor transmitters, either one of which will supply adequate power for velocity measurement, (2) provide two trackers for each of three velocity channels or (3) provide four velocity channels including the receiving antenna, mixer, amplifiers and frequency tracker, any three of which will provide satisfactory operation without degradation.

Two velocity transmitters can be incorporated by at least two methods. One method is to drive two frequency multipliers from a single crystal oscillator. This configuration will prove troublesome because of parallel multiplier phase tracking requirements. Another possibility is to provide two separate transmitters, one of

RELATIVE RATING

	a1	r_1 (0.40)	a2	r_2 (0.30)	a3	r_3 (0.30)	a	Ra (0.35)	b	R_b (0.20)
CW/FM-CW	0.9	0.36	0.4	0.12	0.5	0.15	0.63	0.22	0.60	0.12
ICW	0.9	0.36	0.7	0.21	0.2	0.06	0.63	0.22	0.55	0.11
ICW/FM-CW	0.2	0.08	0.7	0.21	0.8	0.24	0.53	0.19	0.75	0.15
J_2 FM-CW	0.3	0.12	0.2	0.06	0.7	0.21	0.39	0.14	0.55	0.11

	c1	r_1 (0.50)	c2	r_2 (0.50)	c	R_c (0.20)	d	R_d (0.15)	e1	r_1 (0.50)	e2	r_2 (0.50)	e	R_e (0.10)	Rating ΣR
CW FM-CW	0.9	0.45	0.8	0.40	0.85	0.15	0.6	0.09	0.9	0.45	0.8	0.40	0.85	0.09	0.69
ICW	0.1	0.05	0.9	0.45	0.50	0.10	0.5	0.08	0.1	0.05	0.9	0.45	0.50	0.05	0.56
ICW/FM-CW	0.1	0.05	0.7	0.35	0.40	0.08	0.4	0.06	0.1	0.05	0.7	0.35	0.40	0.04	0.52
J_2 FM-CW	0.1	0.05	0.8	0.40	0.45	0.09	0.5	0.08	0.1	0.05	0.8	0.40	0.45	0.05	0.47

Where: a) Probability of Mission Success

a1 Simplicity Concept

a2 Independence of range and velocity measurements

a3 Vulnerability to spurious signals

b) System Performance

Quality of data beyond minimum requirements

c) Development Risk

c1 Similarity to existing equipment

c2 Need for State-of-the-art improvement

d) Versatility

Adaptability to changes in landing concept

e) Cost

e1 Similarity to existing equipment

e2 Need for state-of-the-art improvement

r is weighted subrating
R is weighted rating

Figure 5.9–9

which is selected during in-flight checkout. This would require failure sensing and a means of switching to the alternate transmitter - an undersirable feature.

Providing two trackers for each of the three velocity channels is an effective means of improving reliability but still leaves three highly vulnerable balanced mixers as sources of single point failures.

The four velocity beam receiving and tracking channel redundancy (three of four required) is an effective means of improving reliability with minimum weight increase and overcomes the single point failure sources of the balanced mixers. This redundancy configuration not only materially improves the reliability of the velocity sensing function, but also improves the reliability of the range sensing function as well.

The significance of the improvement resulting from the four velocity beam redundancy configuration can be evaluated by comparing the reliability of the non-redundant and redundant velocity sensor function of the landing radar.

Velocity Sensor Redundancy	Reliability (R)	(1-R)
Nonredundant	.9841	.0159
Redundant	.9949	.0051

The velocity sensing function has been improved by a factor of 3.1. This was accomplished with a weight increase of only five pounds.

The velocity channels are required to remove the doppler component from the range channel. As a consequence of improving the reliability of the velocity sensing function, the range sensing function reliability has been improved also by the addition of a minor amount of logic. The range sensing function reliability has been improved because two of the four velocity channels are available in two configurations for range measurement correction. The reliability analysis from which the above conclusions were derived is presented in Section C, 10.2.

5.9.4.4 Preferred Landing Radar Configuration - In Section 5.9.4.2, the CW/FM-CW radar is evaluated higher than the other three proposed radars. However, it was shown in Section 5.9.4.3 that the reliability of the velocity sensing function should be improved. It was also shown that the best way to improve this reliability is to add a redundant velocity receiving channel.

The addition of an extra velocity channel will also make the Landing Radar less sensitive to pitch variations in the absence of roll control when all four velocity channels are working properly (Reference Sections 5.9.1.1 and 5.9.5.1).

To make the landing radar as nearly independent of roll position as possible, the four velocity beams should have circular shapes, and be spaced symmetrically around the roll axis. Also, the range beam must be pointed parallel to the roll axis. The angle between each of the velocity beams and the roll axis (squint or cone angle) influences the pitch angle sensitivity, and also effects the accuracy of the lateral and vertical velocity measurements. It is shown in Section 5.9.5.6 that a squint angle of 20 degrees provides a good compromise. The beam configuration of the preferred landing radar is shown in Figure 5.9-10.

Thus, the preferred landing radar is similar to the CW/FM-CW system proposed by the manufacturer of the Lunar Module (LM) landing radar, which in turn is similar to the LM landing radar. The similarity between the preferred Landing Radar configuration and the LM landing radar is demonstrated in Figure 5.9-11.

Because of its advanced development status, the LM radar, was used as the basis for identifying required modifications. To make the present LM landing radar suitable the following modifications are required:

Antenna - A new antenna design is required to generate the specified four beam configuration. The Capsule Lander configuration provides sufficient lower surface area to increase the antenna size. For this reason no significant antenna design or development problems are anticipated. The antenna layout is shown in Figure 5.9-12. Although not currently required, the possibility of generating the four beam configuration from a smaller aperture area is currently being investigated.

Antenna Protection - The present LM radar antenna design employs an open slotted waveguide phased array technique. With the selected lander configuration the VOYAGER landing radar antenna is centered among the four terminal propulsion rockets. Consequently, it is anticipated that some protective device will be required to prevent possible exhaust gas backflow into the antenna. (Reference 5.9.5.13). It may take the form of either an RF transparent, bonded protective material on the antenna faces, or individual, dielectric windows for each waveguide slot.

Electronics - With the inclusion of the fourth velocity beam, an additional velocity beam receiving and tracking channel is required. This channel will be similar to the present velocity beam channels, and will consist of in-phase and quadrature microwave mixers, preamplifiers, and doppler frequency tracker. No new design or development is required for the fourth beam electronics through the

LANDING RADAR BEAM CONFIGURATION

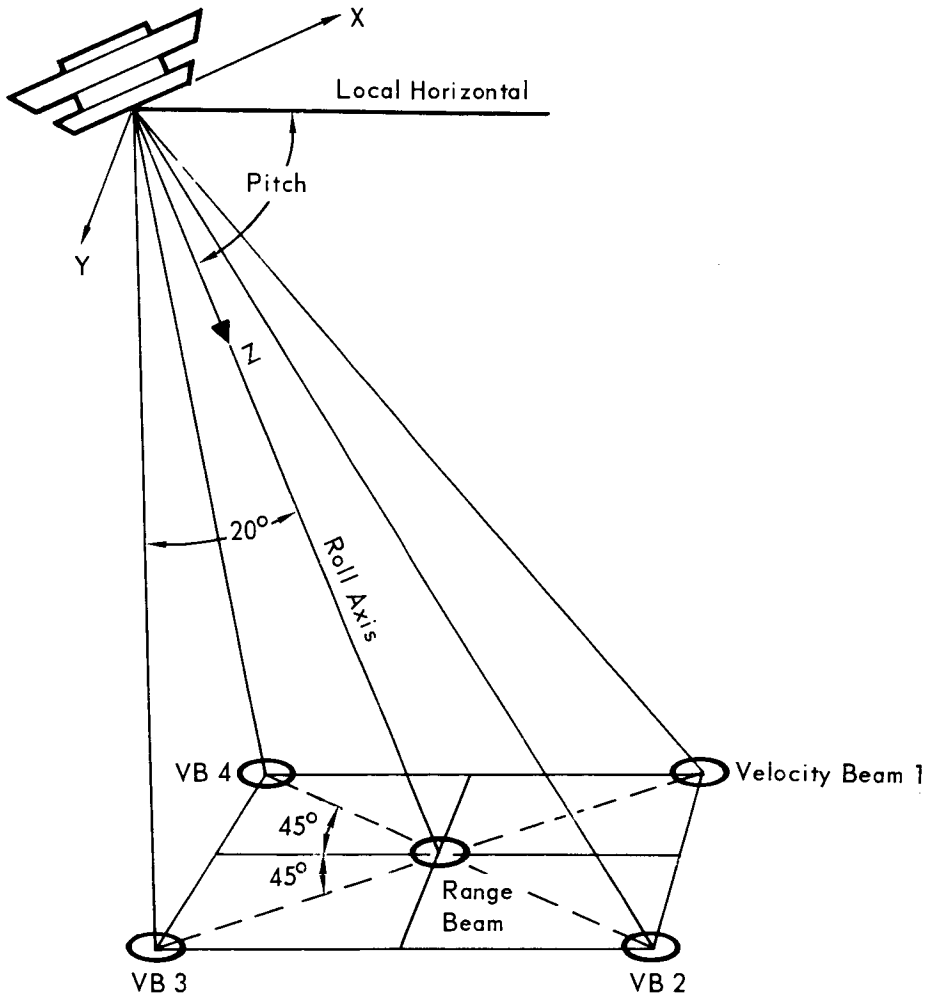

Figure 5.9–10

COMPARISON OF PRESENT LUNAR MODULE (LM) AND THE PREFERRED VOYAGER LANDING RADARS

CHARACTERISTIC	LUNAR MODULE LANDING RADAR	PREFERRED VOYAGER LANDING RADAR
PERFORMANCE		
Accuracy		
Velocity	±(1.5% ± 1.5 fps)	±(1.5% ± 1.5 fps)
Slant Range		
2,500 – 10,000 Ft	±(1.4% + 15 ft)	±(1.4% + 15 ft)
10 – 2,500 Ft	±(1.4% + 5 ft)	±(1.4% + 5 ft)
Smoothing Times (Typical)		
Frequency Tracker	0.1 Sec	0.1 Se
Post Tracker	0.2 Sec	0.2 Sec
Acquisition Time	6 Sec (Max)	3 Sec (Max)
Min. Acquistion SNR	4 dB	4 dB
ANTENNAS		
Type	Planar Arrays	Planar Arrays
Total Aperture	3.4 ft^2	6.2 ft^2
Configuration	Interlaced velocity and range transmitters. Four receivers.	Two velocity transmitters (two beams each). One range transmitter. Five receivers.
Gain ($\sqrt{G_t G_R}$)		
Velocity Beams	27.6 dB	27.9 dB
Range Beam	29.0 dB	26.3 dB
Effective Radiated Power Per Beam		
Velocity Beams	35 mW	35 mW
Range Beam	53 mW	106 mW
Beam Width (2-Way)		
Velocity Beams	3.67 x 7.34 Deg	5.0 Deg (Circular)
Range Beam	3.90 x 7.50 Deg	5.0 Deg (Circular)
BEAM CONFIGURATION	Three velocity beams. One range beam. Two velocity beams 14 deg from range beam. Third velocity beam 42.5 deg from range beam.	Four velocity beams. One range beam. Velocity beams 20 deg from range beam and located symetrically about range beam at 90 deg intervals.
TRANSMITTERS		
Type	Varactor multipliers	Varactor multipliers

Figure 5.9–11

Frequencies		
Velocity	10.51 GHz	10.51 GHz
Range	9.58 GHz	9.58 GHz
Power Output		
Velocity	200 W	200 W
Range	100 W	100 W
Modulation		
Velocity	None (CW)	None (CW)
Range		
Type	Linear Sawtooth FM	Linear Sawtooth FM
Deviation	8 MHz, R>2500 ft 40 MHz, R<2500 ft	8 MHz, R>2500 ft 40 MHz, R<2500 ft
RECEIVER		
Type	Direct-to-audio conversion. Balanced mixers. Detected in quadrature.	Direct-to-audio conversion. Balanced mixers. Detected in quadrature.
Noise Figure	14.5 dB at 10 kHz. Increasing with decreasing frequency.	14.0 dB at 10 kHz. Increasing with decreasing frequency.
SIGNAL PROCESSING		
Type	Frequency Trackers	Frequency Trackers
Tracking Filter Bandwidth		
Velocity	2800 Hz, R>2500 ft 400 Hz, R<2500 ft	1000 Hz, R>2500 ft 400 Hz, R<2500 ft
Range	3200 Hz, R>2500 ft 1000 Hz, R<2500 ft	5000 Hz, R>2500 ft 1000 Hz, R<2500 ft
Converters	Convert velocity to orthogonal components. Correct range for doppler.	Convert velocity to orthogonal components. Correct range for doppler.
PRIMARY POWER	130 W	145 W
SIZE		
Antenna Assembly	20 x 24.6 x 6.5 in. 2400 $in.^3$	32 x 28 x 6.5 in. 5824 $in.^3$
Electronics Assembly	15.75 x 6.75 x 7.38 in. 780 $in.^3$	16.5 x 7-4 x 6.75 in. 824 $in.^3$
Total Volume	1.8 ft^3	3.75 ft^3
WEIGHT		
Antenna Assembly	20.0 lb	25 lb
Electronics Assembly	13.3 lb	15 lb
Total	33.3 lb.	40 lb

5,9-28-2

VOYAGER LANDING RADAR ANTENNA LAYOUT
(DIMENSIONS IN INCHES)

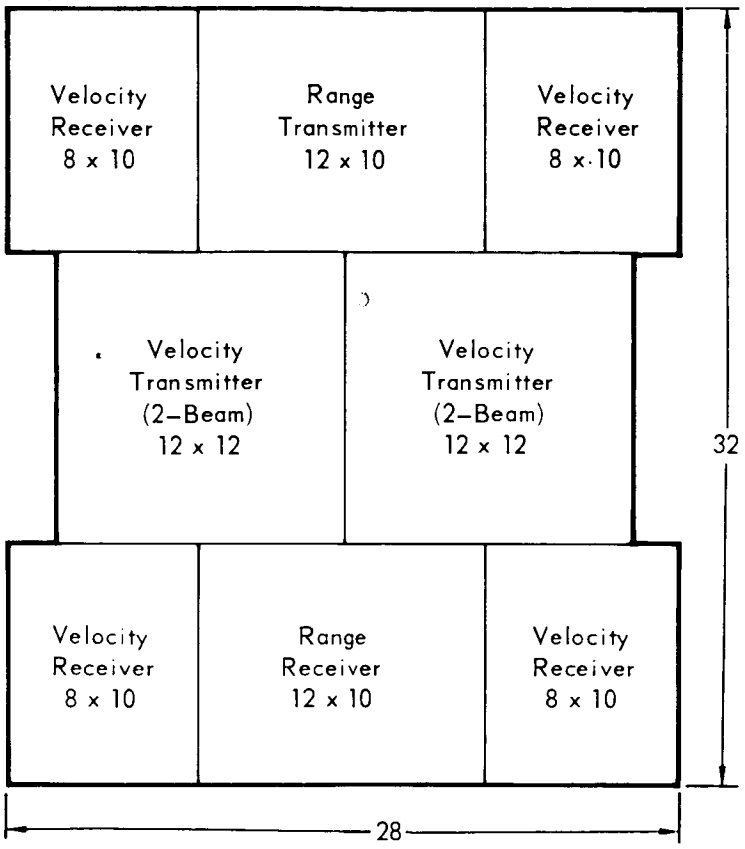

Figure 5.9-12

frequency tracker. A control logic to select the first three of the four velocity beams to acquire must be added. The present LM radar provides reliable operation signals from each frequency tracking channel upon acquisition. These signals can serve as inputs to the selection logic. Only the selection logic itself is a modification. Upon selecting the three reliable velocity beams, the subsequent processing required to derive range and resolve velocity information would be similar to that of the present LM radar.

Power Supply - The present LM radar power supply employes a dc-to-ac converter and a transformer to provide the necessary module voltage levels, and is designed for operation with dc input voltages ranging from 25 to 31.5 volts. The corresponding voltages from the Capsule will range from 22 to 32 volts. Consequently, a modified power supply design will be required. The design changes will result in little or no increase in weight since the present system employs a converter and transformer.

Additional required modifications are the selection of parts and techniques to satisfy the sterilization requirements (see 5.9.5.12); the provision for in-flight monitoring and check-out (see 5.9.5.14); and deleting the LM analog outputs (resolved velocities and slant range) since only the digital information will be used.

In Figure 5.9-11 the physical characteristics listed for the preferred landing radar configuration are based on a conservative extrapolation of present LM radar techniques. If redesign of the electronic circuitry appears desirable during Phase C, and a predominately integrated circuit approach (as opposed to the present LM hybrid combination of conventional parts with integrated circuits) is used, then the total radar weight can be reduced by four to six pounds with an attendant decrease in volume. More efficient design, including the use of step recovery diode frequency multipliers in place of the varactor multipliers, can result in decreasing the primary power requirement by as much as fifty percent.

5.9.5 Landing Radar Performance - Digital and analog simulation combined with analytic techniques were used to evaluate the performance of the preferred landing radar configuration described in 5.9.4 and C,10.2. The results presented here demonstrate that the preferred landing radar configuration is matched to the overall terminal descent concept.

Throughout this section a minimum allowable signal-to-noise ratio of + 4 dB is used in establishing landing radar performance boundaries. This +4 dB value is based on LM radar experimental (and confirming theoretical) data obtained from the

manufacturer, and applies for both acquisition (probability of detection = 0.95) and tracking.

5.9.5.1 Attitude Effects on Landing Radar Performance - Figures 5.9-13 and -14 present the landing radar performance boundaries (+4 dB SNR contours) in the pitch angle vs. roll axis slant range plane for various radar beam configurations, lander roll orientations, and local terrain slopes. A +4 dB signal-to-noise ratio is considered the minimum for sufficient acquisition probability based on the LM radar capability. Figure 5.9-13 is representative of the preferred landing radar beam configuration in that the beam squint angle (angle between each velocity beam and the roll axis) is 20 degrees. Figure 5.9-14 presents similar data for a 25 degree squint angle beam configuration. Performance boundary data as shown in these figures was used to assess the capability of the various landing radar configurations with respect to variations in potential terminal descent techniques (flight path angle, roll position, velocity, and altitude).

In generating these curves the receiver noise figure was assumed constant at 14.5 dB. Lower tracking frequencies will result in higher noise figures, but the curves may be scaled accordingly.

In order to bound the effects of local terrain slopes on landing radar performance, +4 dB signal-to-noise ratio contours are shown for both 0 and 34 degree local terrain slopes. The 34 and 0 degree terrain slope, +4 dB signal-to-noise ratio contours are indicated by solid and dashed lines respectively. For these figures the assumed Martian reflectivity model was $\sigma_o(\theta) = 0.02 \cos^2 \theta$, where θ is the beam angle with the local normal and σ_o is the effective radar cross section per unit surface area. The Martian backscatter model and terrain slope considerations are discussed in Sections 5.9.5.4 and 5.9.5.5 respectively.

In each figure separate contours are shown for the range beam and the limiting velocity beam. Since the range beam signal-to-noise ratio is independent of the lander roll position and velocity beam squint angles, only two range beam contours (cases a and b) are shown corresponding to the 0 and 34 degree local terrain slope cases. That is, the range beam contours shown in Figure 5.9-13 are identical to those of Figure 5.9-14 and are repeated only for reference.

In Figures 5.9-13 and -14 the indicated velocity beam +4 dB signal-to-noise ratio contours are those for the limiting beam (minimum received power) for the particular conditions noted. For the given beam configuration (Figure 5.9-10) and for a given pitch angle, the received power on a particular beam will depend on the lander roll position. The worst roll position when only three velocity beams

RANGE AND VELOCITY BEAM + 4db SNR CONTOURS

- 20 Degree squint angle.
- Number of operating beams, roll position, and local terrain slope shown as running parameters.
- Weakest of three best velocity beams shown for each case.

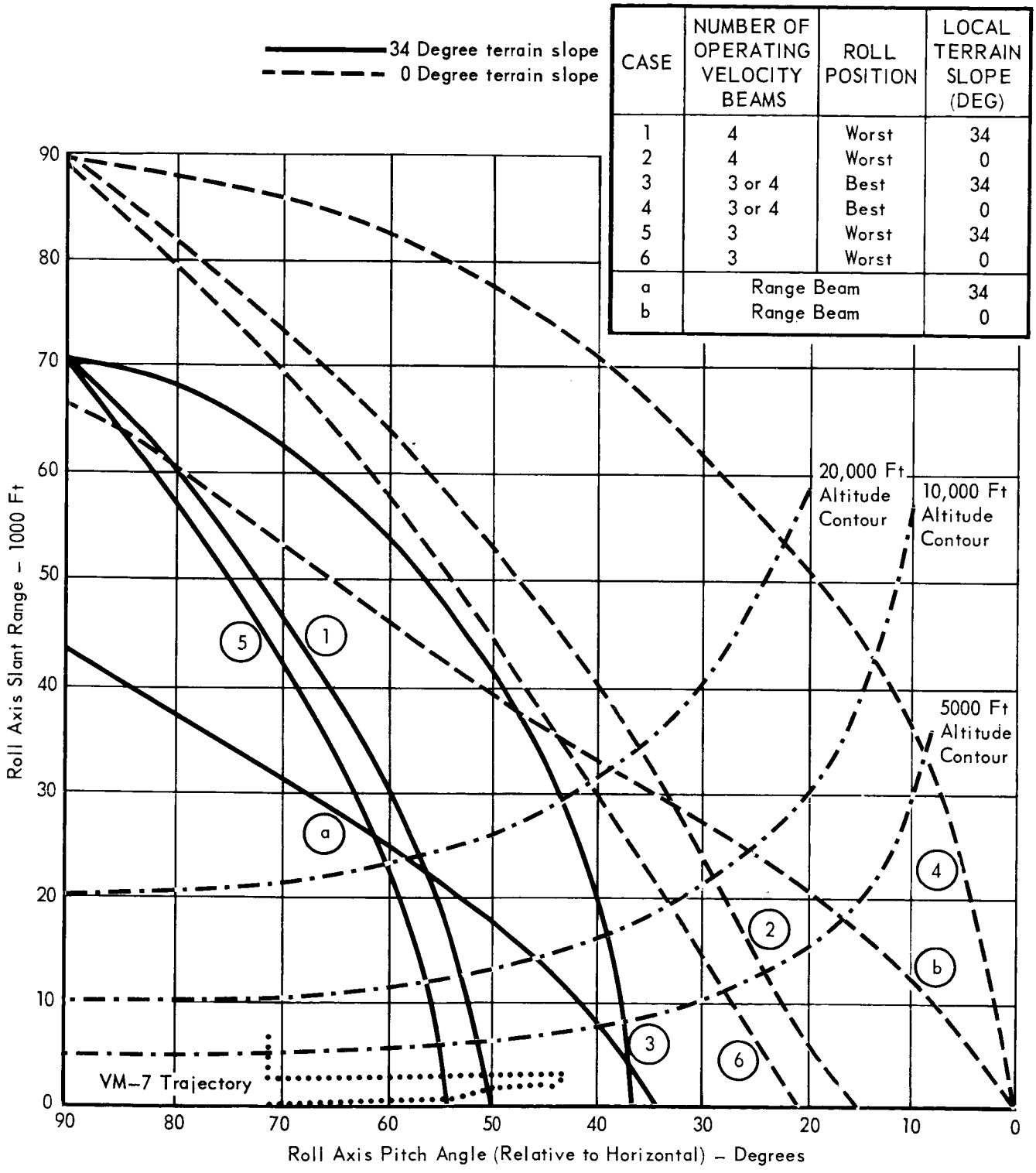

CASE	NUMBER OF OPERATING VELOCITY BEAMS	ROLL POSITION	LOCAL TERRAIN SLOPE (DEG)
1	4	Worst	34
2	4	Worst	0
3	3 or 4	Best	34
4	3 or 4	Best	0
5	3	Worst	34
6	3	Worst	0
a	Range Beam		34
b	Range Beam		0

Figure 5.9–13

RANGE AND VELOCITY + 4db SNR CONTOURS

- 25 Degree squint angle.
- Number of operating beams, roll position, and local terrain slope show as running parameters.
- Weakest of three best velocity beams shown for each case.

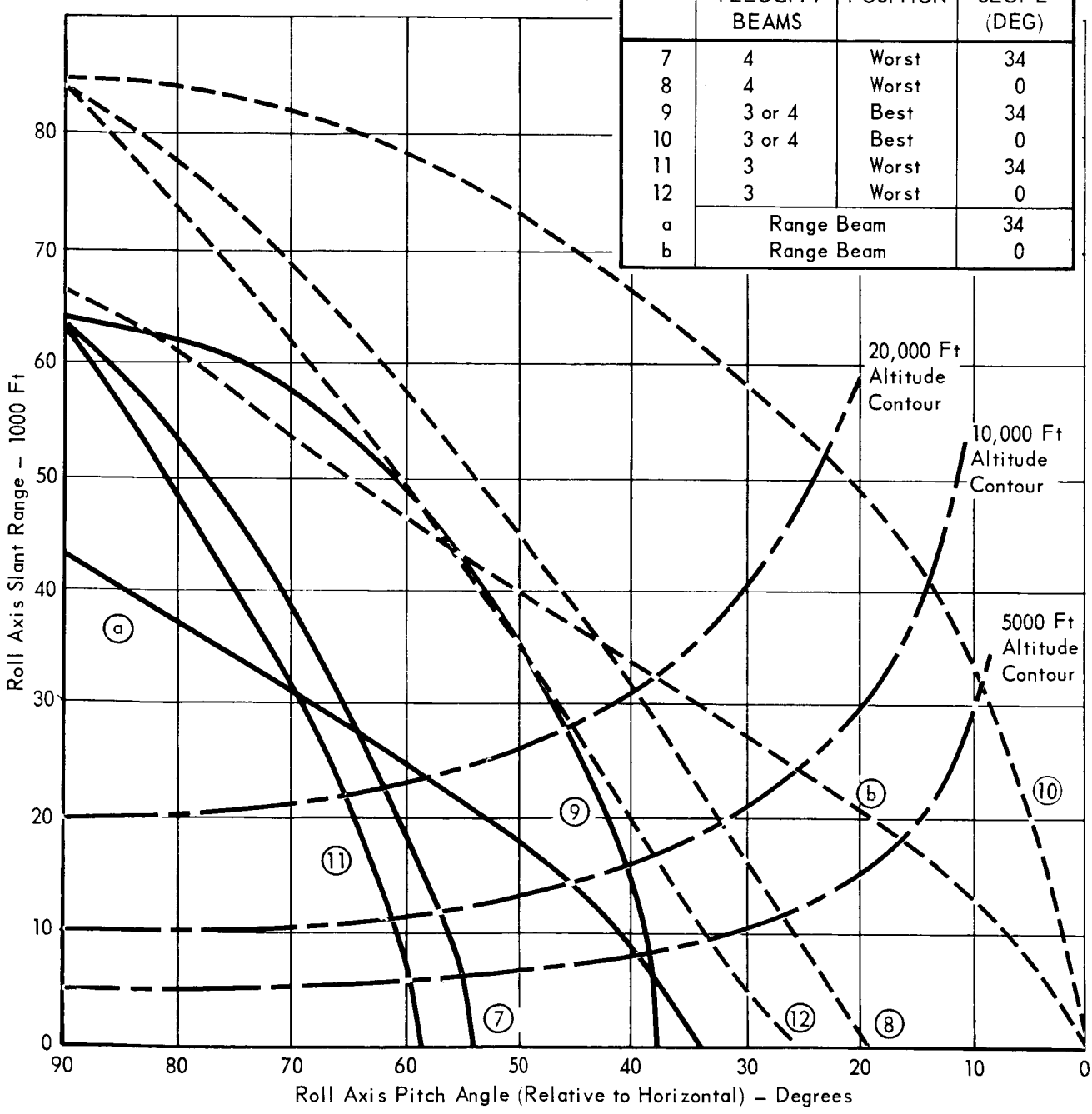

CASE	NUMBER OF OPERATING VELOCITY BEAMS	ROLL POSITION	LOCAL TERRAIN SLOPE (DEG)
7	4	Worst	34
8	4	Worst	0
9	3 or 4	Best	34
10	3 or 4	Best	0
11	3	Worst	34
12	3	Worst	0
a	Range Beam		34
b	Range Beam		0

Figure 5.9–14

are operating is that which causes one velocity beam to be in the pitch plane and above the lander's roll axis. The worst roll position with all four beams operating occurs when adjacent velocity beams are at equal angles from the pitch plane.

For the preferred terminal descent sequence, landing radar operation is nominally required at an altitude of 5,000 feet. Referring to Figures 5.9-13 and -14, and considering the zero local terrain slope case, the following conclusions may be drawn:

- For all cases of three and four operating velocity beams, the range beam limits the allowable pitch angle when a best lander roll position is assumed.
- For all cases of three and four operating velocity beams, the limiting velocity beam determines the allowable pitch angle when a worst roll position is assumed.
- For worst case roll, addition of a fourth velocity beam improves the pitch capability by 3.5 to 6.5 degrees (Cases 6 vs. 2, and 12 vs. 8).
- For worst case roll, reduction of the squint angle from 25 to 20 degrees improves the pitch angle capability by 3 to 5 degrees. (Cases 2 vs. 8, and 6 vs. 12).
- For worst case roll, a four velocity beam, 20 degrees squint angle beam configuration improves the pitch angle capability by about 9.5 degrees relative to the three velocity beam, 25 degree squint configuration (Cases 2 vs. 12).

The dotted line superimposed on Figure 5.9-13 represents the terminal phase of the VM-7 trajectory with a horizontal, 230 ft/sec steady tail wind. This is a representative worst case with respect to lander pitch angle. (In fact, recent modification in the Guidance and Control Subsystem will tend to improve this case.) As indicated in the figure, during the initial acquisition period (inertial hold phase) the roll axis pitch angle is nominally 70.5 degrees. Considering a worst roll, three operating velocity beam (one beam out), and zero local terrain slope case (contour 6 in Figure 5.9-13) a pitch margin of about 43 degrees is available at 5000 feet altitude. This margin is more than adequate to allow for the possible errors in the inertial hold attitude. After landing radar acquisition, the velocity vector alignment maneuver is initiated resulting in a minimum roll axis pitch angle of 43 degrees. As shown in the figure, at this point the pitch margin is about 17 degrees under the same conditions. Note that if all four velocity beams are operating (contour 2 in same figure) the above margins

are increased by 3 to 4 degrees.

Further verification of the landing radar's pitch angle capability is given in Section 5.9.5.11 where the results of the digital/analog simulation of the landing radar over a VM-10 trajectory are given. For the selected VM-10 trajectory with a horizontal, 120 ft/sec tail wind, the minimum roll axis pitch angle relative to horizontal is 49.7 degrees. At this point the minimum signal-to-noise ratio occurs on velocity beam 3 and is about +18.5 dB.

The cases cited above demonstrate that the attitude capability of the preferred landing radar configuration is matched to the requirements imposed by the selected terminal descent concept when zero local terrain slopes are considered. The noted performance margins will allow operation with surface slopes greater than 10 degrees (see Reference 5.9-1), but not with a continuous 34 degree slope. As noted in Section 5.9.5.5, it is believed that the 34 degree ground slope signal-to-noise ratio contours shown in these figures are overly pessimistic when general terrain effects are considered in a statistical sense.

5.9.5.2 Attitude Rate Performance - Lander attitude rates induce frequency rates on both the range and velocity measuring beams of the Landing Radar. After lander separation from the parachute where Landing Radar operation is required, the lander will be held to zero roll rate. Only pitch rates need be considered since beam incident angles are more sensitive to pitch variations than to yaw. The induced range frequency rates will be much greater than the velocity frequency rates. The doppler shift on the velocity beam is proportional to the generally slowly changing beam velocity component; whereas the range beam frequency shift is proportional to the beam slant range. At shallow flight path angles a small change in lander pitch angle results in a large change in beam slant range. Thus, the landing radar's ability to handle pitch rates will generally be determined by the range beam tracking capability.

As discussed in Section 5.9.1.2, the point at which tracker break lock occurs will depend upon the tracker loop gain as well as the induced frequency rate. The loop gain is a function of signal-to-noise ratio, signal bandwidth, and tracking point. The McDonnell analog simulation of the landing radar trackers has been used to evaluate rate tracking capability. The results of one such parametric study are shown in Figure 5.9-15. In the figure the tracker closed loop time constant (which is proportional to the reciprocal of dynamic loop gain) is shown as a function of signal bandwidth with signal-to-noise ratio as a running parameter. A Suryeyor

RANGE TRACKER CLOSED LOOP TIME CONSTANT VARIATION WITH SIGNAL BANDWIDTH AND SIGNAL-TO-NOISE RATIO.

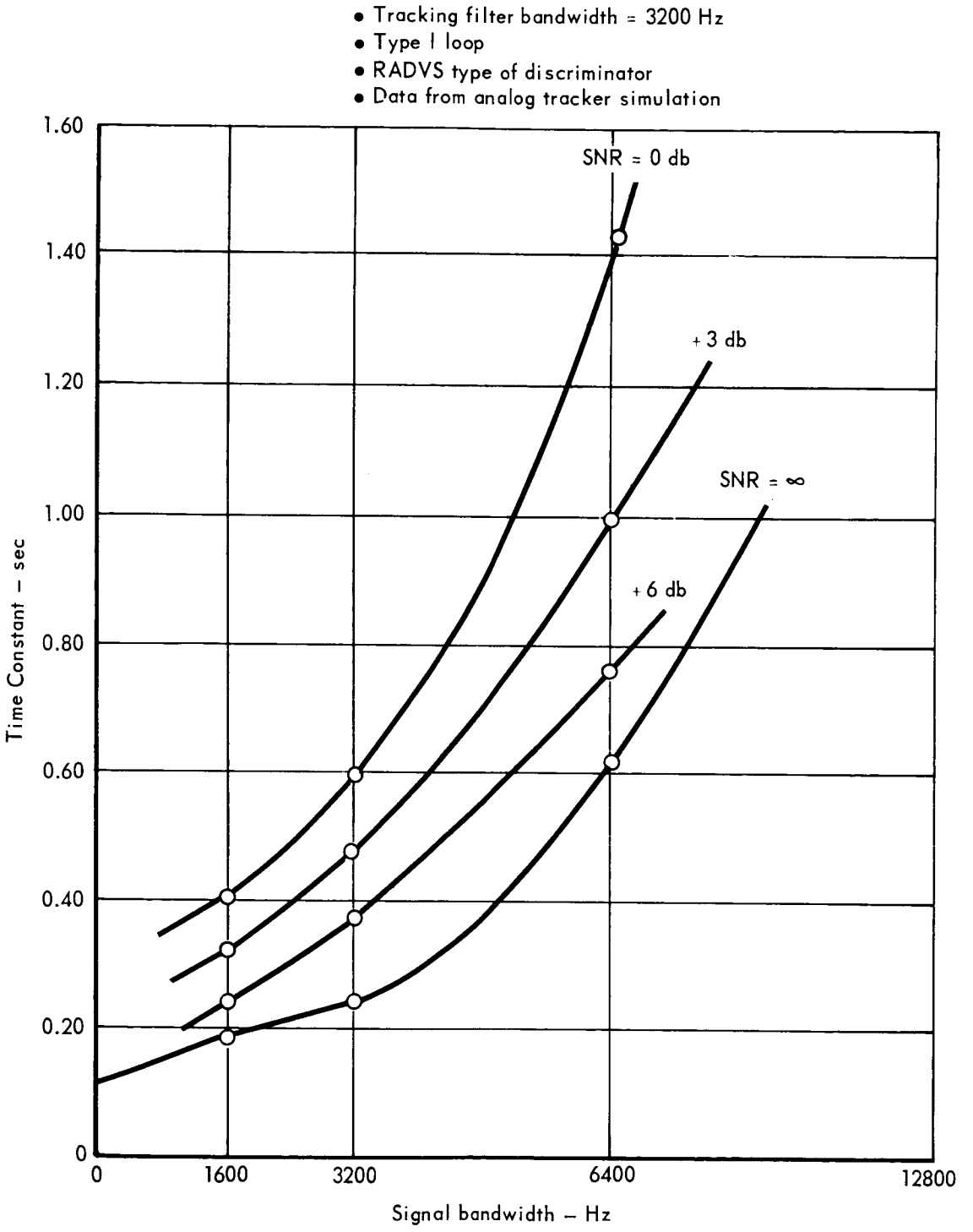

Figure 5.9–15

Radar Altimeter and Doppler Velocity Sensor (RADVS) type of discriminator was assumed in this analysis.

This increased tracker gain with larger signal-to-noise ratios and smaller bandwidths is illustrated in Figure 5.9-16 where contours of constant maximum tolerable pitch rate are shown in the pitch angle vs. slant range plane. A worst case (VM-7 atmosphere with a horizontal, 230 ft/sec steady tail wind) terminal descent trajectory is also shown on Figure 5.9-16. This demonstrates that the pitch rate performance of the landing radar is more than satisfactory, since the maximum terminal descent pitch rates are limited to about 15 degrees per second.

5.9.5.3 Acquisition Time - The landing radar acquisition process will be initiated immediately after engine ignition and lander separation from the parachute at an altitude of 5000 feet with the lander in an attitude hold condition. The velocity vector alignment maneuver is initiated within six seconds after engine ignition. Allowing two seconds for lander attitude stabilization, four seconds are available for landing radar acquisition.

Examination of the landing radar digital simulation data indicates that the maximum frequencies seen by the range and doppler trackers during the acquisition period are less than 45 KHz and 15KHz respectively. These values may be compared to the LM radar where frequency search bands of about 140KHz and 90 KHz are used for the range and velocity beams respectively. The + 4 dB SNR, 95% detection probability, acquisition time for the LM radar is about six seconds. In the VOYAGER application, the acquisition time can be reduced to less than three seconds on the basis of the reduced frequency, search interval requirements alone. In addition, because the signal-to-noise ratios at the acquisition point are well above +4 dB, the sweep rates can be increased to reduce the acquisition time even further.

5.9.5.4 Martian Backscatter Model - The +4 dB signal-to-noise ratio contours of Figures 5.9-13 and -14 assume a Lambert Law Martian backscatter angular dependence with a value of -17 dB at normal incidence. (i.e., $\sigma_o(\theta) = 0.02 \cos^2 \theta$). This model is believed to be conservative and allow adequate margin. For comparative purposes a Muhleman backscatter model is plotted with the assumed Lambert model in Figure 5.9-17. The Muhleman model is based on extrapolation to X-band of the average Mars radar spectogram given by R. M. Goldstein on the basis of 12.5 cm radar measurements made at Goldstone in 1965.

Comparison of the two curves shows that the Muhleman model exhibits a much greater specular effect (+2 dB vs -17 dB at normal incidence). In the region

LANDING RADAR PITCH RATE PERFORMANCE

CONTOURS OF MAXIMUM ALLOWABLE PITCH RATE BASED ON RANGE BEAM TRACK LOSS

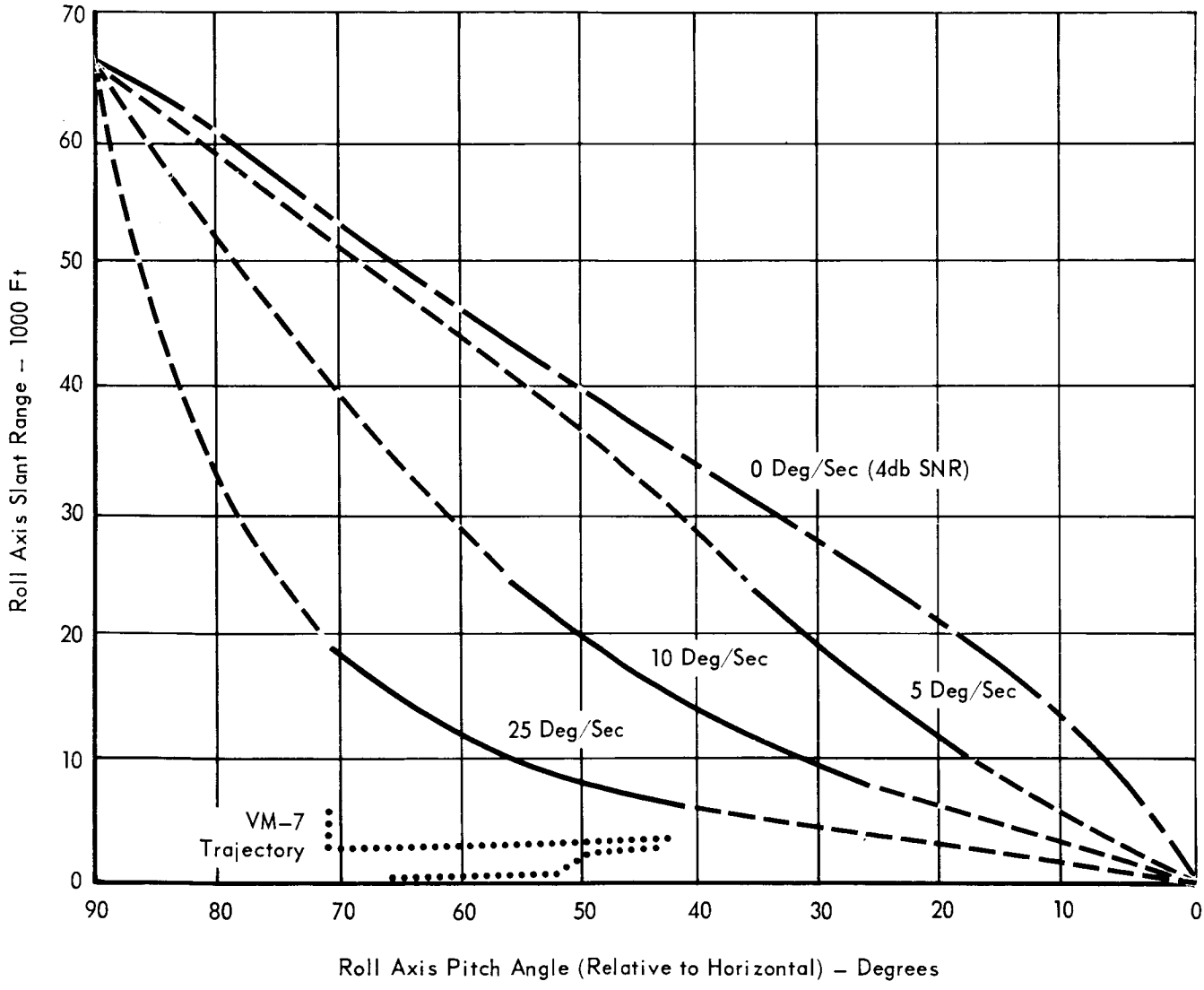

Figure 5.9–16

MARTIAN BACKSCATTER MODEL

Muhleman Equation Approximation
from McDonnell
Directed Study
Reference 5.9–5

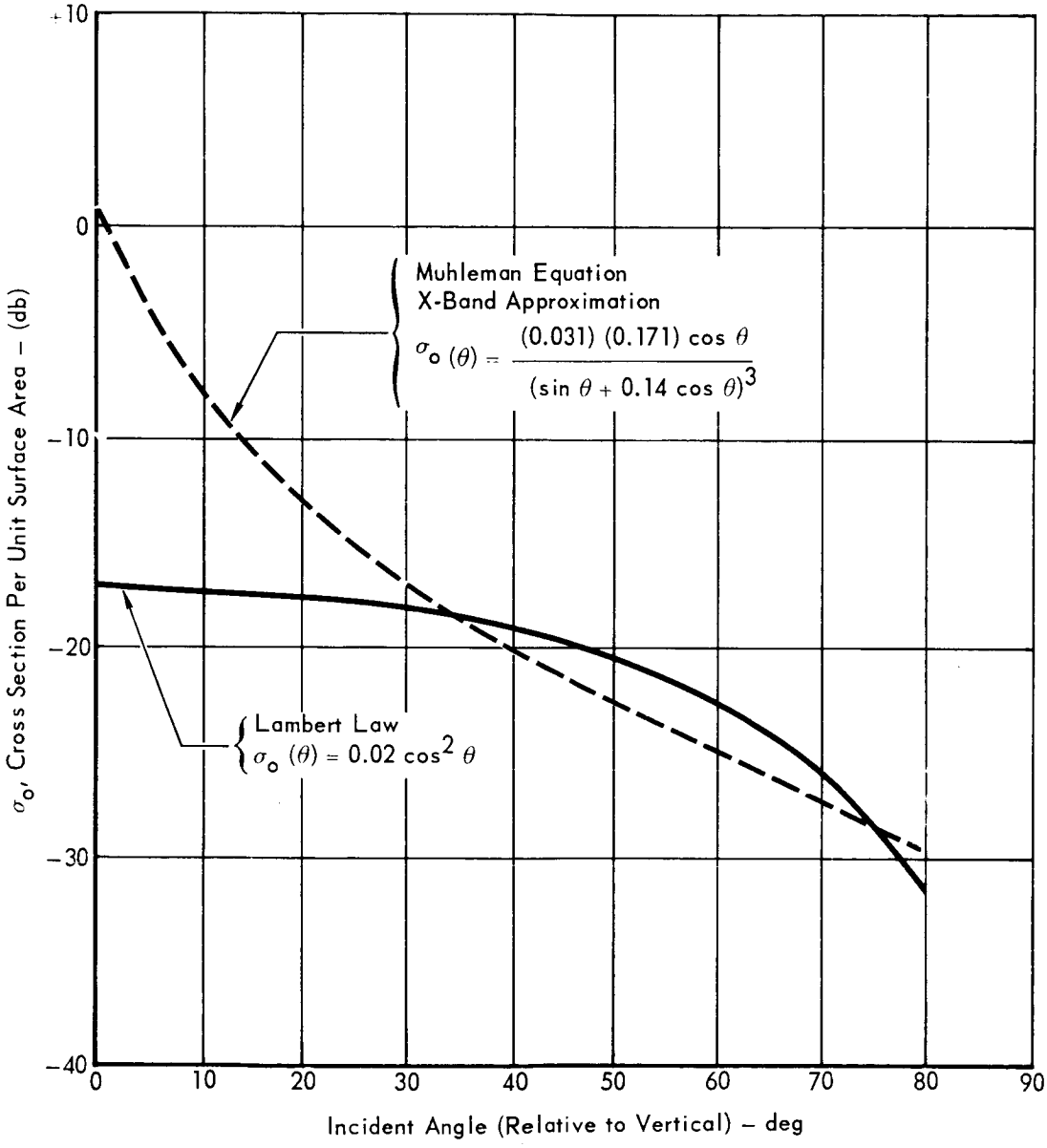

Figure 5.9–17

(near 60 degrees incident angle) where the Lambert curve is above the Muhleman, the difference is only about 2 dB. On this basis it is believed that the Lambert Law backscatter model is generally conservative with respect to the backscatter coefficient amplitude, and it is used here.

A second consideration is the slope of the backscatter model, since higher slopes result in greater radar terrain bias errors. In this regard the Muhleman model is more conservative.

5.9.5.5 Terrain Slope Effects - In determining the energy backscattered to the landing radar, consideration was given to the effects of local terrain slopes up to 34 degrees. A worst case demonstration of the effect of such slopes is shown in Figures 5.9-13 and -14. In allowing for the 34 degrees local terrain slope, the incident angle of the limiting beam was calculated and 34 degrees (Reference 5.9-1) were added to yield the effective local normal incident angle. Then the Lambert backscatter coefficient was corrected for this 34 degree bias. The drastic change in the $\pm$ 4 dB signal-to-noise ratio boundaries is apparent, and the landing radar would certainly lose lock during the velocity vector alignment maneuver.

The worst case ground slope effect cited here may indeed be possible. However, analysis of the Martian ground slope phenomenon in a statistical sense (wherein both the positive and negative backscatter effects are considered) is expected to demonstrate a relatively low weighting factor for this worst case. In Section 5.9.5.1 it was shown that, at the worst case pitch angle, the landing radar provides a pitch attitude margin of 17 degrees. This means that a 17 degree local terrain slope can be accommodated for the most severe trajectory analyzed.

5.9.5.6 Beam Configuration Squint Angle and Terminal Accuracy Considerations - As previously discussed, the squint angle or cone angle of the landing radar beam configuration should be minimized to improve signal-to-noise ratio at shallow flight path angles. The resulting smaller beam incident angles yield a greater radar backscatter coefficient due to the angular dependence of the Martian surface reflectivity model.

However, lateral velocity measurement accuracy decreases with decreasing squint angle. To a first approximation, lateral velocity measurement errors will vary inversely with the sine of the squint angle.

Thus, the problem becomes that of selecting a squint angle small enough to minimize flight path angle sensitivity, and large enough to yield an acceptable lateral velocity measurement accuracy. Figure 5.9-18 presents the results of a

TERMINAL DESCENT VELOCITY MEASUREMENT ACCURACY SENSITIVITY TO BEAM CONFIGURATION SQUINT ANGLE (θ)

Conditions:
- Vertical Descent
- Zero Lateral Velocity
- LM Radar Vibration Noise

Altitude	Axial Velocity
180 ft	20 fps
100 ft	15 fps
30 ft	10 fps
10 ft	5 fps

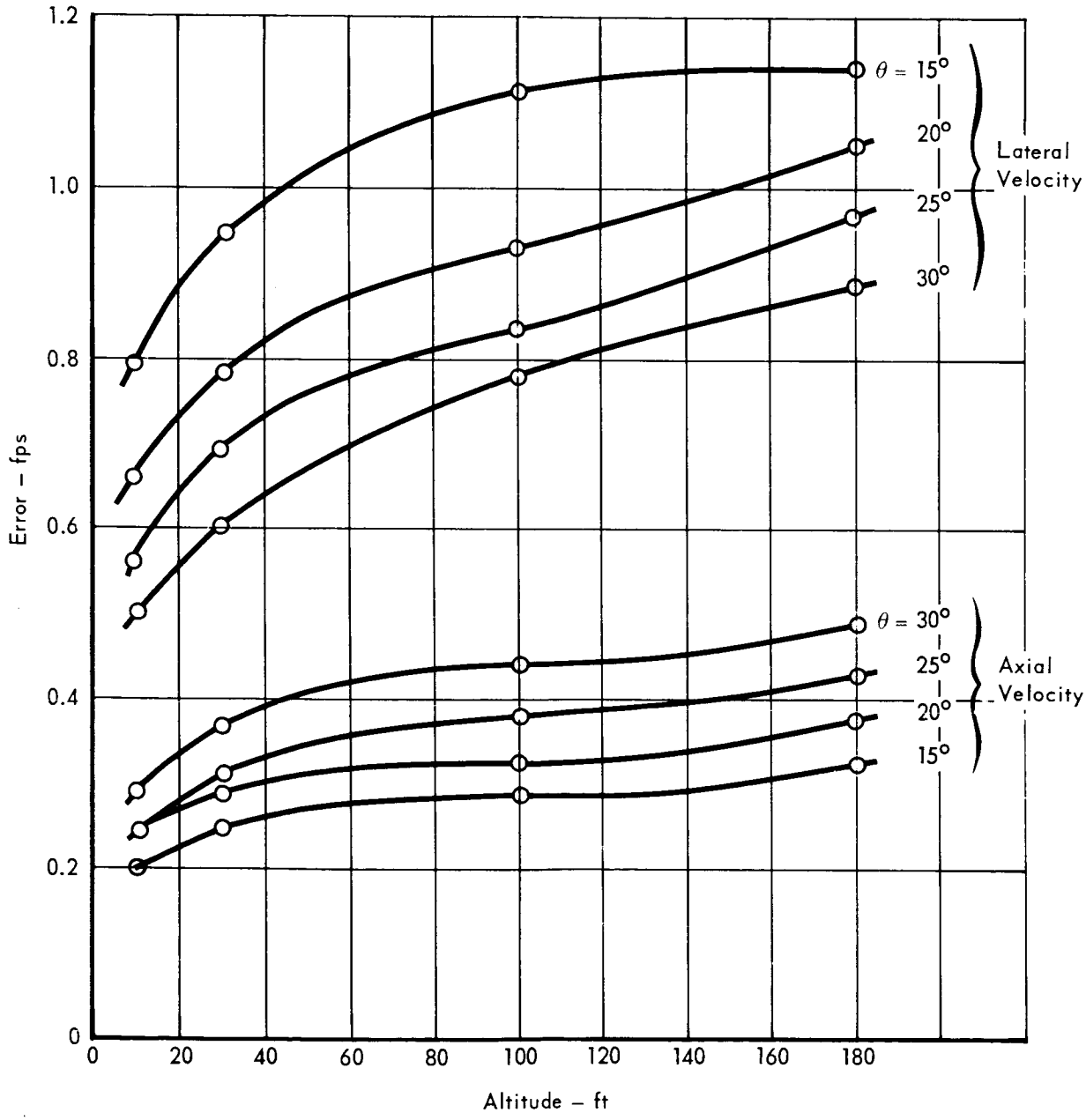

Figure 5.9–18

digital simulation of the landing radar conducted to determine velocity measurement accuracy sensitivity to the beam configuration squint angle. In this figure velocity errors are shown as a function of altitude for a representative terminal descent trajectory and for four squint angle values. Combining this data with the lander attitude sensitivity analysis of Section 5.9.5.1, it is concluded that the twenty degree squint angle selection provides acceptable terminal accuracy and minimizes flight path angle sensitivity.

5.9.5.7 Aeroshell Lock-On - Parachute size and deployment altitude, Aeroshell separation time, and parachute release altitude have been selected to result in the Aeroshell reaching the surface before landing radar operation is required for most atmospheres. (See II, B, 2.3.7).

The VM-7 atmosphere is the worst in this respect because at 5,000 feet the Aeroshell is approximately three seconds away from the surface. The look angle from the lander and aspect angle to the Aeroshell are approximately 23 degrees from the respective roll axes. Thus, the Aeroshell could be within a velocity beam and seeing the peak return from the Aeroshell at 20 degrees (Reference Section 5.9.1.4).

The doppler frequency is positive for the desired surface return at the point where acquisition is desired, for all beams, and for all trajectories and wind conditions. The doppler frequency will be negative for the return from the Aeroshell. The frequency trackers will be searched from positive doppler frequencies to zero, never searching over the negative frequencies corresponding to the doppler frequency of the Aeroshell. The signal-to-noise ratio for all velocity beams is greater than 26 dB for all VM-7 trajectories studied to date. The signal-to-noise ratio from the Aeroshell would be less than 20 dB even if the full 300 square meter flash were directly in a velocity beam at this range (4800 feet). Thus, there should be little chance of the Aeroshell signal pulling the tracker away from the desired lock point. In addition, the probability that all these worst case conditions occur simultaneously is very small.

Another potential Aeroshell lock-on problem consists of the possibility of interference from the Aeroshell after it has impacted with the surface. If the Aeroshell lies within a beam, the return will be from the desired patch of surface and the most that can occur is a degradation in tracker accuracy because of the resulting asymmetrical doppler or range frequency spectrum. The most serious problem occurs if the tracker remains locked to the return from the Aeroshell by virtue of antenna sidelobe gain after the primary lobe had left this

area. It corresponds to tracker gate stealing by the Aeroshell. For this to occur, the return from the Aeroshell in a sidelobe must be larger than the desired surface return in the main lobe.

After examining the Aeroshell structure and the velocities at which it will impact (greater than 175 ft/sec for all atmospheres), it is believed that total deformation will occur on impact. Since this deformation can be assumed random, the large spikes in cross section will be spread over all aspect angles. The return will become diffuse and the radar cross section can be assumed to be independent of frequency and approximately equal to the cross sectional area of the structure (280 square feet).

Reducing this cross section by the relative gain of the sidelobes (down at least 30 dB), and considering that the lander never lands closer to the Aeroshell than 200 feet (Reference Section 2.3.7), the reflections in the sidelobes will not be large enough to steal tracker lock.

A more rigorous analysis of the Aeroshell lock-on problem will be accomplished during the Phase B extension. A more detailed analysis of the radar cross section will be performed, taking into account equipment installation.

A preliminary study indicates that fairly light absorbent materials can be placed over critical areas within the Aeroshell and materially reduce the radar cross section. Figure 5.9-19 shows what can be done with a minimum amount of additional weight. It shows radar cross section with a reflecting screen attached (15 pounds) over the ring stiffeners, plus radar absorbing material (23 pounds) on the back face of the upper stiffener and on the inside of the nose cap. The reflecting screen changes the inside cone angle to 35 degrees, thus shifting the outside peak from 30 to 35 degrees. It also reduces the backscatter at tail-on from the inside ring stiffeners. The absorbing material essentially did away with the 6.5 square meter residual area from the inside of the nose cap and reduced the tail-on and 20 degree spikes due to the upper ring stiffener.

5.9.5.8 Rocket Exhaust Effects - An approximate technique used to evaluate the Gemini retrorocket exhaust recirculation was applied to evaluate the base flow properties of the terminal propulsion engine configuration. Results of this contamination analysis for the 4 terminal propulsion engines operating at full thrust are:

Maximum base total pressure	.0032 psia
Maximum incident base velocity	2083 ft/sec

Base pressure and, therefore, contamination levels are low and are expected to

RADAR CROSS SECTION OF AEROSHELL

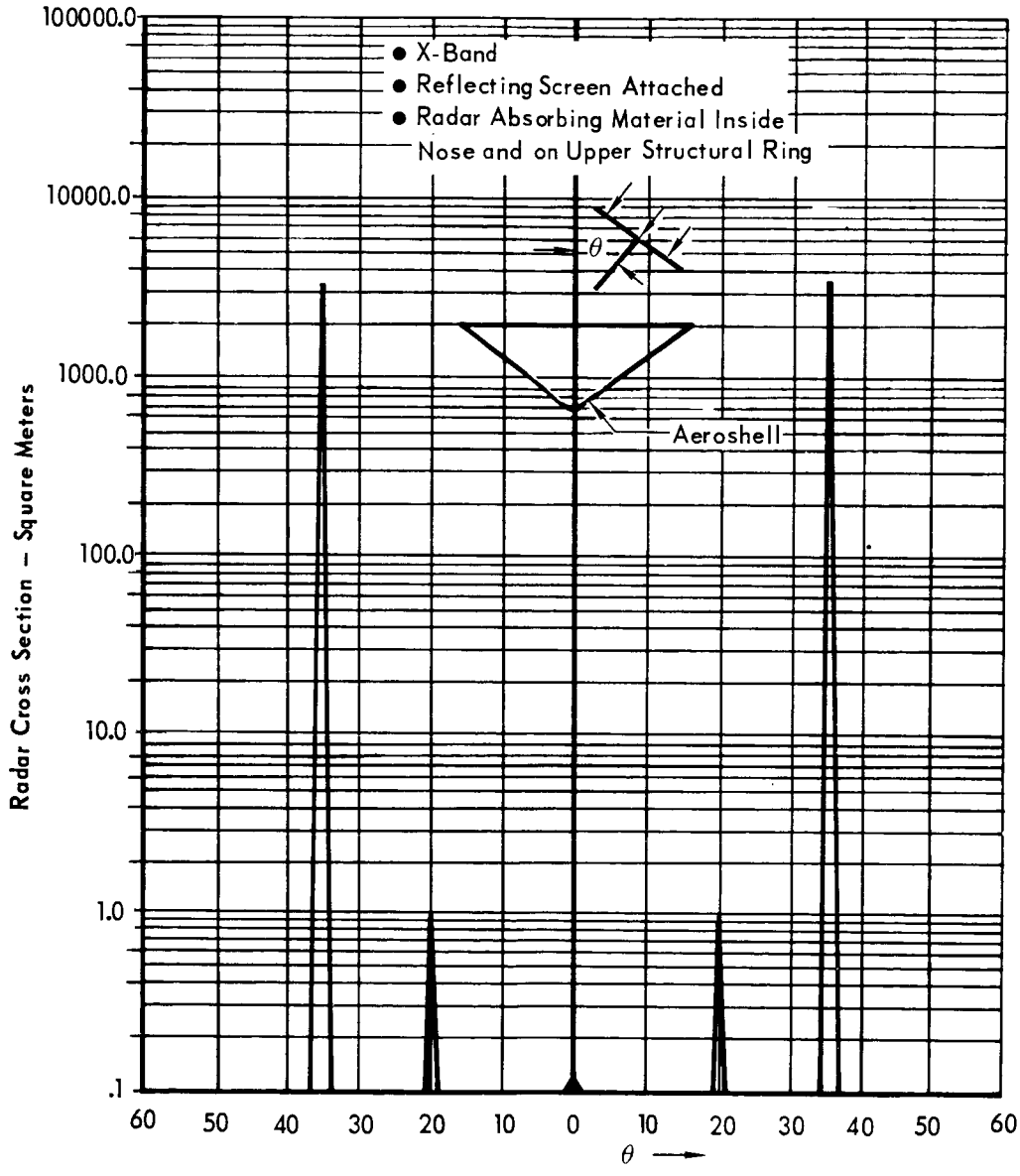

Figure 5.9–19

be no problem. The actual amount of contamination can best be determined empirically.

Propagation Interference - The principal factors determining the degree of interference are electron density, electron collision frequency, transmitting frequency and plasma depth. Free electrons in the rocket exhaust plume may result from a combination of sources including thermal ionization and chemical ionization. However, analytical evaluation of attenuation in rocket exhausts assuming thermal ionization only has compared favorably with experimental measurement. At typical rocket chamber flame temperatures, the predominant contributors to thermal ionization are chemical species having low ionization potentials; specifically the alkali metals (sodium, potassium and lithium) and free carbon. Small amounts of sodium and potassium are usually present in the form of propellant and nozzle material contaminants. Their presence, even in concentrations of a few parts per million, usually account for the bulk of free electrons in rocket exhausts. In the monomethylhydrazine (MMH) nitrogen tetroxide (N_2O_4) system, free carbon is oxidized to carbon dioxide which is an electron scavenger.

Electron density (N_e) and collision frequency (ν) profiles for the terminal propulsion engine exhaust are presented in Figure 5.9-20 for the engine operating at full thrust in the vicinity of a radar beam. These data are for a pressure of 25 millibars, which creates a plume profile more confined than one in a vacuum and should result in worse propagation effects than the more expanded plume. The conservative assumption was made that the concentration of electrons was frozen in the chamber. Since the population of electrons in the exhaust plume is essentially constant, the electron density and collision frequency at any location in the plume were assumed to vary as the ratio of local jet to chamber density. The flow field thermodynamic properties were computed using a method of characteristic solution of the potential flow equations. Only the alkali metal propellant contaminants (sodium and potassium) were considered as electron sources.

The following alkali metal impurity levels were used for MMH and N_2O_4.

	Na (ppm)	K (ppm)
MMH	.49	2.2
N_2O_4	.1	.07

Although the fuel contamination levels reported were for Aerozine 50, it was assumed that the contamination level in MMH would be comparable.

A computer program for calculating transmission characteristics through inhomogeneous plasmas was used to derive the attenuation and phase shift characteristics listed in Figure 5.9-20. The two-way shift of 1.54° and two-way

RADAR REFLECTION FROM ROCKET PLUME

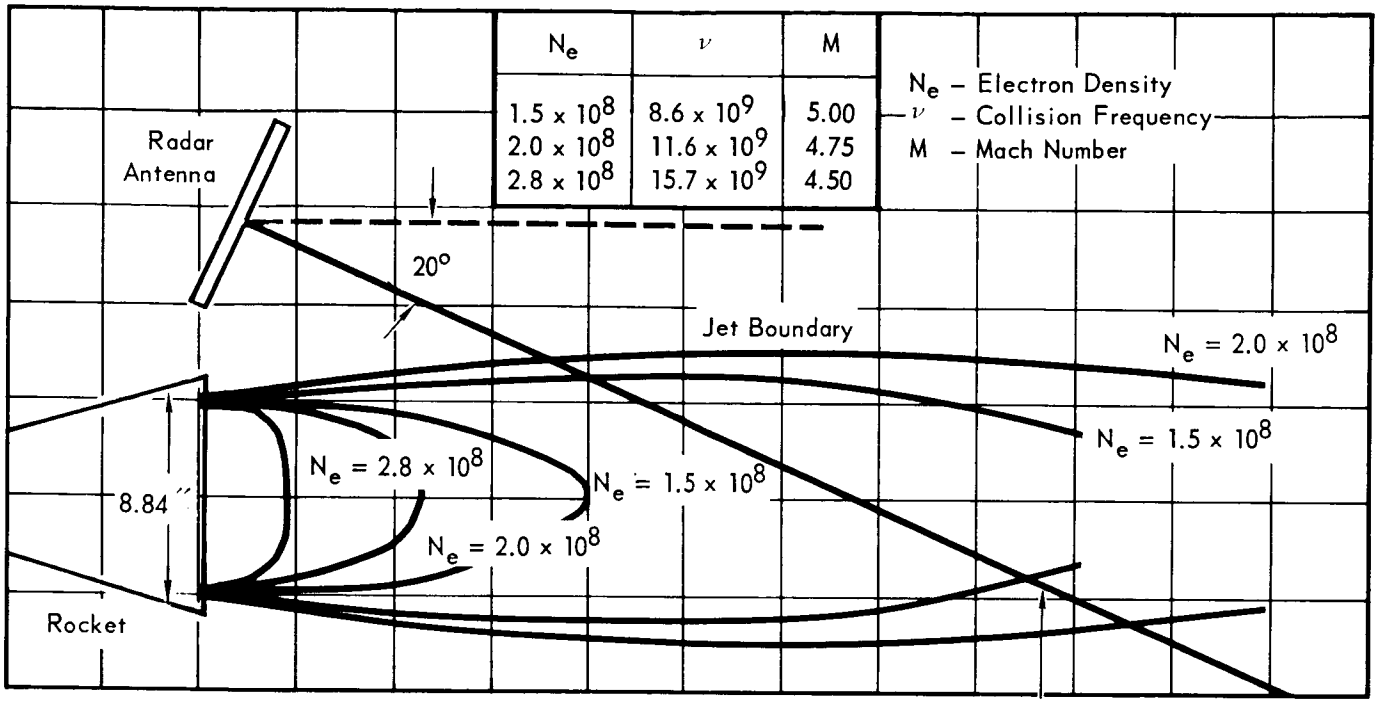

Propellants MMH: NTO
Chamber Temperature – 5545°R
Ambient Pressure – 25 Millibars
Chamber Pressure – 300 psi

Radar Frequency = 10.5 GHz
2-Way Phase Shift = 1.54°
2-Way Attenuation = 0.04 db
Reflected Power = -97 db

POWER SPECTRAL DENSITY OF REFLECTED SIGNAL

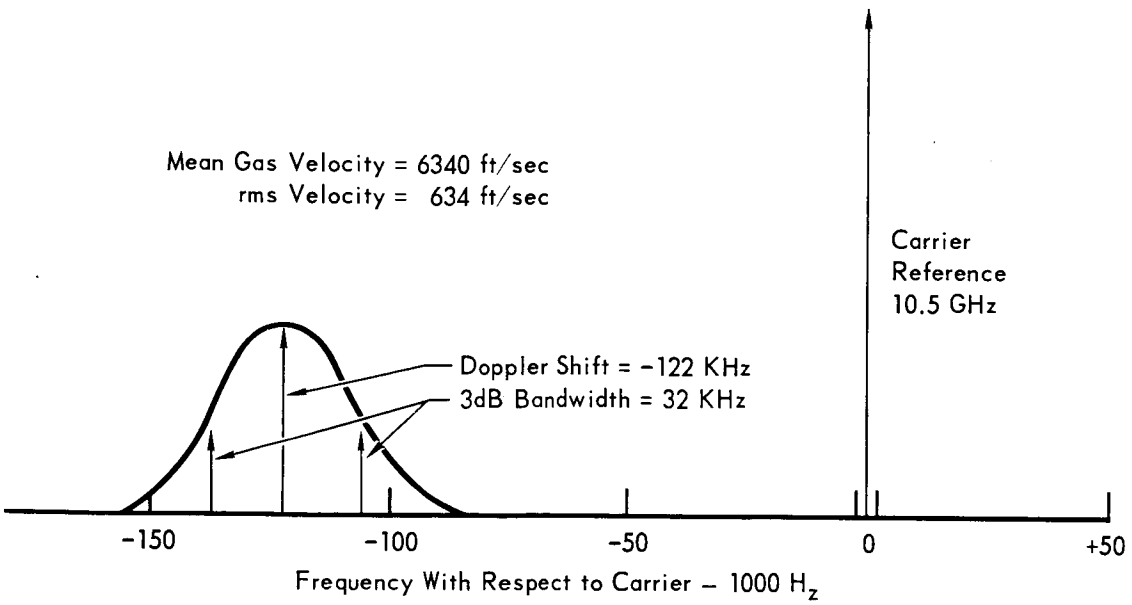

Figure 5.9–20

attenuation of 0.04 dB will not affect radar operation. Backscatter calculations indicate a reflection of -97 dB. The backscatter power spectrum is also shown in Figure 5.9-20. This spectrum will not interfere with the desired signals which are not in this negative frequency region. The spectrum shown is for maximum thrust and would move to a center frequency 113 kHz below the carrier during deep throttling.

These calculations have been made with worst case geometry, i.e., with the propagation path directly through the exhaust plume and with an antenna separation of approximately 1 ft.

The VOYAGER landing radar has an engine to antenna array separation (center to center) of 44 inches with the antenna 6.5 inches below the engine exit plane. The beam angle is 20 degrees off the roll axis while the rocket engines are skewed 5 degrees. The antenna beam and rocket plume do not intersect within the bounds of Figure 5.9-20. In addition, the antenna is rotated with respect to the engines so that the four landing radar velocity beams pass between the four rocket engine plumes. Thus, the propagation interference numbers for the preferred lander and engine configuration, are considerably below the calculated values of Figure 5.9-20, which are themselves insignificant.

5.9.5.9 Dust Clouds - Blue, white and yellow clouds have been observed over Mars. Blue and white clouds occur near the Martian limb and are thought to be due to optical foreshortening of atmospheric haze. If this is the case, particle densities will be too low to affect landing radar operation. Yellow clouds are thought to consist of wind blown dust from the Martian surface. A study has been conducted to determine if these dust clouds will affect operation of the landing radar.

Dust Cloud Model - The dust cloud phenomenon has been modeled based on data from McDonnell wind blown dust tests (Reference 5.9-2) and desert sand storm observations on Earth. It has been determined that two types of clouds are possible.

An upper dust cloud has been hypothesized which extends from the surface to an altitude of 3 to 30 kilometers and has the following characteristics:

- o Particle diameter: 1 to 100 microns
- o Average particle diameter: 20 microns
- o Average particle velocity: 3 - 82 ft/sec
- o Average particle density: 1 to 10 particles per cubic centimeter

A lower saltation cloud could also exist which extends from 4 to 8 centimeters

above the surface and which has the following characteristics:

- o Particle diameter: 1 to 1000 microns
- o Average particle diameter: 90 microns
- o Average particle velocity: 110 to 220 ft/sec (depending on wind velocity)
- o Average particle density: 2 to 100 particles per cubic centimeter

High Altitude Dust Clouds - The high altitude clouds will cause the desired radar return from the surface to be attenuated, and will also result in undesired return, which will be called clutter. The desired return signal to undesired clutter ratio (signal-to-clutter ratio) provides a measure of how well the landing radar can perform.

The signal-to-clutter ratio that can be expected for a LM type radar was calculated assuming the particle density to be uniform throughout the extent of the cloud, and particle size to be distributed according to

$$n(a) = \frac{N_o}{2!\left(\frac{a_o}{2}\right)^3} a^3 \exp\left[\frac{-a}{a_o/2}\right]$$

where (a) is the particle radius in microns, n (a) is the number of particles per cubic centimeter with radius between (a) and (a + da), N_o is the average number of particles per cubic centimeter, and (a_o) is the particle radius at which n(a) is maximum. A value of a_o = 10 microns was chosen, which corresponds to a particle diameter of 20 microns in the upper cloud.

Rayleigh scattering was assumed and the volume scattering cross section calculated for λ = 2.85 centimeters (10.5 GHz), and a complex dielectric constant of ϵ_c = 2.0 + i 1.62 (corresponding to dry powdery earth). Mie scattering theory was then used to find the absorption coefficient.

Using radar reflectivity at normal incidences of 0.0158 and an incidence angle of 25 deg., the signal-to-clutter ratio was calculated as a function of particle density for several values of upper and lower cloud boundaries. For the case of landing radar operation at 5000 feet (at top of, or within the cloud) and the cloud extending all of the way to the surface, the signal-to-clutter ratio is over 40 dB with a particle density of 1 particle per cubic centimeter. The cloud density would have to be greater than 50 particles per cubic centimeter for the signal to clutter ratio to drop to below 20 dB. Since the velocity of the particles is expected to be distributed over such a wide range (3 to 83 feet per second), the clutter spectrum for velocity channels will extend from zero frequency to ap-

proximately 1600 cycles per second, and mix with receiver noise. Thus, a signal-to-clutter ratio of 20 dB would correspond to an equivalent signal-to-noise ratio of 20 dB which is adequate to achieve desired performance. A similar situation exists for the range channel since the major clutter return from the cloud lies within the first 100 feet from the radar. It is believed that high altitude dust clouds will not present a problem.

Low Altitude Saltation Cloud - The same approach was used to calculate the signal-to-clutter ratio for the low altitude saltation cloud. The signal-to-clutter ratio was calculated as a function of particle density for a different cloud thickness, for the average particle diameter of 90 microns, and the same wavelength and dielectric constant. The signal-to-clutter ratio is practically independent of altitude because the range to the surface and range to the saltation cloud are nearly the same.

Wind blown dust tests indicate the particle density should be close to 10 particles per cubic centimeter. For an 8 cm thick cloud with a particle density of 10 particles per cubic centimeter, the signal-to-clutter ratio is 70 dB. The signal-to-clutter ratio is still 50 dB for a particle density of 1000 particles per cubic centimeter. Even if the doppler spectrum from the clutter were relatively narrow, there is little chance that the landing radar would lock on this spectrum. The received signal-to-noise ratio never gets above 50 dB. That is, the noise figure for the LM radar goes up as velocity and range decrease; thus receiver noise will always mask the clutter from the saltation cloud.

These calculations agree very well with preliminary calculations made early in the program for the saltation cloud with a much simpler mathematical model. A homogeneous cloud of spherical particles of uniform size was assumed. Rayleigh scattering was used to calculate the effective reflection coefficient which is plotted for a cloud thickness of 3 centimeters in Figure 5.9-21. The minimum expected reflection coefficient from the surface (-30 dB) is also plotted. From the figure, for the operating frequency used by the LM radar (f = 10 GHz), and a particle density of 100, the reflection coefficient from the dust cloud is approximately 3×10^{-10}. For a cloud 8 centimeters thick, the return would be $(8/3) \times 3 \times 10^{-10}$, or 8×10^{-10}. Assuming no loss through the cloud, the effective signal-to-clutter ratio is the ratio of reflection coefficient of the surface to the reflection coefficient of the cloud, or $10^{-3}/8 \times 10^{-10} = 1.25 \times 16^{6}$ which corresponds to 61 dB. (A more sophisticated model gives a signal to clutter ratio of 60 dB for the same particle density.)

REFLECTION COEFFICIENT OF SURFACE CLOUD

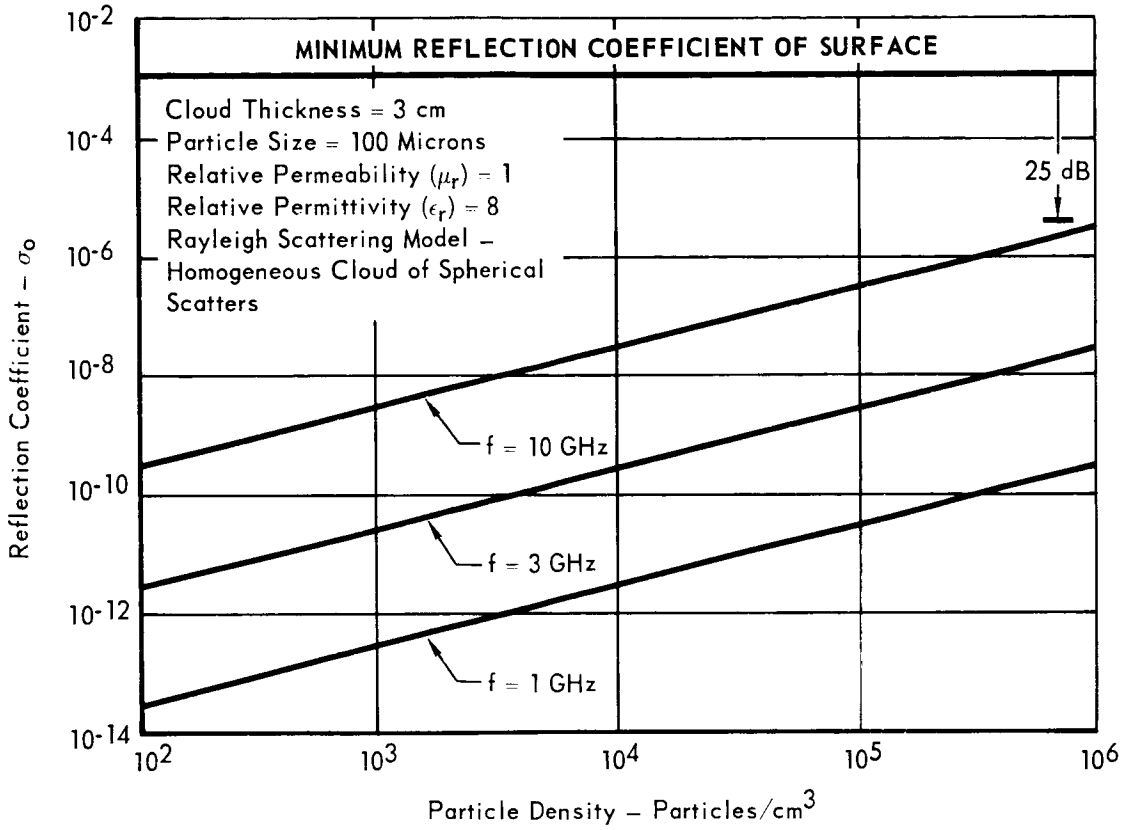

Figure 5.9–21

5.9.5.10 Spurious Signals - Consideration must be given to all potential noise and spurious signal sources in evaluating the landing radar performance. These interfering signals may be classified as either double or single sideband depending on their spectral symmetry about the zero doppler line in the received spectrum.

In addition to receiver thermal noise, other potential sources of double sideband interfering spectra include signals reflected from vibrating surfaces, modulation resulting from microwave equipment vibration, and transmitter noise. The desired ground return signal is single sideband. During the acquisition process, the landing radar compares the power of the apparent signal with that in the image sideband. If the comparison yields equal power levels (as in the case of double sideband modulation), that signal is rejected and the searching process is resumed; thus, avoiding locking onto double sideband signals. The net effect of a double sideband noise or spurious signal is to degrade the receiver sensitivity.

Single sideband spurious signals present a more difficult discrimination problem because of their similarity to the desired signal. These signals generally result from a false target possessing a velocity relative to the landing radar antenna. Potential sources of single sideband spurious signals include the Aeroshell after separation from the Capsule Lander, Martian dust clouds, and rocket exhaust plumes as discussed previously in Sections 5.9.5.7, 8, and 9.

Vibrating Structure Reflections - A reflecting surface in the field of view of the landing radar antenna will result in double sideband modulation about the zero doppler frequency point in the receiver spectrum, providing that relative motion exists between the antenna and reflector. This phenomenon would be a major problem if the landing radar were required to operate through the structure (e.g., radome). In the selected terminal descent concept the landing radar is not required to operate behind a radome. Any required antenna protective material will be fixed to the antenna. Furthermore, the lander configuration is essentially free of potential reflecting surfaces. Consequently, this source of spurious signals is virtually non-existant.

Microwave Equipment Vibration - In the preferred landing radar configuration all microwave equipment will be located in the antenna assembly. This equipment consists of the slotted waveguide phased arrays, solid state transmitters, range beam FM modulator, microwave mixers, and audio frequency preamplifiers. When subjected to vibration, the receiver noise as measured at the output of the preamplifiers will be increased. This resultant noise spectrum can generally be characterized by a continuous spectrum together with isolated spikes. These

spikes generally result from antenna assembly resonance modes, and will depend upon the specific antenna physical design and mounting. The effect of the continuous portion of this noise spectrum may be treated by defining an equivalent receiver noise figure. The spectral spikes are treated as discrete interfering signals.

Figure 5.9-22 presents the estimated equivalent noise figures (i.e., including both thermal and vibrational noise) for the range and velocity channels of the preferred landing radar configuration. These equivalent noise figures are based on a representative antenna vibrational spectrum (during entry) equal to 0.005 g^2/cps from 20 to 2000 cps, and were used in the digital simulation from which the signal characteristics were generated. (Section 5.9.5.11)

In order to confirm the validity of these estimated equivalent noise figures, experimental data was obtained from the LM radar manufacturer. The data consisted of a spectral analysis of noise appearing at the output of each velocity beam preamplifier with the LM antenna subjected to a 0.005 g^2/cps vibration spectrum (20 to 2000 cps). The experimental data indicated that the estimated equivalent noise figure that is shown in Figure 5.9-22 is generally correct within $\pm$ 4 dB. The largest exception occurred for only one of the three velocity channels at a frequency of 1250 cps where the experimentally measured noise figure was about 10 dB above that of Figure 5.9-22.

Examination of the VM-10 signal parameter time histories presented in Section 5.9.5.11, shows that the signal-to-noise ratio when the doppler frequency reaches 1250 cps is 40 dB. Thus, even with this worst case experimental data, the signal-to-noise ratio at this point would only be reduced to 30 dB.

It is concluded that the equivalent noise figure data of Figure 5.9-22 is a good estimate of actual receiver performance under vibration.

Transmitter noise - AM and FM noise will accompany the generation of the landing radar X-band CW signals. The LM radar performance indicates that the AM and FM noise on the basic CW signals can be suppressed to the point where there is essentially no effect on receiver performance. However, in the generation of the FM/CW ranging signal, incidental amplitude modulation results. A portion of the range beam transmitted signal is used as the reference signal at the microwave mixers in the range channel. The incidental AM is effectively envelope detected at this mixer, resulting in interfering noise which may be represented by discrete spectral components (double sideband) appearing at multiples of the modulating frequency (130 H_z).

LANDING RADAR EQUIVALENT NOISE FIGURE AS A FUNCTION OF TRACKING FREQUENCY

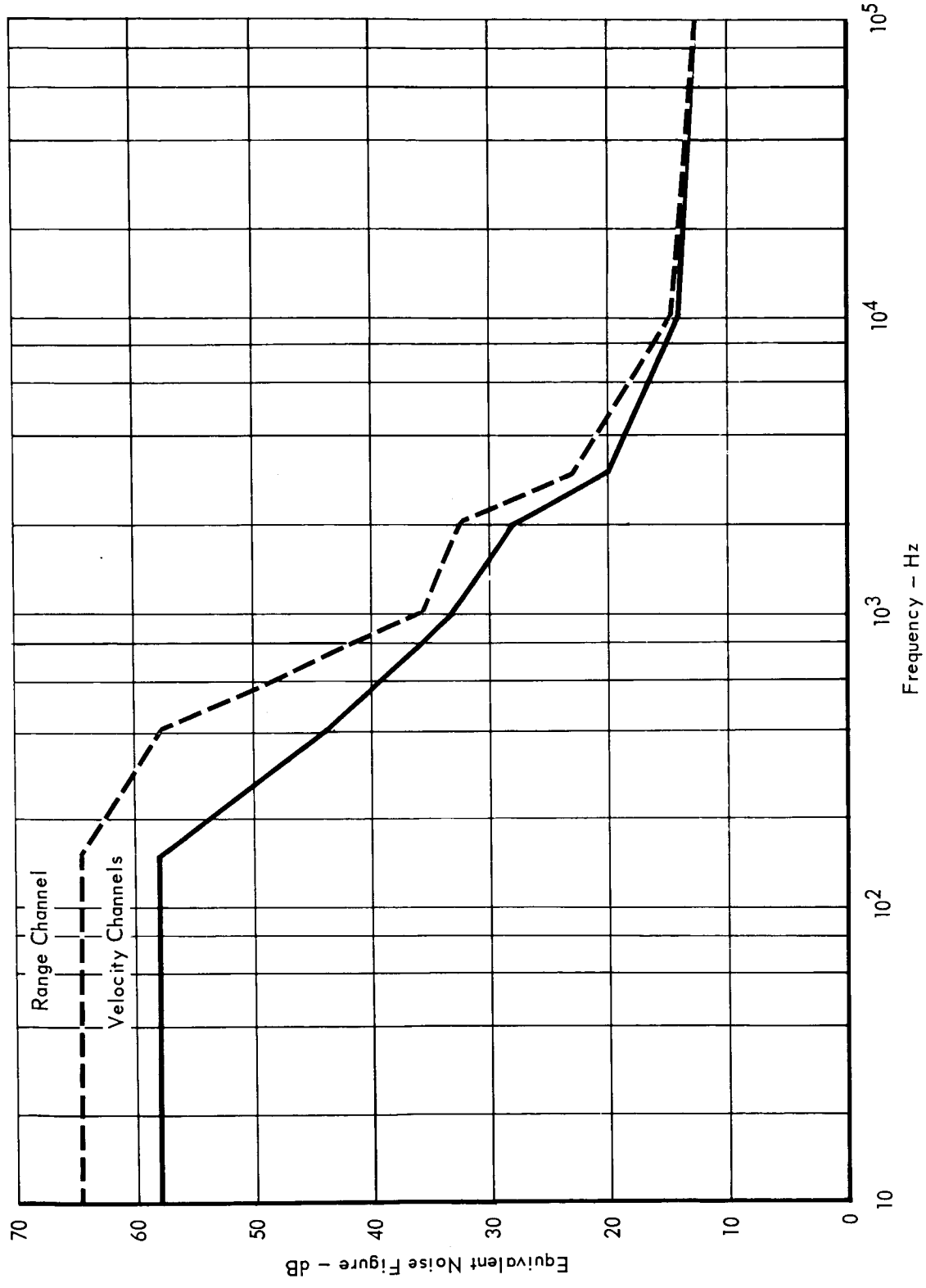

Figure 5.9–22

The amplitude of these incidental AM discretes will depend upon the AM on the first mixer reference signal and the characteristics of the mixer. In generating the curves for range beam signal-to-noise ratio and tracking performance of Section 5.9.5.11, it was assumed that the incidental AM noise was masked by the equivalent continuous receiver noise figure of Figure 5.9-22. However, for purposes of the error analysis of Section 5.9.5.11 discrete spectral components were included at multiples of the modulating frequency. These discretes varied from -83.2 dBW at 130 Hz to -112.8 dBW at 1040 Hz, and are considered to be an upper bound.

Single Sideband Spurious Effects - In order to evaluate the landing radar tracking performance in the presence of spurious signals, a number of tests were conducted using the McDonnell analog simulation of the frequency trackers. The results of one such parametric study are shown in Figure 5.9-23. In this case a spurious signal was introduced at a specified relative power level and frequency from the signal being tracked, and the resultant tracking error was measured. For the particular case shown, the desired velocity tracker signal frequency was 10 KHz (placing it well above the preamplifier break frequency at 3KHz), and the desired signal bandwidth was 300 Hz (representative of the VOYAGER terminal descent conditions). Results are shown for spurious-to-signal power ratios of -3, 0, and + 3 dB.

The results are self-evident. For example, it is seen that, for the conditions shown, an equal power spurious signal can cause a tracking error of 220 Hz which corresponds to a beam velocity error of 10 ft/sec. The significance of this error will depend upon the point in the terminal descent trajectory at which it occurs. Results from this and other similar parametric studies have been used to evaluate spurious signal effects as a function of the terminal descent phase.

5.9.5.11 Landing Radar Performance During Descent - In order to illustrate the capability of the preferred landing radar when operating with the selected VOYAGER terminal descent concept, a specific trajectory is considered and the results are discussed in this section. The McDonnell digital and analog landing radar simulations were used for this performance evaluation, with the descent profile used as the simulation driving function.

For the trajectory evaluation, a VM-10 atmosphere was considered with a 120 fps horizontal tail wind. Zero terrain slope is assumed. The Capsule Lander roll position was such that velocity beams 1 and 3 were in the pitch plane with velocity beam 3 nearest the horizontal and velocity beam 1 nearest the vertical.

SINGLE SIDEBAND SPURIOUS SIGNAL RESPONSE

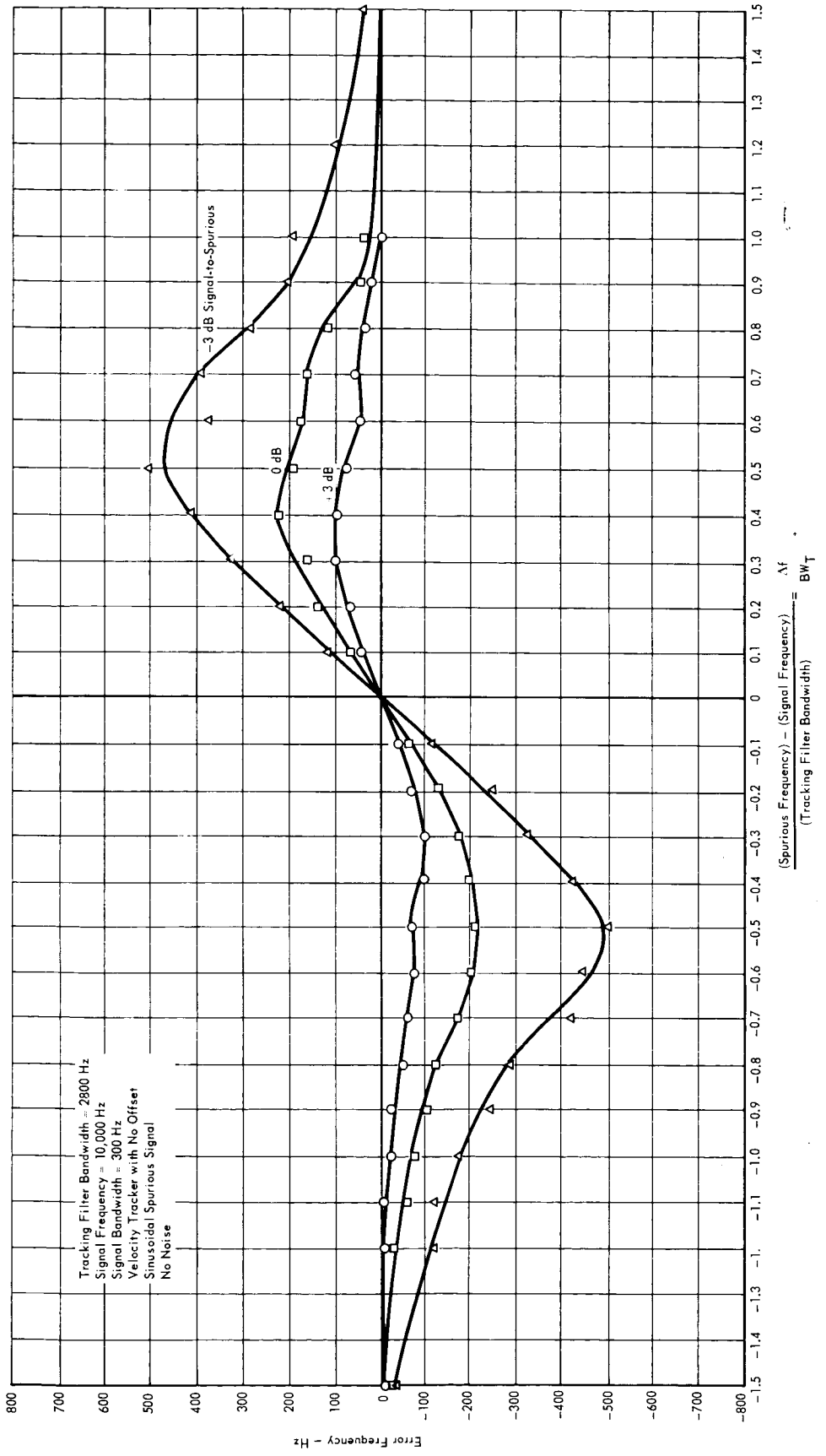

Figure 5.9–23

In this roll position velocity beams 2 and 4 experienced equal, intermediate incident angles. It was also assumed that guidance information was derived from velocity beams 1, 2, and 3 (corresponding to a beam 4 out condition). This particular choice of operating beams and roll position results in a worst case with respect to signal-to-noise ratios for two reasons. First, beam 3 is nearest the horizon, and thus operates with the minimum backscatter coefficient and maximum free space loss. Second, the horizontal tail wind causes a reduction in the doppler frequency shift on beam 1 and forces beam 1 tracker operation into the low frequency, higher receiver noise (thermal and vibrational) region.

Various aspects of the landing radar performance during the VM-10 terminal descent are shown in Figures 5.9-24 through -30. In order to provide a basis for subsequent discussion, event sequencing during the later portion of this VM-10 trajectory is described here. At time zero the lander roll axis is aligned with the vertical, and the lander altitude is 5000 ft. For the first six seconds the lander is in an inertial attitude hold mode. It is during this six second period that landing radar acquisition must be completed. At about the sixth second the velocity vector alignment maneuver is initiated. The maneuver is essentially completed at about the eleventh second. From about time 11 sec to time 22 sec a constant minimum thrust level is maintained with the lander control system providing velocity vector/thrust axis alignment. During this period the Capsule Lander reaches a landing radar measured roll axis slant range equal to 2500 feet (at time 16.5 sec) where mode switching in the landing radar occurs. The mode switching in the landing radar consists of reducing the tracker bandwidths and increasing the range beam frequency deviation by a factor of five. From time 22 sec on, the lander is controlled to the specified decent profile.

Signal-to-Noise Ratio and Tracking Performance - Figures 5.9-24 through -30 present the significant landing radar performance parameters over the selected VM-10 terminal descent trajectory. Velocity beam 1 characteristics are shown in Figures 5.9-24 and 5.9-25 and velocity beam 3 characteristics are shown in Figures 5.9-26 and 5.9-27. Similar data for velocity beams 2 and 4 is not shown as these beams represent an intermediate case. The range beam parameters are shown in Figures 5.9-28 and 5.9-29.

In Figures 5.9-24 through -30 all curves have been generated from the McDonnell landing radar digital simultation with the exception of the curves labeled tracker error frequency. The tracker error frequency curves and indicated acquisition points are results of the McDonnell analog simulation of the range and velocity beam

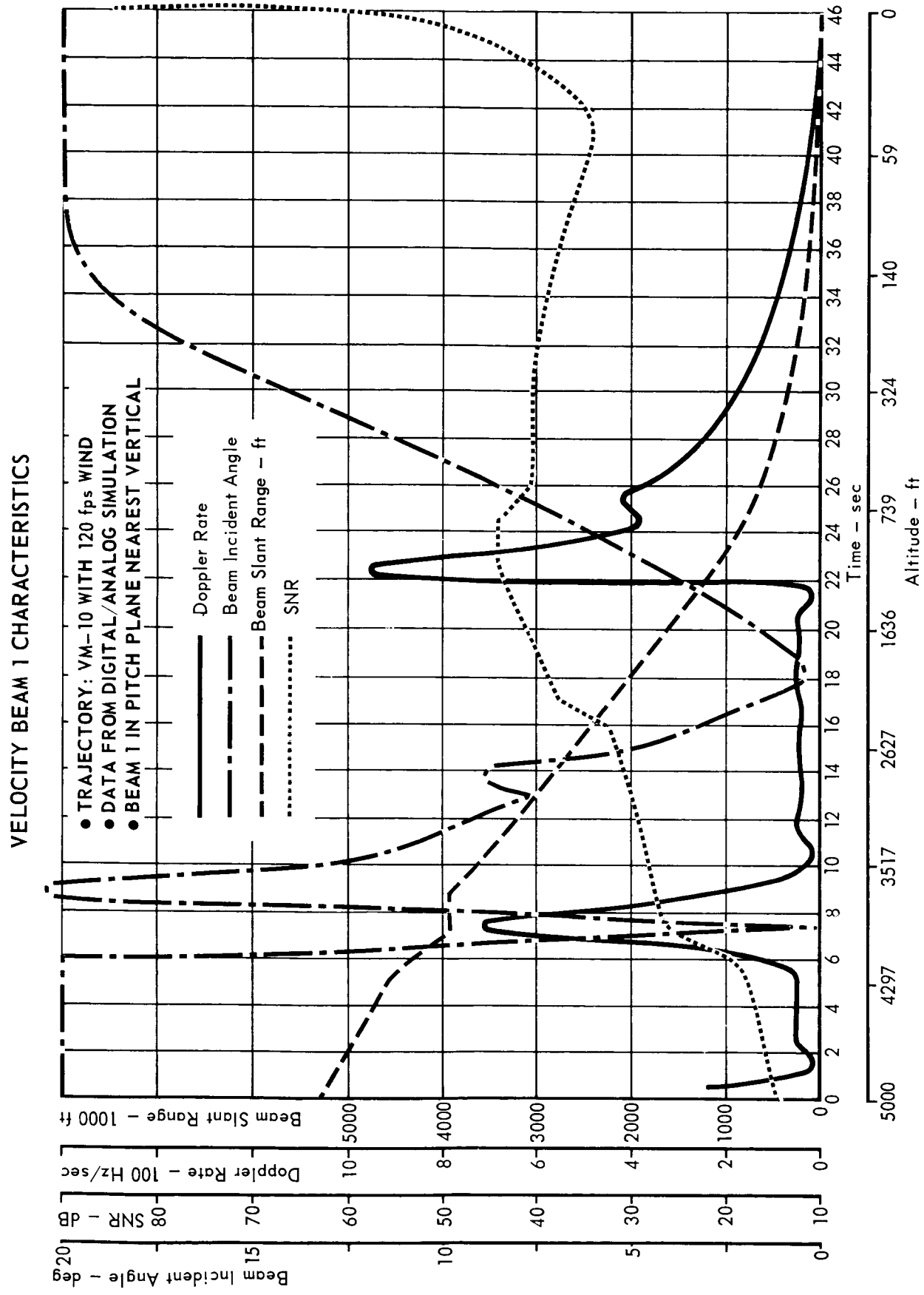
VELOCITY BEAM 1 CHARACTERISTICS
● TRAJECTORY: VM-10 WITH 120 fps WIND
● DATA FROM DIGITAL/ANALOG SIMULATION
● BEAM 1 IN PITCH PLANE NEAREST VERTICAL
Doppler Rate
Beam Incident Angle
Beam Slant Range – ft
SNR
Beam Incident Angle – deg
SNR – dB
Doppler Rate – 100 Hz/sec
Beam Slant Range – 1000 ft
Time – sec
Altitude – ft

Figure 5.9–24

VELOCITY BEAM 1 CHARACTERISTICS

Trajectory: VM-10 with 120 FPS Wind
Data from Digital/Analog Simulation
Beam 1 in Pitch Plane Nearest Vertical

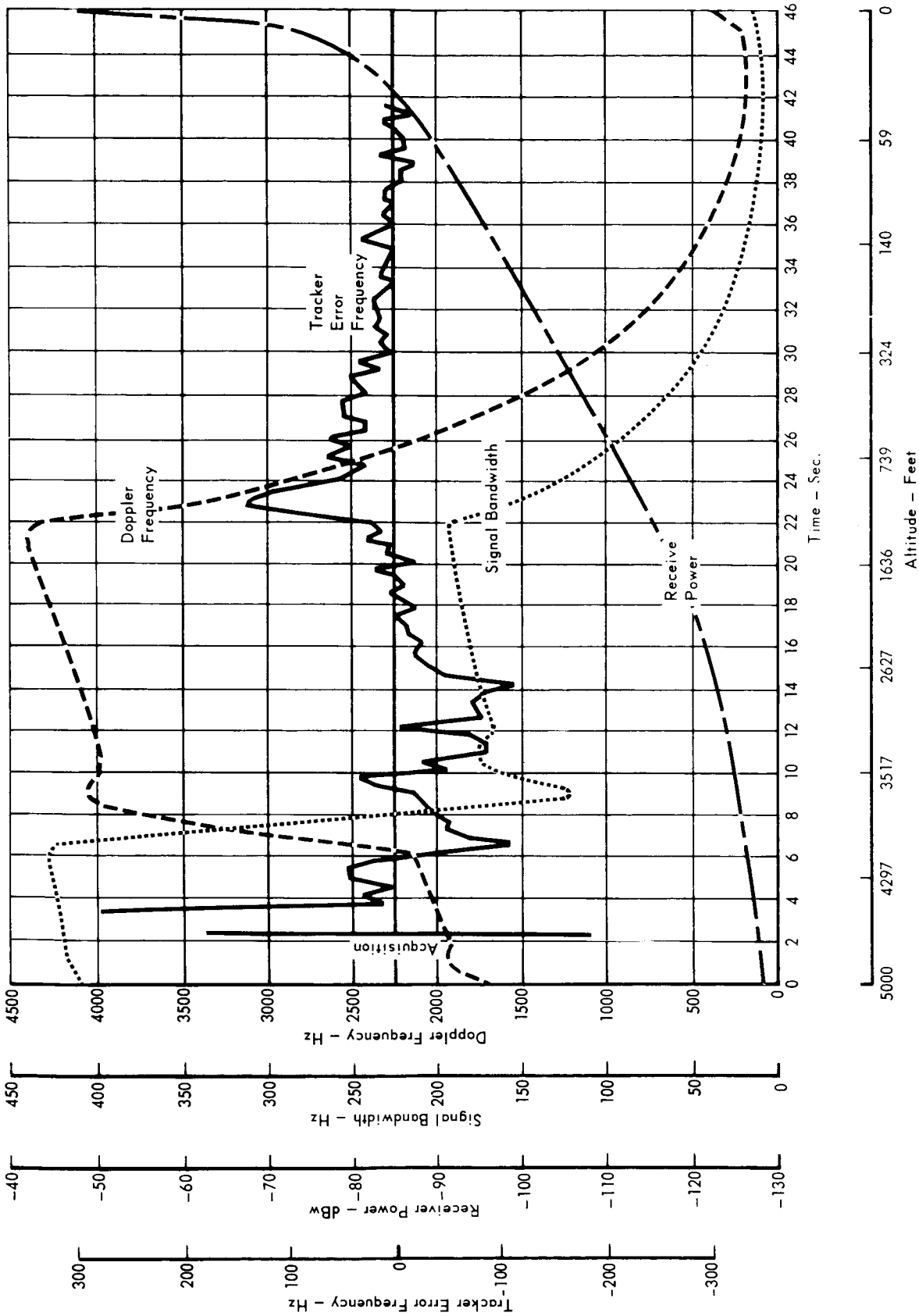

Figure 5.9–25

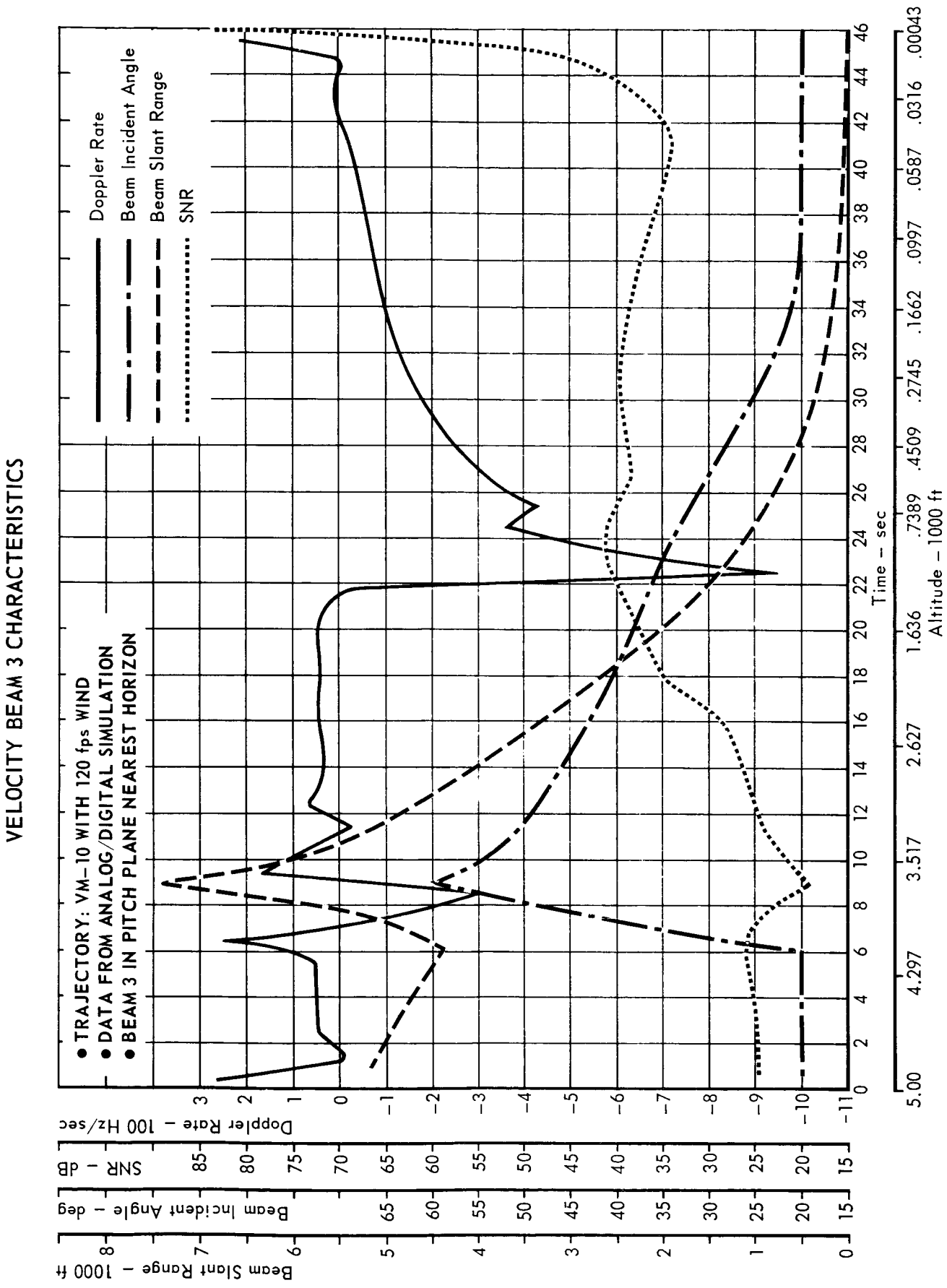
VELOCITY BEAM 3 CHARACTERISTICS
• TRAJECTORY: VM-10 WITH 120 fps WIND
• DATA FROM ANALOG/DIGITAL SIMULATION
• BEAM 3 IN PITCH PLANE NEAREST HORIZON
Doppler Rate
Beam Incident Angle
Beam Slant Range
SNR
Doppler Rate – 100 Hz/sec
SNR – dB
Beam Incident Angle – deg
Beam Slant Range – 1000 ft
Time – sec
Altitude – 1000 ft

Figure 5.9–26

VELOCITY BEAM 3 CHARACTERISTICS

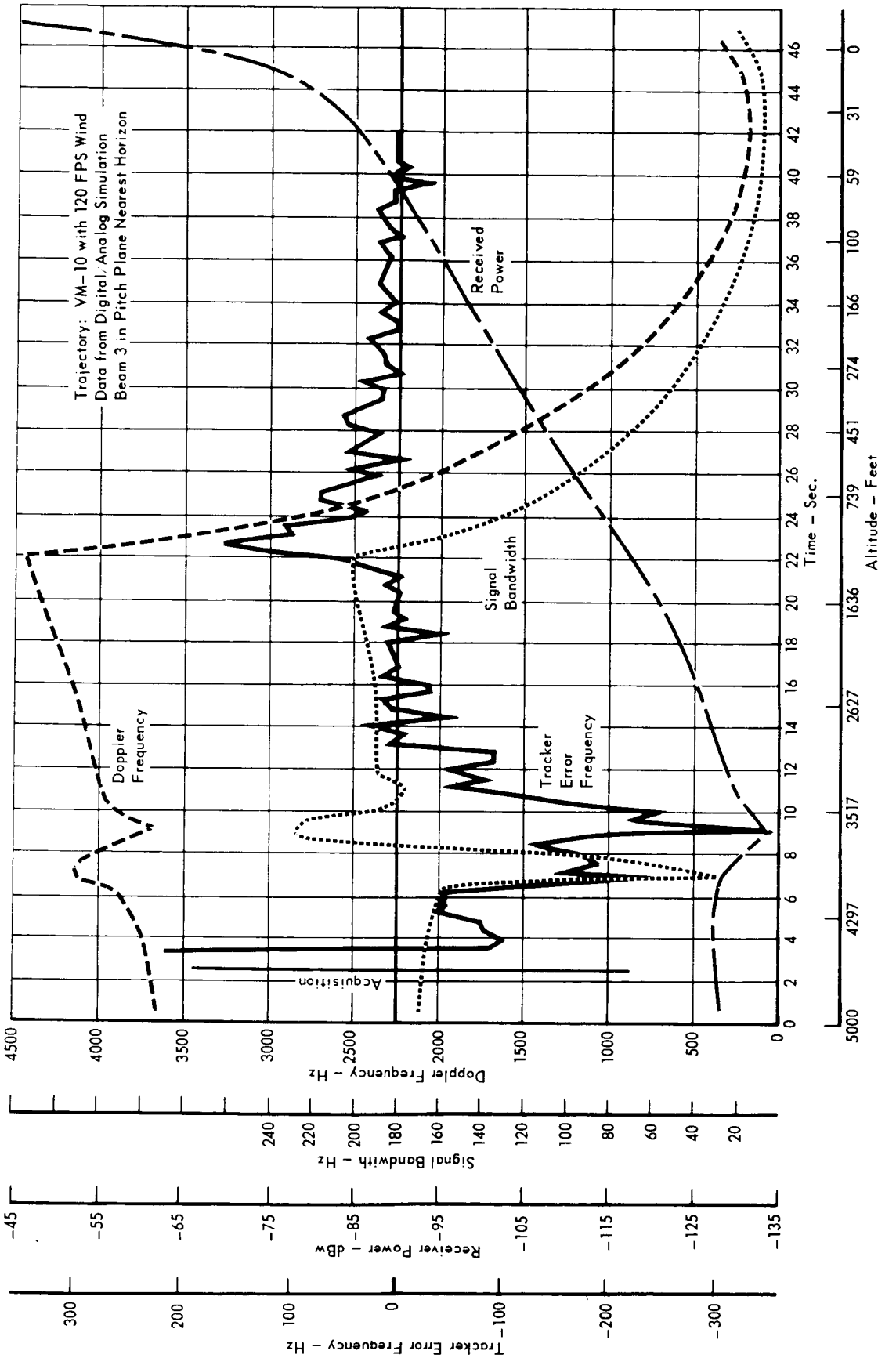

Figure 5.9-27

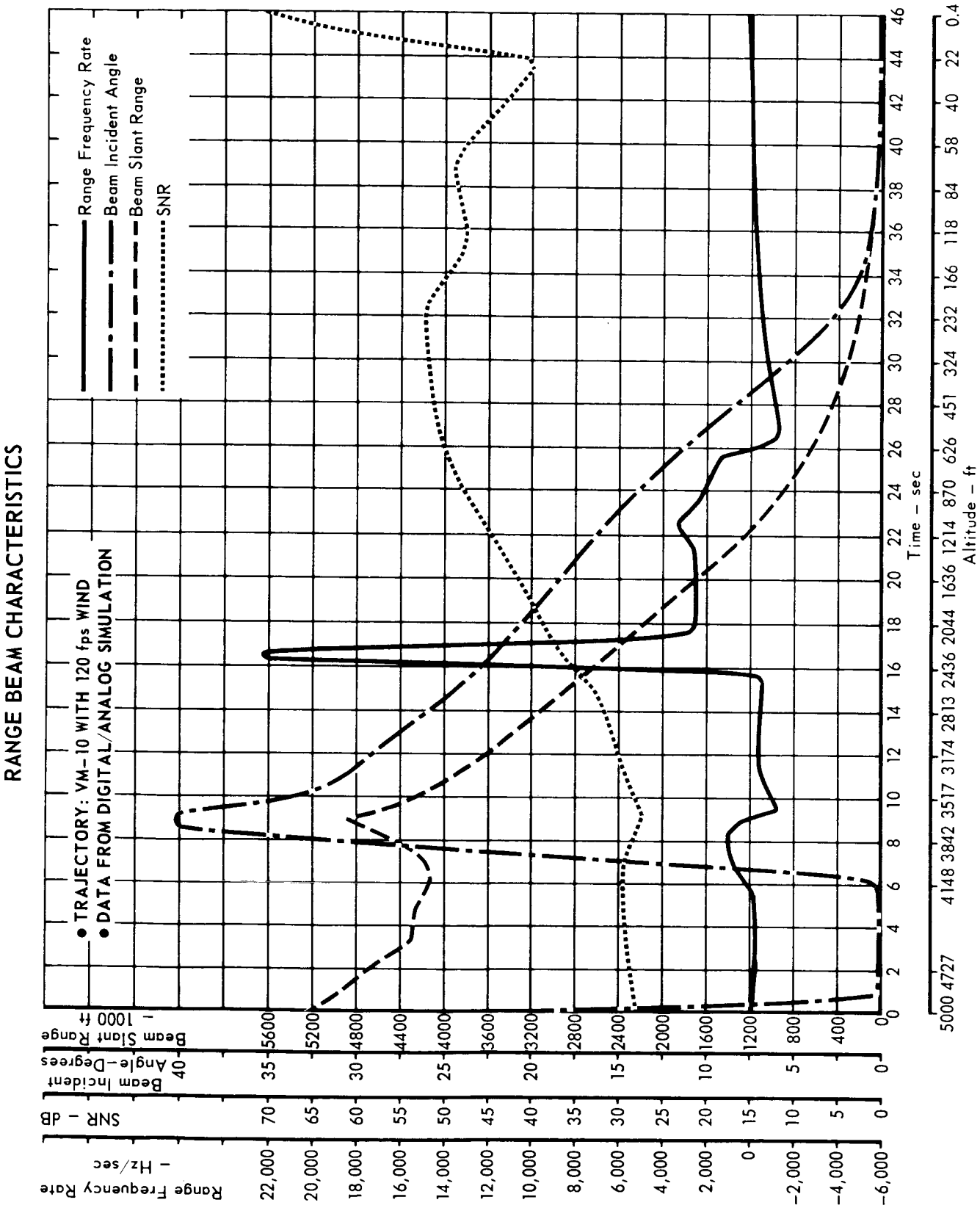
RANGE BEAM CHARACTERISTICS
● TRAJECTORY: VM-10 WITH 120 fps WIND
● DATA FROM DIGITAL/ANALOG SIMULATION
Range Frequency Rate
Beam Incident Angle
Beam Slant Range
SNR
Range Frequency Rate – Hz/sec
SNR – dB
Beam Incident Angle–Degrees
Beam Slant Range – 1000 ft
Time – sec
Altitude – ft

Figure 5.9–28

RANGE BEAM CHARACTERISTICS (Continued)

- Trajectory = VM-10 with 120 fps Wind
- Data from Digital Analog Simulation

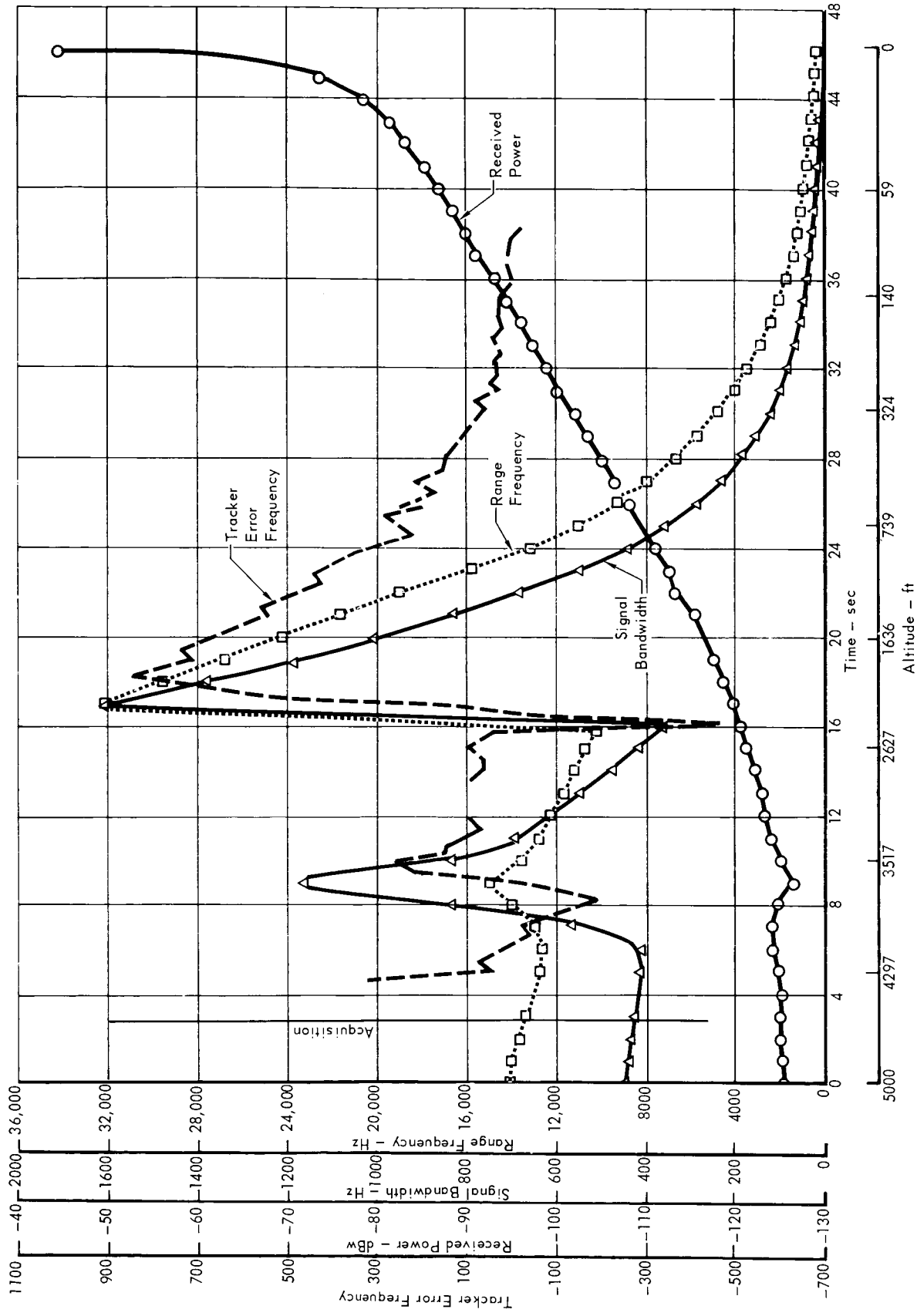

Figure 5.9-29

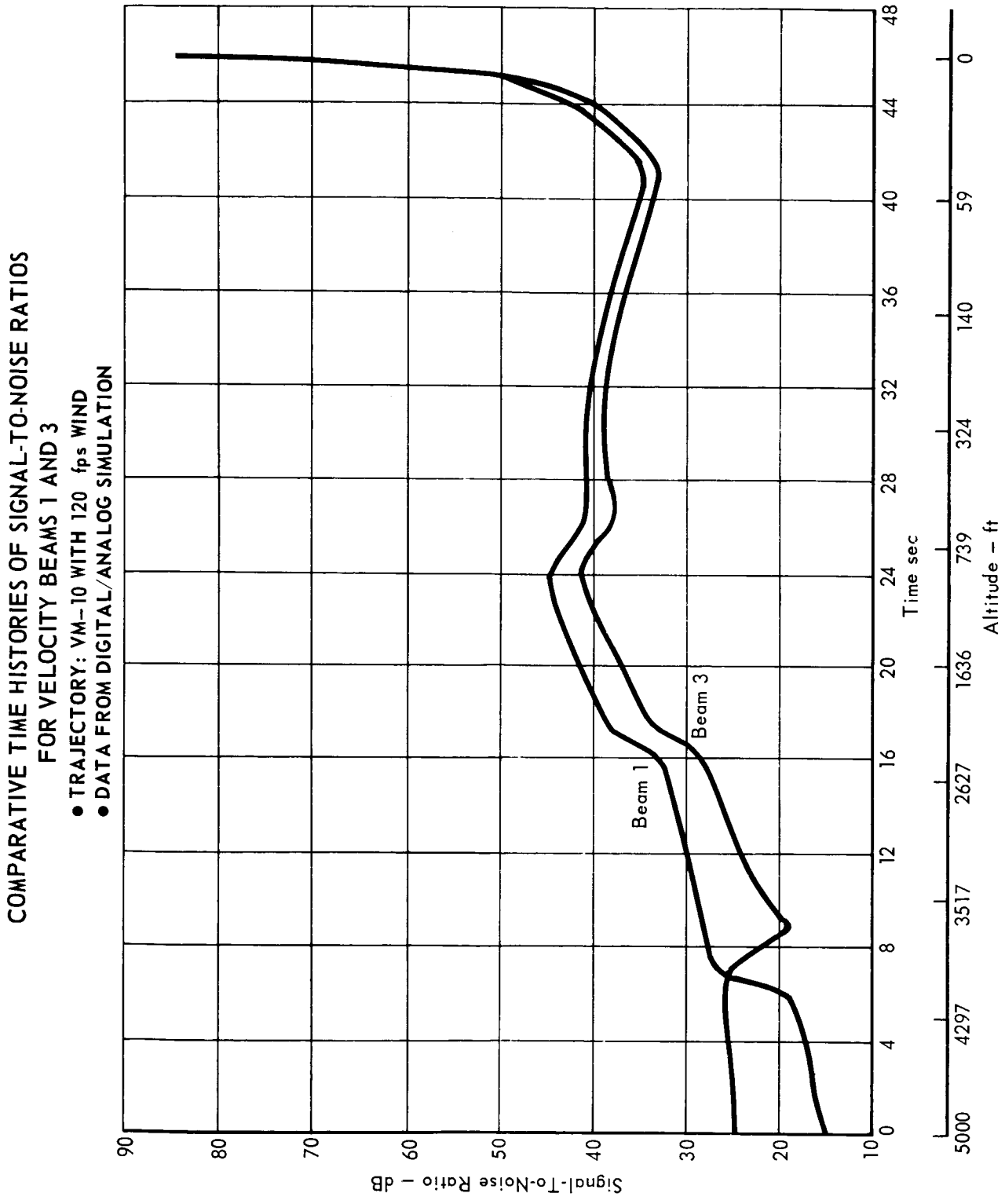
COMPARATIVE TIME HISTORIES OF SIGNAL-TO-NOISE RATIOS
FOR VELOCITY BEAMS 1 AND 3
• TRAJECTORY: VM-10 WITH 120 fps WIND
• DATA FROM DIGITAL/ANALOG SIMULATION
Signal-To-Noise Ratio – dB
90
80
70
60
50
40
30
20
10
Beam 1
Beam 3
0
4
8
12
16
20
24
28
32
36
40
44
48
Time sec
5000
4297
3517
2627
1636
739
0
59
140
324
Altitude – ft

Figure 5.9-30

frequency trackers. Examination of these figures shows that the signal-to-noise ratio on each beam is more than adequate for acquisition. The minimum initial signal-to-noise ratio occurs on velocity beam 1 and is about + 14 dB. The required value for acquisition is + 4 dB. The analog tracker simulation demonstrates that each beam is acquired during the first frequency sweep. Acquisition points are indicated on the figures.

It is noted that the signal-to-noise ratio on velocity beam 1 is below that of velocity beam 3 during the initial six second inertial hold period allowed for acquisition although both beams have equal 20 degree incident angles. This is true because the steady 120 fps horizontal wind tends to increase and decrease the doppler shifts on beams 3 and 1 respectively. The greater tracking frequency results in lower receiver noise. Figure 5.9-30 indicates the comparative signal-to-noise ratios on velocity beams 1 and 3. At about 7 sec the velocity beam 1 signal-to-noise ratio becomes greater than that for velocity beam 3. This is due to the velocity vector alignment maneuver which causes the beam 3 incident angle to be greater.

The improvement in signal-to-noise ratio on all beams is apparent from the figures when mode switching occurs at about time 16 sec. At this point the range beam signal bandwidth and signal frequency experience large changes due to the factor of five increase in the transmitter frequency deviation. The range beam tracker is designed to accommodate this sudden change in signal parameters by introducing an artificial frequency step into the tracker loop, and by providing a fixed time delay before switching to the narrow band tracking filter. The maximum range frequency tracking error occurs at 19.2 sec and is equal to 850 Hz (Figure 5.9-29). There is no danger of breaking lock at this point, since the range channel tracking filter bandwidth used was 3200 Hz, and the signal-to-noise ratio is 40 dB. Since the 850 Hz tracking error is the maximum experienced by the range channel frequency tracker, it is concluded that at no point will the range beam break lock.

A complete examination of the signal-to-noise ratios and frequency tracking errors for velocity beams 1 and 3 (Figures 5.9-24 through -27) shows that at no point will the velocity beams break lock. The maximum velocity beam tracking error occurs at 9.2 sec on beam 3 and is equal to -340 Hz. At this point the signal-to-noise ratio is about + 19 dB. The velocity beam tracking filter bandwidth used in this run was 1500 Hz (wideband mode).

Parameter Estimation Accuracy - Errors in the Landing Radar measured slant range and orthogonal velocity components are shown in Figure 5.9-31. These curves

LANDING RADAR RANGE AND VELOCITY ERRORS

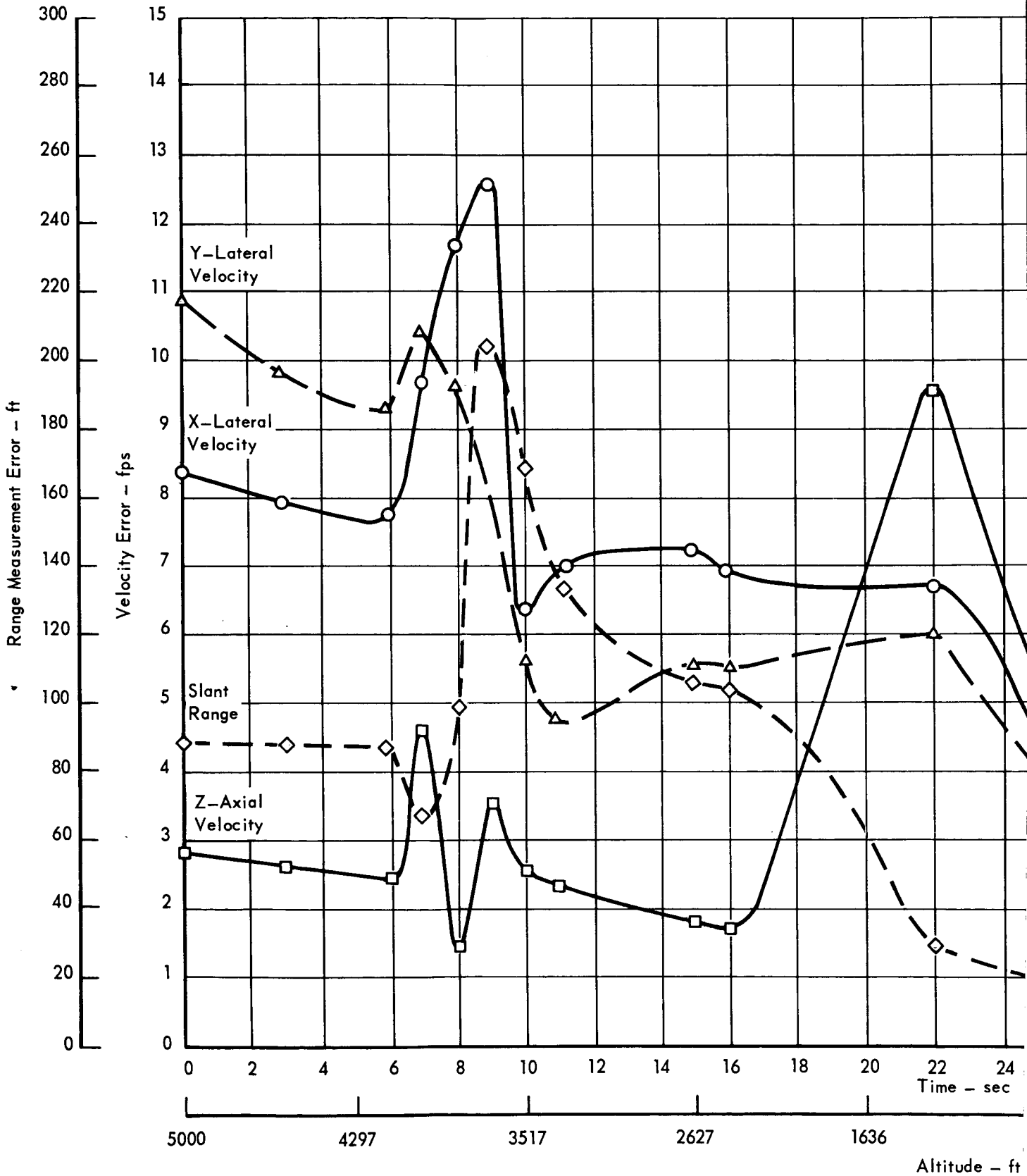

Figure 5.9–31

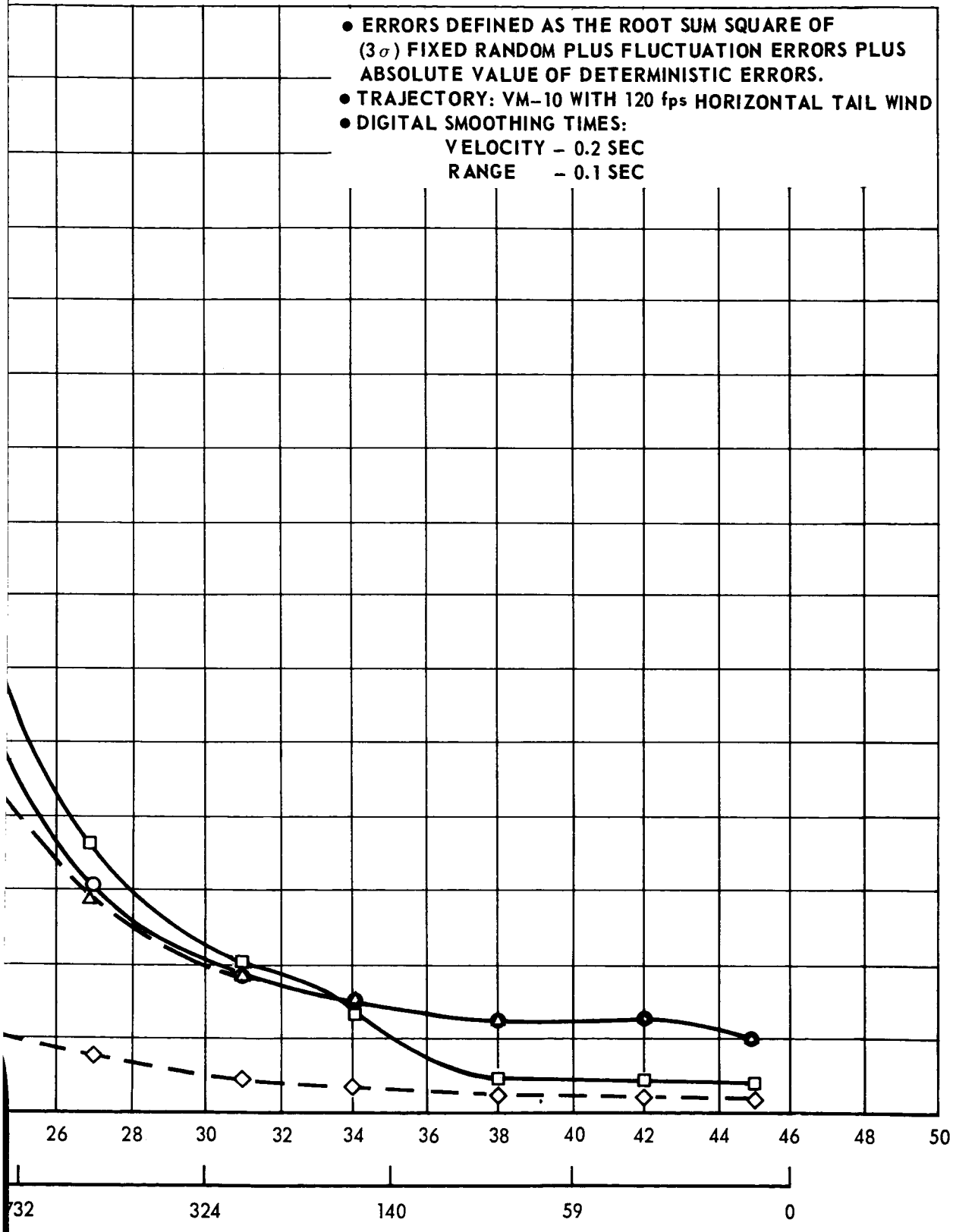
• ERRORS DEFINED AS THE ROOT SUM SQUARE OF (3σ) FIXED RANDOM PLUS FLUCTUATION ERRORS PLUS ABSOLUTE VALUE OF DETERMINISTIC ERRORS.
• TRAJECTORY: VM-10 WITH 120 fps HORIZONTAL TAIL WIND
• DIGITAL SMOOTHING TIMES:
VELOCITY - 0.2 SEC
RANGE - 0.1 SEC
26
28
30
32
34
36
38
40
42
44
46
48
50
732
324
140
59
0

5.9-65-2

are based on a complete Landing Radar, digital computer error analysis performed by the LM radar manufacturer. The net errors shown in Figure 5.9-31 reflect all error sources including: thermal noise, vibrational noise, fluctuations due to signal bandwidth, antenna boresight and alignment errors, parameter drifts, terrain bias, time lags, quantization errors, etc. The data is for a 0.2 second counting time on the digital landing radar velocity outputs. A 0.1 second counting time was used for the digital range outputs. The errors shown in Figures 5.9-31 are the computed root-sum-square of all fixed random errors (3σ) and fluctuating errors (3σ) plus the absolute value of the deterministic errors. From Figure 5.9-31 it is seen that the lateral velocity errors during the initial six second attitude hold mode are less than 11 fps. During this period the axial velocity error is less than 3 fps and the slant range measurement error less than 85 ft. During the velocity vector alignment maneuver (approximately 6 sec to 11 sec) the change in flight path angle (resulting in increased terrain bias, time lag errors, fluctuation errors, etc.) causes all errors to increase. Note that all errors, except the Y lateral velocity error, are maximum at the ninth second. At the ninth second the roll axis incident angle is maximum and equal to 40.3 degrees.

After completion of the velocity vector alignment maneuver all errors (excepting the axial velocity error) remain nearly constant until about 22 sec where the descent profile is intercepted. Thereafter all errors decrease; with velocity and range errors becoming less than 2 fps and 10 ft respectively, at 31 sec (altitude equal to 274 ft).

From these results it is concluded that the Landing Radar tracking error and signal-to-noise ratio performance is adequate. Additional parametric studies are planned to optimize the Landing Radar tracking capability. For example, on the basis of the data presented herein and other similar trajectory runs, it is believed that a more nearly matched condition will be obtained with velocity and range tracking filter bandwidths equal to 1000 Hz and 5000 Hz, respectively.

5.9.5.12 Sterilization - The LM radar has been reviewed relative to its ability to withstand sterilization procedures without degradation. The analysis considered all parts (less tilt control and transmitters) and weighted each part type according to the following criteria:

a. JPL Listing: ZPP-2010

The part type is considered a likely sterilization candidate as witnessed by inclusion in JPL Specification ZPP-2010-SPL-C, (1 December 1966), Electronic Part Sterilization Candidates for Spacecraft Applications.

b. Sterilization Capability Indicated

Specified part type operating or storage maximum temperatures exceed the temperature which will most likely be used in sterilization.

c. Sterilization Capability Questionable

No specification requirement or test exists which indicates that the part is capable of withstanding sterilization temperatures. This does not indicate that the part does not have sterilization capability, but only that no presently available data indicates appropriate thermal exposures. Hence, the part has been categorized questionable until further data can be acquired.

From the following sterilization capability summary it is seen that less than 2% (79 total parts) of the existing LM radar part population is in the questionable category with regard to sterilization capability:

Quantity and Part Type	Max Temp Range	JPL Listing ZPP 2010	Sterilization Capability Indicated	Sterilization Capability Questionable
861 Capacitors	85-175	765	92	4
2238 Resistors	150-195	1573	665	-
576 Diodes	100-200	27	532	20
534 Transistors	170-200	283	251	-
404 Integrated	150-175	368	36	-
77 Other Parts	85-125	14	8	55
		Totals for Above Parts		
4693		3030	1584	79
		Unlisted Parts		
(178)*				178
		Percentages		
4871 (100%)		62.20%	32.52%	*5.28%

* All 178 nonlisted parts (from the two-transmitters) have been placed in the questionable category for the present even though a majority are known to fall into the other two categories. These 178 parts are:

Velocity Frequency Multiplier	107
Range Frequency Multiplier	71
	178

Of these 79 parts, 36 appear to be devoid of sterilization degradation mechanisms and probably can be removed from the questionable category subsequent to testing without need for revision of part design. However, the following 5 part types (0.88% of total population) have recognized handicaps as indicated.

Part	Quantity	Reason and Resolution
1) Capacitor	3	Uses a low temperature sealant. Modify parts using a high temperature sealant.
2) FA2089 Diode matched pair	20	High temperature exposure may alter temperature compensation of some device pairs. Select by acceptance test performed after high temperature cycling.
3) Filter	2	Same as for Item I
4) XM-254 Isolator, RF Ferrite	2	High temperature may change characteristics of ferrite used. a) change type of ferrite used or b) select by acceptance testing after high temperature cycling
5) Coil, RF Shielded	16	Same as for Item 4

5.9.5.13 Thermal Effects - Thermal environment is most severe while operating during planetary entry and landing. Thermal control during non-operating launch and interplanetary cruise will be maintained by the Thermal Control Subsystem.

The thermal design of the Landing Radar is primarily concerned with survival during entry and terminal descent. Principal heat sources are:

- o Aerodynamic heating during entry.
- o Internal power dissipation.
- o Descent engine radiation.
- o Recirculation of hot gases from the descent engine.
- o Reradiation from the Martian surface due to descent engine surface plume impingement.

Effects such as solar radiation and planetary infrared heat loads are orders of magnitude less and need not be considered.

Choice of the VOYAGER preferred landing concept has done much to minimize radar heat rise. Use of differential drag separation, rather than fire-in-the-hole, removes any heating problem during separation. Engine ignition at the relatively low altitude of 5000 ft reduces the heat load from recirculating engine exhaust. Also the wide spacing of the terminal descent engines reduces base recirculation heating. Radiant heat flow is also low.

Exposure is most severe for the antenna and antenna mounted electronics. Insulation and predetermined heat flow blockage paths are employed to prevent the external, and rather severe heat loads from significantly heating the interior portions of the antenna. Since the internal power dissipation phase of the mission is a transient condition, the joulean heat produced is stored in an internal thermal heat sink. The heat sink is sized to the mass required to keep the internal temperature rise below safe limits.

The LM antenna was used as a model for investigating thermal survivability . With the relatively short descent time and the high external heat loads (relative to internal power dissipation), the first thermal effects appear to be slight distortions of the antenna due to the high temperature gradients between the antenna and antenna electronics. High antenna temperatures with high heating rates may result in sufficiently high temperature gradients to cause slight boresight shifts. A conservative maximum antenna temperature of 200°F is used for preliminary thermal analysis.

An antenna temperature profile for the LM antenna using a worst case soak temperature of 40°F at entry is given in Figure 5.9-32 for the estimated heat load of Figure 5.9-33. The abrupt rise in temperature near touchdown is due to engine radiant heat reflection off the Martian surface. Antenna surfaces are assumed to have an emissivity of 0.4. Antenna temperature at touchdown is below 200°F. The entry heating curve is conservative and does not consider placement of the radar altimeter antenna in front of the Landing Radar within the Aeroshell. This will provide additional insulation during entry. The terminal heating rate is due to descent engines and considers engine ignition at the termination of entry heating. In fact, a time lag will exist between Aeroshell release and engine ignition. Engine heating rate is for an engine separation of 50 inches and a duration of 150 seconds. Review of the trajectories for 5000 ft parachute release and engine ignition shows a maximum time to touchdown of 46 seconds. Start temperature at entry is expected to fall between -150°F and +40°F.

Under very conservative estimates the present LM antenna and, therefore, LM electronics would servive all mission phases. It is felt that while additional thermal control is not difficult it is not necessary. It is anticipated that the new antenna thermal design will follow that of the existing LM antenna with sufficient protection for both antenna and electronics.

5.9.5.14 Test - The Landing Radar self test capability is discussed in more detail.

Sterilization subjects the equipment to a difficult environment. Unfortunately, access to the equipment after sterilization will be limited to an umbilical connector and TCM. Post sterilization performance will be a launch contingency and therefore, it becomes important that pre-launch checkout give an accurate evaluation of subsystem performance without violation of sterilization.

It is the post sterilization checkout requirements along with in flight checkout requirements that dictate Landing Radar built-in test design. End-to-end test requiring a simulated input is considered simplest and most complete.

Monitoring would be largely by TM with use of the umbilical connector reserved for control and monitoring of critical items. Waveguide coupled, transmitter power monitors will be used. RF absorbent material in front of the antenna will approximate a free space environment.

TIME-TEMPERATURE HISTORY OF ANTENNA ARRAY

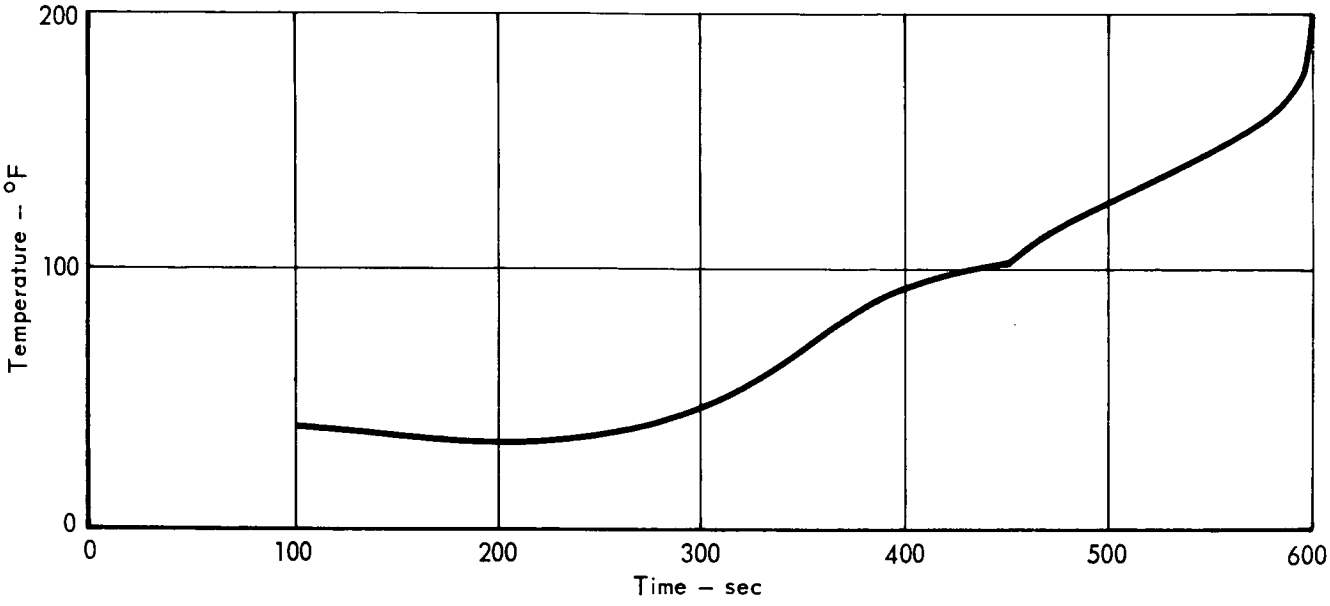

Figure 5.9–32

TYPICAL HEATING RATE HISTORY ON LANDING RADAR ANTENNA DURING ENTRY AND TERMINAL DESCENT

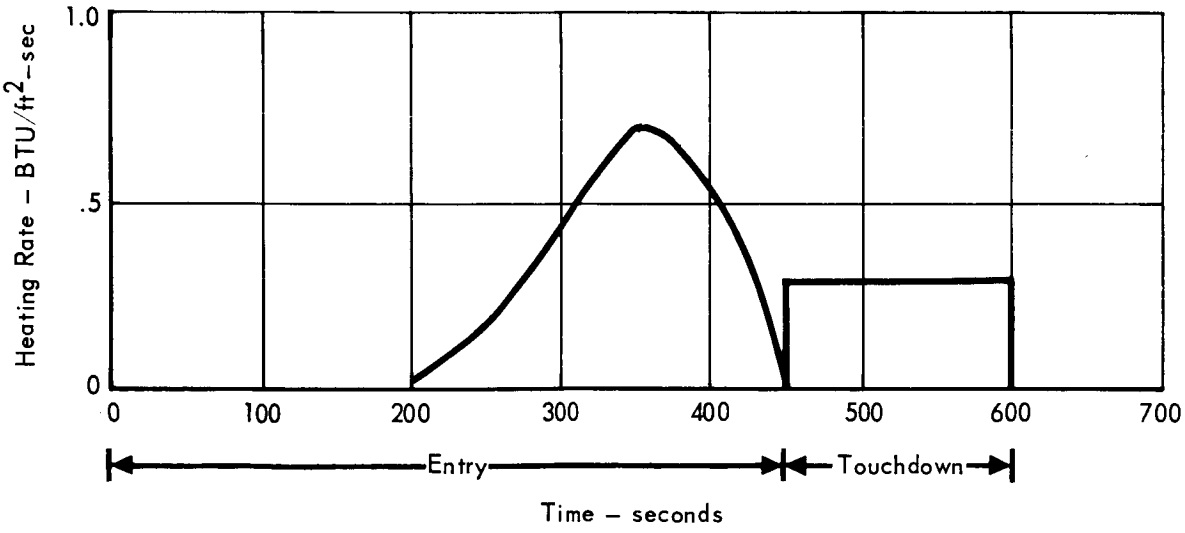

Figure 5.9–33

Test stimuli injection were considered at the RF level into the antenna, at the RF level into the mixers and at the IF level into the preamplifiers. IF signal generation is undoubtedly simplest (with the homodyne receiver the frequency of the test signal would range from approximately 100Hz to 30KHz). The major drawback is that performance of the mixers is not evaluated. Sterilization survival of the mixer crystals at this point should not be assumed. Alternate methods of evaluating mixer performance, such as noise measurement, are inadequate. The IF injection is therefore, rejected in favor of an RF test signal with mixer checkout.

RF signal injection into the antenna would require an antenna coupler and either a source external to the Landing Radar or interconnection from the Landing Radar to the antenna coupler. A source external to the Landing Radar operating as a transponder would be required for complete checkout of the Landing Radar. It must sense Landing Radar transmitter frequency and return a frequency shifted target. This complexity should only be considered in a part of the ground equipment. A cable from the Landing Radar out to an antenna coupler (which must be attached to the Aeroshell) is undesirable, also. The antenna itself is devoid of sterilization failure mechanisms. Injection of a simulated signal into the antenna would be little more than a form of continuity check and has little to offer. Conventional antenna checks of pattern, boresight, etc. are impossible due to its placement within the canister and Capsule.

This leaves two major pre-launch candidates. Signal injection from ground OSE via cable, or signal generation within the Landing Radar via directional couplers. The former is lighter and allows more checkout versatility. Use of a cable from an antenna or waveguide coupler to ground OSE (through the Sterilization Canister) involves certain implementation unknowns. This concept will be given further study. The alternative is to use voltage controlled oscillators (VCO), mixed with a sample of the velocity and range transmitter outputs with the resultant signal injected after the antenna but before the mixers. The present concept calls for the use of single sideband generators (SSBG), but a simple amplitude modulation of the transmitter by the VCO might be acceptable. A single RF signal for velocity simulation would serve to checkout all velocity mixers and requires only one SSBG (one would also be required for the range channel). However, it would result in only a roll axis component of velocity. Use of a single RF signal for mixer checkout, coupled with IF

injection for velocity data conversion checkout, is an attractive compromise. Three VCOs would suffice; one for the range channel and two for the velocity channels. VCO #1 would be supplied to channels one and three, and VCO #2 to channels two and four. The VCOs would be controlled via hardline from ground OSE. This would allow complete checkout of all channels with some variety of simulated profile.

Removal of hardline control would leave the VCO self test oscillator at a pre-programmed frequency (several could be used) for in-flight checkout, and would only require an enable from the test programmer to initiate the self test cycle.

Weight increase for the built-in test has not been estimated and is only partially included in system weight figures.

5.9.6 Altimeter Requirements, Alternatives and Selection of a Preferred Design

Selection of a preferred altimeter design was accomplished by:

a. Examining the major constraints placed on subsystem operation
b. Determining the functional performance range and accuracy which satisfied dependent subsystems requirements
c. Evaluating the various alternatives
d. Selecting a design providing the best functional performance, considering all constraints

5.9.6.1 Major Constraints - Figure 5.9-34 provides a list of the major constraints applicable to an altimeter design, and the design approach selected. Hemispherical antenna coverage was selected when it was determined that roll stabilization for the purpose of antenna pointing required excessive weight, power and complexity. Suppression of electrical breakdown by using insulation to eliminate high voltage contact with the atmosphere became mandatory after low power CW systems proved to be unsuitable for high altitude altimetry. Operation during the plasma blackout period was required only for improved Entry Science data correlation. A decision was made to accept the small degradation in Entry Science atmospheric data if a blackout period occurred. Operating with the same altimeter, using a secondary antenna after Aeroshell release eliminated the added weight and complexity of a second altimeter.

5.9.6.2 Functional Performance Range and Accuracy Requirements - Aerodynamic decelerator deployment, Aeroshell release and terminal propulsion engine start depend on an accurate measurement of altitude. Uncertainties in the Martian atmospheric model eliminate all triggering methods such as time from peak deceleration, static pressure, calculated velocities, etc. due to the wide

MAJOR ALTIMETER CONSTRAINTS

CONSTRAINT	DESIGN APPROACH
1. Perform required functions on a vehicle that does not provide preferred roll orientation (rate damping only).	Provide coverage which does not depend on stabilized attitude – hemispherical antenna pattern.
2. Perform required functions in atmospheres and pressures which cause electrical breakdown.	Provide a subsystem design which protects high voltage gradients from partial pressures.
3. Operate reliably behind an Aeroshell.	Design Aeroshell to provide a Dielectric window for R.F. transmission.
4. Operate during periods where plasma generation may produce severe electromagnetic radiation attenuation.	Accept period of blackout, operate during period to obtain plasma data and altitude data when plasma generation ceases.
5. Operate after Aeroshell is released.	Use secondary antenna, and near return blanking which rejects Aeroshell as a target.

Figure 5.9–34

altitude interval in which these triggers could occur. Radar altimetry was selected to provide the primary means of initiating altitude dependent functions. Maximum altitude for descent function sequencing was selected to be 100,000 ft for Landing Radar turn-on.

Accuracy of entry science atmospheric measurements depends on accurate altitude measurement during descent. Improvement in entry science data accuracy by measuring altitudes higher than 100,000 ft appeared desirable if size, weight and power requirements were not excessive. An estimation of atmospheric data for altitudes higher than actually measured by the altimeter is possible by using iterative extrapolation. The accuracy of this estimated data will be influenced by the highest altitude measured and the accuracy of the measurement. The selection of the altitude, and altimeter accuracy to provide best overall science data with minimum power and weight was aided by a computer study. The computer program simulated the altimeter altitude data beginning at altitudes of 100, 200, 300 and 500 thousand feet, with 1% and 3% accuracy. Results of these runs can be seen in Figures 5.9-35 and 5.9-36. Figure 5.9-35 shows the error in estimating altitudes above the highest measured altitude. The accuracy of these estimations depend equally on highest altitude measured and altimeter accuracy. Figure 5.9-36 shows the error in estimating atmospheric density above the highest altitude measured. From this curve it can be seen that, for iterative extrapolation of density, an accurate altitude measurement at a lower altitude is more desirable than an inaccurate measurement at high altitude.

A 200,000 ft maximum altitude, and an accuracy of 1% $\pm$400 ft for long ranges and 1% $\pm$25 ft for short ranges is a requirement for the altimeter, to provide good entry science data. The next highest altitude where altitude measurements can be made reliably is at 500,000 ft, above the blackout region. Operation at this altitude will require up to 12 times more transmitter primary power than operation at 200,000 ft. Operation higher than 200,000 ft was rejected due to the small improvement in science data accuracy for a large increase in input power.

Minimum altitude of operation was set at 50 ft. This allows the altimeter to be used as a functional backup to the Landing Radar during terminal descent.

5.9.6.3 Evaluation of Alternatives - Selection of the best modulation technique from the four available (Pulse, CW, Interrupted CW and PN-Code), and selection of an optimum operating frequency is influenced by the factors shown in Figure 5.9-37. Selection of an altimeter antenna to fulfill the coverage constraint listed in

ALTITUDE ESTIMATION ACCURACY ($3\sigma_{HE}$) AS A FUNCTION OF ALTIMETER ACCURACY ($3\sigma_H$), AND DISTANCE OF FIRST ALTITUDE MEASUREMENT

(VM-3 ATMOSPHERE)

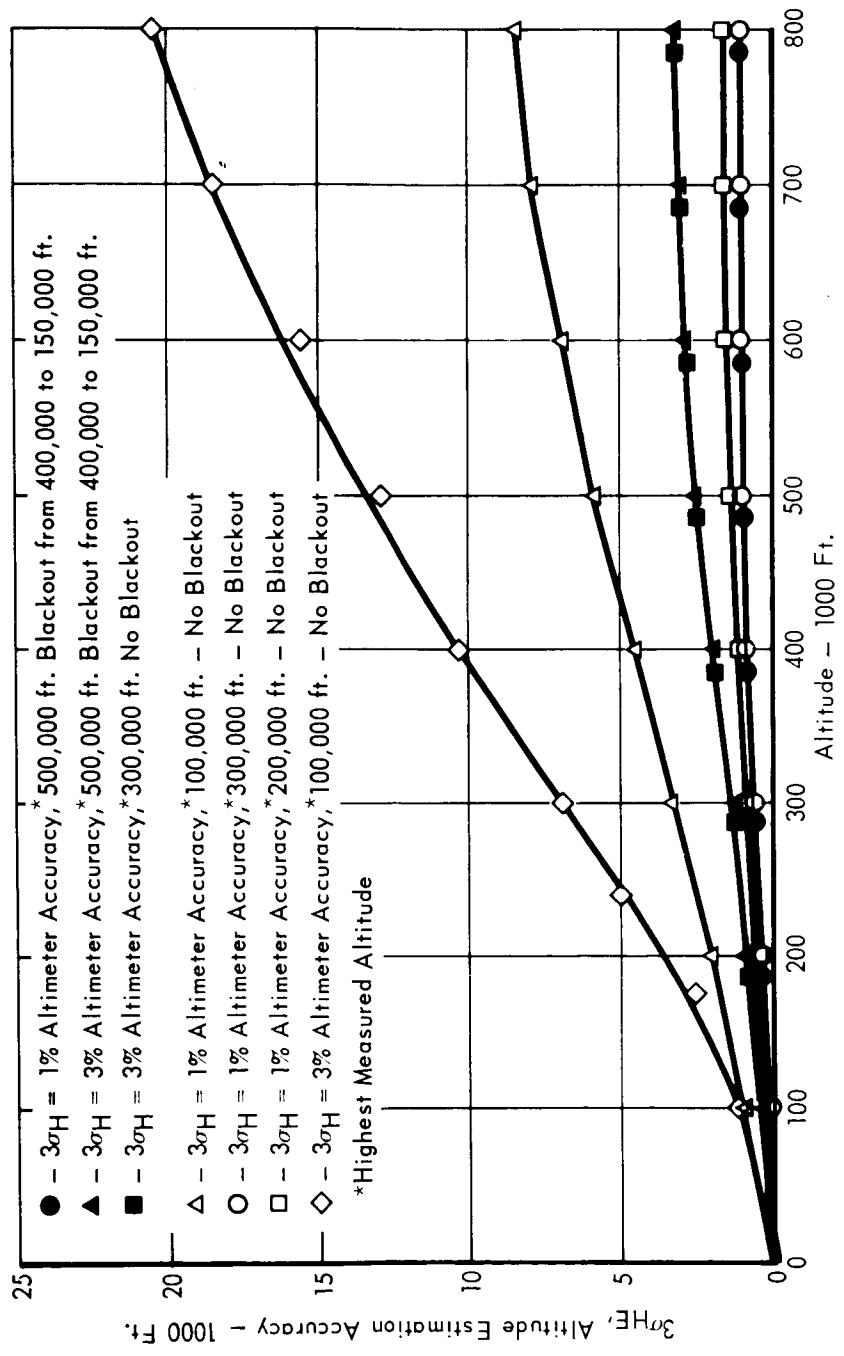

Figure 5.9–35

ATMOSPHERIC DENSITY ESTIMATION ACCURACY ($3\sigma_\rho/\rho$) AS A FUNCTION OF ALTIMETER ACCURACY ($3\sigma_H$) AND DISTANCE OF FIRST ALTITUDE MEASUREMENT

(VM-3 ATMOSPHERE)

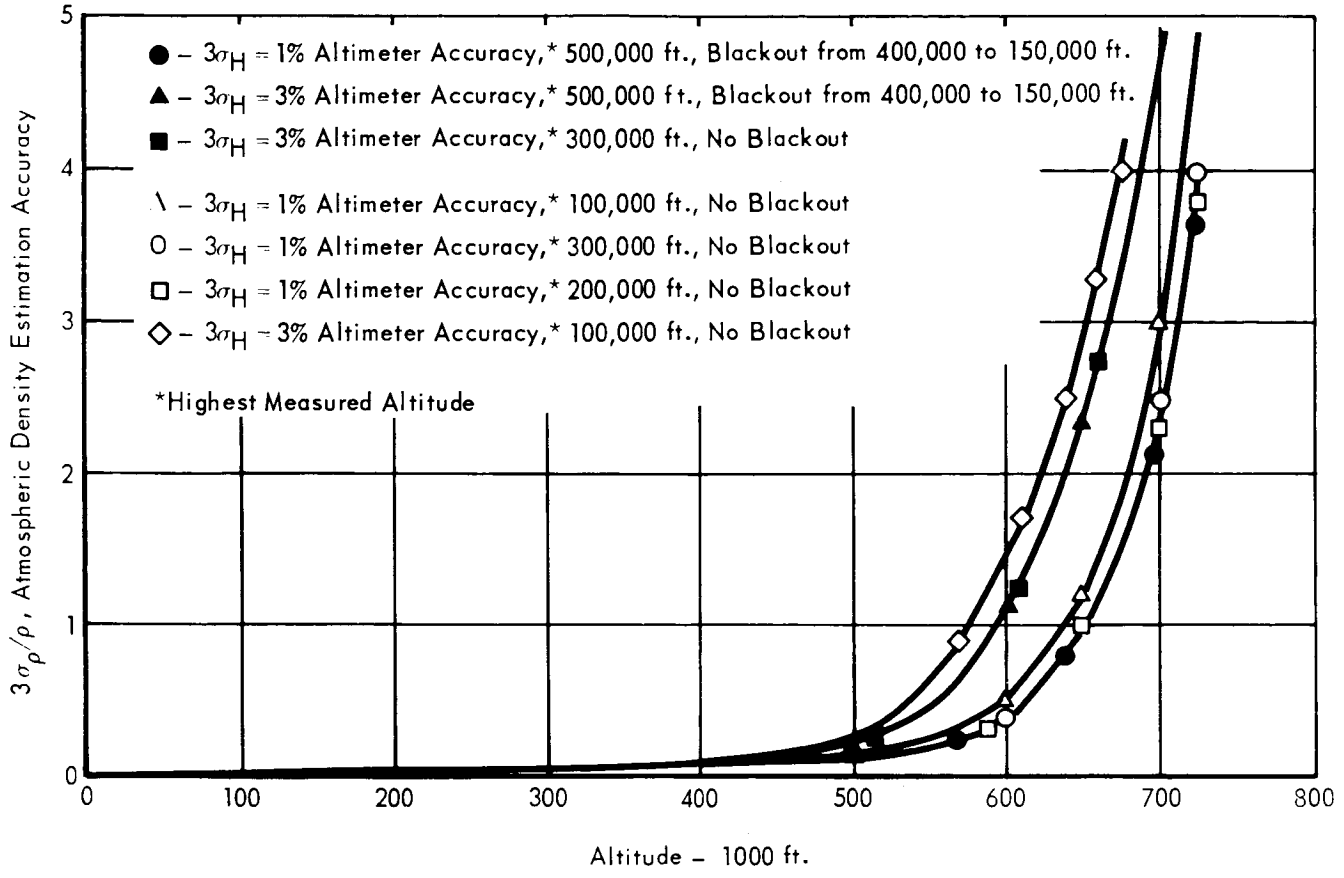

Figure 5.9-36

FACTORS AFFECTING FREQUENCY AND MODULATION SELECTION

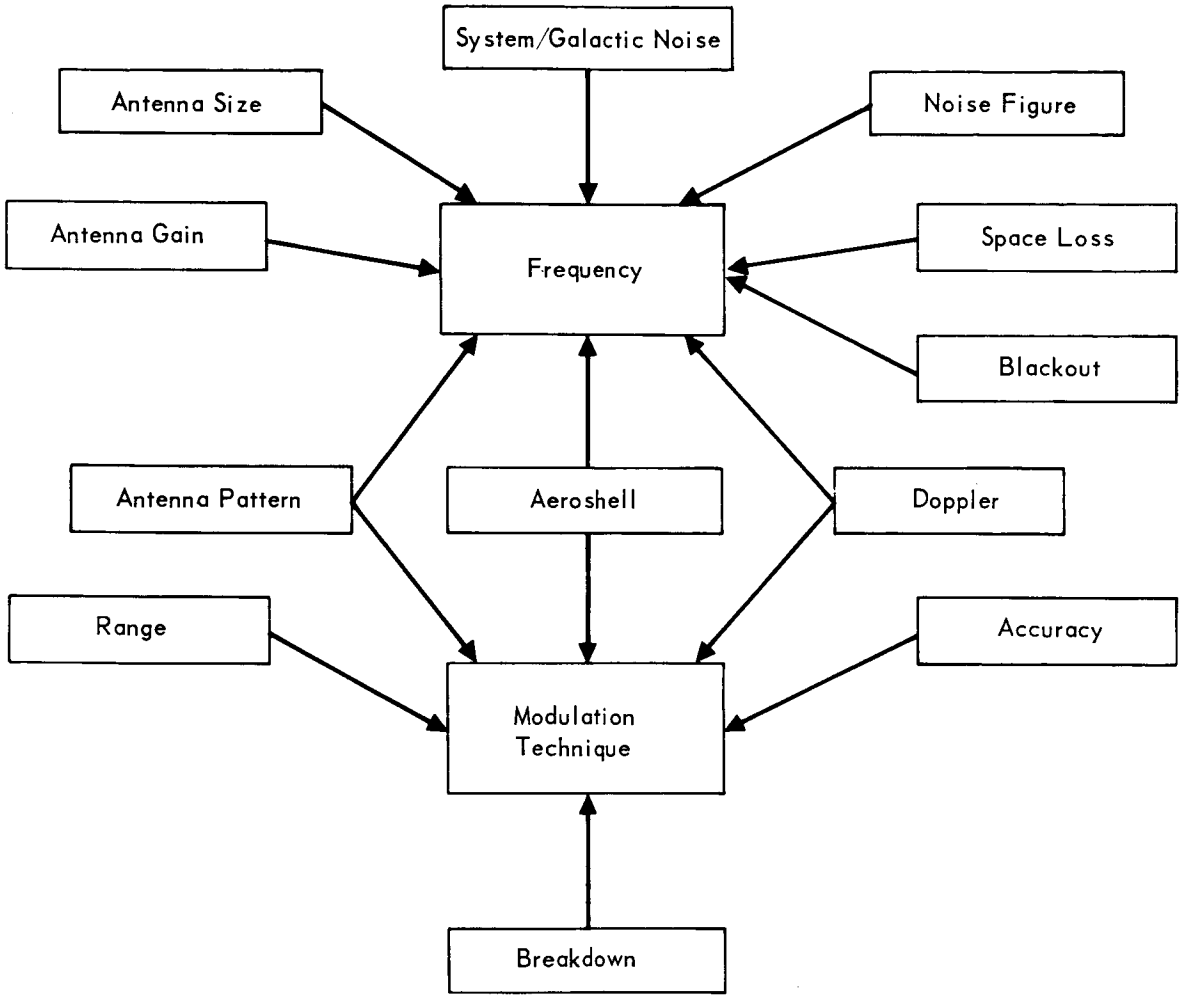

Figure 5.9–37

Figure 5.9-34 will have the greatest effect in influencing frequency and modulation selection. Selection of the preferred antenna design must be made prior to frequency or modulation selection.

- o Antenna Alternatives - Antennas which were considered for providing the required hemispherical coverage include:

a. Steered pencil beams

b. Switched fan beams

c. Single element radiators which provide an approximation to hemispherical coverage.

Steered beams were rejected because of volume and weight considerations with mechanical steering, and because of complexity, reliability and the excessive weight required to provide hemispherical coverage with an electronically scanned antenna. Lack of development and space qualified equipment make electronically scanned antennas unattractive. Switched fan beams were also rejected because of weight complexity and reliability reasons.

A conical monopole radiating element, backed by a ground plane, was selected because of its simplicity, reliability and the good approximation to hemispherical coverage it provided. The conical element allows Entry Science stagnation point temperature and pressure transducer installation in the nose cap with no interference to the antenna radiation pattern. Use of the Aeroshell as a low-frequency asymmetrical dipole radiator was rejected because of the difficulty in Aeroshell design, antenna matching, installation and checkout.

- o Frequency Alternatives - Frequency-dependent factors from Figure 5.9-37 and their relative effect on return signal-to-noise ratio in the radar range equation

$$S/N = \frac{P_{Pk}\, G^2\, \lambda^2\, \sigma o\, (AREA)}{(4\pi)^3\, h^4\, L\, KT\, B\, N_f} \qquad (1)$$

are shown in Figure 5.9-38. From this figure it is apparent that the frequency range from 10 to 500 MHz provides the best signal-to-noise (S/N) ratio for an altimeter using low gain dipole-type radiation patterns. However, selection of the conical monopole which best fits the nose cap dimensions and also provides the best approximation to hemispherical coverage, requires the frequency to be 1 GHz or higher. By selecting 1 GHz for the altimeter, rather than the optimum 500 MHz, 4 times more transmitter power was required. The increase from about 2.5 watts to 10 watts of input power to the transmitter was considered an acceptable trade for a compatible design.

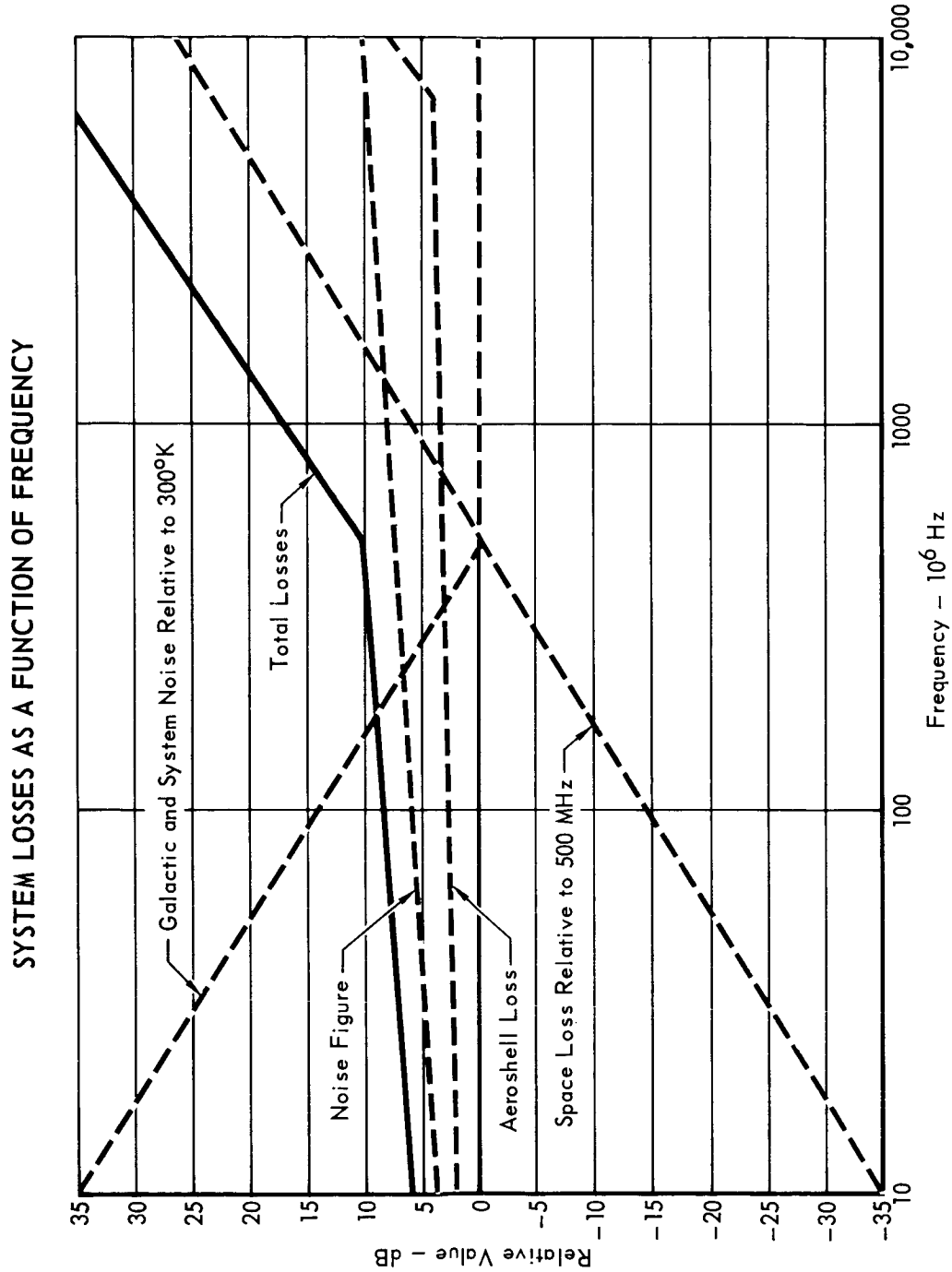
SYSTEM LOSSES AS A FUNCTION OF FREQUENCY
Galactic and System Noise Relative to 300°K
Total Losses
Noise Figure
Aeroshell Loss
Space Loss Relative to 500 MHz
Relative Value – dB
35
30
25
20
15
10
5
0
-5
-10
-15
-20
-25
-30
-35
10
100
1000
10,000
Frequency – 10^6 Hz

Figure 5.9–38

- Modulation Alternatives - Continuous wave (CW), Interrupted CW, Pseudo-noise Code, and standard Short Pulse modulation techniques were considered for the altimeter. Conventional CW systems which require two antennas are obviously incompatible with the hemispherical coverage requirement unless undesirably complex switching schemes are used. A modified CW system which uses Bessel sideband, or zero IF techniques for information processing might be developed for use with a single, omni-directional coverage antenna. Operation to 200,000 ft with these systems, and obtaining accuracies better than 3% will be very difficult to achieve due to the high noise level caused by transmitter to receiver leakage and Aeroshell reflections. Accuracy will be severely degraded due to the extensive spectrum spreading of the returned signal, caused by extensive ground illumination. Aeroshell discrimination after separation will be difficult to achieve.

  Interrupted CW (ICW) techniques reduce the transmitter to receiver leakage problem and allow greater dynamic range. This is done by alternate operation of the transmitter and receiver, to position the return signal energy between the transmitter pulses. Two-way altitude delay determines the pulse repetition frequency (PRF), which is inversely proportional to altitude. Return signal rise and fall time distortions prevent accurate positioning of the returned signal, which reduces accuracy. Obtaining 1% to 3% accuracy appears difficult to achieve. Ambiguity in altitude will also exist at multiples of the PRF, requiring ambiguity resolution. Using ambiguity resolution and a high PRF will improve accuracy, but greatly increases the system complexity. High transmitter average power required for operation at 200,000 feet makes this system undesirable. Aeroshell discrimination after separation will be difficult to achieve.

  A pseudo-noise code correlation altimeter using a two-frequency, frequency shift keyed (FSK) program and a stored correlation program to determine delay time (and hence altitude) could also be used. This system suffers from complexity and long acquisition times because of combined doppler and range uncertainty. Large area illumination, transmitter to receiver leakage and Aeroshell reflections reduce accuracy.

The least complex and most-used technique for high altitude altimetry is short pulse modulation. Accuracy better than 1% is typical of most systems. Pulse-width limiting allows this system to be most compatible with hemispherical antenna coverage. Two disadvantages are high peak transmitter power, which may cause electrical breakdown, and limited low altitude operation due to the pulse length. Modifications must be made to prevent breakdown in partial-pressures expected in the Martian atmosphere. Pulse-width switching circuits have been developed which allow operation down to lower altitudes. Normal receiver blanking during transmitter operation, and range gate tracking allows this modulation technique to effectively discriminate between the Aeroshell and ground returns. It is the best technique for rejecting the Aeroshell as a target.

Figure 5.9-39 shows the various modulation techniques investigated and also assigns a relative rating from 1 to 4 based on the following:

1. Unusable, severe problem exists and no solution is readily apparent.
2. Not adequate, has problem but solution is available.
3. Adequate, no problems.
4. Exceeds requirements, superior concept or only choice.

The total ratings are listed at the bottom of each column. Simple pulse modulation, with a total score of 31, rated highest. It best fulfills the requirements for the VOYAGER Radar Altimeter. Pseudo-Noise Code is second at 25, and ICW is a close third at 24. The Pseudo-Random Code and ICW systems are about equal as a second choice of modulation.

5.9.6.4 Selection of a Preferred Altimeter - A short pulse (non-coherent) altimeter using a conical monopole primary antenna and a dipole secondary antenna is selected as the concept which performs the required functions best. Section C.10.1 provides a detailed functional description of the design. A considerable amount of previous experience and development effort has been performed on this type of altimeter. The altimeter used on the Saturn Launch Vehicle and an improved version using microminiaturized circuit techniques (Ref. 5.9 -3), built under NASA study contracts, use short pulse modulation and L-Band transmitter frequencies for high altitude operation. Another altimeter for space applications which uses short pulse modulation techniques at X-Band was developed during Phase IV of the referenced NASA study. This altimeter has the capability

MODULATION TECHNIQUE RATING

MODULATION TYPE / SELECTION FACTORS	SIMPLE PULSE, WITH PULSE WIDTH SWITCHING	FM/CW, ZERO IF	FM/CW BESSEL SIDEBAND	ICW HIGH-PRF WITH AMBIGUITY RESOLUTION	FSK PSEUDO-RANDOM CODE (CORRELATION)
Omnidirectional Antenna Coverage Constraint	3	Reduced accuracy, increased TX/RX coupling, decreased maximum range. 1	Reduced accuracy, increased TX/RX coupling and system noise reduces dynamic range. 1	Degrades risetime, reduces accuracy. 2	3
Accuracy	Best accuracy if pulse width switch used. 4	Ranging, step error, return noise, leakage noise. 2	Phase linearity, phase distortion of ground return. 2	3	3
Maximum/Minimum Altitude	Breakdown susceptible, pulse-width switching required. 2	TX/RX isolation limits dynamic range. 2	TX/RX isolation limits dynamic range. 2	System isolation, PRF servoing. 2	Correlation delay, system isolation. 2
High Voltage Breakdown	Most susceptible, design must overcome. 2	3	3	3	3
Complexity/ Reliability	3	3	Complexity in signal processing. 2	Complexity in waveform generation, tracking and ambiguity. 2	Complexity in correlation generator and correlation tracker. 2
Operation through Aeroshell and after Aeroshell Release	Natural Aeroshell discrimination. 4	Severe reflection, vibration, no discrimination of Aeroshell. 1	Severe reflection, vibration, no discrimination of Aeroshell. 1	3	Reflection will cause system noise. 2
Ambiguity Resolution	3	3	3	Special modulation circuitry. 2	3
Weight	3	3	3	3	3
Previous Use and Development Risk	All techniques and concepts previously used. Much development done. 4	No previous use as a high altitude altimeter. 2	No previous use as a high altitude altimeter. 2	Proposed for high altitude system, but not used. 2	Previously proposed by GE for Apollo, but not used. 2
Input Power	3	Inefficient transmitter, high duty cycle. 2	Inefficient transmitter, high duty cycle. 2	Inefficient transmitter, high duty cycle. 2	Inefficient transmitter, high duty cycle. 2
Total Rating	31	22	21	24	25

Figure 5.9–39

to operate down to about 30 feet by the use of pulse-width switching.

5.9.6.5 Summary of Recommended Altimeters - Technical information on altimeter concepts was solicited from 6 vendors. Responses to the request for information, for an altimeter capable of providing hemispherical coverage are tabulated in Figure 5.9-40. From the tabulation it is apparent that pulse modulation is favored.

5.9.7 Altimeter Performance - The following analysis will show the Radar Altimeter detection/acquisition capability, estimated accuracy, and the degradations caused by the constraints shown in Figure 5.9-34.

5.9.7.1 Detection and Acquisition - A complete tabulation of parameters applicable to the selected altimeter design are given in Figure 5.9-41. To achieve the single-sweep .95 detection probability (Pd) at 200,000 feet and the one hour false alarm time (Tfa) specified, a signal to noise ratio (S/N) of 15 dB will be required. (Ref. 5.9-4) An additional 11 dB improvement is required for the Swerling Case 2 fluctuations expected from the surface target, requiring a total integrated S/N ratio of 26 dB. Integrating 25 pulses will provide 23 dB S/N improvement, which allows a single pulse S/N of 3 dB to be adequate for maximum range detection. Substituting the applicable values from Figure 5.9-41 and a conservative value of -10 dB for the backscattering coefficient per unit surface area (σ_o) in the radar equation:

$$S/N = \frac{P_{pk} G^2 \lambda^2 \sigma_o \pi (hc\tau)}{(4\pi)^3 h^4 L KT B N_f}$$

shows that a peak power of 500 watts provides the required 3 dB S/N at 200,000 feet. Average power is determined from $Pav = (\tau \cdot F_R \cdot P_{pk})$, = 2.5 watts.

Maximum acquisition time will be set by Ti, the time required to sweep a 5μ sec. range gate from 220,000 to 20,000 feet, while integrating 25 pulses at each position.

$$T_{aq} = (T_i)(N_i) / (f_R)(\tau) = 2 \text{ sec.}$$

This two second acquisition time will be sufficient for both the high altitude and low altitude modes of operation. An auxiliary gate will be set at 250,000 feet to enable early detection if returned signal power is greater than anticipated due to a greater σ_o. If the maximum altitude rate of 4,000 ft/sec occurs during the time the vehicle is at 220,000 feet and acquisition sweeps are made at 216,000 ft, 208,000 ft, and 200,000 ft., the cumulative probability of detection at the end of the 200,000 foot sweep is .9985.

RADAR ALTIMETER EVALUATION (NO REDUNDANCY OR SECONDARY ANTENNA)

CRITERIA	WEC	RYAN	SPERRY	STEWART-WARNER	HONEYWELL	TEXAS INST.
1. Size	5.20" x 4.75" x 9.75"	6.4" x 7.4" x 10.6"	12" x 8" x 6"	6" x 7" x 8.5"	6" x 4" x 8.5"	6.5" x 6.5" x 6.1" 6.1 In.
2. Weight	11 Lb.	11.6 Lb.	13 Lb.	10 Lb.	10 Lb.	6.959 Lb.
3. Power	25 Watts	34.3 Watts	39 Watts	25 Watts	35 Watts	14.64 Watts
4. Performance						
a) Range Accuracy (3σ)	±200 Ft. or ±0.3%	±200	±200 or ±1%	±50 Ft. or ±.025%	±100 Ft. or ±.0.5%	1%
b) Rate Accuracy (3σ)	±20 FPS or ±5%	±40 FPS or ±5%	±5%	±5%	±5%	
c) Mark Generation	Range Bit Comparison	Range Bit Comparison	And Gate W/Slow Count	Available Any Bit		
d) Altitude, Ft.	300K	300K	50K	Wrong Calculations Used	50K	50K
5. System Concept						
a) Transmitter	Triode/Stripline	Triode/Stripline	Magnetron	Jan 7815 Planar Triode	Cavity/Triode	MERA RFBB
b) Modulator	Pulse – 15 μ sec	Pulse – 1 μ sec	Pulse – 0.8 μ sec	Pulse – 0.75 μ sec	Pulse – 1 μ sec	Pulse – 2–4 μ sec
c) Tracker	Centroid-Digital	L.E. (Shaper)	L.E.	L.E., "Synthetic Pulse"	L.E., 10% Ampl.	L.E. Type I Loop
d) AGC	Digital	Analog	Analog-Noise Gate			
e) False Alarm Time	1 Hour	60 Hours	1 Hour			
f) Pd	99%	99%	99%		99%	
g) Frequency	1 KMH_z	225 MH_z	4.2 GHz	260 MHZ	4.3 GH_z	
6. Self-Test	Delayed Attenuated Transmitter Signal	Synthetic IF, Mark Check, Reliable Operation			Delayed, Gated Local Oscillator	Each MERA Block Tested Individually
7. Short Range	30-40 Feet (Adds 2 Lb., 75 $In.^3$, 8w)	Use Alternate System		Minimum of 100 Ft.	Dual Antenna Switched, 10 Ft.	
8. Mechanical Design	Multifunction Integrated Circuits, Thin Film and Modules	Integrated Circuits and Modules			Hybrid Integrated Circuits Thick Film and Modules	MERA Blocks, Plus Electronics
9. Sterilizability	Component Selection and Design Adequate	Previous Work and Component Selection	"Can Meet"	"Will Confirm"	Components to 150°C, Design to Meet	All Solid-State or I.C.
10. Environment and Storage	(Previous Space Experience)	Covered Shock, Vibration (Previous Spacework)	"Can Meet"	"Will Confirm"	"As Specified"	
11. Reliability	Calculated .9999 Probability of Success	600 Parts, 9×10^3hr MTBF		5066 Hr. MTBF	.999936 Prob. of 10-Min. Operation	
12. Development Risk	Similar System is in Prototype State	Modify Saturn Altimeter	Develop New System with Proven Subsystem	New System	Modified Aircraft System	New Concept, Not Space-Qualified

Figure 5.9-40

RADAR ALTIMETER FUNCTIONAL CHARACTERISTICS

CHARACTERISTIC	SYMBOL	VALUE
Frequency	f	1 GHz
Wavelength	λ	1 foot
Transmitter Repetition Frequency	f_R	10^3 Hz
Pulse Width	τ	5×10^{-6} seconds (Long Range) 1×10^{-7} seconds (Short Range)
Peak Transmitter Power	P_{pk}	500 watts (27 dBw)
Pulses Integrated (for acquisition)	N_i	25 – Long Range Mode 5 – Short Range Mode
Acquisition Sweep Time	T_{aq}	2 seconds
I.F. Bandwidth	B	2×10^5 Hz – Long Range 1×10^7 Hz – Short Range
Single Pulse Signal to Noise Ratio	S/N	3 db – Long Range Mode 27 db – Short Range Mode
Probability of Detection (Single-Sweep)	P_d	.95 – Long Range .99 – Short Range
False Alarm Time	T_{fa}	1 hour
System Noise Figure	N_f	6 db
System Losses (including Aeroshell)	L	9 db
System Noise Power	KT	4.14×10^{-21} watt-seconds (–204 dBw) (assumes 300°K system temperature)
Antenna Gain	G	1 (0 db) Long Range 1.59 (2 db) Short Range

Figure 5.9-41

At 23,500 feet, the altimeter updates the sequencer to allow aerodynamic decelerator deployment. Aeroshell release occurs 12 sec later, at approximately 18,000 feet. One second prior to and until 4 seconds after Aeroshell release the altimeter modulator will be held off. Reacquisition will commence with the pulse width still at 5 microseconds. This allows the altimeter to disregard the early return from the Aeroshell because the receiver is blanked for 5 microseconds (during the transmitter on time) providing 2,500 foot discrimination distance. Integrated signal-to-noise has increased to 56 dB at 20,000 feet which provides a .999 or better probability of detection on the first sweep. At 5,000 feet, after the final marking function has been satisfied, an internal mark will switch the pulse width (and bandwidth) to 0.1 μ sec (and 10 MH_z) to allow improved resolution and accuracy. The signal to noise ratio at 5,000 feet, using a 0.1 μ sec pulse width, is about 41 dB* which provides a .999 or better probability of detection. This assures reacquisition within two seconds if tracking should be lost during pulse width switching.

5.9.8.2 Altimeter Accuracy - Basic error sources are caused by:

a. Thermal noise
b. Quantization
c. Deceleration lag
d. Ground return fluctuations
e. Insufficient near-surface illumination

Two different tracking loops will be analyzed to give an indication of the magnitude of the errors.

For the digital tracking loop similar to that in Reference 5.9.6, the total RMS error resulting from receiver noise, ground fluctuations, and quantization is given by:

$$U_R = \left(\frac{\tau}{4\sqrt{S/N}} \sqrt{B_n} f_s \right)^2 + \left(\frac{\tau}{4\sqrt{S/F}} B_n f_s \right)^2 + \frac{q_R^2}{12} \Bigg)^{1/2}$$

where $B_n = \dfrac{(b + a/b + a/2)\, fs/2}{2 - b - a/2}$

$b = 1/8$, $a = 1/256$, $f_s = 18.75$ Hz

q_R = 200 feet/bit (long range mode)

S/N = 3 dB at 200,000 feet

* 41 dB is a result of a 27 dB single pulse signal-to-noise ratio at 5,000 feet, and a 14 dB integration improvement from:

$Ni = (T_{aq})\ (fr)\ (\tau)\ /\ Ti$ = 5 pulses integrated.

S/F is an equivalent signal-to-fluctuation "noise power", calculated from statistical data obtained from a computer program which provided simulated pulsed RF returns from the Martian surface. S/F was calculated by using the expression for the RMS time delay error in a triangular pulse corrupted by noise

$$\delta TR = 2\tau / \sqrt{12}(2S/N)^{1/2}$$

Assuming the 1σ dispersion of the simulated pulse 50% point due to fluctuations has the same effect on the tracking loop error as a 1σ dispersion caused by thermal noise, an equivalent S/F can be calculated. Taking the 1σ value obtained from the computer study (δ_{TR} = 3 μsec for τ= 10 μsec) and substituting into the above equation gives S/F = 3 dB. Substituting in the original equation yields U_R = 145 feet (1σ), or 435 feet (3σ), at maximum range.

Acceleration lag error for the digital tracking loop is given by

$$E_R = \frac{\ddot{R} \sin \gamma}{a (f_s)^2}$$

where $\ddot{R}$ is a 580 ft/sec^2 peak deceleration expected, occurring at about 100,000 feet for $M/C_D A$ = 0.3, γe = 20, in a VM-8 atmosphere. Upon substitution, E_R = 146 feet.

For an analog tracking loop similar to the one used in the Saturn altimeter, noise and fulctuation error is given by:

$$U_R = \tau \left(\frac{1}{2 f_R T_s} \right)^{1/2} \left(\frac{.287}{\varepsilon \, S/N \, \tau \, B_i} + .274 \right)^{1/2}$$

where $f_R = 10^3$ Hz, τ = 5 μsec,

T_s = .008 sec, S/N = 2 (3dB)

$B_i = 2 \times 10^5$, ε = .96

On substitution, U_R = 405 feet (1 σ), or 1210 feet, (3σ).

Deceleration error is given by:

$$E_R = (\ddot{R}) \cdot (T_c) \cdot (t)$$

where T_c is loop time constant (1/56π). Since $\ddot{R}$ is a function of time (t), an approximation to it must be made. A constant 100 feet/sec^2 deceleration for 50 sec will be assumed.

On substitution, E_R = 280 feet error at the end of 50 seconds.

System errors such as bias drift, IF delay uncertainty, velocity error, timing, and calibration are small compared to the noise and tracker fluctuation errors. An additional error may occur at the end of dynamic deceleration, due to the antenna pattern null around the roll axis failing to illuminate the surface directly below the lander. This may occur at 30,000 feet, for a VM-10 atmosphere. The magnitude of this error can be determined from the difference in the average rise time of the pulse leading edge when the surface is illuminated (1) by the main lobe, and (2) by the null in the primary antenna pattern (See Figure 5.9-42). Figure 5.9-43 shows the difference in the 50% point of the two rise times (ε) to be about 1 microsecond, causing a 500 foot error.

Figure 5.9-44 gives an estimate of total percent error as they occur in the trajectory as a function of altitude for two tracking loops. This data serves only to indicate the approximate error expected, and represents the worst case. Differences in error between the digital and analog tracking loops are caused by selection of different tracking loop constants. The analog loop has a wide bandwidth to enable rapid acquisition and is more sensitive to fluctuation errors. The digital and analog tracking loops provide about the same measurement accuracy, when comparable loop parameters are used. The digital loop does, however, provide better long-term performance because the digital nature of the design eliminates temperature and time drift errors. Selection of a preferred tracking loop design will be made during Phase C, based on a computer program now being developed, which will simulate the mechanization of both tracking loops. This program will be used in conjunction with the existing program providing pulse returns from a simulated Martian surface, to allow selection of tracking loop parameters and constants which provide the best overall accuracy considering all error sources.

5.9.7.3 Potential Problem Areas and Solutions - Degradations will occur due to (1) the hemispherical antenna pattern approximation (null) causing delay error when the vehicle trajectory becomes vertical, (2) electrical breakdown causing a data lapse, (3) Aeroshell attenuation causing reduced altitude capability, (4) blackout periods extending below the calculated levels, and (5) Aeroshell interference after release.

- Rise-Time Delay - These have been previously examined and found to contribute about 500 feet of error in a VM-10 trajectory. Since this error occurs only in a dense atmosphere, where the Capsule Bus velocity is relatively slow, it has no appreciable affect on the sequencing function,

RADAR ALTIMETER ANTENNA RADIATION PATTERNS

A PRIMARY ANTENNA (CONICAL MONOPOLE)
B SECONDARY ANTENNA (DIPOLE)

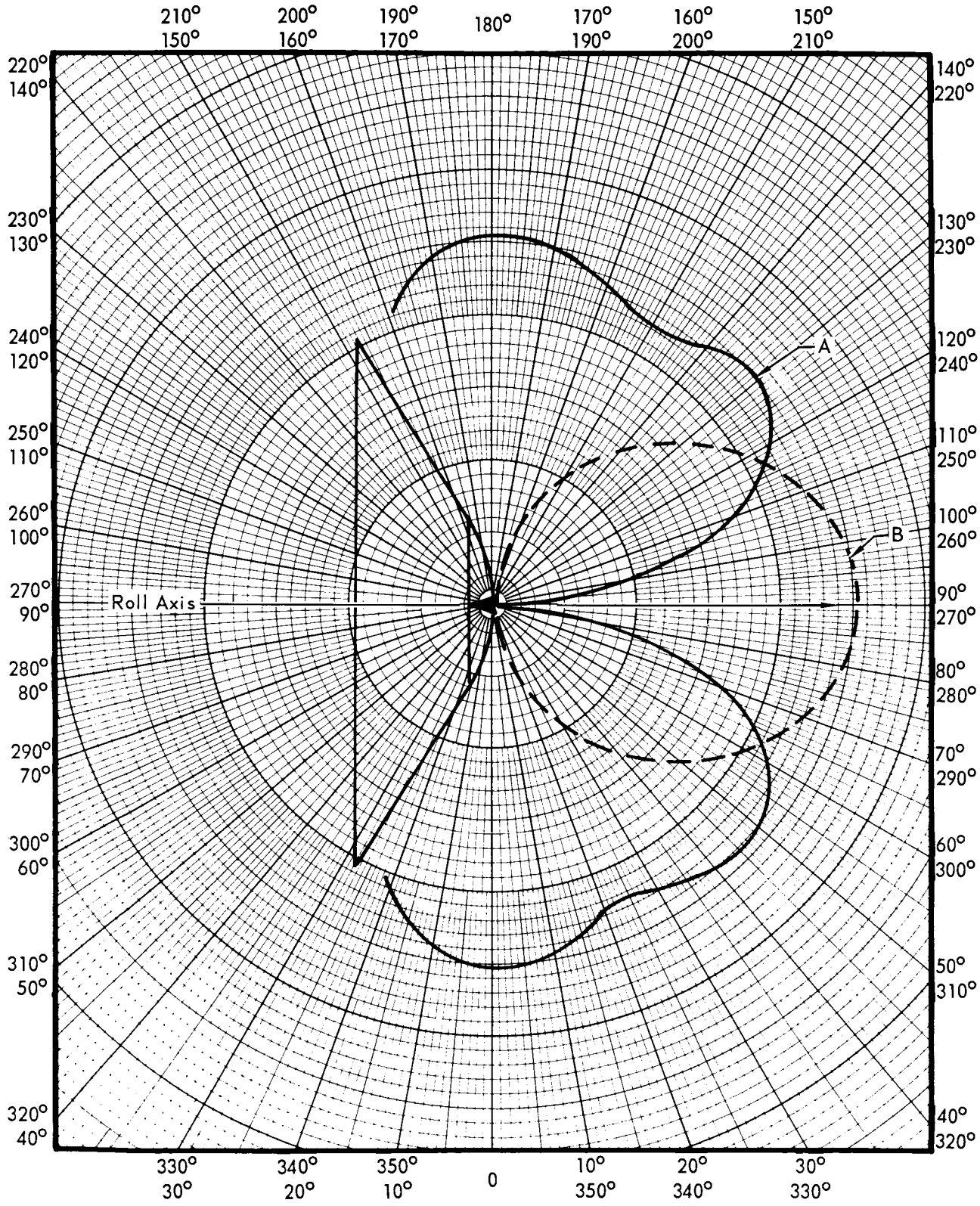

Figure 5.9–42

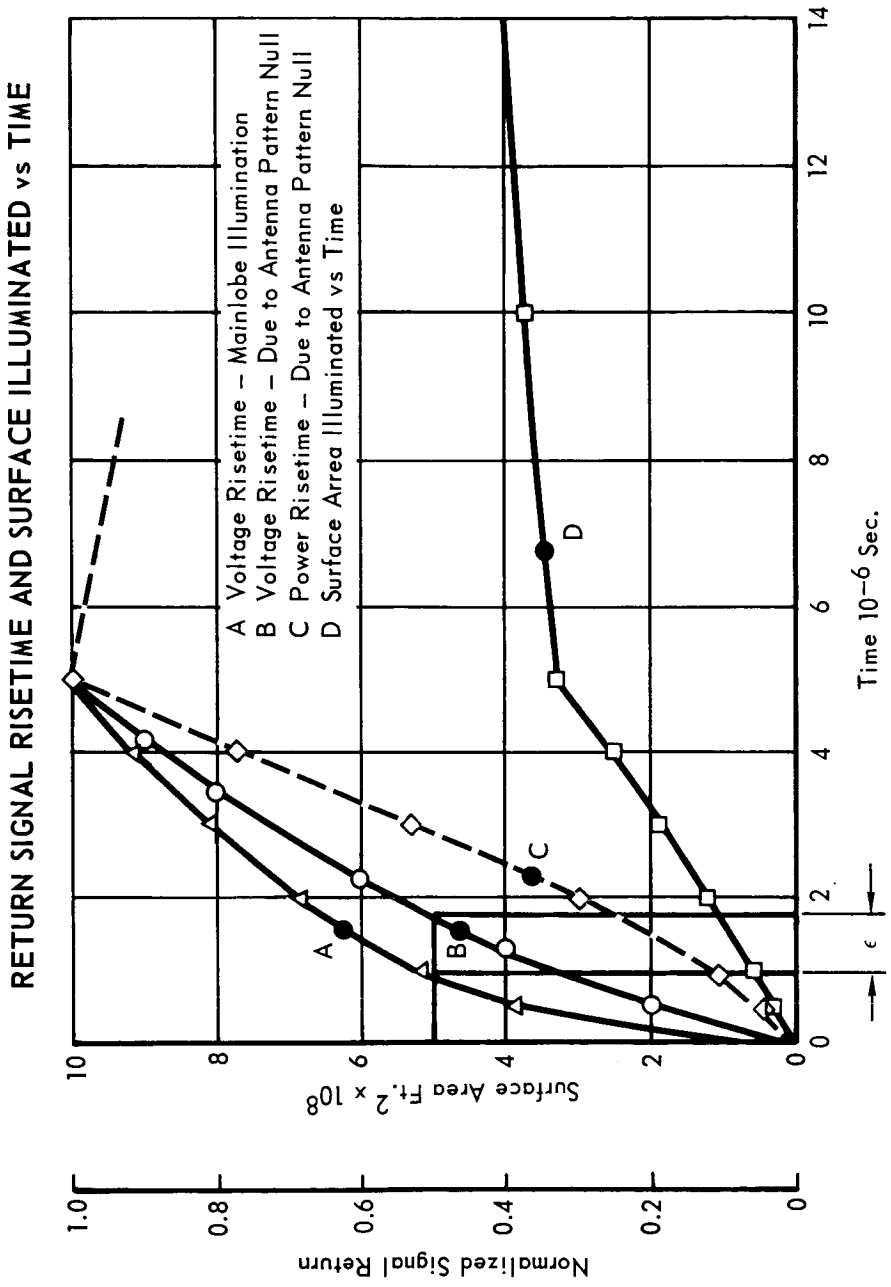
RETURN SIGNAL RISETIME AND SURFACE ILLUMINATED vs TIME
A Voltage Risetime – Mainlobe Illumination
B Voltage Risetime – Due to Antenna Pattern Null
C Power Risetime – Due to Antenna Pattern Null
D Surface Area Illuminated vs Time
Normalized Signal Return
Surface Area Ft.2 x 10^8
Time 10^-6 Sec.
A
B
C
D
ε

Figure 5.9–43

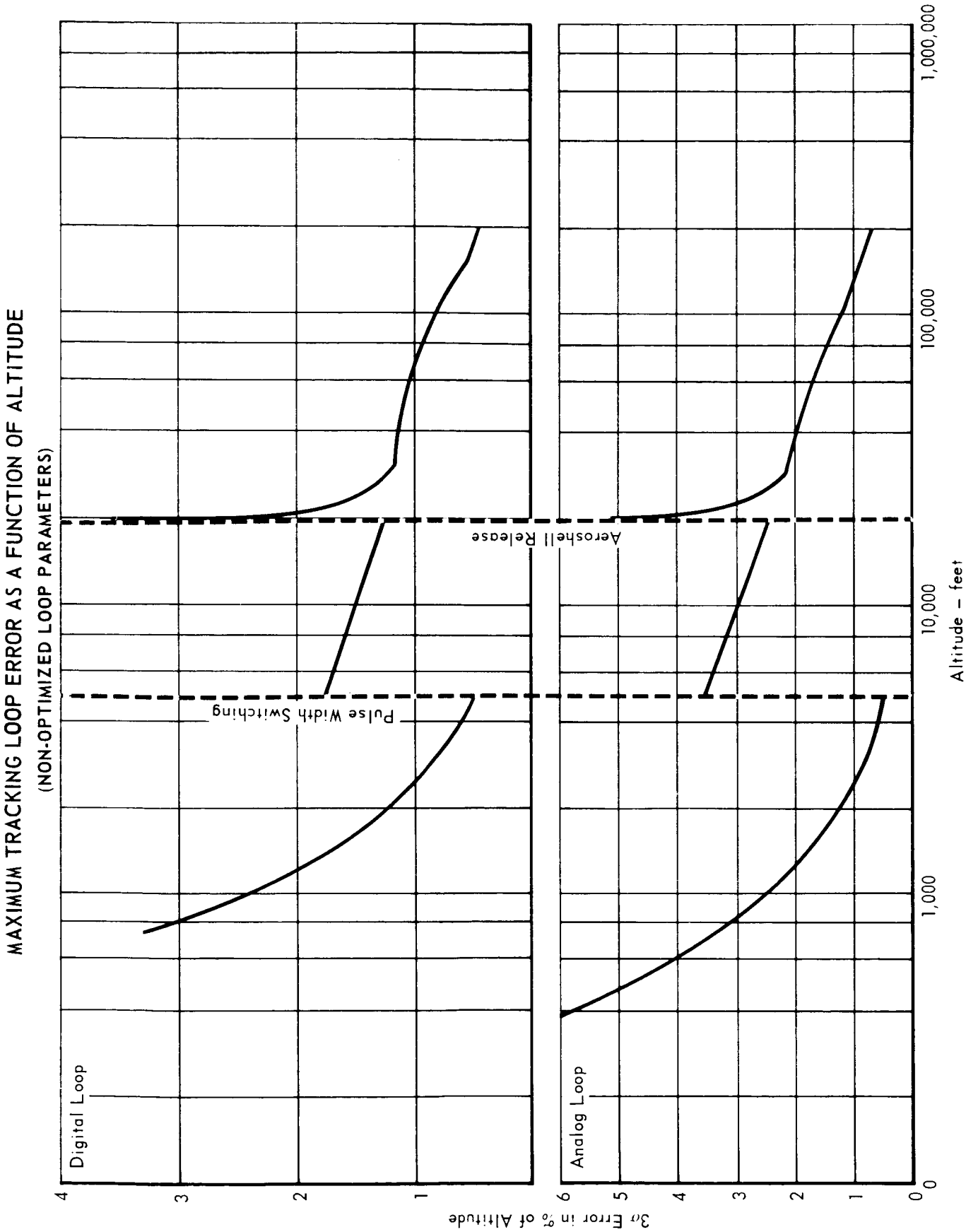
MAXIMUM TRACKING LOOP ERROR AS A FUNCTION OF ALTITUDE
(NON-OPTIMIZED LOOP PARAMETERS)
Digital Loop
Analog Loop
Pulse Width Switching
Aeroshell Release
3σ Error in % of Altitude
Altitude – feet
0
1
2
3
4
5
6
1,000
10,000
100,000
1,000,000

Figure 5.9–44

and will not affect the mission. After Aeroshell release the secondary antenna is used (which has no null along the roll axis) and this error is eliminated.

b. Electrical Breakdown - Degradation from a slight loss of data, to a catastrophic failure can result from electrical breakdown. Techniques to prevent breakdown have been developed and must be implemented in the design to eliminate all possibility of electrical breakdown.

c. Aeroshell Attenuations - Losses of 3 dB must be included in system parameter calculations. This results in twice the transmitter power; no performance degradation will occur.

d. Plasma Blackout - Figure 5.9-45 shows how worst case blackout regions could occur down to about 140,000 feet. If this should occur the estimation of atmospheric properties back to an altitude of 800,000 feet will have a greater error, but will still be usable. This figure was obtained from a comprehensive plasma analysis performed during the study. A more complete discussion of plasma induced blackout can be found in Part B, Section 5.5.1.4 of this volume.

e. Aeroshell Release - Built-in blanking during the transmitter-on period effectively ignores the near return from the Aeroshell. No degradation is anticipated with this provision.

5.9.7.4 Conclusion - The preceding analysis shows the preferred VOYAGER altimeter design to be a pulse-modulated altitude measuring radar using broad-beam, approximately hemispherical antenna coverage, and servo controlled range tracking. The analysis also shows that the selected design provides the required performance, with sufficient margins, to ensure an optimum mission providing good Entry Science data, and a successful soft landing.

BLACKOUT DURATION AS A FUNCTION OF FREQUENCY

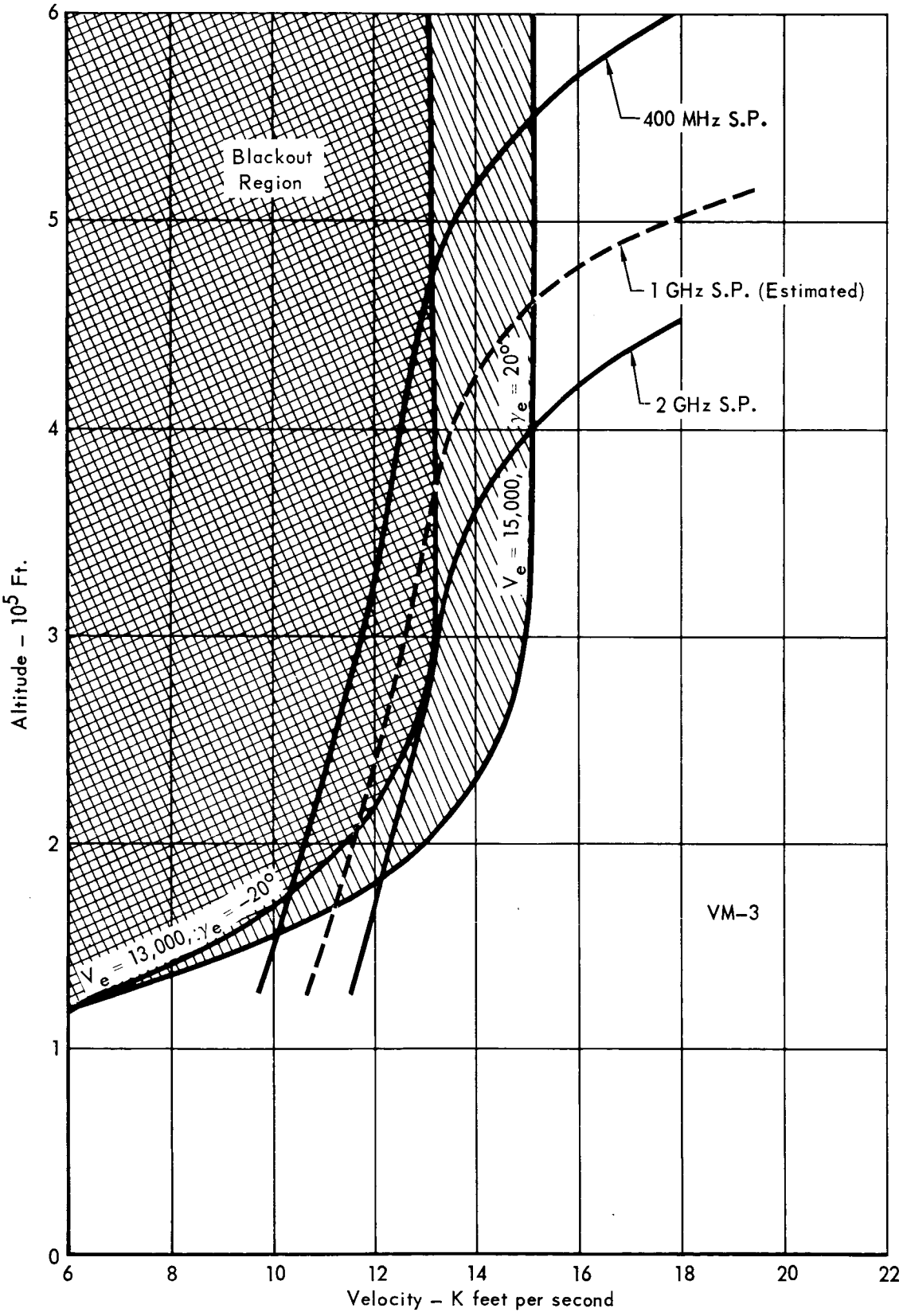

Figure 5.9–45

REFERENCES

5.9.1 1973 VOYAGER Capsule Systems Constraints and Requirements Document - Revision 2, dated 12 June 1967.

5.9.2 MAC Report E6610-174, Final Report, VOYAGER Wind Blown Sand and Dust Tests

5.9.3 Phase I Completion Report - Research and Development of Microminaturization Techniques and Circuitry and It's Adapatability to Radar Altimeters, Westinghouse Elect. Corp., 30 April 1965, Contract No. NAS 8-11682 for NASA, Marshall Space Flight Center

5.9.4 M. I. Skolnik, Introduction to Radar Systems, McGraw-Hill, 1962.

5.9.5 Report 29170-75, Proposal for a VOYAGER Landing Radar, Ryan Aeronautical Company, 29 May 1967.

5.9.6 Phase IV Final Report - Research and Development of Microminiaturization Techniques and Circuitry and its Adaptability to Radar Altimeters, Westinghouse Elect. Corp., 31 Jan. 1967, Contract No. NAS 8-11682 for NASA, Marshall Space Flight Center.